Decentralized Estimation and Control for Power Systems

Abhinav Kumar Singh

Thesis submitted for the degree of
Doctor of Philosophy

Imperial College London
Department of Electrical and Electronic Engineering
Control and Power Research Group

November 2014

Dedicated to my family

I hereby declare that all the work in the thesis is my own. The work of others has been properly acknowledged.

Declaration of Copyright

Abstract

This thesis presents a decentralized alternative to the centralized state-estimation and control technologies used in current power systems. Power systems span over vast geographical areas, and therefore require a robust and reliable communication network for centralized estimation and control. The supervisory control and data acquisition (SCADA) systems provide such a communication architecture and are currently employed for centralized estimation and control of power systems in a static manner. The SCADA systems operate at update rates which are not fast enough to provide appropriate estimation or control of transient or dynamic events occurring in power systems. Packet-switching based networked control system (NCS) is a faster alternative to SCADA systems, but it suffers from some other problems such as packet dropouts, random time delays and packet disordering. A stability analysis framework for NCS in power systems has been presented in the thesis considering these problems. Some other practical limitations and problems associated with real-time centralized estimation and control are computational bottlenecks, cyber threats and issues in acquiring system-wide parameters and measurements.

The aforementioned problems can be solved by a decentralized methodology which only requires local parameters and measurements for estimation and control of a local unit in the system. The cumulative effect of control at all the units should be such that the global oscillations and instabilities in the power system are controlled. Such a decentralized methodology has been presented in the thesis. The method for decentralization is based on a new concept of 'pseudo-inputs' in which some of measurements are treated as inputs. Unscented Kalman filtering (UKF) is applied on the decentralized system for dynamic state estimation (DSE). An extended linear quadratic regulator (ELQR) has been proposed for the optimal control of each local unit such that the whole power system is stabilized and all the oscillations are adequately damped. ELQR requires DSE as a prerequisite. The applicability of integrated system for dynamic estimation and control has been demonstrated on a model 16-machine 68-bus benchmark system.

Acknowledgements

First of all, I would like to express my most sincere gratitude to my supervisor Prof. Bikash C. Pal for his continuous support of my Ph.D study and research, for his patience, motivation, expertise and understanding. His guidance helped me throughout the research period. It is difficult to imagine a better advisor and mentor for my Ph.D study.

A very special thanks to my B. Tech. professors, Prof. Nilanjan Senroy and Prof. G. Bhuvaneshwari, who motivated and inspired me to pursue a research career.

I thank my fellow labmates and ex-labmates in Control and Power Group, especially Dr. Ravindra Singh, Dr. Yashodhan Prakash Agalgaonkar, Dr. Mohd Aifaa bin Mohd Ariff, Mr. Georgios Anagnostou and Mr. Ankur Majumdar for their thought provoking and stimulating discussions and for their constant help and support.

Last but not the least, I would like to thank my family: my parents Mr. Arun Kumar Singh and Mrs. Smita Singh, my wife Jayeeta and my brother Abhineet for always being there for me, through thick and thin.

Contents

List of Figures

List of Tables

List of Abbreviations

AC	Alternating current
AGC	Automatic generation control
AVR	Automatic voltage regulator
CT	Current transformer
DAC	Discrete to analog converter
DAE	Differential and algebraic equation
DC	Direct current
DSE	Dynamic state estimation
DSP	Digital signal processing
EKF	Extended Kalman filter
ELQR	Extended linear quadratic regulator
EMS	Energy management system
FACTS	Flexible AC transmission system
GPS	Global positioning system
JLS	Jump linear system
LMI	Linear matrix inequality
LQG	Linear quadratic Gaussian
LQR	Linear quadratic regulator
LTI	Linear time invariant
MPDP	Marginal packet delivery probability
NCPS	Networked control power system
NCS	Networked control system
NETS	New England test system
NYPS	New York power system
PDP	Packet delivery probability
PMU	Phasor measurement unit
POD	Power oscillation damping
PSS	Power system stabilizer
PT	Potential transformer

RTU	Remote terminal unit
SCADA	Supervisory control and data acquisition
SD	Standard deviation
SMIB	Single machine infinite bus
SSSC	Static synchronous series compensator
STATCOM	Static synchronous compensator
SVC	Static VAR compensator
TCP	Transmission control protocol
TCSC	Thyristor-controlled series capacitor
UDP	User datagram protocol
UKF	Unscented Kalman filter
WACS	Wide area control system
WAMS	Wide area measurement system
ZOH	Zero order hold

List of Symbols

$\mathbf{0}_{a\times b}$	denotes a zero matrix of size $(a \times b)$
$\boldsymbol{\alpha}$	diagonal binary matrix representing input packet dropout
α	difference of rotor angle and stator voltage phase in rad
α^c	c^{th} diagonal element of $\boldsymbol{\alpha}$
$\boldsymbol{\beta}$	diagonal binary matrix representing output packet dropout
β^c	c^{th} diagonal element of $\boldsymbol{\beta}$
$\boldsymbol{\gamma}^-$	a predicted-measurement sigma point
δ	rotor angle in rad
ζ	damping ratio of an electromechanical mode
θ	stator voltage phase in rad
θ_w	associated noise in the measured value of θ in rad
θ_y	measured value of θ in rad
λ_0	absolute bounding value of λ_y
λ_y	normalized innovation ratio for the measurement y
σ_η	standard deviation of η, for η=$V_w, \theta_w, I_w, \phi_w$ and f_w
ϕ	stator current phase in rad
ϕ_w	noise in the measured value of stator current phase in rad
ϕ_y	measured value of stator current phase in rad
$\boldsymbol{\chi}$	a sigma point
$\boldsymbol{\chi}^-$	a predicted-state sigma point
$\Psi_{1\mathrm{d}}$	subtransient emf due to d axis damper coils in p.u.
$\Psi_{2\mathrm{q}}$	subtransient emf due to q axis damper coils in p.u.
ω	rotor-speed in p.u.
ω_b	base-value of the rotor-speed in rad/s
$\boldsymbol{A}$	state-space matrix of system states
A_x, B_x	AVR exciter saturation constants in p.u.
$\arg\{C\}$	denotes the angle of a complex number C, in rad
$\boldsymbol{B}$	state-space matrix of system inputs
$\boldsymbol{B}'$	state-space matrix of system pseudo-inputs

$\boldsymbol{C}$	state-space matrix of system measurements
D	rotor damping constant in p.u.
diag$\{\boldsymbol{D}\}$	denotes a diagonal matrix of the elements in a vector $\boldsymbol{D}$
$\mathbb{E}[\boldsymbol{D}]$	denotes the expectation value of a random variable $\boldsymbol{D}$
E_{fd}	field excitation voltage in p.u.
E_{fdmax}	upper-limit value of E_{fd} in p.u.
E_{fdmin}	lower-limit value of E_{fd} in p.u.
E'_d	transient emf due to flux in q-axis damper coil in p.u.
E'_{dc}	state of the dummy-rotor coil in p.u.
E'_q	transient emf due to field flux linkages in p.u.
$\boldsymbol{F}$	state-feedback gain in the LQR and ELQR solutions
f	frequency of the phase of the stator voltage in p.u.
$\boldsymbol{G}$, $\boldsymbol{G'}$	feedback gains corresponding to $\boldsymbol{u'}$ in the ELQR solution
$\boldsymbol{g}$	a column vector of the system difference functions
$\bar{\boldsymbol{g}}$	a column vector of the system differential functions
H	generator inertia constant in s
$\boldsymbol{h}$	a column vector of the system algebraic functions
$\boldsymbol{I}_c$	denotes an identity matrix of size $(c \times c)$
I	stator current magnitude in p.u.
I_d	d-axis component of the stator current in p.u.
I_q	q-axis component of the stator current in p.u.
I_w	noise in the measured stator current magnitude in p.u.
I_y	measured stator current magnitude in p.u.
i	refers to the i^{th} generation unit or the i^{th} bus in the power system
$\boldsymbol{J}$	quadratic cost for a discrete LTI system without pseudo-inputs
$\boldsymbol{J'}$	quadratic cost for a discrete LTI system with pseudo-inputs
j	refers to $\sqrt{-1}$
$\boldsymbol{K}$	Kalman gain matrix
K_a	AVR-regulator gain in p.u.
K_c	initial value of degree of compensation of a TCSC
K_{c-ss}	control signal (change in degree of compensation) of a TCSC
K_{cmax}	upper-limit value of K_c
K_{cmin}	lower-limit value of K_c
K_{d1}	ratio $(X''_d - X_l)/(X'_d - X_l)$
K_{d2}	ratio $(X'_d - X''_d)/(X'_d - X_l)$
K_{pss}	PSS gain in p.u.
K_{q1}	ratio $(X''_q - X_l)/(X'_q - X_l)$
K_{q2}	ratio $(X'_q - X''_q)/(X'_q - X_l)$

K_x	AVR-exciter gain in p.u.
k	refers to the k^{th} time sample
$\boldsymbol{L}$	state-feedback gain in the stochastic LQR used in NCPS modeling
l	refer to the l^{th} sigma-point
$\boldsymbol{M}$	positive-definite matrix corressponding to $\boldsymbol{L}$
M	number of generation units in power system
m	number of elements in $\boldsymbol{x}$
N_0	number of buses in power system
N	final time sample of reaching steady state in LQR/ELQR solution
n	number of elements in $\boldsymbol{X}$
opt	denotes the optimal value of a variable
$\boldsymbol{P}$	positive-definite matrix corressponding to $\boldsymbol{F}$
P_{a-b}	denotes the active power flow in the line from bus a to bus b
P_G	active component of a power generation in p.u.
P_L	active component of a load in p.u.
$P_{s\tau}$	τ^{th} PSS state in p.u., for τ=1,2,3
$P'_{s\tau}$	τ^{th} PSS algebraic quantity in p.u., for τ=1,2,3
$\boldsymbol{P}_v$	covariance matrix of $\boldsymbol{v}$
$\boldsymbol{P}_w$	covariance matrix of $\boldsymbol{w}$
$\boldsymbol{P}_X$	estimated covariance matrix of $\boldsymbol{X}$
$\boldsymbol{P}_X^-$	estimated covariance matrix of $\boldsymbol{X}^-$
$\boldsymbol{P}_{Xy}^-$	estimated cross-correlation between $\boldsymbol{X}^-$ and $\boldsymbol{y}^-$
$\boldsymbol{P}_x$	estimated covariance matrix of $\boldsymbol{x}$
$\boldsymbol{P}_{xz}$	estimated cross-correlation between $\boldsymbol{x}$ and $\boldsymbol{z}$
$\boldsymbol{P}_x^-$	estimated covariance matrix of $\boldsymbol{x}^-$
$\boldsymbol{P}_y^-$	estimated covariance matrix of $\boldsymbol{y}^-$
p	number of elements in $\boldsymbol{u}$
p_u	PDP of an input channel
p_y	PDP of an output channel
$\boldsymbol{Q}$	state cost matrix
Q_G	reactive components of a power generation in p.u.
Q_L	reactive components of a load in p.u.
q	number of elements in $\boldsymbol{y}$
r	number of elements in $\boldsymbol{u}'$
$\mathbb{R}$	denotes the set of real numbers
$\boldsymbol{R}$	input cost matrix
R	denotes reduced form of state-space matrices, for example $\boldsymbol{A}_R$
$\boldsymbol{R}'$	pseudo-input cost matrix

R_a	armature resistance in p.u.
R_L	resistance of a line in p.u.
$\boldsymbol{S}$	matrix corressponding to $\boldsymbol{G}$ in the ELQR solution
$\boldsymbol{S}'$	matrix corressponding to $\boldsymbol{G}'$ in the ELQR solution
T	denotes matrix transpose
T_0	system sampling period in s
$T_{\tau 1}$	PSS's τ^{th} stage lead time constants in s for τ=1,2
$T_{\tau 2}$	PSS's τ^{th} stage lag time constants in s for τ=1,2
T_a	time constant of AVR's regulator in s
T_c	time constant for the dummy rotor coil (usually 0.01) in s
T_{tcsc}	time constant representing delay in firing sequence of a TCSC in s
T_e	electrical torque input in p.u.
T_m	mechanical torque input in p.u.
T_r	time constant of AVR's filter in s
T_w	PSS-washout time constant in s
T_x	time constant of AVR-exciter in s
T'_{d0}	d-axis transient time constant in s
T'_{q0}	q-axis transient time constant in s
T''_{d0}	d-axis subtransient time constant in s
T''_{q0}	q-axis subtransient time constant in s
t	system time in s
$\boldsymbol{u}$	a column vector of the inputs to the system
$\boldsymbol{u}'$	a column vector of the pseudo-inputs to the system
$\bar{\boldsymbol{u}}$	inputs to the system which have suffered packet dropout
$\boldsymbol{V}$	a column vector of the bus voltages, $V_\tau e^{\theta_\tau}$, τ=$1, 2, \ldots, N$; in p.u.
V	stator voltage magnitude in p.u.
V_a	AVR regulator voltage in p.u.
V_r	AVR-filter voltage in p.u.
V_{ref}	AVR reference voltage in p.u.
V_{ss}	PSS output voltage in p.u.
V_{ssmax}	upper-limit value of V_{ss} in p.u.
V_{ssmin}	lower-limit value of V_{ss} in p.u.
V_w	associated noise in V in p.u.
V_y	measured value of V in p.u.
$\boldsymbol{v}$	a column vector of process noise in discrete form
$\bar{\boldsymbol{v}}$	a column vector of process noise in continuous form
$\hat{\boldsymbol{v}}$	mean of $\boldsymbol{v}$
$\boldsymbol{w}$	a column vector of measurement noise

$\hat{\boldsymbol{w}}$	mean of $\boldsymbol{w}$
$\boldsymbol{X}$	augmented-state random variable
$\boldsymbol{X}^-$	predicted augmented-state random variable
X_d	d-axis synchronous reactance in p.u.
X_L	reactance of a line in p.u.
X_l	armature leakage reactance in p.u.
X_q	q-axis synchronous reactance in p.u.
X'_d	d-axis transient reactance in p.u.
X'_q	q-axis transient reactance in p.u.
X''_d	d-axis subtransient reactance in p.u.
X''_q	q-axis subtransient reactance in p.u.
$\hat{\boldsymbol{X}}$	estimated mean of $\boldsymbol{X}$
$\hat{\boldsymbol{X}}^-$	estimated mean of $\boldsymbol{X}^-$
$\boldsymbol{x}$	column vector of the states
$\boldsymbol{x}^-$	predicted state random variable
$\hat{\boldsymbol{x}}$	estimated mean of $\boldsymbol{x}$
$\hat{\boldsymbol{x}}^-$	estimated mean of $\boldsymbol{x}^-$
$\boldsymbol{Y}$	bus admittance matrix in p.u.
$\boldsymbol{y}$	column vector of the observed measurements
$\bar{\boldsymbol{y}}$	observed measurements which have suffered packet dropout
$\boldsymbol{y}^-$	predicted-measurement random variable
$\hat{\boldsymbol{y}}^-$	estimated mean of $\boldsymbol{y}^-$
Z_a	armature impedance ($\sqrt{{R_a}^2 + X''^2_d}$) in p.u.
$\boldsymbol{z}$	a column vector of noise in pseudo-inputs
$\hat{\boldsymbol{z}}$	mean of $\boldsymbol{z}$

Chapter 1

Introduction

The electrical power systems are over 120 years old and they are a key infrastructural asset for socio-economic development of the world. As power systems are considered to be the biggest and the most complex 'machines' ever built by mankind, the control of these systems, so that they operate within their stability margins, is an equally complex and challenging task. According to [1], stability of a power system is defined as "the ability of the system, for a given initial operating condition, to regain a state of operating equilibrium (or steady-state of operation) after being subjected to a physical disturbance, with most system variables bounded so that practically the entire system remains intact." As alternating current (AC) of near-constant frequency is the most widely adopted standard for generation and delivery of power using synchronous machines, the most important criterion for steady-state operation is that all the synchronous machines in the system remain in synchronism, or 'in-step'. This synchronism of generators in power systems is called rotor angle stability and is achieved using automatic generation control (AGC) [2]. Another criterion which should be satisfied during steady-state operation is that all the oscillations which develop after a small disturbance in the system should be controlled and damped within a specified period of time. This stability criterion is referred to as 'small signal stability'. Traditionally, small signal stability in power systems is achieved using automatic voltage regulators (AVRs) and power system stabilizers (PSSs) [2].

The growth of power requirements in the last few decades has been quite fast, in contrast to the slow and incremental nature of the evolution of power systems. The grid interconnections have increased manifold and there is an assimilation of more and varied (both centralized and decentralized) sources of energy into

the grid. Deregulation has led to increased separation of power producers and consumers, and there is an increased demand for not only power but also for high-quality power. In order to meet these growing demands, power systems have not only grown larger and more complex than ever (mainly due to large scale interconnections and integration of renewable sources of energy), but are increasingly operating closer to their stability limits as well, as elaborated in [3]. The European Network of Transmission System Operators for Electricity (ENTSO-E) interconnected system is an example of a stressed power system which is being operated more and more at its limits [3]. Small signal stability of such stressed systems is increasingly becoming more difficult to achieve using traditional schemes based on AVRs and PSSs. For instance, in some power blackout analyses the ineffectiveness of the control of small signal stability was identified as an important link to inception of the events leading to system-wide blackouts [4], [5].

It has been observed that under certain conditions, a small disturbance in a power system can initiate spontaneous oscillations in the power-flows in the transmission lines. These oscillations grow in magnitude within few seconds if they are undamped or poorly damped. This can lead to loss in synchronism of generators or voltage collapse, ultimately resulting in system separations and blackouts. The power blackout of August 10, 1996 in the Western Electricity Co-ordination Council region is a famous example of blackouts caused by such oscillations [6], [7]. The frequencies of these oscillations are in the range of 0.2 to 1.0 Hz, and as these oscillations are not local to a particular generator and involve two or more groups of generators (also known as areas), they are termed as inter-area oscillations [8], [9]. The local control actions of AVRs and PSSs are insufficient to control interarea oscillations, and therefore more global control schemes are needed to achieve small signal stability in current power systems.

Today there is an increase in the research, development and investment in global control schemes for power systems. Phasor measurement units (PMUs) and flexible AC transmission system (FACTS) are starting to form the core of such a global control infrastructure for power systems. New techniques for dynamic state estimation (DSE) and dynamic control are emerging which can not only strengthen but potentially revolutionize this control infrastructure. There is also a requirement of reliable communication network to be in place which can deliver real-time system-wide information to and from these devices and controllers. The next section explores the state of the art and current research in power system estimation and control.

1.1 State of the art

1.1.1 Energy management system and SCADA

Energy management system (EMS) in a power system plays an important role in system operation and control [10]. EMS has a host of network computation functions such as static state estimation, optimal power flow, contingency analysis etc. These drive scheduling and dispatch of load and generation in the time scale of minutes to hours. Supervisory control and data acquisition (SCADA) forms the heart of EMS and performs data acquisition, update of system status through alarm processing and user interface updating, as well as execution of control actions [11]. Remote terminal units (RTUs) perform the role of sensors and actuators in SCADA. Different types of telemetering and communication protocols are used in SCADA (which vary with SCADA vendors), but majority of them use serial communication based on DNP3.0 protocol [12]; and their update rates lie in the range of 2-10 seconds [13], [14]. Although these rates are fast enough to provide the traditional functions performed by EMS, they are not enough to deliver time critical measurements and control actions needed for dynamic estimation and control. Besides communication systems, there are several other aspects of EMS/SCADA (such as metering, security, visualization, database and control capabilities) which need to be upgraded to meet the requirements of today's power systems [15].

1.1.2 Phasor measurement units

An electrical quantity which has both phase and magnitude (for example bus voltage, line current and line power) is called a phasor. A PMU is a device which can accurately measure a phasor. This is done by time synchronization of all the PMUs in the power system to an absolute time reference provided by the global positioning system (GPS) [16], [17]. PMUs are capable of providing sampling rates of over 600 Hz and time synchronization accuracy of ± 0.2 μs [18]. The speed and accuracy of measurement by PMUs has led to the development of several techniques and algorithms for fast and reliable control and dynamic state estimation, which will be more evident in the following subsections.

1.1.3 Flexible AC transmission system

FACTS devices are static power-electronic devices installed in AC transmission networks to increase power transfer capability, stability and controllability of the networks through series and/or shunt compensation [19]. These devices can also be employed for congestion management and loss optimization. Static synchronous series compensator (SSSC) and thyristor-controlled series capacitor (TCSC) are some of the FACTS devices which provide series compensation to reactance of the lines to which they are connected, while static synchronous compensator (STATCOM) and static VAR compensator (SVC) are some FACTS devices which provide shunt compensation to transmission lines. FACTS devices can also provide adequate damping of interarea oscillations by acting as actuators in robust control schemes and PMU based wide area control schemes [7], [19].

1.1.4 Wide-area measurements and wide-area control

Wide area measurement system (WAMS) refers to a measurement system composed of strategically placed time synchronized sensors (which are PMUs) which can monitor in real time the current status of a critical area. The critical area can be a whole power system or a part of the system. The strategic locations are decided in a way that the number of locations are minimized and the critical area remains completely observable [20]. The measurements from WAMS are utilized by the wide area control system (WACS) to control the transient and oscillatory dynamics of system voltage and frequency [21]. A fast communication network which can operate at update rates of 10-20 Hz is crucial for WAMS/WACS in order to deliver measurements from sensors to control-center and control signals from control-center to actuators (AVRs, PSSs and FACTS devices). As the communication requirements of WAMS/WACS are very high, at present WAMS/WACS have only been implemented in small scale power systems. The WAMS/WACS implemented by Bonneville Power Administration for the wide area stability and voltage support of their power system is such an example [21]. A revamp of communication architecture for power systems needs to be done in order to implement WAMS/WACS on large scale power systems [22]-[24].

1.1.5 Dynamic state estimation and dynamic control

DSE, which refers to the estimation of state variables representing oscillatory dynamics of a power system, can also be utilized for effective control of these dynamics besides the aforementioned techniques of robust control and wide-area control. With growing deployment of PMUs across the system, DSE algorithms have been proposed by several research groups for the real time estimation of dynamic states (typically machine load angle, acceleration, transient speed voltages etc.) using Kalman filtering [25]-[31]. However, as all of these algorithms present a centralized approach to DSE, a reliable and fast communication network is needed to bring system-wide measurements to a central location to implement these algorithms. Thus, a slow communication network used in EMS/SCADA (with update rates of 2-10 s) is a bottleneck for both WACS and DSE.

DSE forms an integral part of many dynamic control techniques proposed for today's power system. Algorithms based on real time dynamic security assessment ([32],[33]) and model predictive control ([34],[35]) are a few examples of such control techniques.

1.2 Challenges to power system estimation and control

The majority of control and monitoring tools in present power systems are provided by EMSs and are based on steady state system model, which cannot capture the dynamics of power system very well. This limitation is primarily due to the dependency of EMSs on slow update rates of the SCADA systems. Therefore, the state estimates of the system are updated in a time scale of ten seconds, and most of the dynamic control schemes are local to a generator or a FACTS device and are based on locally available information and measurements. The chief challenge in implementing dynamic estimation and global control schemes is unavailability of a fast, reliable and secure communication network.

Packet based communication is the most widely adopted communication technology today, on which even the highly complex 'Internet' is based. There is an option of using packet based communication network (instead of the slow and outdated communication technology used in SCADA) for DSE, WAMS/WACS and dynamic control in power systems. But this option also poses a question that whether the

overall system will remain stable or not as packet based communication suffers from problems such as packet dropout, packet disordering and time-delay.

Another option for implementing DSE, WAMS/WACS and dynamic control in power systems is to implement them in a completely decentralized manner. This means that the complete knowledge of states and controllability of the oscillatory system dynamics are obtained at decentralized locations in the system using only local information and measurements at those locations. This option remains an important research challenge as finding a solution to this challenge would remove the necessity of a fast and reliable communication network for dynamic estimation and control. Presently, an algorithm for decentralized DSE is not available in literature. Some algorithms for decentralized control of power systems are available which are based on Lyapunov theory ([36]-[38]), but these algorithms assume a simplistic model of power system and also require the knowledge of dynamic states at the decentralized locations of control.

1.3 Research objectives

This research intends to answer the following two questions based on the aforementioned challenges to dynamic estimation and control of power systems:

1. What is the effect on small-signal stability of a power system in which a packet based communication network is included in its control loops (that is, a communication network is used for the transmission of measurement signals from sensors to a control center and for the transmission of control signals from control center to actuators)?
2. Can the dynamic estimation and control of a power system be performed in a decentralized manner so that the requirement of a fast and reliable communication network is eliminated?

1.4 Research contributions and dissemination

The contributions of the research can be summarized as follows:

1. A model of a networked controlled power system has been developed in which the control loops of the system are closed using a packet based communication network. The stability analysis of such a system has been performed under an assumption that stochastic packet dropout is taking place in the network. The lower limit on the probability of packet dropout has been computed which guarantees specified stability margin of the system.

2. A new concept of 'pseudo-inputs' has been developed for decentralization of power system equations. This concept, along with the concept of non-linear unscented Kalman filtering, has been applied for decentralized dynamic estimation of states and parameters of power systems.

3. An extended linear quadratic regulator has been developed for optimal control of a linear system in which both controllable inputs and uncontrollable pseudo-inputs are present.

4. The concepts of decentralized DSE and extended linear quadratic regulator have been integrated together for decentralized estimation and control of a power system.

5. A benchmark 68-bus 16-machine system has been implemented in MATLAB. The developed technique of decentralized estimation and control has been successfully implemented and validated on the benchmark system.

The research work on decentralized parameter estimation was conducted jointly with Dr. Mohd Aifaa bin Mohd Ariff, a colleague of the author in Imperial College London. Mr. Ariff was the principal researcher in this work, and the author helped him with the concepts of pseudo-inputs and unscented Kalman filtering and also helped him with the implementation of these concepts in MATLAB. The theory and results of this work are available in [39].

The complete research findings have been disseminated in the following papers, posters and reports.

1.4.1 Journal papers

1. A. K. Singh, R. Singh, B. C. Pal, "Stability Analysis of Networked Control in Smart Grids," *IEEE Transactions on Smart Grid*, vol. PP, no. 99, pp. 1–10, May 2014.

Abstract: A suitable networked control scheme and its stability analysis framework have been developed for controlling inherent electromechanical oscillatory dynamics observed in power systems. It is assumed that the feedback signals are obtained at locations away from the controller/actuator and transmitted over a communication network with the help of phasor measurement units (PMUs). Within the generic framework of networked control system (NCS), the evolution of power system dynamics and associated control actions through a communication network have been modeled as a hybrid system. The data delivery rate has been modeled as a stochastic process. The closed-loop stability analysis framework has considered the limiting probability of data dropout in computing the stability margin. The contribution is in quantifying allowable data-dropout limit for a specified closed loop performance. The research findings are useful in specifying the requirement of communication infrastructure and protocol for operating future smart grids.

2. A. K. Singh, B. C. Pal, "Decentralized Dynamic State Estimation in Power Systems Using Unscented Transformation," *IEEE Transactions on Power Systems*, vol. 29, no. 2, pp. 794–804, Mar. 2014.

   Abstract: This paper proposes a decentralized algorithm for real-time estimation of the dynamic states of a power system. The scheme employs phasor measurement units (PMUs) for the measurement of local signals at each generation unit; and subsequent state estimation using unscented Kalman filtering (UKF). The novelty of the scheme is that the state estimation at one generation unit is independent from the estimation at other units, and therefore the transmission of remote signals to a central estimator is not required. This in turn reduces the complexity of each distributed estimator; and makes the estimation process highly efficient, accurate and easily implementable. The applicability of the proposed algorithm has been thoroughly demonstrated on a representative model.

3. M. A. M. Ariff, B. C. Pal, A. K. Singh, "Estimating Dynamic Model Parameters for Adaptive Protection and Control in Power System," *IEEE Transactions on Power Systems*, vol. PP, no. 99, pp. 1–10, 2014.

   Abstract: This paper presents a new approach in estimating important parameters of power system transient stability model such as inertia constant H and direct axis transient reactance x'_d in real time. It uses a variation of unscented Kalman filter (UKF) on the phasor measurement unit (PMU) data. The accurate estimation of these parameters is very important for

assessing the stability and tuning the adaptive protection system on power swing relays. The effectiveness of the method is demonstrated in a simulated data from 16-machine 68-bus system model. The paper also presents the performance comparison between the UKF and EKF method in estimating the parameters. The robustness of method is further validated in the presence of noise that is likely to be in the PMU data in reality.

4. A. K. Singh, B. C. Pal, "Decentralized Control of Oscillatory Dynamics in Power Systems using an Extended LQR," *IEEE Transactions on Power Systems*, 2014 (under second stage of review).

   Abstract: This paper proposes a decentralized algorithm for real-time control of oscillatory dynamics in power systems. The algorithm integrates dynamic state estimation (DSE) with an extended linear quadratic regulator (ELQR) for optimal control. The control for one generation unit only requires measurements and parameters for that unit, and hence the control at a unit remains completely independent of other units. The control gains are updated in real-time, therefore the control scheme remains valid for any operating condition. The applicability of the proposed algorithm has been demonstrated on a representative power system model.

1.4.2 Conference posters

1. A. K. Singh, A. Majumdar, B. C. Pal, "Effect of Network Packet-Dropout on the Control Performance of Power Systems," *IEEE Power and Energy Society General Meeting '12 - Student-poster*, San Diego, USA, 21-25 July, 2012.

   Abstract: With the introduction of wide area measurement system (WAMS) and flexible AC transmission system (FACTS) in Power Technology, remote signals need to be transmitted over distances as large as even hundreds of kilometers to centralized or distributed controllers. The number of such signals and controllers is bound to increase with an increase in the complexity of power systems as they are going to operate closer to their operating limits and also become larger by integration of more and varied sources of energy. The introduction of a packet based network is soon going to be indispensable for the communication of such a 'smart' grid. This poster aims to study the effect of packet-dropout rate on the stability of such a networked controlled power system, specifically on the stability of the damping control using a thyristor controlled series capacitor (TCSC).

2. A. K. Singh, B. C. Pal, "Distributed Data Fusion for State Estimation in Cyber Physical Energy Systems," *IEEE Power and Energy Society General Meeting '13 - Student-poster*, Vancouver, Canada, 21-25 Jul., 2013.

   Abstract: This poster proposes an adaptive algorithm for dynamic state estimation in cyber physical energy systems. The algorithm involves distributed estimation based on unscented Kalman filtering, and subsequent multi-path data fusion of the local estimates. The distributed estimation takes into account the inherent shortcomings of networked systems, viz., packet dropout, packet disordering and variable time delays. The multi-path data fusion strategy endeavours to convert the highly stochastic and uncertain packet delivery model of present day networks into a deterministic model with very high packet delivery probabilities and fixed time delays. The combined strategy of distributed estimation and multi-path data fusion has been demonstrated on a representative 68-bus power system model.

1.4.3 IEEE Task Force reports

1. A. K. Singh, B. C. Pal, *IEEE PES Task Force on Benchmark Systems for Stability Controls*–Report on the 68-Bus, 16-Machine, 5-Area System, ver. 2.0, 9 Jul. 2013 [Online]. http://www.sel.eesc.usp.br/ieee/

   Abstract: The present report refers to a small-signal stability study carried over the 68-Bus, 16-Machine, 5-Area System and validated on a widely known software package: MATLAB-Simulink (ver. 2011b). The 68-bus system is a reduced order equivalent of the inter-connected New England test system (NETS) and New York power system (NYPS), with five geographical regions out of which NETS and NYPS are represented by a group of generators whereas, the power import from each of the three other neighboring areas are approximated by equivalent generator models. This report has the objective to show how the simulation of this system must be done using MATLAB in order to get results that are comparable and exhibit a good match with respect to the electromechanical modes with the ones presented in the PES Task Force website on Benchmark Systems.

2. R. Ramos, L. Lima, N. Martins, I. Hiskens, B. Pal, D. Vowles, M. Gibbard, C. Canizares, L. G. Lajoie, F. Marco, B. Tamimi, R. Kuiava, and A. K. Singh, *IEEE PES Task Force on Benchmark Systems for Stability Controls*–Final Report (Draft), ver. 9, 16 Jun. 2014.

Abstract: This report describes the work by the members of the IEEE PES Task Force (TF) on Benchmark Systems for Stability Controls. The following sections present the objectives of the TF, the guidelines used to select the benchmarks, a brief description of each benchmark system (so the reader can select the most suitable system for the intended application), the input data and results for each benchmark system and a set of conclusions.

1.5 Thesis organization

The organization of the rest of the thesis is as follows. In Chapter 2, a stability analysis framework for packet-switching based networked control system (NCS) in power systems is presented. Some practical limitations and problems associated with real-time centralized estimation and control using NCS are also presented. Chapter 3 presents the method for decentralization. This method is based on the concept of pseudo-inputs in which some of measurements are treated as inputs. Unscented Kalman filtering is then applied on the decentralized system for dynamic state estimation. An extended linear quadratic regulator is proposed and developed in Chapter 4 for the optimal control of a linear system with pseudo-inputs. In Chapter 5, the developed regulator is used for decentralized control of each local unit such that the whole power system is stabilized and all oscillations in the system are adequately damped. Modeling and implementation details for MATLAB are presented in the Appendices.

Chapter 2

Stability analysis of networked control in power systems

This chapter addresses the first research question of the thesis: *What is the effect on small-signal stability of a power system in which a packet based communication network is included in its control loops?* Networked control system (NCS) approach utilizing modern communication concepts is very appropriate in this context. An NCS is defined as a system in which the control loops are closed through a real-time communication network [40]. Networked control enables execution from long distance by connecting cyberspace to physical space. It has been successfully applied in other technology areas such as space and terrestrial exploration, aircraft, automobiles, factory automation and industrial process control. NCS offers many advantages over traditional control architectures. Addition of new sensors, actuators or controllers in traditional control architectures can result in significant increase in wiring and complexity of the control system, leading to increased costs and reduced flexibility with each new component. Utilizing a communication network for connecting these components can effectively reduce the complexity of the system and maintenance costs, with nominal economical investments, as networked controllers allow data to be shared efficiently. Furthermore, networked control offers high flexibility as new control system components can be added with little costs and without making significant structural changes to the system. The advantages of NCS over traditional control systems have been elaborated in [40].

Packet-switching based communication networks are the most widely adopted systems for fast, economic and stable data transfer over both large and small distances through dynamic path allocation. They are in contrast to the traditional

circuit-switching based networks in which a dedicated link is established between the sending and the receiving ends. Circuit switching is not only inefficient and costlier than packet-switching, but also the link failure rate increases for large transmission distances, and the failure cannot be dynamically corrected, unlike packet-switching [41]. This is the reason that most of the current research in NCS is based on packet-switching technology. However, packet-switching based networks also suffer from some problems such as packet-dropout, network induced delays and packet-disordering [40]. These factors can possibly degrade the performance of the control of power system dynamics and small signal stability. As explained in Chapter 1, in the context of interconnected power systems, the control of oscillatory stability is very time critical as uncontrolled oscillations in past have led to several power blackouts. Therefore these factors need to be analyzed thoroughly for assessing the suitability of the NCS approach to wide area control of power systems.

Over the past decade, substantial research has been undertaken to model NCS and study the effects of packet-dropout and time delays on the control design and the stability of the NCS ([42], [43], [44] and [45]), but this research is not reflected in the power system literature. In most of the literatures relating to power systems, it is assumed that the transmission of signals to and from the central control unit occurs over an ideal, lossless and delay-free communication network. A few exceptions to this are [46], [47] and [48]. In [46] the effect of network induced time-delays has been considered using a WAMS based state-feedback control methodology. In [47] an estimation of distribution algorithm based speed control of networked DC motor system has been studied; and in [48] the effect of communication-bandwidth constraints on the stability of WAMS based power system control has been studied. But all these papers have other limitations. For instance, in [46] it is not explained how the various system states (such as the rotor angle, rotor velocity and transient voltages) are estimated before using them for state-feedback; and also the power system model considered in the paper is too simplistic to represent actual power system dynamics. In [47] only a local network based control of a single dc-motor system is considered instead of considering the networked control of a complete power-system. In [48], the chief problems associated with networked-control, which are packet-loss and delay, are not considered. This chapter has made an attempt to address the aforementioned limitations by analyzing the effects of packet-dropout on the oscillatory stability response of a networked controlled power system (NCPS).

A rigorous model for a NCPS is presented in Section 2.1. Section 2.2 presents LMI based stability analysis of the developed NCPS, and derives the probability threshold of the packet-dropout rate while guaranteeing specified level of damping of the NCPS. A case study of a representative 68-bus New-England/New-York inter-connected NCPS model has been presented in Section 2.3. In the case study, the inter-area oscillations in the power system are controlled using feedback signals which are transmitted over a communication network. Section 2.4 presents the limitations of the developed NCPS model and Section 2.5 summarizes the chapter.

2.1 NCPS Modeling with Output-feedback

A block diagram of the output-feedback controlled NCPS is shown in Fig. 2.1. The model is described as hybrid continuous-discrete system in which power system is the continuous, while networked-controller is the discrete part. The NCPS model is hybrid in one other sense that the power system is deterministic while the networked controller is stochastic in nature.

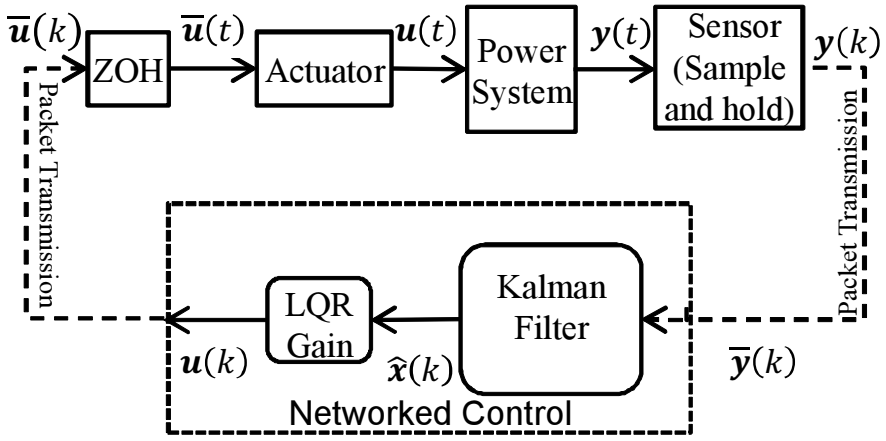

Figure 2.1: A reduced model of the NCPS

In Fig. 2.1, the block 'Power System' represents the open-loop power system, oscillatory dynamics of which need to be controlled. To this effect, real-power deviations in some of the lines are measured in real-time using current transformers (CTs) and potential transformers (PTs) [49], and represented by $\boldsymbol{y}(t)$ in the block diagram. These are then sampled at the sampling rate of the communication network using digital devices such as phasor measurement units (PMUs) and intelligent electronic devices (IEDs) and then sent over the communication network as discrete data-packets, $\boldsymbol{y}(k)$. User datagram protocol (UDP) is used for packet

transmission, and packet-loss occurs during transmission. The final data which is received at the control unit after packet loss is given by $\bar{\boldsymbol{y}}(k)$. The control unit consists of a LQG controller, which is a combination of a Kalman filter and a linear quadratic regulator (LQR). Kalman filter uses linearized, discretized and reduced power system model and the output data-packets arriving at the controller, $\bar{\boldsymbol{y}}(k)$, to estimate the states, $\hat{\boldsymbol{x}}(k)$. The state estimates are then multiplied by the LQR gain to produce the control signals $\boldsymbol{u}(k)$, which are then sent over the communication network to the actuators. The packets arrive at discrete to analog converters (DACs), which are zero-order-hold devices and convert the discrete control signals after packet-loss, $\bar{\boldsymbol{u}}(k)$, into continuous control signals, $\bar{\boldsymbol{u}}(t)$. These continuous signals control the actuators, which are the FACTS devices, more commonly known as FACTS controllers. The inputs $\boldsymbol{u}(t)$ to the power system are the percentage compensations provided by the FACTS controllers to control the power-flow in the lines on which the FACTS controllers are installed. All the variables in the model have been expressed in per unit (p.u.), except the time variables which are expressed in s. A detailed description of each component of the NCPS model is presented as follows.

2.1.1 Power system

An interconnected power system is represented through important components such as the generators, their excitation systems, power system stabilizers (PSS), FACTS controllers such as a thyristor controlled series capacitor (TCSC), loads and transmission network [50] as shown in Fig. 2.2.

The dynamics of the system is modeled using a set of non-linear differential and algebraic equations (DAEs) ([51] and [50]). The state space representation of the system is obtained through linearization of the DAEs around an initial operating point. The order of the system is reduced to speed up the controller design algorithm and also to reduce the order of the controller. On applying balanced model reduction based on singular value decomposition, as given in [52], only the unstable and/or poorly damped electromechanical modes of the power system are retained in the reduced model. The reduced model is written as:

$$\Delta\dot{\boldsymbol{x}}\,(t) = \boldsymbol{A}_R\Delta\boldsymbol{x}\,(t) + \boldsymbol{B}_R\Delta\boldsymbol{u}\,(t) \tag{2.1}$$

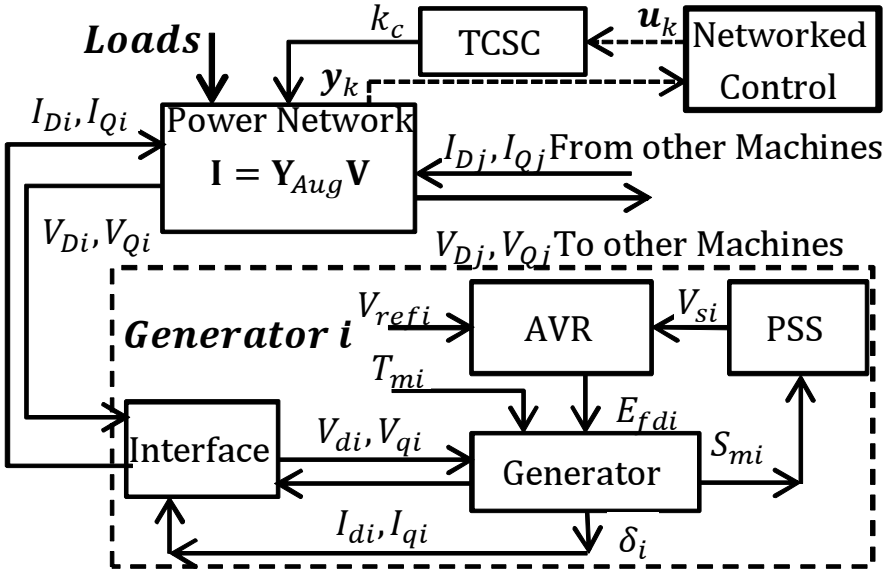

Figure 2.2: Details of the power system in the NCPS

$$\Delta \boldsymbol{y}(t) = \boldsymbol{C}_R \Delta \boldsymbol{x}(t) \tag{2.2}$$

$\boldsymbol{A}_R \in \mathbb{R}^{m\times m}, \boldsymbol{B}_R \in \mathbb{R}^{m\times p}$ and $\boldsymbol{C}_R \in \mathbb{R}^{q\times m}$ are the reduced state space matrices and $\boldsymbol{x} \in \mathbb{R}^m, \boldsymbol{u} \in \mathbb{R}^p$ and $\boldsymbol{y} \in \mathbb{R}^q$ are the vectors of state variables, inputs and outputs, respectively. It should be noted that after balanced reduction of the full model, only the state variables and the state matrices get reduced in order; the inputs $\boldsymbol{u}$ and the outputs $\boldsymbol{y}$ remain same as in the original full model. Also, out of the various possible measurable outputs (which are the line-powers in the context of NCPS), only those outputs are selected in $\boldsymbol{y}$ which have high observability of the unstable and/or poorly damped electromechanical modes of the power system.

2.1.2 Sensors and actuators

The sensors (in the context of NCPS, they are CTs, PTs and PMUs) send the feedback signals to the controller over the communication network at a regular interval of T_0, which is the sampling period of the communication network. The discrete to analog converters (DACs) convert the discrete control signals after packet-loss into continuous control signals. The DACs are event-driven zero-order-hold (ZOH) devices, each one of which holds the input to the power system in a given cycle. In the next cycle it holds its previous value if there is no new input due to packet drop, otherwise it holds the new input. The outputs of the DACs control the FACTS controllers, which are the actuators; and the inputs $\boldsymbol{u}(t)$ to the power

system are the percentage compensations provided by the FACTS controllers. For the $(k+1)^{th}$ time cycle, (2.1) reduces to:

$$\Delta\dot{\boldsymbol{x}}(t) = \boldsymbol{A}_R\Delta\boldsymbol{x}(t) + \boldsymbol{B}_R\Delta\boldsymbol{u}(kT_0); 0 \leq t - kT_0 < T_0 \tag{2.3}$$

Solving (2.3) with initial condition $(\Delta\boldsymbol{x}(kT_0), \Delta\boldsymbol{u}(kT_0))$ and a constant input $\Delta\boldsymbol{u}(kT_0)$ [53], we get:

$$\Delta\boldsymbol{x}((k+1)T_0) = \boldsymbol{A}\Delta\boldsymbol{x}(kT_0) + \boldsymbol{B}\Delta\boldsymbol{u}(kT_0); \tag{2.4}$$

$$\boldsymbol{A} = e^{\boldsymbol{A}_R T_0}; \boldsymbol{B} = \boldsymbol{A}_R^{-1}\left(e^{\boldsymbol{A}_R T_0} - \boldsymbol{I}\right)\boldsymbol{B}_R \tag{2.5}$$

Denoting $\Delta\boldsymbol{x}(kT_0)$ as $\boldsymbol{x}_k$, $\Delta\boldsymbol{u}(kT_0)$ as $\bar{\boldsymbol{u}}_k$ (where $\bar{\boldsymbol{u}}_k$ is the uncertain input after packet dropout), $\Delta\boldsymbol{y}(kT_0)$ as $\boldsymbol{y}_k$, $\boldsymbol{C}_R$ as $\boldsymbol{C}$, and also including a white Gaussian measurement noise $\boldsymbol{v}_k$ and a white Gaussian process noise $\boldsymbol{w}_k$ in the model, we get:

$$\boldsymbol{x}_{k+1} = \boldsymbol{A}\boldsymbol{x}_k + \boldsymbol{B}\bar{\boldsymbol{u}}_k + \boldsymbol{w}_k;\ \boldsymbol{y}_k = \boldsymbol{C}\boldsymbol{x}_k + \boldsymbol{v}_k \tag{2.6}$$

2.1.3 Communication protocol, packet delay and packet dropout

In the model design process two classes of communication protocols have been considered. In transmission control protocol (TCP)-like protocols the acknowledgments that the receiver received the packets are sent back to the sender, while in user datagram protocol (UDP)-like protocols they are not sent. In TCP-like case, unlike in the UDP-like case, the lost packets can be re-sent because of the availability of the acknowledgments. So the separation principle, as explained in [54], holds only in the case of TCP-like protocols, and hence the controller and the estimator can be designed independently [55]. In UDP-like case no known optimal regulator exists and one can design a suboptimal solution based on a Kalman-like estimator and a LQG-like state feedback controller, as shown in Fig. 2.1. Although UDP-like protocol results in a sub-optimal solution, it is preferred over a TCP-like protocol as it may be extremely difficult to both analyze and implement a TCP-like control scheme [55]. In this chapter, a UDP-like scheme has been used. The time delays

and dropouts of packets have been modeled such that a packet is assumed to be lost, unless its time-delay is less than the sampling interval of the system. This fact is one of the factors while deciding the sampling duration, the other factor being the type of control needed, as explained in Section 2.3.2.1. If a packet is lost, the output of the receiver is held at the last successfully received packet.

The packet loss over the network usually follows a random process. In the present analysis an independent Bernoulli process has been used to model the packet loss [55]. The input $\bar{\boldsymbol{u}}_k$ at the actuator and $\bar{\boldsymbol{y}}_k$ at the estimator are modeled as:

$$\bar{\boldsymbol{u}}_k = \boldsymbol{\alpha}_k \boldsymbol{u}_k;\ \bar{\boldsymbol{y}}_k = \boldsymbol{\beta}_k \boldsymbol{y}_k \tag{2.7}$$

$\boldsymbol{\alpha}_k = diag\,(\alpha_k^1, \alpha_k^2, ..., \alpha_k^p)$ is a stationary diagonal binary random matrix, in which the value of α_k^i is equal to one with a probability p_{ui}, indicating that the i^{th} component of $\boldsymbol{u}_k$ is delivered; while its value is equal to zero with a probability $(1 - p_{ui})$, indicating that the component is lost (Fig. 2.3). Similarly, $\boldsymbol{\beta}_k = diag\,(\beta_k^1, \beta_k^2, ..., \beta_k^q)$ is the stationary diagonal binary random matrix for the delivery indication of $\boldsymbol{y}_k$. p_{ui} is termed as the packet delivery probability (PDP) of the i^{th} input channel, while p_{yi} is the PDP of the i^{th} output channel.

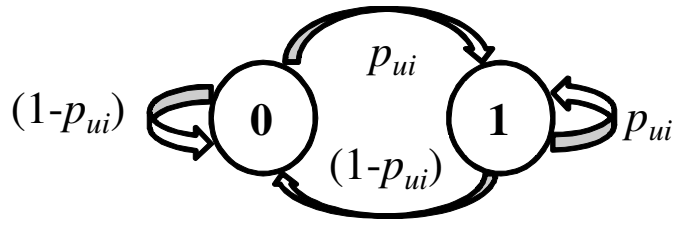

Figure 2.3: Markov chain for the i^{th} input-channel's delivery indication

Remark: The assumption of an independent Bernoulli packet loss model is not valid when the communication channel is congested. In a congested channel the packet loss occurs in bursts, and follows a two-state Markov chain model, also known as Gilbert model [56]. Fig. 2.4 shows this model, where '1' represents the state of packet delivery and '0' represents the state of packet loss; and the probability of transition from state '0' to state '1' is p and the probability of transition from state '1' to state '0' is q. When p is equal to $(1 - q)$, this model reduces to Bernoulli model.

The drawback of using Gilbert model in stability analysis is that this model is not a memory-less model, which means that the probability of packet delivery depends on the current channel state, and it fluctuates between p and $(1 - q)$ depending on

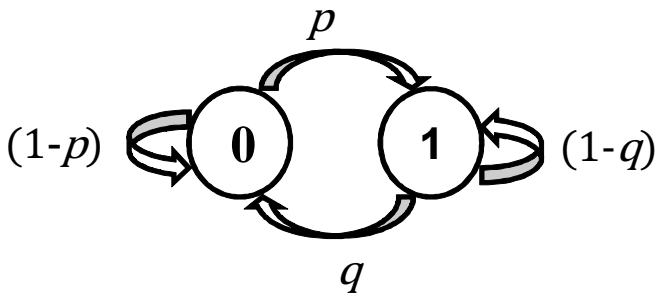

Figure 2.4: Markov chain for Gilbert process

whether the current channel state is '0' or '1', respectively. Mathematical representation of such a fluctuating probability of packet delivery becomes practically infeasible. A practical alternative for approximating Gilbert model with Bernoulli model can be to set the communication channel's probability of packet delivery as p if $p < (1-q)$, and as $(1-q)$ if $(1-q) \leq p$. Thus, the approximated Bernoulli model represents the worst case scenario of packet delivery performance given by Gilbert model, as the smaller probability of the two possible packet delivery probabilities from Gilbert model is assumed to be the constant packet delivery probability in the approximated Bernoulli model.

2.1.4 Controller

For an open-loop LTI system given by (2.6), whose input $\bar{\boldsymbol{u}}_k$ is defined by (2.7), the quadratic cost function $\boldsymbol{J}$ is given by:

$$\boldsymbol{J} = \frac{1}{N}\mathbb{E}\Big\{\boldsymbol{x}_N^T\boldsymbol{Q}\boldsymbol{x}_N + \sum_{k=1}^{N-1}\Big[\boldsymbol{x}_k^T\boldsymbol{Q}\boldsymbol{x}_k + \boldsymbol{u}_k^T\boldsymbol{\alpha}_k\boldsymbol{R}\boldsymbol{\alpha}_k\boldsymbol{u}_k\Big]\Big\} \tag{2.8}$$

where N is the number of samples, $\mathbb{E}$ is the expectation value, T denotes the transpose of a vector or a matrix, $\boldsymbol{Q}$ is a positive definite matrix denoting state costs, $\boldsymbol{R}$ is a positive semi-definite matrix denoting input costs and it is assumed that the full state information of the LTI system is available (we get this information from the state-estimator). Minimizing $\boldsymbol{J}$ with respect to $\boldsymbol{u}_k$ results in the following Riccati-like difference equation, as explained in [57]:

$$\boldsymbol{M}_{k+1} = \boldsymbol{A}^T \boldsymbol{M}_k \boldsymbol{A} + \boldsymbol{Q} - \boldsymbol{A}^T \boldsymbol{M}_k \boldsymbol{B} \mathbb{E}[\boldsymbol{\alpha}](\boldsymbol{R} + \mathbb{E}[\boldsymbol{\alpha} \boldsymbol{B}^T \boldsymbol{M}_k \boldsymbol{B} \boldsymbol{\alpha}])^{-1} \mathbb{E}[\boldsymbol{\alpha}] \boldsymbol{B}^T \boldsymbol{M}_k \boldsymbol{A} \quad (2.9)$$

where $\boldsymbol{M}_0$ is $\boldsymbol{Q}$ and $\mathbb{E}[\boldsymbol{\alpha}]$ is the expectation value of $\boldsymbol{\alpha}_k$ (subscript k is removed in $\mathbb{E}[\boldsymbol{\alpha}]$ as $\boldsymbol{\alpha}_k$ is stationary). If we obtain a steady state solution $\boldsymbol{M} = \boldsymbol{M}_\infty$ for (2.9) as $k \to \infty$ then the LTI open-loop system is infinite horizon stabilizable in mean-square sense, provided the pair $(\boldsymbol{A}, \boldsymbol{B})$ is controllable; the pair $(\boldsymbol{A}, \boldsymbol{Q}^{1/2})$ is observable, where $\boldsymbol{Q} = (\boldsymbol{Q}^{1/2})^T \boldsymbol{Q}^{1/2}$. The infinite horizon control policy for such a system is a state feedback policy, given by:

$$\boldsymbol{u}_k = \boldsymbol{L} \widehat{\boldsymbol{x}}_k;\ \boldsymbol{L} = -(\boldsymbol{R} + \mathbb{E}[\boldsymbol{\alpha} \boldsymbol{B}^T \boldsymbol{M} \boldsymbol{B} \boldsymbol{\alpha}])^{-1} \mathbb{E}[\boldsymbol{\alpha}] \boldsymbol{B}^T \boldsymbol{M} \boldsymbol{A} \quad (2.10)$$

where $\widehat{\boldsymbol{x}}_k$ is the estimated state, and $\boldsymbol{L}$ is the LQG gain.

2.1.5 Estimator

The controller uses the output from the state estimator to generate the control command which is sent over the network to the actuator in the power system. The estimator uses the information vector, which consists of the control command and the intermittent plant output delivered to the estimator via the network, to generate a best estimate of the state of the system. It was shown in [58] that even in the case of intermittent observations, Kalman filter is still the best linear estimator for LTI systems with stationary Gaussian noise processes, provided that only time update is performed when a measurement packet is dropped. When a measurement is received, both the time and measurement update steps are performed. The filtering equations for such a closed-loop system, using (2.10), are:

2.1.5.1 Prediction step

$$\hat{\boldsymbol{x}}_k^- = \boldsymbol{A}' \hat{\boldsymbol{x}}_{k-1};\ \boldsymbol{A}' = (\boldsymbol{A} + \boldsymbol{B} \mathbb{E}[\boldsymbol{\alpha}] \boldsymbol{L}) \quad (2.11)$$

$$\boldsymbol{P}_{xk}^- = \boldsymbol{A}' \boldsymbol{P}_{x(k-1)} \boldsymbol{A}'^T + \boldsymbol{P}_{vk} \quad (2.12)$$

2.1.5.2 Estimation step

$$\hat{\boldsymbol{x}}_k = \hat{\boldsymbol{x}}_k^- + \boldsymbol{K}_k\boldsymbol{\beta}_k(\boldsymbol{y}_k - \boldsymbol{C}\hat{\boldsymbol{x}}_k^-) \tag{2.13}$$

$$\boldsymbol{P}_{xk} = \boldsymbol{P}_{xk}^- - \boldsymbol{K}_k\boldsymbol{\beta}_k\boldsymbol{C}\boldsymbol{P}_{xk}^- \tag{2.14}$$

$$\boldsymbol{K}_k = \boldsymbol{P}_{xk}^-\boldsymbol{C}^T[\boldsymbol{C}\boldsymbol{P}_{xk}^-\boldsymbol{C}^T + \boldsymbol{P}_{wk}]^{-1} \tag{2.15}$$

For the k^{th} sample, $\hat{\boldsymbol{x}}_k^-$ is the estimated mean of the predicted states, $\boldsymbol{P}_{xk}^-$ is the predicted-state covariance matrix, $\hat{\boldsymbol{x}}_k$ is the estimated mean of the states, $\boldsymbol{P}_{xk}$ is the state covariance matrix, $\boldsymbol{P}_{wk}$ is the covariance matrix of $\boldsymbol{w}_k$, $\boldsymbol{P}_{vk}$ is the covariance matrix of $\boldsymbol{v}_k$, $\boldsymbol{K}_k$ is the Kalman gain. The equations are valid if and only if $(\boldsymbol{A}', \boldsymbol{C})$ is observable and $(\boldsymbol{A}', \boldsymbol{P}_{vk}^{1/2})$ is controllable. In (2.11) the estimator takes the closed loop state-space matrix $\boldsymbol{A}'$ as $(\boldsymbol{A}+\boldsymbol{B}\mathbb{E}[\boldsymbol{\alpha}]\boldsymbol{L})$ as it can at best have an estimate of the packet dropout rate of the network because it does not receive the acknowledgments of the control packets it sends out to the power system.

2.2 Closed-loop stability and damping response

The closed loop model of the NCPS can be summarized as follows, using (2.6)-(2.15):

$$\boldsymbol{x}_{k+1} = \boldsymbol{A}\boldsymbol{x}_k + \boldsymbol{B}\boldsymbol{\alpha}_k\boldsymbol{L}\widehat{\boldsymbol{x}}_k + \boldsymbol{w}_k; \tag{2.16}$$

$$\widehat{\boldsymbol{x}}_{k+1} = \boldsymbol{A}'\widehat{\boldsymbol{x}}_k + \boldsymbol{K}_{k+1}\boldsymbol{\beta}_{k+1}(\boldsymbol{y}_{k+1} - \boldsymbol{C}\boldsymbol{A}'\widehat{\boldsymbol{x}}_k) \tag{2.17}$$

$$\boldsymbol{y}_{k+1} = \boldsymbol{C}(\boldsymbol{A}\boldsymbol{x}_k + \boldsymbol{B}\boldsymbol{\alpha}_k\boldsymbol{L}\widehat{\boldsymbol{x}}_k + \boldsymbol{w}_k) + \boldsymbol{v}_{k+1} \tag{2.18}$$

A steady state solution for $\boldsymbol{P}_{xk}$ in (2.14), and hence for $\boldsymbol{K}_k$, may or may not exist for given $\boldsymbol{\alpha}_k$ and $\boldsymbol{\beta}_k$, even if the conditions for the existence of steady state solution for a standard Kalman filter hold; but a steady state estimate $\boldsymbol{K} = \mathbb{E}[\boldsymbol{K}_\infty]$ for the

Kalman gain may be obtained by iteratively solving (2.12), (2.14) and (2.15) after substituting $\boldsymbol{\beta}_k$ with its expected value $\mathbb{E}[\boldsymbol{\beta}]$. This is the sub-optimal Kalman gain which is used for deriving the condition for mean square stability and adequate damping of the developed NCPS. Writing (2.16)-(2.18) in composite form, after replacing $\boldsymbol{K}_{k+1}$ with its steady state estimate $\boldsymbol{K}$, we get:

$$\begin{bmatrix} \boldsymbol{x}_{k+1} \\ \widehat{\boldsymbol{x}}_{k+1} \end{bmatrix} = \begin{bmatrix} \boldsymbol{I}_m \\ \boldsymbol{K}\boldsymbol{\beta}_{k+1}\boldsymbol{C} \end{bmatrix} \boldsymbol{w}_k + \begin{bmatrix} \boldsymbol{0}_{m\times q} \\ \boldsymbol{K}\boldsymbol{\beta}_{k+1} \end{bmatrix} \boldsymbol{v}_{k+1} + \underbrace{\begin{bmatrix} \boldsymbol{A} & \boldsymbol{B}\boldsymbol{\alpha}_k\boldsymbol{L} \\ \boldsymbol{K}\boldsymbol{\beta}_{k+1}\boldsymbol{C}\boldsymbol{A} & \boldsymbol{A}' + \boldsymbol{K}\boldsymbol{\beta}_{k+1}\boldsymbol{C}(\boldsymbol{B}\boldsymbol{\alpha}_k\boldsymbol{L} - \boldsymbol{A}') \end{bmatrix}}_{\mathbb{A}(\boldsymbol{\alpha}_k, \boldsymbol{\beta}_{k+1})} \begin{bmatrix} \boldsymbol{x}_k \\ \widehat{\boldsymbol{x}}_k \end{bmatrix} \quad (2.19)$$

The presence of α_k and β_{k+1} in (2.19) makes it a jump linear system (JLS): a system whose state matrices vary randomly with α_k and β_{k+1}. The framework of a JLS and its stability analysis are described in [59] and [60]. A brief overview of the criterion for the stability and the damping in mean square sense of the NCPS has been presented in the next section.

2.2.1 Stability analysis framework of a jump linear system

Let $\boldsymbol{S}_i$ be a set of all the subsets of $\{1, 2, 3, ..., i\}$. Let $\boldsymbol{r} \in \boldsymbol{S}_p$ be a set of indices of all those input delivery indicators whose values are one, i.e. $\boldsymbol{r} = \{i$, such that (s.t.) $\alpha_k^i = 1\}$. E.g., for a 2 input system (p=2), $\boldsymbol{r}$ can either be $\emptyset$ (both the inputs failed to deliver), or $\{1\}$ (only 1^{st} input delivered), or $\{2\}$ (only 2^{nd} input delivered), or $\{1, 2\}$ (both the inputs delivered). Similarly, let $\boldsymbol{s} \in \boldsymbol{S}_q$ be a set of indices of successful output delivery indicators. As each input delivery indicator α_k^i has two modes (0 or 1) and $\alpha_k^i s$ are p in total, $\boldsymbol{\alpha}_k$ has 2^p modes. Any mode of $\boldsymbol{\alpha}_k$ is expressed as $\boldsymbol{T}_p(\boldsymbol{r})$, $\boldsymbol{r} \in \boldsymbol{S}_p$, where $\boldsymbol{T}_p(\boldsymbol{r})$ is a $p \times p$ diagonal matrix whose $(i, i)^{th}$ element is 1 if $i \in \boldsymbol{r}$, else it is 0. Similarly, $\boldsymbol{\beta}_{k+1}$ has 2^q modes, and any mode is expressed as $\boldsymbol{T}_q(\boldsymbol{s})$, $\boldsymbol{s} \in \boldsymbol{S}_q$, where $\boldsymbol{T}_q(\boldsymbol{s})$ is a $q \times q$ diagonal matrix whose $(i, i)^{th}$ element is 1 if $i \in \boldsymbol{s}$, else it is 0. The probability distributions of $\boldsymbol{T}_p(\boldsymbol{r}), \boldsymbol{r} \in \boldsymbol{S}_p$ and $\boldsymbol{T}_q(\boldsymbol{s}), \boldsymbol{s} \in \boldsymbol{S}_q$ are given by:

$$\mathcal{P}_p(\boldsymbol{r}) = \mathbf{P}\left[\boldsymbol{\alpha}_k = \boldsymbol{T}_p(\boldsymbol{r})\right] = \prod_{i \in r} p_{ui} \prod_{i \notin r} 1 - p_{ui} \quad (2.20)$$

$$\mathcal{P}_q(\boldsymbol{s}) = \mathbf{P}\left[\boldsymbol{\beta}_{k+1} = \boldsymbol{T}_q(\boldsymbol{s})\right] = \prod_{i \in s} p_{yi} \prod_{i \notin s} 1 - p_{yi} \tag{2.21}$$

$\mathcal{P}_p(\boldsymbol{r})$ is the resultant probability of data delivery for any combination of input to the plant by the channel characterized by $\boldsymbol{T}_p(\boldsymbol{r})$. Similarly $\mathcal{P}_q(\boldsymbol{s})$ is the resultant probability of data delivery for any combination of plant output channel mode characterized by $\boldsymbol{T}_q(\boldsymbol{s})$.

As $\mathbb{A}(\boldsymbol{\alpha}_k, \boldsymbol{\beta}_{k+1})$ in (2.19) is a function of $\boldsymbol{\alpha}_k$ and $\boldsymbol{\beta}_{k+1}$, it may be re-expressed as $\mathcal{A}(\boldsymbol{r}, \boldsymbol{s})$ in (2.22):

$$\mathcal{A}(\boldsymbol{r}, \boldsymbol{s}) = \begin{bmatrix} \boldsymbol{A} & \boldsymbol{B}\boldsymbol{T}_p(\boldsymbol{r})\boldsymbol{L} \\ \boldsymbol{K}\boldsymbol{T}_q(\boldsymbol{s})\boldsymbol{C}\boldsymbol{A} & \boldsymbol{A}' + \boldsymbol{K}\boldsymbol{T}_q(\boldsymbol{s})\boldsymbol{C}(\boldsymbol{B}\boldsymbol{T}_p(\boldsymbol{r})\boldsymbol{L} - \boldsymbol{A}') \end{bmatrix} \tag{2.22}$$

As the value of $\mathcal{A}(\boldsymbol{r}, \boldsymbol{s})$ depends on the values of $\boldsymbol{r}$ and $\boldsymbol{s}$, it can take any value in a given sample out of the possible 2^{p+q} values, with a corresponding overall probability distribution $\mathcal{P}_p(\boldsymbol{r})\mathcal{P}_q(\boldsymbol{s})$. The NCPS in (2.19) is said to be mean-square stable if $\lim_{k\to\infty} \mathbb{E}\left\| \begin{smallmatrix} \boldsymbol{x}_k \\ \widehat{\boldsymbol{x}}_k \end{smallmatrix} \right\|^2 = 0$, starting with any state $\left[\begin{smallmatrix} \boldsymbol{x}_0 \\ \widehat{\boldsymbol{x}}_0 \end{smallmatrix} \right]$. Mean-square stability and damping response of (2.19) can be checked using the following inequalities formed with linear combination of symmetric matrices, which are known as linear matrix inequalities (LMIs):

2.2.1.1 LMIs for mean-square stability

The criterion for the stability of discrete-time JLS in [59] is applied to obtain the condition for the mean-square stability of the NCPS in (2.22). The satisfaction of the criterion requires the existence of positive definite matrices $\boldsymbol{P}_{\boldsymbol{r},\boldsymbol{s}}$, $\forall \boldsymbol{r} \in \boldsymbol{S}_p$, $\forall \boldsymbol{s} \in \boldsymbol{S}_q$, such that:

$$\boldsymbol{P}_{\boldsymbol{r},\boldsymbol{s}} > \mathcal{A}(\boldsymbol{r}, \boldsymbol{s}) \left(\mathcal{P}_p(\boldsymbol{r})\mathcal{P}_q(\boldsymbol{s}) \sum_{\boldsymbol{r}' \in \boldsymbol{S}_p, \boldsymbol{s}' \in \boldsymbol{S}_q} \boldsymbol{P}_{\boldsymbol{r}',\boldsymbol{s}'} \right) \mathcal{A}(\boldsymbol{r}, \boldsymbol{s})^T \tag{2.23}$$

There are in total 2^{p+q} LMIs in (2.23).

2.2.1.2 LMIs for adequate damping response

The concept of $\mathcal{D}$-stability [61] has been used to study the adequate damping response of the developed NCPS. This is very practical and useful in the context of power oscillation damping. If $\mathcal{D}$ is a sub-region of the complex left half plane, and all the closed loop poles of a dynamical system $\dot{\boldsymbol{x}} = \boldsymbol{A}\boldsymbol{x}$ lie in $\mathcal{D}$, then the system and its state transition matrix $\boldsymbol{A}$ are called $\mathcal{D}$-stable. When $\mathcal{D}$ is the entire left-half plane, then $\mathcal{D}$-stability reduces to asymptotic stability. For damping control analysis, the $\mathcal{D}$-region of interest is $\mathcal{D}(\Theta)$ of complex numbers $(x + jy)$ s.t. $|y/x| < |\tan\Theta|$ (Fig. 2.5). Thus a specified and required damping of inter-area modes becomes an important criterion for NCS design and analysis.

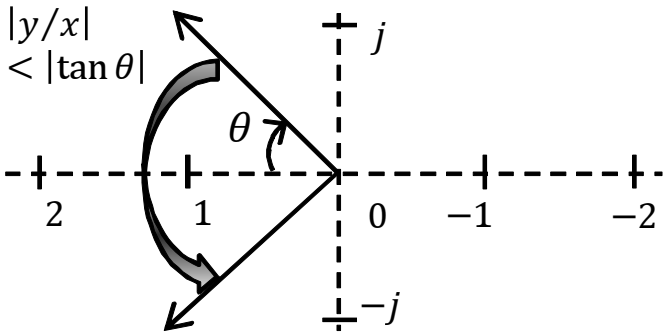

Figure 2.5: $\mathcal{D}$-stability region for damping control of a continuous system

Confining the closed loop poles of the system to the region shown in Fig. 2.5 ensures a minimum damping ratio $\zeta_0 = \cos\Theta$. This in turn bounds the decay rate and the settling time for the corresponding oscillatory inter-area modes of the system. Power systems usually require an operating constraint that all the disturbances in the system should settle to less than a fixed percent (usually 15%) of the maximum overshoot within a few seconds (usually $10-15s$) of the start of the disturbance to the system [7]. As the inter-area modes usually lie in the frequency range $0.2-1.0$ Hz, they have longer settling times and lower decay rates than other modes. In this chapter, the margin for $\mathcal{D}$-stability is taken as a minimum damping ratio of 0.1 for all the closed-loop interarea modes, as a damping ratio of 0.1 corresponds to a setting time of $15s$ for a modal frequency of 0.2 Hz.

Lemma 2.1. *The closed-loop NCPS in* (2.19) *is expected to have all of its equivalent continuous-time poles with damping ratios* $\zeta > \cos\Theta$ *if and only if there exist positive definite matrices* $\boldsymbol{Q}_{\boldsymbol{r},\boldsymbol{s}}$, $\forall \boldsymbol{r} \in \boldsymbol{S}_p$, $\forall \boldsymbol{s} \in \boldsymbol{S}_q$, *such that:*

$$(\boldsymbol{W} \otimes \mathcal{A}_{\boldsymbol{c}}(\boldsymbol{r},\boldsymbol{s}))\boldsymbol{Q}_{\boldsymbol{r},\boldsymbol{s}} + \boldsymbol{Q}_{\boldsymbol{r},\boldsymbol{s}}(\boldsymbol{W} \otimes \mathcal{A}_{\boldsymbol{c}}(\boldsymbol{r},\boldsymbol{s}))^T + \left(\mathcal{P}_p(\boldsymbol{r})\mathcal{P}_q(\boldsymbol{s}) - 1\right)\boldsymbol{Q}_{\boldsymbol{r},\boldsymbol{s}} + \mathcal{P}_p(\boldsymbol{r})\mathcal{P}_q(\boldsymbol{s})\Big(\sum_{\boldsymbol{r}' \in \boldsymbol{S}_p, \boldsymbol{s}' \in \boldsymbol{S}_q, \boldsymbol{r}' \neq \boldsymbol{r}, \boldsymbol{s}' \neq \boldsymbol{s}} \boldsymbol{Q}_{\boldsymbol{r}',\boldsymbol{s}'}\Big) < 0 \quad (2.24)$$

$$\textit{where, } \mathcal{A}_{\boldsymbol{c}}(\boldsymbol{r},\boldsymbol{s}) = \mathit{ln}(\mathcal{A}(\boldsymbol{r},\boldsymbol{s}))/T_0, \boldsymbol{W} = \begin{bmatrix} \sin\Theta & \cos\Theta \\ -\cos\Theta & \sin\Theta \end{bmatrix}, \quad (2.25)$$

ln is the natural logarithm of a square matrix and T_0 is the sampling-period of the NCPS.

Proof: The damping-region of interest $\mathcal{D}(\Theta)$ shown in Fig. 2.5 is applicable only to the continuous-time representation of a dynamic system; the discrete-time equivalent of this region is a logarithmic spiral and is very difficult to represent using matrices and LMIs. We therefore consider the continuous-time equivalent of $\mathcal{A}(\boldsymbol{r},\boldsymbol{s})$ which is given by (2.24) as $\mathcal{A}_{\boldsymbol{c}}(\boldsymbol{r},\boldsymbol{s})$. Using [62] we know that a dynamic system $\dot{\boldsymbol{x}} = \boldsymbol{A}\boldsymbol{x}$ is $\mathcal{D}$-stable in the region $\mathcal{D}(\Theta)$ if and only if $\boldsymbol{W} \otimes \boldsymbol{A}$ is asymptotically stable. This holds because the eigenvalues of $\boldsymbol{W}$ are $e^{\pm j(\frac{\pi}{2} - \Theta)}$. The eigenvalues of the Kronecker product of 2 matrices are the product of the eigenvalues of individual matrices. Hence, the eigenvalues of $\boldsymbol{W} \otimes \boldsymbol{A}$ are two sets of eigenvalues of $\boldsymbol{A}$, one set rotated by an angle $(\frac{\pi}{2} - \Theta)$ and another one by $-(\frac{\pi}{2} - \Theta)$. All those eigenvalues of $\boldsymbol{A}$ which lie outside $\mathcal{D}(\Theta)$ get rotated into the right half plane in $\boldsymbol{W} \otimes \boldsymbol{A}$, and hence $\boldsymbol{W} \otimes \boldsymbol{A}$ is asymptotically stable if and only if none of the eigenvalues of $\boldsymbol{A}$ lie outside $\mathcal{D}(\Theta)$, i.e. if and only if $\boldsymbol{A}$ is adequately damped. So, the asymptotic stability of $\boldsymbol{W} \otimes \mathcal{A}_{\boldsymbol{c}}(\boldsymbol{r},\boldsymbol{s})$ implies $\mathcal{D}$-stability of $\mathcal{A}_{\boldsymbol{c}}(\boldsymbol{r},\boldsymbol{s})$. As $\mathcal{A}_{\boldsymbol{c}}(\boldsymbol{r},\boldsymbol{s})$ is a jump-linear mode of the stochastic system in (2.19) with a modal probability of $\mathcal{P}_p(\boldsymbol{r})\mathcal{P}_q(\boldsymbol{s})$, the matrix $\boldsymbol{W} \otimes \mathcal{A}_{\boldsymbol{c}}(\boldsymbol{r},\boldsymbol{s})$ is also a modal matrix of same probability as $\mathcal{A}_{\boldsymbol{c}}(\boldsymbol{r},\boldsymbol{s})$; and the mean-square stability of $\boldsymbol{W} \otimes \mathcal{A}_{\boldsymbol{c}}(\boldsymbol{r},\boldsymbol{s})$ [59] (given by (2.24)) implies the $\mathcal{D}$-stability of $\mathcal{A}_{\boldsymbol{c}}(\boldsymbol{r},\boldsymbol{s})$ in a mean square sense, i.e. its electro-mechanical modes are expected to have $\zeta > \cos\Theta$. □

Remark: It should be noted that an additional pole-placement constraint which is desired (besides the constraint of a minimum damping ratio) is that the real part of each mode should be less than a specified minimum value (usually -0.1), so that none of the modes are very close to the imaginary axis. This constraint is relevant to the modes which have very small modal frequencies (in the range of $0.0 - 0.16$ Hz) as the real parts of only these modes can be greater than -0.1 even if they satisfy the constraint of a minimum damping ratio of 0.1. Thus, this additional

constraint has been relaxed in the aforementioned stability analysis, as the analysis focuses on interarea modes (which have modal frequencies greater than 0.2 Hz). Another reason for relaxing the constraint is that it is mathematically difficult to include an additional constraint in the above lemma.

Remark: If all the channels have same characteristics, their PDPs become equal to each other ($p_{ui} = p_{yi} = p_{y0} \forall i$). The marginal packet delivery probability (MPDP), such that the NCPS remains properly damped $\forall p_{y0}$ >MPDP, is given by $\sup \{\gamma > 0, \text{s.t. LMIs in (2.24) remain feasible}, \forall p_{y0} \in [\gamma, 1]\}$.

2.2.2 Physical significance of the developed LMIs

The physical meaning of the mathematical result given by the developed LMIs will be better understood using the concepts of observability and controllability. As mentioned in Section 2.1.1, the output measurements have high observability of the unstable and/or poorly damped electromechanical modes of the power system. The LQG controller requires the knowledge of these measurements and the state matrices to correctly estimate the states, which are then multiplied by the LQR gain to get the control input for the power system. The LQG controller requires the knowledge of these measurements and the state matrices in order to correctly estimate the states, which are then multiplied with the LQR gain to get the control input for the power system. The closed loop system is properly stabilized and damped, provided the packet delivery rate is 100%. The decrease in packet delivery rate from 100% results in the loss of the output measurements in the communication network. The measurements which finally arrive at the controller after packet loss have an overall decrease in their observability for a given period of time, and the controller estimates the states with decreased accuracy. For a packet delivery rate of zero percent, none of the measurements arrive at the LQG controller, and thus the observability is zero, and controller cannot estimate the states at all.

This concept of probabilistic observability will be better understood with an example. For example, if there are two measurements which are sent over the network then there are four possibilities in a given time sample: (1) none of the measurements arrive, (2) only first measurement arrives, (3) only second measurement arrives, and (4) both the measurements arrive. Each of these four possibilities has a probability associated with it depending on the packet delivery rates of the two communication channels. The overall observability of the arriving measurements

depends on these four probabilities, and is thus a probabilistic quantity in itself. For q measurements, there are 2^q possibilities, and the overall observability will depend on all of these possibilities. Similar analogy applies for the controllability of the power system by the control inputs sent over the communication network, and thus the overall controllability is also a probabilistic quantity. The stability and the $\mathcal{D}$-stability of the closed loop system depend on these probabilistic observability and controllability, and are written in mathematical forms as (2.23) and (2.24), respectively.

2.3 Case study: 68-bus 16-machine 5-area NCPS

2.3.1 System description

A 16-machine, 68 bus model test system [63], shown in Fig. 2.6, has been used for the case study.

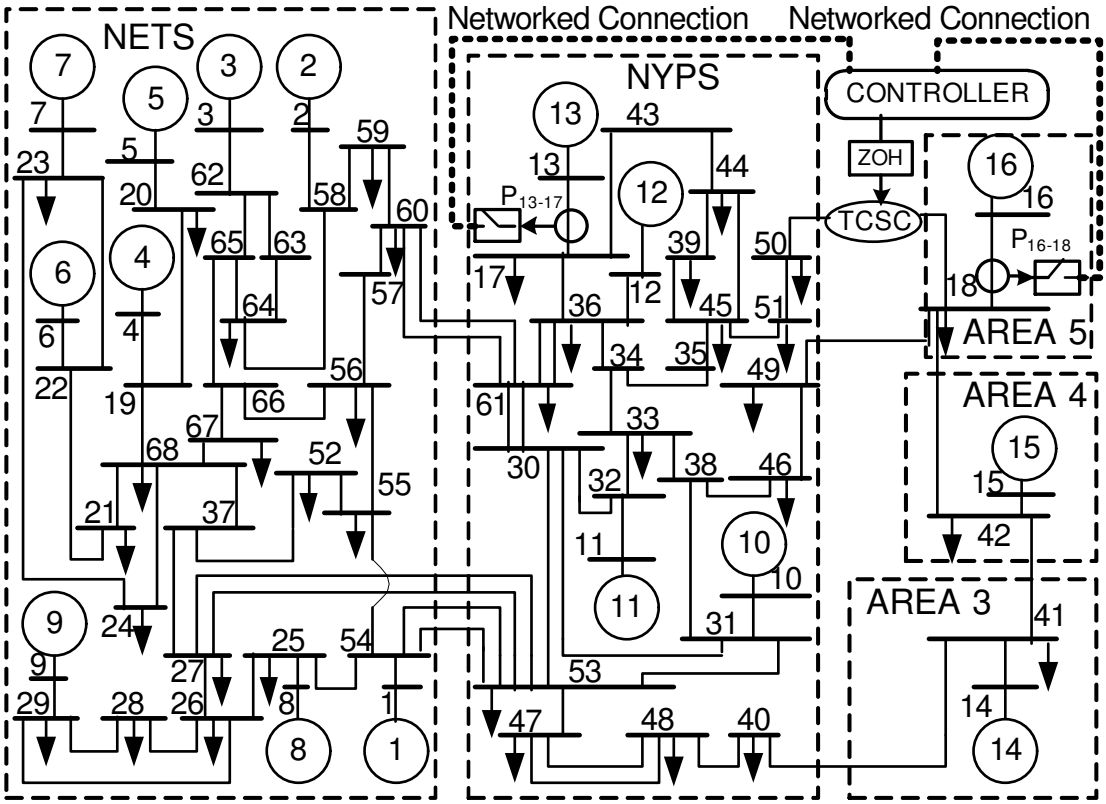

Figure 2.6: Line diagram of the 16-machine, 68-bus, 5-area NCPS

This is a reduced order equivalent of the interconnected New England test system (NETS) and New York power system (NYPS) of 1970s. NETS and NYPS are

represented by a group of generators, while the power import from each of the three other neighboring areas are approximated by equivalent generator models (G14 to G16). NYPS needs to import around 1.5 GW from Area 5, for which a TCSC is installed on the 18-50 tie-line. Percentage compensation of the TCSC needs to be dynamically controlled to control the reactance of the tie-line. A detailed system description is available in Appendix D, which is used to simulate the NCPS model in MATLAB SIMULINK. Fully non-linear sub-transient model of power system is used for simulation.

2.3.2 Simulation results and discussion

2.3.2.1 Operating condition 1 (base case)

For the first case of system operation (total tie-line flow between NETS and NYPS = 700MW, no line outages), the damping and the frequency of the three poorly damped modes of the linearized system were computed. The normalized participation factors (P.F.) of all the states in these modes were also calculated and arranged in decreasing order [7]. Table 2.1 gives the normalized P.F. of the top four states in these modes. As one can see in Table 2.1, the three poorly damped modes are indeed the inter-area modes as they have strong participation from the electro-dynamical modes of all the three generators G14, G15 and G16, which model the power generation in three different areas.

Table 2.1: Normalized participation factors of the top 4 states in the 3 modes

Mode 1, $\zeta = 0.020$, $f = 0.394Hz$		Mode 2, $\zeta = 0.041$, $f = 0.505Hz$		Mode 3, $\zeta = 0.032$, $f = 0.598Hz$	
State	P.F.	State	P.F.	State	P.F.
δ_{16}	1.000	Slip_{15}	1.000	Slip_{14}	1.000
Slip_{16}	0.999	δ_{15}	0.999	δ_{14}	0.999
δ_{15}	0.936	Slip_{14}	0.727	Slip_{6}	0.493
Slip_{15}	0.935	δ_{14}	0.726	δ_{6}	0.492

The open loop system response confirmed that the other electromechanical modes including one inter-area mode of the system settled in less than 10 seconds and hence they have been left from the consideration of providing additional damping. The remote feedback signals were chosen based on modal observability analysis [64] for various active line power signals. For the fixed location of actuator, the modal controllability does not change so modal residue is related to modal observability

by a scale factor. Table 2.2 gives the normalized residues of top 3 active power flows in the 3 inter-area modes. There are other means of robust signal selection to obtain the best signal(s) out of all the available signals, as described in [65], [66] and [67], to guarantee effectiveness of the signals for various operating scenarios.

Table 2.2: Normalized residues of the active power-flows in the 3 modes

Mode 1, $\zeta = 0.020$, $f = 0.394Hz$		Mode 2, $\zeta = 0.041$, $f = 0.505Hz$		Mode 3, $\zeta = 0.032$, $f = 0.598Hz$	
Signal	Residue	Signal	Residue	Signal	Residue
P_{13-17}	1.000	P_{16-18}	1.000	P_{13-17}	1.000
P_{51-45}	0.773	P_{14-41}	0.760	P_{17-36}	0.698
P_{51-50}	0.665	P_{42-18}	0.727	P_{43-17}	0.600

The signals P_{13-17} (having highest residues for modes 1 and 3) and P_{16-18} (having highest residue for mode 2) have been selected as output signals (Here P_{13-17} denotes the active power flow in the line from bus number 13 to bus number 17). With these two signals as output and Δk_{c-ss}, (the control signal of the TCSC) as the input, the open-loop system was linearized to find the state space matrices. System order was reduced (Section 2.1.1) to the lowest possible order such that the reduced system still remained a very good approximation of the full system in the frequency range of 0.2-1.0 Hz, and thus a reduced seventh order system was obtained. Table 2.3, which compares frequencies and damping ratios of the three modes for the full and the reduced systems, and Fig. 2.7, which shows frequency response of both the full and the reduced systems, prove that the reduced system is a good approximation of the full system in the frequency range of 0.2-1.0 Hz.

Table 2.3: Comparison of modes for the full vs. the reduced system

	Frequency (in Hz)		Damping Ratio	
Mode	Full System	Reduced System	Full System	Reduced System
Mode 1	0.394	0.394	0.020	0.020
Mode 2	0.505	0.500	0.041	0.046
Mode 3	0.598	0.598	0.032	0.034

Remark: *Deciding the sampling period*: The controller needs to observe the system in the range of 0.2-1.0 Hz; hence the minimum required sampling frequency is 2.0 Hz (i.e. a maximum allowed sampling period of 0.5 s) according to the Nyquist−Shannon sampling theorem. This upper limit of sampling period is also the threshold requirement for average time delay of the packets, as if the average delay is more than this upper limit, then the packet loss rate will be very high and

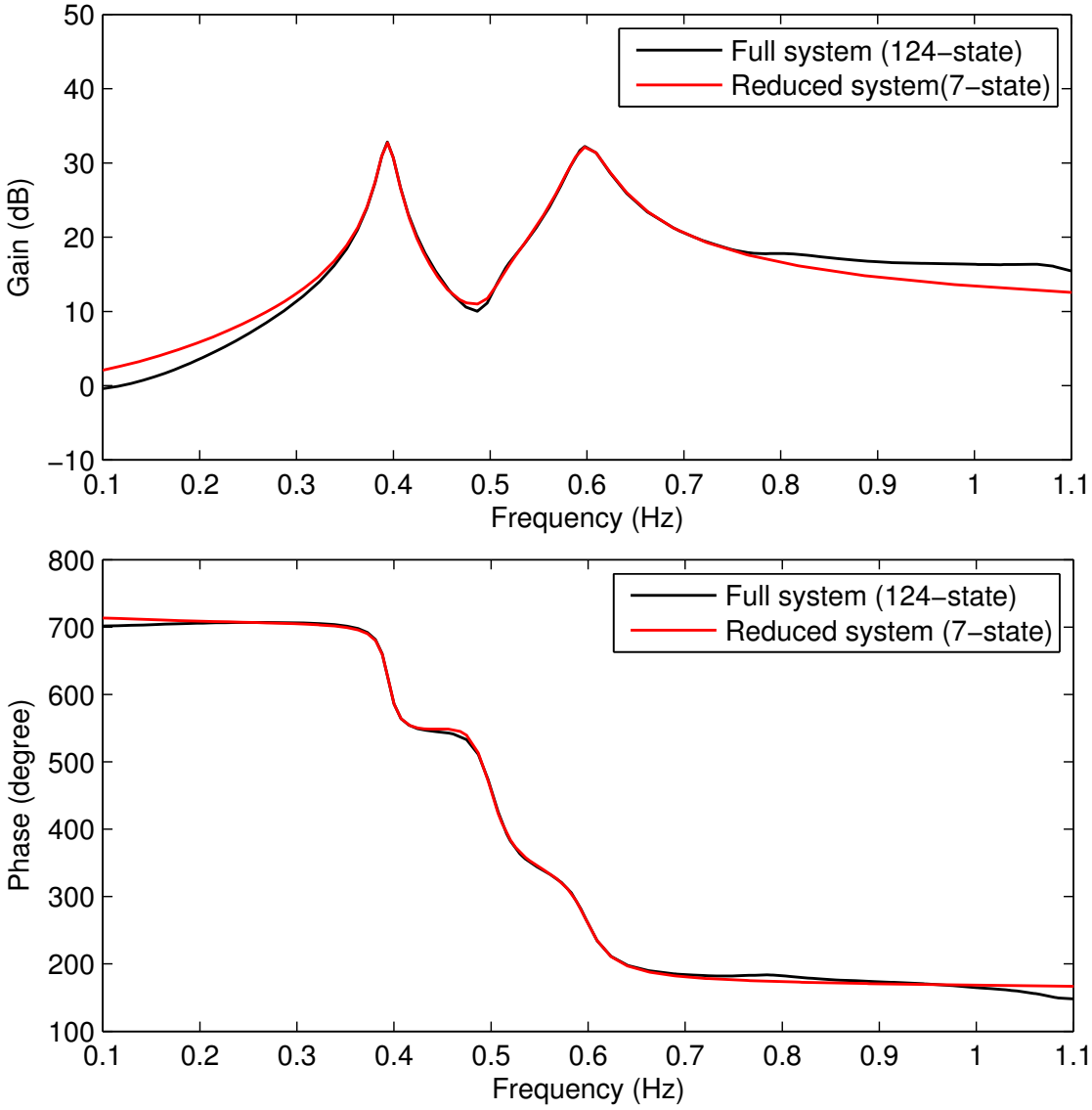

Figure 2.7: Frequency response of the full vs. the reduced system

the network would not support the communication needs of the system. In the case study, a conservative sampling period of $T_0 = 0.1\ s$ was assumed.

The packet loss in the path of the input and output signals was modeled as a Bernoulli's process. So, $\boldsymbol{\alpha}_k = \alpha_k^1$, while $\boldsymbol{\beta}_{k+1} = diag(\beta_{k+1}^1, \beta_{k+1}^2)$, in (2.7). The steady state controller gain for the reduced system was found using the results of Section 2.1.4 and the modified Kalman filter was modeled using the principle described in Section 2.1.5. Simulation was started and after one second a disturbance was created in the NCPS model by a three-phase fault and immediate outage of one of the tie lines between buses 53-54.

The open loop system is a minimum-phase system (which means that all of its

zeros and poles are in the left half plane); thus it was required to check only the damping response of the system for various packet drop rates. For $\boldsymbol{\alpha}_k$, $\boldsymbol{S}_p = \{\emptyset, \{1\}\}$, and $\boldsymbol{T}_p(\boldsymbol{r})$ has two modes, $\boldsymbol{T}_1(\emptyset)$ and $\boldsymbol{T}_1(\{1\})$. For $\boldsymbol{\beta}_k$, $q = 2$ and $\boldsymbol{S}_q = \{\emptyset, \{1\}, \{2\}, \{1,2\}\}$, and $\boldsymbol{T}_q(\boldsymbol{s})$ has four modes viz. $\boldsymbol{T}_2(\emptyset)$, $\boldsymbol{T}_2(\{1\})$, $\boldsymbol{T}_2(\{2\})$ and $\boldsymbol{T}_2(\{1,2\})$. The corresponding jump state matrices $\mathcal{A}(\boldsymbol{r}, \boldsymbol{s})$ are $\mathcal{A}(\emptyset, \emptyset)$, $\mathcal{A}(\emptyset, \{1\})$, $\mathcal{A}(\emptyset, \{2\})$, $\mathcal{A}(\emptyset, \{1,2\})$, $\mathcal{A}(\{1\}, \emptyset)$, $\mathcal{A}(\{1\}, \{1\})$, $\mathcal{A}(\{1\}, \{2\})$ and $\mathcal{A}(\{1\}, \{1,2\})$, and their probabilities of occurrences are $(1-p_{u1})(1-p_{y1})(1-p_{y2})$, $(1-p_{u1})p_{y1}(1-p_{y2})$, $(1-p_{u1})(1-p_{y1})p_{y2}$, $(1-p_{u1})p_{y1}p_{y2}$, $p_{u1}(1-p_{y1})(1-p_{y2})$, $p_{u1}p_{y1}(1-p_{y2})$, $p_{u1}(1-p_{y1})p_{y2}$, and $p_{u1}p_{y1}p_{y2}$, respectively. Using these parameters, eight pairs of LMIs in (2.24) were obtained. Θ was taken as 84.3 degrees corresponding to 10% damping line, as shown in Fig. 2.5. Assuming same network characteristics for all the network-channels, i.e. $p_{u1} = p_{y1} = p_{y2} = p_y$, the feasibility of the LMI's was checked for various values of p_y using LMI toolbox in MATLAB. The toolbox returned a minimum feasible value of $p_y = 0.81$, i.e. the LMIs were feasible for $0.81 < p_y < 1.0$.

As data loss is a random process, multiple simulations were performed for a given value of marginal PDP. Fig. 2.8 shows the rotor slip response for G16 for 100 simulations at a marginal PDP of 0.81. The mean value of rotor-slip for the 100 simulations has also been plotted in Fig. 2.8. In rest of the plots in the case study only the mean-value of multiple simulations has been shown.

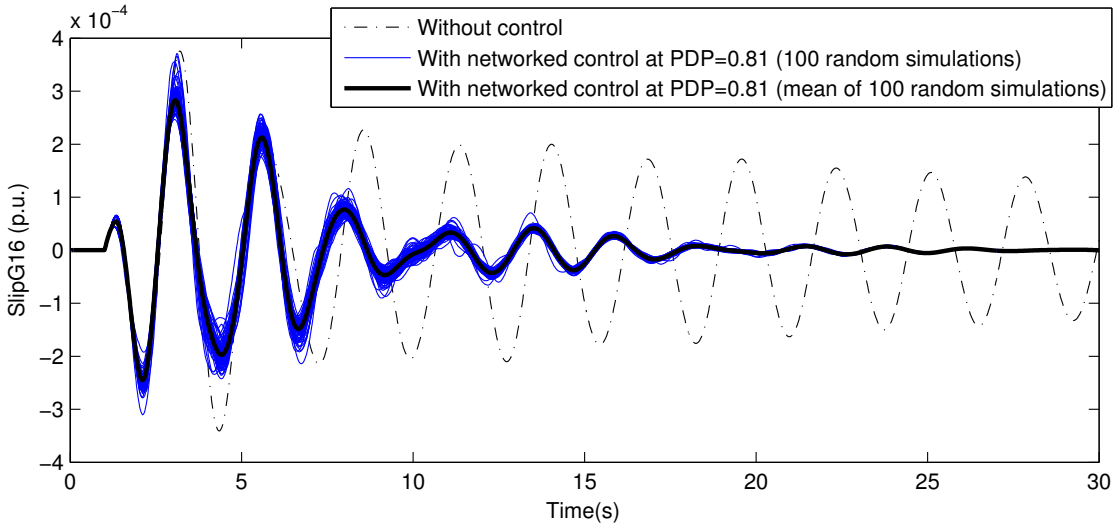

Figure 2.8: Rotor-slip response for G16 at operating point 1

System response using a classical damping controller (assuming a perfect communication link in its control loop, with infinite sampling rate and zero packet loss) has been shown for comparison in Fig. 2.9. Corresponding values of control signal have also been shown in Fig. 2.10. The transfer function for the classical power

oscillation damping (POD) controller has been evaluated using the theory and results given in [68], and it is as follows:

$$\Delta k_{c\text{-}ss} = P_{13\text{-}17} \times (-0.738) \left[\frac{1+0.138s}{1+0.725s}\right]^2 + P_{16\text{-}18} \times 0.925 \left[\frac{1+0.182s}{1+0.949s}\right]^2 \quad (2.26)$$

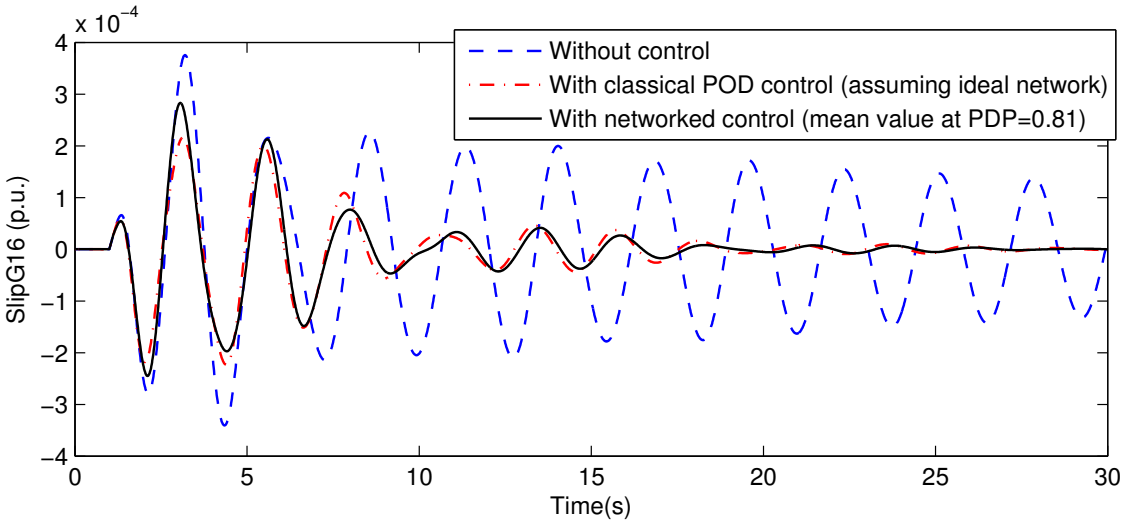

Figure 2.9: Comparison of rotor-slip response at operating point 1

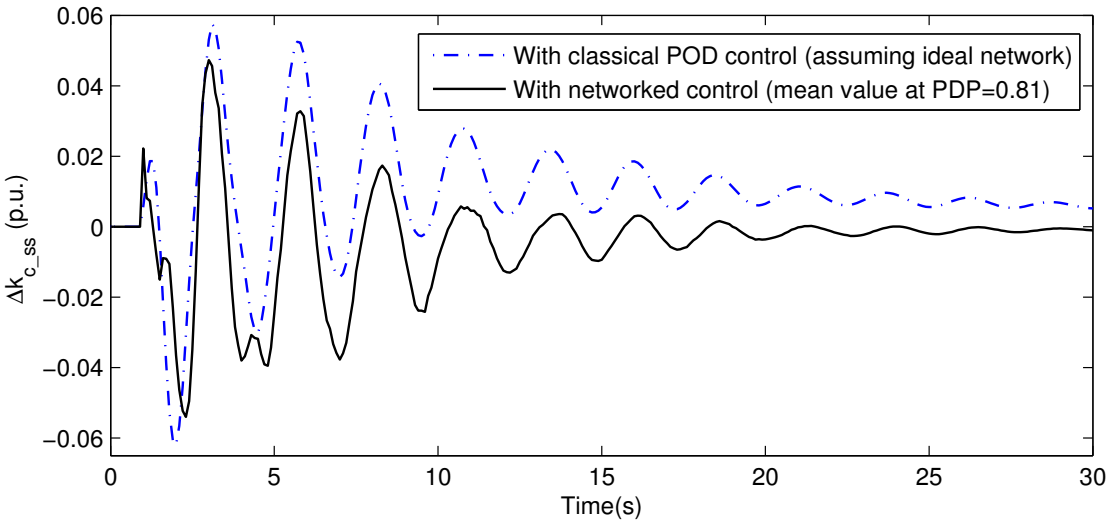

Figure 2.10: Comparison of control signals at operating point 1

The rotor-slip response of G16 for the first operating point was also found for four other values of p_y, as shown in Fig. 2.11.

Remark: It should be understood that it is not the sole purpose of Fig. 2.9 (and subsequent figures) to show that the performance of the networked controller is

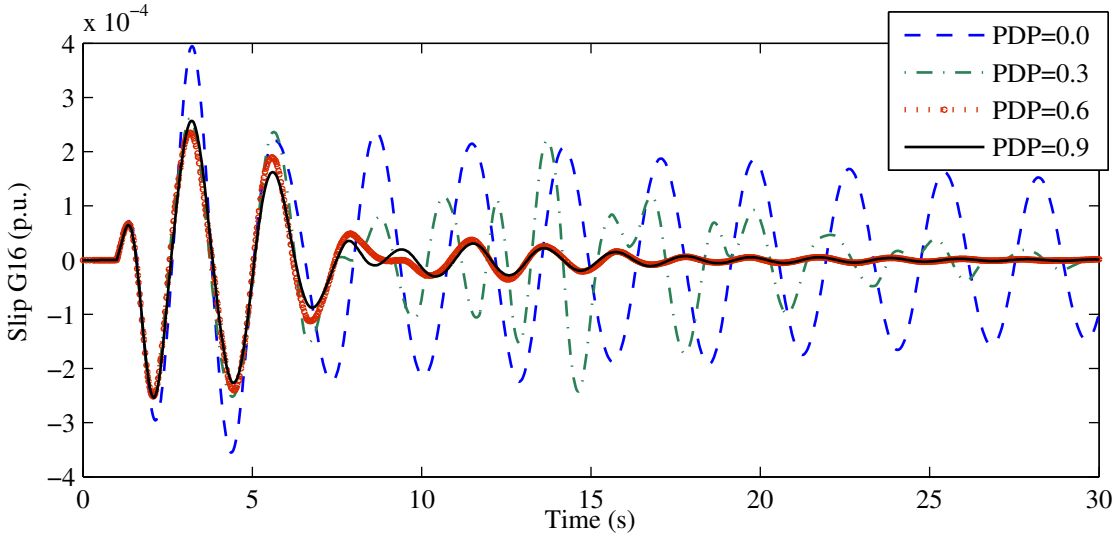

Figure 2.11: Rotor-slip response for various packet delivery probabilities (PDPs)

better than the classical damping controller. Rather, its another important purpose is to show that the performance of the networked control with communication packet-dropout, even with marginal PDP, is comparable to the performance of classical control in which an ideal, lossless and delay-free communication network is assumed. Fig. 2.12 shows the comparison of the performance of networked control with that of classical control, when in both the cases an ideal communication network is assumed (that is PDP=1). It can be clearly verified from the figure that the performance of networked control is much better than classical control when ideal network conditions are assumed for both the cases. Also, a metric which is used to assess the control effort required by a control method is the 2-norm of the output from the controller, or $\|\boldsymbol{u}\|_2$. The control effort for classical control is 0.32 p.u., while for networked control (with PDP=1) it is 0.25 p.u. Thus networked control at 100% packet delivery rate is better than classical control, and it can damp the oscillations in a smaller amount of time, even when the control effort required by networked control is decreased by 22 % as compared to the control effort required by classical control.

2.3.2.2 Operating condition 2

In the second operating condition (total tie-line flow between NETS and NYPS = 900MW, no line outages), the open-loop system becomes unstable after the line-outage, unlike the first operating condition. This is due to the presence of an unstable mode with negative damping ratio in the system. Therefore we can apply

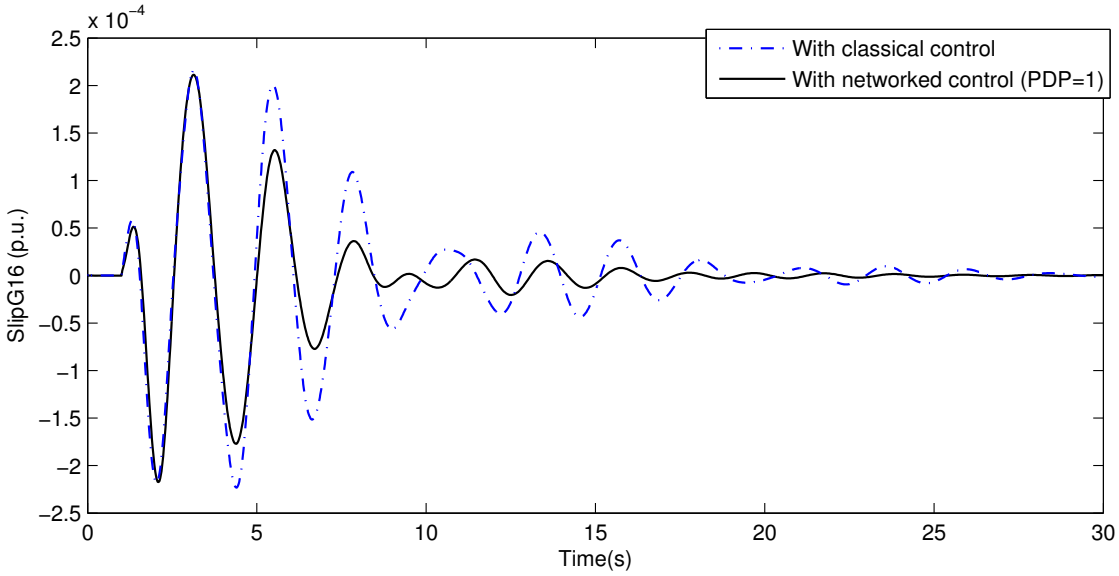

Figure 2.12: Classical vs. networked control, with assumption of an ideal network

the LMI analysis (Section 2.2.1.1) to find the marginal PDP which can ensure closed-loop stability of the NCPS. It was found that the stability of the NCPS under this operating condition was ensured at a marginal PDP of 0.24, while the adequate damping of the system was ensured at a marginal PDP of 0.87 (using Section 2.2.1.2). The slip response of G16 has been shown at both of these marginal PDPs in Fig. 2.13.

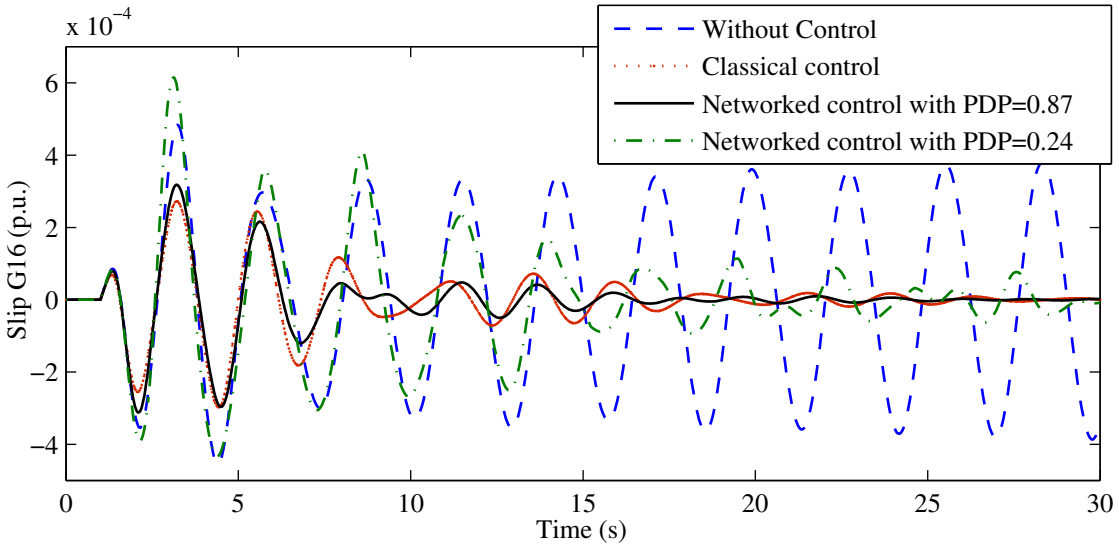

Figure 2.13: Rotor-slip response for G16 at operating point 2

It is evident in Fig. 2.9 and Fig. 2.11, for $T_0 = 0.1\ s$ and PDPs more than or equal to 0.81, the inter-area modes of the system are properly damped. Similarly, it may be observed from Fig. 2.13 that the system in second operating condition is

stabilized at the marginal PDP of 0.24 while adequately damped at the marginal PDP of 0.87. So the results of the LMI analysis stand verified. It is also clear from Fig. 2.9 and Fig. 2.13 that the performance of the networked controller is better than the classical damping controller, at realistic packet delivery qualities that can be easily delivered by present day telecom networks.

2.3.2.3 Effect of sampling period

Next, the effect of sampling period on the marginal delivery probability for $\mathcal{D}$-stability is being investigated. Fig. 2.14 shows the plot of the marginal delivery probability versus sampling period.

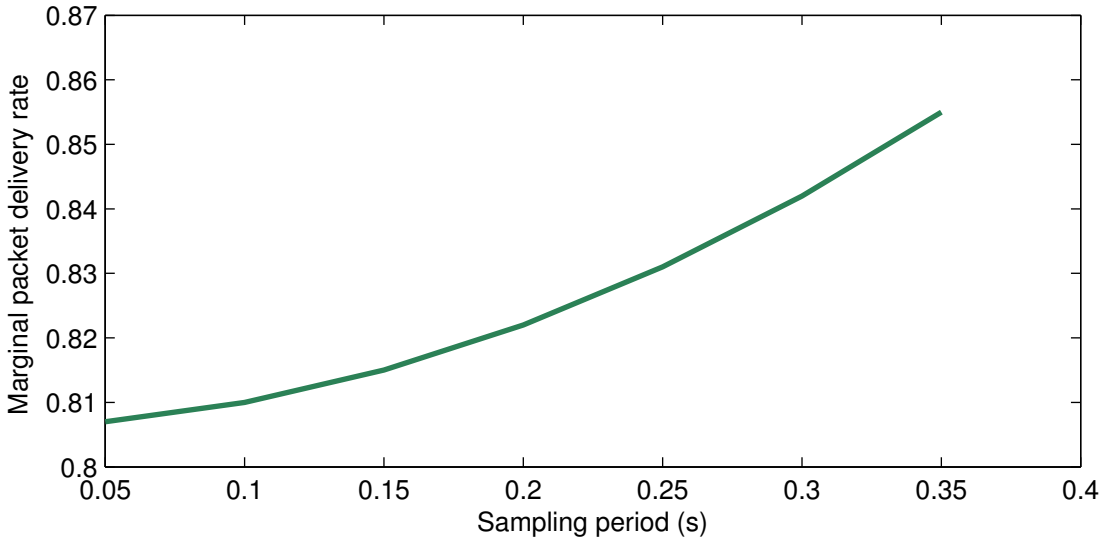

Figure 2.14: Marginal delivery probability vs. sampling period

One can easily infer from Fig. 2.14 that higher sampling period requires increase in p_y to guarantee feasibility. This is in line with the expectation that a packet has to be delivered with higher probability with an increase in sampling time.

2.3.2.4 Robustness

The robustness of the NCPS has been checked by obtaining the probabilities of marginal packet delivery for various operating conditions as listed in Table 2.4.

In Table 2.4, serial number 1 (S.No.1) was considered the base case of operation. For each operating condition, the control scheme was required to be updated to give a corresponding LQG gain and reduced-order state space matrices for the

Table 2.4: Marginal packet delivery probability vs. operating point

S.No.	Total tie-line flow (MW)	Line-outage	Marginal PDP
1.	700	no-outage	0.81
2.	700	60-61	0.83
3.	700	27-53	0.81
4.	100	no-outage	0.79
5.	900	no-outage	0.87
6.	100	27-53	0.79

Kalman filter. The stability performance of the NCPS was also studied with a constant control scheme, i.e. the control scheme obtained for the base case was used for all the operating conditions. Fig. 2.15 shows the rotor-slip response for 3 operating conditions with such constant control scheme.

It is clear from Table 2.4 and Fig. 2.15 that the NCPS is $\mathcal{D}$-stable for various operating points, even with a constant control scheme, at a feasible delivery probability of 0.85.

2.4 Limitations

The NCPS model developed in this chapter is a rigorous and generalized model, but it still suffers from limitations. Some of its limitations are as follows.

1. The time-delay model of the packets is integrated in the packet dropout model, as any packet with delay more than one sampling period is assumed to be dropped while rest of the packets are deemed to be delivered successfully. A more accurate model for NCPS would have been the one in which the time-delays and the packet dropouts are modeled independently.

2. The model is only valid as long as the operating conditions don't change significantly from the operating point at which the system is linearized. For instance, if a generator goes out of service then the transmission system operator (TSO) should get this information in real-time so that the system model and control gains are accordingly updated.

3. Linearization of the system at an operating point is non-trivial, and requires an exact knowledge of steady-state state values and system-wide parameters.

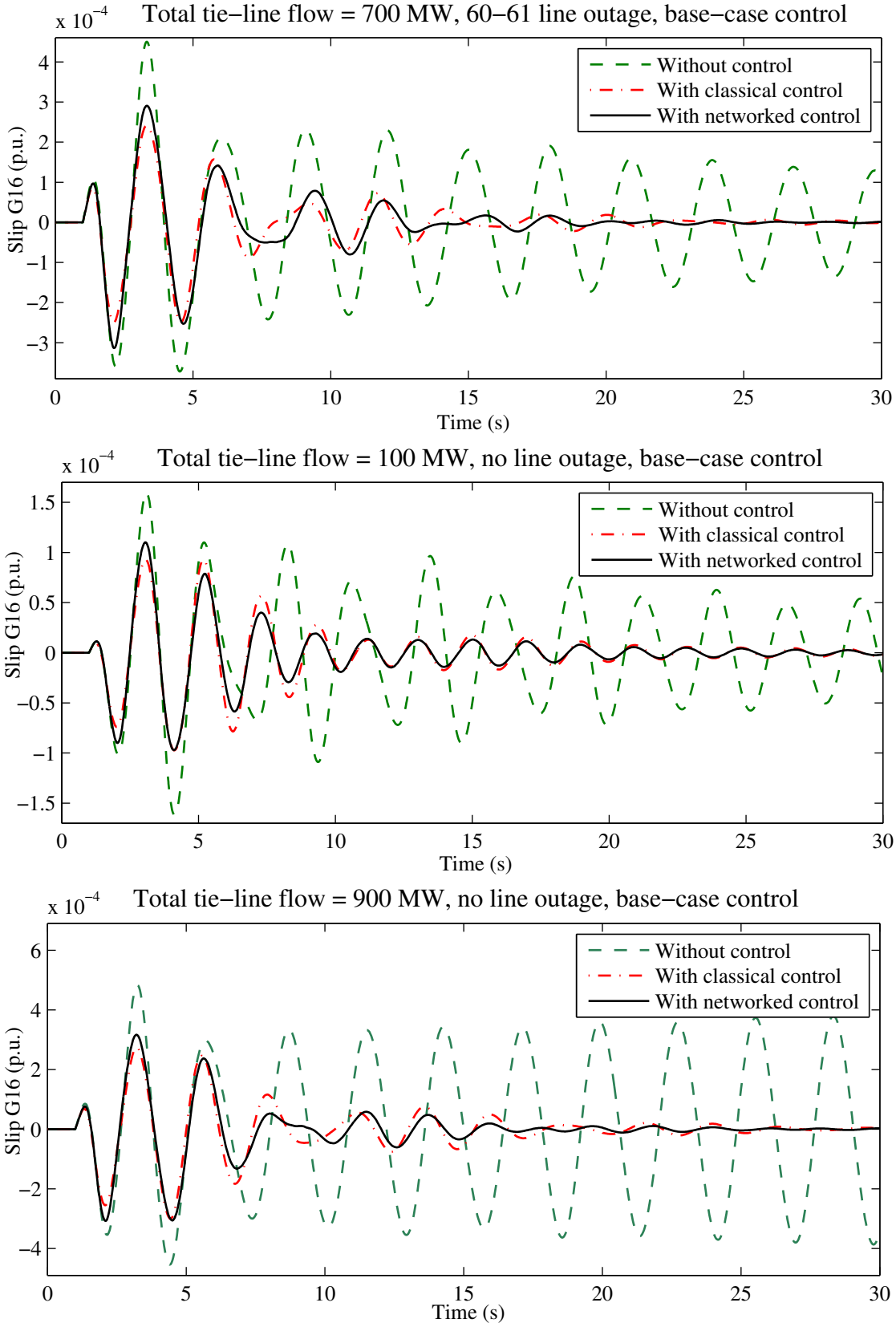

Figure 2.15: Rotor-slip response for various operating points at $p_y = 0.85$

2.5 Summary

This chapter has made an attempt to analyze the stability effects of introducing a packet-based communication network in the control loops of a power system. A Kalman filtering and linear quadratic Gaussian (LQG) based optimal control scheme for damping oscillatory dynamics has been adopted as the centralized estimation and control scheme. The random loss in the delivery of the packets has been modeled as a stochastic process. Using the developed linear matrix inequalities, the lower limit on the probability of packet delivery has been computed which guarantees specified damping. It was found that under varying operating conditions the performance of the NCPS was robust.

The main contribution of this research study lies in the development of a generalized framework to assess the stability and damping of a NCPS. It also presents a formal approach for finding the minimum network requirements in terms of packet delivery quality, so that the specified stability and damping margins can be ensured for any operating condition of a power system. Specifically, the contributions may be summarized as follows.

1. A detailed characterization of packet transmission process and the probability of packet loss have been considered in the framework of NCS for power system control.

2. A practical output-feedback methodology has been used for control (instead of state-feedback), and the signals which are required to be transmitted to the control unit are measurable line-power signals. Also, a detailed and realistic sub-transient power system model has been used.

3. The optimal control scheme which has been used for centralized control can be easily integrated with the WAMS or FACTS devices already present in the system.

The research findings show that although the NCPS framework has limitations, it still has a good potential to guarantee small signal stability margin for modern power systems.

Chapter 3

Decentralized dynamic state estimation in power systems

It was stated in the last chapter that update-rates of communication networks which are used in present day power systems are not as fast as those assumed in the NCPS model. Therefore, the networked control model of the last chapter can only be applied to future power systems in which faster communication networks replace the existing ones. This leads to the second research question, *Can the dynamic estimation and control of a power system be performed in a decentralized manner so that the requirement of a fast and reliable communication network is eliminated*? This and the next two chapters address this research question. This chapter proposes a decentralized algorithm for DSE, which eliminates the requirement of a communication network for dynamic estimation in power systems.

Past studies in DSE are mostly based on linear schemes [26]-[27]. These schemes involve linearization of system's differential and algebraic equations (DAEs), followed by calculation of Jacobian matrices. Linearization introduces approximation errors, which may become significant over time, especially for a complex and high-order power system [30]. Moreover, calculation of Jacobian matrices is computationally expensive, as it has to be done at every iteration of the algorithm.

The drawbacks of linear schemes have been addressed in more recent research papers which propose application of unscented transformation to eliminate linearization and calculation of Jacobians [28]-[31]. In [28], an unscented Kalman filter (UKF) based algorithm has been proposed for DSE of a synchronous machine connected to an infinite bus (also called as single machine infinite bus (SMIB) system). [29] performs DSE of a SMIB system using an extended particle filter. A

SMIB system is an ideal approximation of a real power system. This limitation has been addressed in [30], which proposes a centralized UKF algorithm for DSE of a multi-machine power system. This algorithm requires that remote signals from all the machines in the system are transmitted to a central location. This method has its own limitations that many of the signals required for estimation, such as rotor speed and state variables of excitation system, are difficult to measure. Even if these signals are measured somehow, it is difficult to ensure their transmission to a central location at a high sampling rate. Unless these problems are dealt with, these methods may not be applied to a practical system.

The rest of the chapter is organized as follows. The problem statement and an overview of the proposed scheme are given in Section 3.1. Section 3.2 presents a description of discrete DAEs for power system while the concept of decentralization is explained in Section 3.3. Theory of unscented Kalman filter and algorithm for decentralized DSE are given in Section 3.4. Section 3.5 presents case study of a 68-bus test model and Section 3.6 presents algorithm for bad-data detection. Section 3.7 summarizes the chapter.

3.1 Problem statement and methodology in brief

It is assumed that the power system is represented using a set of continuous-time non-linear DAEs, given by (3.1):

$$\dot{\boldsymbol{x}}(t) = \bar{\boldsymbol{g}}[\boldsymbol{x}(t), \boldsymbol{u}(t)] + \bar{\boldsymbol{v}}(t);\ \boldsymbol{y}(t) = \boldsymbol{h}[\boldsymbol{x}(t), \boldsymbol{u}(t)] + \boldsymbol{w}(t) \tag{3.1}$$

After sampling (3.1) at a sampling period T_0, one gets:

$$\frac{\boldsymbol{x}(kT_0) - \boldsymbol{x}((k-1)T_0)}{T_0} = \bar{\boldsymbol{g}}[\boldsymbol{x}((k-1)T_0), \boldsymbol{u}((k-1)T_0)] + \bar{\boldsymbol{v}}((k-1)T_0); \tag{3.2}$$

$$\boldsymbol{y}(kT_0) = \boldsymbol{h}[\boldsymbol{x}(kT_0), \boldsymbol{u}(kT_0)] + \boldsymbol{w}(kT_0) \tag{3.3}$$

Rewriting kT_0 as k and $(k-1)T_0$ as $k-1$, (3.3) gets converted into discrete form given by (3.5)-(3.6).

$$\boldsymbol{x}(k) = \boldsymbol{x}(k-1) + T_0\bar{\boldsymbol{g}}[\boldsymbol{x}(k-1), \boldsymbol{u}(k-1)] + T_0\bar{\boldsymbol{v}}(k-1) \tag{3.4}$$

$$\Rightarrow \boldsymbol{x}(k) = \boldsymbol{g}[\boldsymbol{x}(k-1), \boldsymbol{u}(k-1)] + \boldsymbol{v}(k-1); \tag{3.5}$$

$$\boldsymbol{y}(k) = \boldsymbol{h}[\boldsymbol{x}(k), \boldsymbol{u}(k)] + \boldsymbol{w}(k) \tag{3.6}$$

In state estimation the state $\boldsymbol{x}(k)$ is treated as a random variable with an estimated mean $\hat{\boldsymbol{x}}(k)$ and an estimated covariance $\boldsymbol{P}_x(k)$.

$\boldsymbol{v}(k)$ and $\boldsymbol{w}(k)$ are assumed to be white Gaussian noises. The constant covariance matrices for the noises are denoted as $\boldsymbol{P}_v$ for $\boldsymbol{v}(k)$ and $\boldsymbol{P}_w$ for $\boldsymbol{w}(k)$.

Remark: Although white Gaussian noises have been used in this chapter, other types of noises may also be used (such as colored noises) as unscented Kalman filter remains applicable in wide variety of noise models, as shown in [39].

3.1.1 Problem statement

Find $\hat{\boldsymbol{X}}(k)$ and $\boldsymbol{P}_X(k)$, given $\hat{\boldsymbol{X}}(k-1)$, $\boldsymbol{P}_X(k-1)$, $\boldsymbol{g}$, $\boldsymbol{h}$, $\boldsymbol{u}(k-1)$, $\boldsymbol{u}(k)$, $\boldsymbol{y}(k)$, $\boldsymbol{P}_v$ and $\boldsymbol{P}_w$, under constraints that:

the algorithm is decentralized, that is, the algorithm for one generation unit should work independently from the algorithms for other units; and

only those measurements may be used which are easily measurable using PMUs, and are locally available.

Stating the problem in simpler terms, an iterative algorithm for finding real-time estimates of the mean and covariance of the states needs to be devised, provided the system DAEs, the inputs, the local PMU measurements, and all the noise covariances are available. The algorithm should be such that the estimation process for each generation unit remains independent of other units.

3.1.2 Methodology

A block diagram of the system and the proposed decentralized methodology for finding a solution for the aforementioned problem statement is shown in Fig. 3.1.

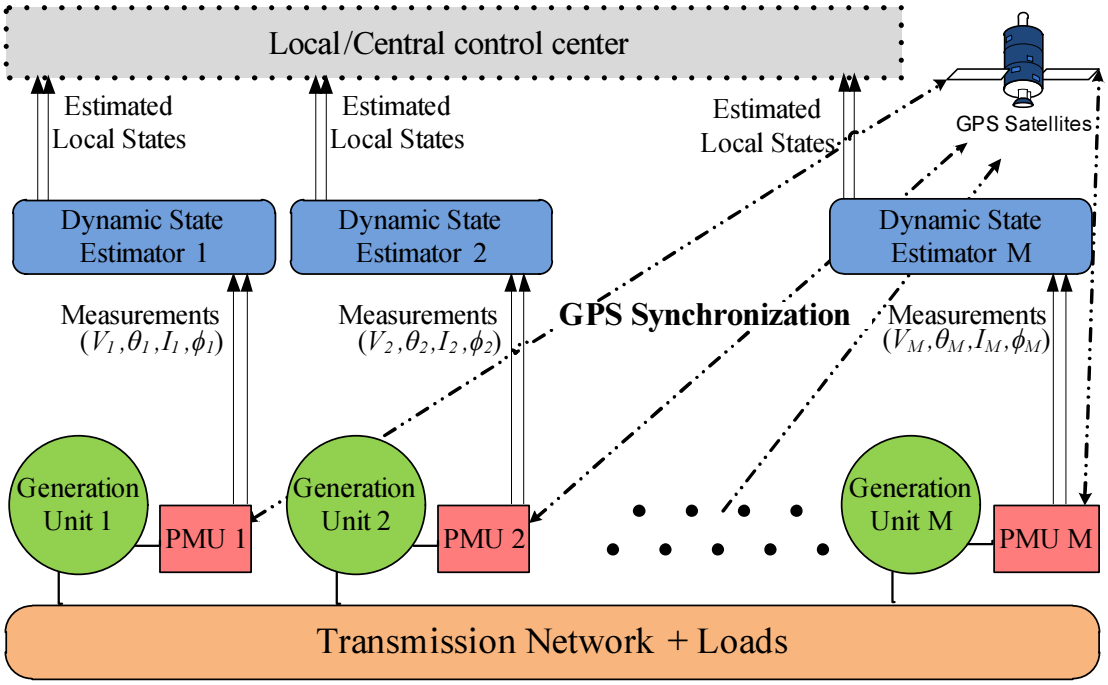

Figure 3.1: System block-diagram and an overview of the methodology

Each generation unit is equipped with a PMU responsible for measuring various phasors associated with that unit, specifically voltage and current phasors. Power systems usually operate at a near constant system frequency of 50 or 60 Hz, and thus all the measured signals from the system have a fundamental harmonic component which is equal to the system frequency. Assuming that other harmonics are present in relatively small quantities, when the measured signals are sampled at more than twice the system frequency, the sampling does not lead to any loss in information in the signals, as per Nyquist-Shannon sampling theorem. PMUs provide sampling rates of over 600 Hz [17]; and hence they are capable of preserving signal-information for state estimation purpose.

Any measuring device in a system (such as a PMU) has finite accuracy. This finite accuracy for a given measurement represented in the model as a white-Gaussian noise superimposed over correct value of the signal. Each noise is assumed to have a zero mean and a standard deviation equal to accuracy of the corresponding measurement. The sampled measurements, along with their noise variances, are sent from PMU to a local estimator. The estimator is located in the vicinity

of PMU and hence communication requirements are assumed to be easily met. DSE is performed at the estimator using non-linear unscented transformation in association with Kalman-like filtering. Estimates of all the dynamic states of the machine are then sent to local and/or central control centers for taking control decisions.

3.2 Power system modeling and discrete DAEs

Discrete DAEs of the power system derived using continuous time DAEs given in [7] (and also in Appendix A), and a brief description of the various components of the system are as follows:

3.2.1 Generators

Each generator in the system has been represented using sub-transient model [50]. Slow dynamics of speed-governor have been ignored as they have practically no influence on the fast small-signal oscillatory dynamics of a power system [2]. Thus, mechanical torque, T_m, has been treated as a constant parameter. If T_m and other parameters for the machine (such as H and D) are not known, they may be estimated in real-time using the parameter estimation algorithm given in [39] or [69]. Discrete DAEs for the i^{th} generator are given by (3.7)-(3.18).

$$\delta_i(k+1) = \delta_i(k) + T_0\omega_b(\omega_i(k) - 1); \tag{3.7}$$

$$\omega_i(k+1) = \omega_i(k) + \frac{T_0}{2H_i}\left(T_{mi} - T_{ei}(k) - D_i\left(\omega_i(k) - 1\right)\right); \tag{3.8}$$

$$\begin{aligned} E'_{qi}(k+1) = E'_{qi}(k) + \frac{T_0}{T'_{d0i}}[E_{fdi}(k) - E'_{qi}(k) \\ + (X_{di} - X'_{di})\{K_{d1i}I_{di}(k) + K_{d2i}\frac{\Psi_{1di}(k) - E'_{qi}(k)}{X'_{di} - X_{li}}\}]; \end{aligned} \tag{3.9}$$

$$E'_{di}(k+1) = E'_{di}(k) - \frac{T_0}{T'_{q0i}}[E'_{di}(k) + (X_{qi} - X'_{qi})\{K_{q1i}I_{qi}(k) + K_{q2i}\frac{\Psi_{2qi}(k) + E'_{di}(k)}{X'_{qi} - X_{li}}\}]; \quad (3.10)$$

$$\Psi_{2qi}(k+1) = \Psi_{2qi}(k) + \frac{T_0}{T''_{q0i}}[I_{qi}(k)(X'_{qi} - X_{li}) - E'_{di}(k) - \Psi_{2qi}(k)]; \quad (3.11)$$

$$\Psi_{1di}(k+1) = \Psi_{1di}(k) + \frac{T_0}{T''_{d0i}}[I_{di}(k)(X'_{di} - X_{li}) + E'_{qi}(k) - \Psi_{1di}(k)]; \quad (3.12)$$

$$E'_{dci}(k+1) = E'_{dci}(k) + \frac{T_0}{T_{ci}}((X''_{di} - X''_{qi})I_{qi}(k) - E'_{dci}(k)); \quad (3.13)$$

where $T_{ei}(k)$, $I_{di}(k)$ and $I_{qi}(k)$ are algebraic functions of $E'_{di}(k)$, $E'_{qi}(k)$, $\Psi_{1di}(k)$, $\Psi_{2qi}(k)$, $E'_{dci}(k)$, $V_i(k)$, $\theta_i(k)$ and $\delta_i(k)$, and are given by:

$$T_{ei}(k) = K_{q1i}E'_{di}(k)I_{di}(k) + K_{d1i}E'_{qi}(k)I_{qi}(k) + K_{d2i}\Psi_{1di}(k)I_{qi}(k) - K_{q2i}\Psi_{2qi}(k)I_{di}(k) + (X''_{di} - X''_{qi})I_{di}(k)I_{qi}(k); \quad (3.14)$$

$$I_{di}(k) = [R_{ai}\{E'_{di}(k)K_{q1i} - \Psi_{2qi}(k)K_{q2i} + E'_{dci}(k) - V_{di}(k)\} - X''_{di}\{E'_{qi}(k)K_{d1i} + \Psi_{1di}(k)K_{d2i} - V_{qi}(k)\}]/Z^2_{ai}; \quad (3.15)$$

$$I_{qi}(k) = [R_{ai}\{E'_{qi}(k)K_{d1i} + \Psi_{1di}(k)K_{d2i} - V_{qi}(k)\} + X''_{di}\{E'_{di}(k)K_{q1i} - \Psi_{2qi}(k)K_{q2i} + E'_{dci}(k) - V_{di}(k)\}]/Z^2_{ai}; \quad (3.16)$$

$$\text{where, } V_{di}(k) = -V_i(k)\sin(\delta_i(k) - \theta_i(k)); \quad (3.17)$$

$$V_{qi}(k) = V_i(k)\cos(\delta_i(k) - \theta_i(k));\ i = 1, 2, \ldots, M. \tag{3.18}$$

3.2.2 Excitation systems

Each generation unit may be excited manually or by using an automatic voltage regulator (AVR). Two types of AVRs have been considered in the case study. Discrete DAEs for IEEE-DC1A type of AVR are given by (3.19)-(3.21), while for IEEE-ST1A type of AVR they are given by (3.22)-(3.23). In case of manual excitation, the field excitation voltage, E_{fd}, is equal to a constant reference, V_{ref}.

$$V_{ri}(k+1) = V_{ri}(k) + \frac{T_0}{T_{ri}}[V_i(k) - V_{ri}(k)]; \tag{3.19}$$

$$V_{ai}(k+1) = V_{ai}(k) + \frac{T_0}{T_{ai}}[K_{ai}(V_{refi} + V_{ssi}(k) - V_{ri}(k)) - V_{ai}(k)]; \tag{3.20}$$

$$E_{fdi}(k+1) = E_{fdi}(k) - \frac{T_0}{T_{xi}}[E_{fdi}(k)(K_{xi} + A_{xi}e^{B_{xi}E_{fdi}(k)}) - V_{ai}(k)];$$
$$E_{fdmini} \leq E_{fdi}(k+1) \leq E_{fdmaxi};\ i = 1, 2, \ldots, M. \tag{3.21}$$

$$V_{ri}(k+1) = V_{ri}(k) + \frac{T_0}{T_{ri}}[V_i(k) - V_{ri}(k)]; \tag{3.22}$$

$$E_{fdi}(k+1) = [K_{ai}(V_{refi} + V_{ssi}(k+1) - V_{ri}(k+1))];$$
$$E_{fdmini} \leq E_{fdi}(k+1) \leq E_{fdmaxi};\ i = 1, 2, \ldots, M. \tag{3.23}$$

3.2.3 Power system stabilizer (PSS)

A PSS is used to provide supplementary damping control to the local modes of a generation unit. Transfer function of PSS for the i^{th} generation unit, as considered in the case study, is given as follows.

$$V_{ssi} = K_{pss}(\omega_i - 1)\frac{(sT_{wi})}{(1+sT_{wi})}\frac{(1+sT_{11i})}{(1+sT_{12i})}\frac{(1+sT_{21i})}{(1+sT_{22i})} \tag{3.24}$$

The discrete form of this transfer function is given by (3.25)-(3.31).

$$P_{s1i}(k+1) = P_{s1i}(k) + \frac{T_0}{T_{wi}}P'_{s1i}(k); \tag{3.25}$$

$$P_{s2i}(k+1) = P_{s2i}(k) + \frac{T_0}{T_{12i}}P'_{s2i}(k); \tag{3.26}$$

$$P_{s3i}(k+1) = P_{s3i}(k) + \frac{T_0}{T_{22i}}P'_{s3i}(k); \tag{3.27}$$

$$\text{where, } P'_{s1i}(k) = K_{pssi}(\omega_i(k) - 1) - P_{s1i}(k); \tag{3.28}$$

$$P'_{s2i}(k) = P'_{s1i}(k) - P_{s2i}(k); \tag{3.29}$$

$$P'_{s3i}(k) = P'_{s1i}(k) + \frac{T_{11i} - T_{12i}}{T_{12i}}P'_{s2i}(k) - P_{s3i}(k); \tag{3.30}$$

$$\text{and, } V_{ssi}(k) = P'_{s1i}(k) + \frac{T_{11i} - T_{12i}}{T_{12i}}P'_{s2i}(k) + \frac{T_{21i} - T_{22i}}{T_{22i}}P'_{s3i}(k);$$
$$V_{ssmini} \leq V_{ssi}(k+1) \leq V_{ssmaxi};\ i = 1, 2, \ldots, M. \tag{3.31}$$

3.2.4 Network model

Network current balance equations for the generator buses are given by (3.32), while power-balance equations for the non-generator buses are given by (3.33).

$$(I_{qi}(k) + jI_{di}(k))e^{j\delta_i(k)} = I_i(k)e^{j\phi_i(k)} = \boldsymbol{Y}_i(k)\boldsymbol{V}(k) + \frac{P_{Li}(k) - jQ_{Li}(k)}{V_i(k)e^{-j\theta_i(k)}};$$
$$\text{where } \boldsymbol{Y}_i(k) \text{ is the } i^{th} \text{ row of } \boldsymbol{Y}(k), \text{ and } i = 1, 2, \ldots, M. \tag{3.32}$$

$$(P_{Li}(k) - jQ_{Li}(k)) + V_i(k)e^{-j\theta_i(k)}(\boldsymbol{Y}_i(k)\boldsymbol{V}(k)) = 0;$$
where $\boldsymbol{Y}_i(k)$ is the i^{th} row of $\boldsymbol{Y}(k)$, and $i = (M+1), (M+2), \ldots, N_0$. (3.33)

3.3 Pseudo inputs and decentralization of DAEs

A generation unit consists of a generator, its AVR and PSS when present. The DAEs for a unit, given by (3.7)-(3.31), are coupled to the DAEs for other units through the network equations, given by (3.32)-(3.33). Inputs to the power system come in form of system-disturbances, such as load changes, line-faults and generation failures. If it is provided that none of the dynamic states are directly measured, a centralized state estimation scheme would require real-time information about all system-wide disturbances, besides an information of line parameters, parameters for all the generation units and system-wide PMU measurements. Obtaining such real-time information is practically not feasible. A decentralized scheme of estimation is the only practical alternative.

An inspection of (3.7)-(3.31) would reveal that the i^{th} generation unit's I, ϕ and the dynamic states for the $(k+1)^{th}$ sample are explicit functions of V, θ and the dynamic states for the k^{th} sample. This inspection leads to an idea which forms the basis of the decentralized estimation scheme: *if V and θ are treated as inputs, rather than as measurements, and I and ϕ are treated as outputs (i.e. as normal measurements), then the dynamic equations for one generation unit can be decoupled from the dynamic equations for other units.* This idea of 'pseudo-inputs' forms the central theme of rest of the thesis and is also the most important contribution of the thesis. It must be noted here that this representation is not unique, and the DAEs can be rearranged in such a way that V and θ become the outputs, and I and ϕ become the inputs. The idea is, therefore, to use one of the pair of measurements as an input pair, and the other pair as an output pair. In this chapter the pair of V and θ is treated as the input pair.

The idea of pseudo-inputs may be better understood with a simpler model of a power system. Classical model of a power system in discrete form is given by the following DAEs for the i^{th} machine.

$$\delta_i(k+1) = \delta_i(k) + T_0\omega_b(\omega_i(k) - 1); \tag{3.34}$$

$$\omega_i(k+1) = \omega_i(k) + \frac{T_0}{2H_i}\left(T_{mi} - T_{ei}(k) - D_i\left(\omega_i(k) - 1\right)\right); \tag{3.35}$$

$$\text{where, } T_{ei}(k) = E'_{qi} I_i(k)\cos(\delta_i(k) - \phi_i(k)) = \frac{E'_{qi}}{x'_d} V_i(k)\sin(\delta_i(k) - \theta_i(k)); \tag{3.36}$$

$$\text{and } (V,\theta) \text{ and } (I,\phi) \text{ are related as: } I_i(k)e^{j\phi_i(k)} = \frac{E'_{qi}e^{j\delta_i(k)} - V_i(k)e^{j\theta_i(k)}}{jx'_d} \tag{3.37}$$

E'_{qi} is treated as a constant parameter in the classical model. The various bus voltages and currents in the system are coupled by the same network equations as in the sub-transient model (that is, by (3.32)-(3.33)). In the centralized method of dynamic state estimation (such as in [30]), the central estimator requires complete system model and a real-time knowledge of all the changes/disturbances occurring in the system. When a disturbance occurs, the estimator predicts the new states of all the machines (in state prediction step) and the new voltages and currents of all the buses (in measurement prediction step) by incorporating the disturbance in the complete system model. The predicted values are then corrected using the measured values of bus voltages and currents in Kalman-update step, and thus new state estimates are generated.

In the proposed decentralized method of dynamic state estimation, each machine has its own estimator. Each decentralized estimator treats one of the pairs of (V,θ) and (I,ϕ) as input and the other pair as normal measurement, and hence requires only equations (3.34)-(3.36) for state prediction and (3.37) for measurement prediction. If the pair (V,θ) is used as pseudo-input, then $T_{ei}(k) = (E'_{qi}/x'_d)V_i(k)\sin(\delta_i(k)-\theta_i(k))$ is used in the state prediction step and $I_i(k)e^{j\phi_i(k)} = (E'_{qi}e^{j\delta_i(k)} - V_i(k)e^{j\theta_i(k)})/(jx'_d)$ is used in measurement prediction step. Otherwise, if the pair (I,ϕ) is used as pseudo-input then $T_{ei}(k) = E'_{qi}I_i(k)\cos(\delta_i(k)-\phi_i(k))$ is used in the state prediction step and $V_i(k)e^{j\theta_i(k)} = E'_{qi}e^{j\delta_i(k)} - jx'_d I_i(k)e^{j\phi_i(k)}$ is used in the measurement prediction step. Thus the network equations (3.32)-(3.33) are not required, and the machine equations are decoupled.

Physical significance of the above idea of decentralization may be understood by going deeper into the physics of power system dynamics. Any change or disturbance which takes place at one point in a large-scale power system is propagated

quickly throughout the system. This is because the propagation of disturbances takes place over an electromechanical traveling wave which travels at a high speed and takes less than a second to propagate changes throughout all the bus voltages and currents in the system (as elaborated in the chapter on 'Electromechanical Wave Propagation' in [16]). These changes in voltage and current levels are in fact responsible for initiating slower small-signal oscillatory dynamics of devices which are connected to the buses. Therefore, just the knowledge of local bus voltage and current is sufficient to predict and estimate the dynamics of the devices that are connected to that local bus; and in our case this device is a synchronous generator. But this knowledge of local voltage and current must be complete (both magnitude and phase are required), and this makes the synchronization of various PMU devices through the GPS satellites crucial to the estimation process. This synchronization of PMUs may also be considered as an indirect coordination between the decentralized estimators.

The idea of decoupling by treating V and θ as inputs leads to a problem: only measured values of V and θ are available (given by V_y and θ_y, respectively), instead of their actual values, and hence they have associated noises, given by V_w and θ_w, respectively. One way of including these noises in the DAEs is to model them as input noises [75]. But this would require linearization and would therefore defeat the purpose of unscented transformation and non-linear filtering. Another way of including the measurement noises is to redefine the values of V and θ according to (3.38), based on the fact that the actual inputs are equal to the differences of their measured values and the associated noises.

$$V_i(k) = V_{yi}(k) - V_{wi}(k);\ \theta_i(k) = \theta_{yi}(k) - \theta_{wi}(k); \tag{3.38}$$

If the expressions for $V_i(k)$ and $\theta_i(k)$ from (3.38) are used in (3.7)-(3.31), the resultant DAEs give the decentralized process model for the i^{th} generation unit, which is written in the following form, with $\boldsymbol{x}_i$ as the vector of the dynamic states, and $\boldsymbol{g}_i$ as the corresponding state functions:

$$\boldsymbol{x}_i(k) = \boldsymbol{g}_i[\boldsymbol{x}_i(k-1), \boldsymbol{u}'_i(k-1), \boldsymbol{z}_i(k-1)] + \boldsymbol{v}_i(k-1);\ i = 1, 2, \ldots, M \tag{3.39}$$

In the above model, $\boldsymbol{u}'_i(k-1)$ acts as a *pseudo-input* vector and $\boldsymbol{z}_i(k-1)$ is its noise. $\boldsymbol{u}'_i(k-1)$ and $\boldsymbol{z}_i(k-1)$ are given as:

$$\boldsymbol{u}_i'(k-1) = [V_{yi}(k-1), \theta_{yi}(k-1)]^T; \tag{3.40}$$

$$\boldsymbol{z}_i(k-1) = [V_{wi}(k-1), \theta_{wi}(k-1)]^T;\ i = 1, 2, \ldots, M \tag{3.41}$$

V_{wi} and θ_{wi} are white noises with zero mean and constant standard deviations given by $\sigma_{V_{wi}}$ and $\sigma_{\theta_{wi}}$, respectively. Thus, the mean and covariance of $\boldsymbol{z}_i(k-1)$ also remain constant for each sample; and, for $i = 1, 2, \ldots, M$, they are given by:

$$\hat{\boldsymbol{z}}_i(k-1) = \boldsymbol{0}_{2\times 1}; \boldsymbol{P}_{zi}(k-1) = \boldsymbol{P}_{zi} = \text{diag}\{{\sigma_{V_{wi}}}^2 {\sigma_{\theta_{wi}}}^2\} \tag{3.42}$$

If $\hat{\boldsymbol{x}}_i(k-1)$ and $\boldsymbol{P}_{xi}(k-1)$ are the estimates of mean and covariance of $\boldsymbol{x}_i(k-1)$; and $\boldsymbol{P}_{xzi}(k-1)$ is the cross-correlation between $\boldsymbol{x}_i(k-1)$ and $\boldsymbol{z}_i(k-1)$; and if $\boldsymbol{x}_i(k-1)$ is augmented with $\boldsymbol{z}_i(k-1)$ to give $\boldsymbol{X}_i(k-1) = [\boldsymbol{x}_i(k-1)^T, \boldsymbol{z}_i(k-1)^T]^T$, the estimates of mean and covariance of $\boldsymbol{X}_i(k-1)$, for $i = 1, 2, \ldots, M$, are given by:

$$\hat{\boldsymbol{X}}_i(k-1) = \begin{bmatrix} \hat{\boldsymbol{x}}_i(k-1) \\ \hat{\boldsymbol{z}}_i(k-1) \end{bmatrix}; \tag{3.43}$$

$$\boldsymbol{P}_{Xi}(k-1) = \begin{bmatrix} \boldsymbol{P}_{xi}(k-1) & \boldsymbol{P}_{xzi}(k-1)^T \\ \boldsymbol{P}_{xzi}(k-1) & \boldsymbol{P}_{zi}(k-1) \end{bmatrix} \tag{3.44}$$

The augmented state $\boldsymbol{X}(k)$ is also a random variable with an estimated mean $\hat{\boldsymbol{X}}(k)$ and an estimated covariance $\boldsymbol{P}_X(k)$. Rewriting (3.39) in the augmented state form, one gets:

$$\boldsymbol{X}_i(k) = \boldsymbol{g}_i[\boldsymbol{X}_i(k-1), \boldsymbol{u}_i'(k-1)] + \begin{bmatrix} \boldsymbol{v}_i(k-1) \\ \boldsymbol{0}_{2\times 1} \end{bmatrix};\ i = 1, 2, \ldots, M \tag{3.45}$$

Measurement equations for measured magnitude, I_{yi}, and measured phase, ϕ_{yi}, of the stator current of the i^{th} unit are (using (3.32)):

$$I_{yi}(k) = \sqrt{(I_{qi}(k))^2 + (I_{di}(k))^2} + I_{wi}(k); \tag{3.46}$$

$$\phi_{yi}(k) = \arg\{I_{qi}(k) + jI_{di}(k)\} + \delta_i(k) + \phi_{wi}(k);\ i = 1, 2, \ldots, M \tag{3.47}$$

In (3.46), $I_{qi}(k)$ and $I_{di}(k)$ are given by (3.18) after replacing the expressions of $V_i(k)$ and $\theta_i(k)$ from (3.38). Writing $[I_{yi}, \phi_{yi}]^T$ as the output vector $\boldsymbol{y}_i$, the corresponding measurement functions (given by (3.46), (3.38) and (3.18)) as $\boldsymbol{h}_i$, and $[I_{wi}, \phi_{wi}]^T$ as the output-noise vector $\boldsymbol{w}_i$, the measurement model comes out as:

$$\boldsymbol{y}_i(k) = \boldsymbol{h}_i[\boldsymbol{X}_i(k), \boldsymbol{u}_i'(k)] + \boldsymbol{w}_i(k);\ i = 1, 2, \ldots, M. \tag{3.48}$$

The mean and covariance of $\boldsymbol{w}_i(k)$, for $i = 1, 2, \ldots, M$, are:

$$\hat{\boldsymbol{w}}_i(k) = \boldsymbol{0}_{2\times 1};\ \boldsymbol{P}_{wi}(k) = \boldsymbol{P}_{wi} = \text{diag}\{{\sigma_{I_{wi}}}^2, {\sigma_{\phi_{wi}}}^2\} \tag{3.49}$$

The aggregate model for the i^{th} unit, given by (3.45) and (3.48), is the decentralized equivalent of (3.5)-(3.6).

3.4 Unscented Kalman filter

Unscented transformation was proposed by J. K. Uhlmann as a general method for approximating nonlinear transformations of probability distributions [71] . Based on an idea that it is easier to approximate a probability distribution than to approximate a non-linear function; this method is used to find consistent, efficient and unbiased estimates of mean and covariance of a random variable undergoing a non-linear transformation [72]. If the non-linear transformation given by (3.45) is applied to $\boldsymbol{X}(k-1)$ (the suffix i has been ignored), then the estimated mean and covariance of the resultant state $\boldsymbol{X}(k)$ are derived in four steps:

3.4.1 Generation of sigma points

The first step is to generate a set of points, called as sigma points, whose sample mean and covariance are same as that of $\boldsymbol{X}(k-1)$. If the dimension of $\boldsymbol{X}(k-1)$ is n, then just $2n$ sigma points, $\boldsymbol{\chi}_l(k-1)$, $l = 1, 2, \ldots, 2n$, need to be generated

to capture its distribution [71]. The following algorithm is used for generation of the sigma points [28]:

$$\boldsymbol{\chi}_l(k-1) = \hat{\boldsymbol{X}}(k-1) + (\sqrt{n\boldsymbol{P}_X(k-1)})_l,\ l = 1, 2, \ldots, n; \tag{3.50}$$

$$\boldsymbol{\chi}_l(k-1) = \hat{\boldsymbol{X}}(k-1) - (\sqrt{n\boldsymbol{P}_X(k-1)})_l, l = (n+1), (n+2), \ldots, 2n \tag{3.51}$$

Here, $(\sqrt{n\boldsymbol{P}_X(k-1)})_l$ is the l^{th} column of lower triangular matrix $\sqrt{n\boldsymbol{P}_X(k-1)}$ obtained by Cholesky decomposition, which is given by:

$$n\boldsymbol{P}_X(k-1) = \sqrt{n\boldsymbol{P}_X(k-1)}\sqrt{n\boldsymbol{P}_X(k-1)}^T \tag{3.52}$$

3.4.2 State prediction

In second step predicted-state sigma points are generated, which are given by $\boldsymbol{\chi}_l^-(k) = \boldsymbol{g}[\boldsymbol{\chi}_l(k-1), \boldsymbol{u'}(k-1)]$, $l = 1, 2, \ldots, 2n$. Sample mean of these points is equal to $\hat{\boldsymbol{X}}^-(k)$, while sum of augmented $\boldsymbol{P}_v$ and sample covariance of these points is equal to $\boldsymbol{P}_X^-(k)$. Here, $\hat{\boldsymbol{X}}^-(k)$ and $\boldsymbol{P}_X^-(k)$ are estimated mean and estimated covariance, respectively, of a predicted-state random variable, $\boldsymbol{X}^-(k)$.

3.4.3 Measurement prediction

The third step is to generate predicted-measurement sigma points, which are given by $\boldsymbol{\gamma}_l^-(k) = \boldsymbol{h}[\boldsymbol{\chi}_l^-(k), \boldsymbol{u'}(k)]$, $l = 1, 2, \ldots, 2n$. Sample mean of these points is equal to $\hat{\boldsymbol{y}}^-(k)$, while sum of $\boldsymbol{P}_w$ and sample covariance of these points is equal to $\boldsymbol{P}_y^-(k)$. Here, $\hat{\boldsymbol{y}}^-(k)$ and $\boldsymbol{P}_y^-(k)$ are estimated mean and estimated covariance, respectively, of a predicted-measurement random variable, $\boldsymbol{y}^-(k)$. Cross-correlation between the predicted-state sigma points and the predicted-measurement sigma points is equal to $\boldsymbol{P}_{Xy}^-(k)$, which is taken as estimated cross-correlation between $\boldsymbol{X}^-(k)$ and $\boldsymbol{y}^-(k)$.

3.4.4 Kalman update

The final step is to find $\hat{\boldsymbol{X}}(k)$ and $\boldsymbol{P}_X(k)$ using the normal Kalman filter equations [73]:

$$\boldsymbol{K}(k) = \boldsymbol{P}_{Xy}^{-}(k)(\boldsymbol{P}_{y}^{-}(k))^{-1}; \tag{3.53}$$

$$\hat{\boldsymbol{X}}(k) = \hat{\boldsymbol{X}}^{-}(k) + \boldsymbol{K}(k)(\boldsymbol{y}(k) - \hat{\boldsymbol{y}}^{-}(k)) \tag{3.54}$$

$$\boldsymbol{P}_X(k) = \boldsymbol{P}_X^{-}(k) - \boldsymbol{K}(k)[\boldsymbol{P}_{Xy}^{-}(k)]^T \tag{3.55}$$

The above four steps constitute the UKF. As stated in the beginning of this chapter, the superiority of UKF has been established over other non-linear filters, such as extended Kalman filter [74].

Coming back to power systems, the aggregate model for one generation unit, given by (3.48) and (3.45), is completely independent from other units. Thus, the four steps of UKF may be directly applied to the i^{th} aggregate model to give its filtering algorithm, summarized as follows.

Algorithm 1: Decentralized DSE for the i^{th} generation unit

Begin Find $\boldsymbol{g}_i$, $\boldsymbol{h}_i$, $\boldsymbol{P}_{zi}$ and $\boldsymbol{P}_{wi}$ according to (3.45), (3.48), (3.42) and (3.49), respectively. Find $\boldsymbol{P}_{vi}$. Let m_i denote the total number of states to be estimated for the unit. Denote $n_i = m_i + 2$. Denote the steady-state values of $\hat{\boldsymbol{x}}_i$ as $\boldsymbol{x}_{0i}$.

While $(k \geq 1)$

{ **STEP 1: Initialize**

if $(k = 1)$ **then** initialize $\hat{\boldsymbol{x}}_i(0) = \boldsymbol{x}_{0i}$, $\hat{\boldsymbol{z}}_i(0) = \boldsymbol{0}_{2\times 1}$, $\boldsymbol{P}_{xi}(0) = \boldsymbol{P}_{vi}$, $\boldsymbol{P}_{xzi}(0) = \boldsymbol{0}_{2\times m_i}$, $\boldsymbol{P}_{zi}(0) = \boldsymbol{P}_{zi}$ in (3.43) to get $\boldsymbol{P}_{Xi}(0)$ and $\hat{\boldsymbol{X}}_i(0)$.

else reinitialize $\hat{\boldsymbol{z}}_i(k-1) = \boldsymbol{0}_{2\times 1}$ and $\boldsymbol{P}_{zi}(k-1) = \boldsymbol{P}_{zi}$, leaving rest of the elements in $\hat{\boldsymbol{X}}_i(k-1)$ and $\boldsymbol{P}_{Xi}(k-1)$ unchanged.

STEP 2: Generate sigma points

$$\boldsymbol{\chi}_{il}(k-1) = \hat{\boldsymbol{X}}_i(k-1) + (\sqrt{n_i \boldsymbol{P}_{Xi}(k-1)})_l,\ l=1,2,\ldots,n_i$$

$$\boldsymbol{\chi}_{il}(k-1) = \hat{\boldsymbol{X}}_i(k-1) - (\sqrt{n_i \boldsymbol{P}_{Xi}(k-1)})_l, l = (n_i+1), (n_i+2), \ldots, 2n_i$$

STEP 3: Predict states

$$\boldsymbol{\chi}_{il}^{-}(k) = \boldsymbol{g}_i[\boldsymbol{\chi}_{il}(k-1), \boldsymbol{u}_i'(k-1)], l=1,\ldots,2n_i;\ \hat{\boldsymbol{X}}_i^{-}(k) = \tfrac{1}{2n_i}\textstyle\sum_{l=1}^{2n_i}\boldsymbol{\chi}_{il}^{-}(k)$$

$$\boldsymbol{P}_{Xi}^{-}(k) = \tfrac{1}{2n_i}\textstyle\sum_{l=1}^{2n_i}[\boldsymbol{\chi}_{il}^{-}(k) - \hat{\boldsymbol{X}}_i^{-}(k)][\boldsymbol{\chi}_{il}^{-}(k) - \hat{\boldsymbol{X}}_i^{-}(k)]^T + \begin{bmatrix} \boldsymbol{P}_{vi} & \boldsymbol{0}_{m\times 2} \\ \boldsymbol{0}_{2\times m} & \boldsymbol{0}_{2\times 2} \end{bmatrix}$$

STEP 4: Predict measurements

$$\boldsymbol{\gamma}_{il}^{-}(k) = \boldsymbol{h}_i[\boldsymbol{\chi}_{il}^{-}(k), \boldsymbol{u}_i'(k)],\ l=1,2,\ldots,2n_i;\ \hat{\boldsymbol{y}}_i^{-}(k) = \tfrac{1}{2n_i}\textstyle\sum_{l=1}^{2n_i}\boldsymbol{\gamma}_{il}^{-}(k)$$

$$\boldsymbol{P}_{yi}^{-}(k) = \tfrac{1}{2n_i}\textstyle\sum_{l=1}^{2n_i}[\boldsymbol{\gamma}_{il}^{-}(k) - \hat{\boldsymbol{y}}_i^{-}(k)][\boldsymbol{\gamma}_{il}^{-}(k) - \hat{\boldsymbol{y}}_i^{-}(k)]^T + \boldsymbol{P}_{wi}$$

$$\boldsymbol{P}_{Xyi}^{-}(k) = \tfrac{1}{2n_i}\textstyle\sum_{l=1}^{2n_i}[\boldsymbol{\chi}_{il}^{-}(k) - \hat{\boldsymbol{X}}_i^{-}(k)][\boldsymbol{\gamma}_{il}^{-}(k) - \hat{\boldsymbol{y}}_i^{-}(k)]^T$$

STEP 5: Kalman update

$$\boldsymbol{K}_i(k) = \boldsymbol{P}_{Xyi}^{-}(k)(\boldsymbol{P}_{yi}^{-}(k))^{-1}; \hat{\boldsymbol{X}}_i(k) = \hat{\boldsymbol{X}}_i^{-}(k) + \boldsymbol{K}_i(k)(\boldsymbol{y}_i(k) - \hat{\boldsymbol{y}}_i^{-}(k))$$

$$\boldsymbol{P}_{Xi}(k) = \boldsymbol{P}_{Xi}^{-}(k) - \boldsymbol{K}_i(k)[\boldsymbol{P}_{Xyi}^{-}(k)]^T$$

STEP 6: Output and time update

output $\hat{\boldsymbol{X}}_i(k)$ and $\boldsymbol{P}_{Xi}(k)$

$k \leftarrow (k+1)$ }

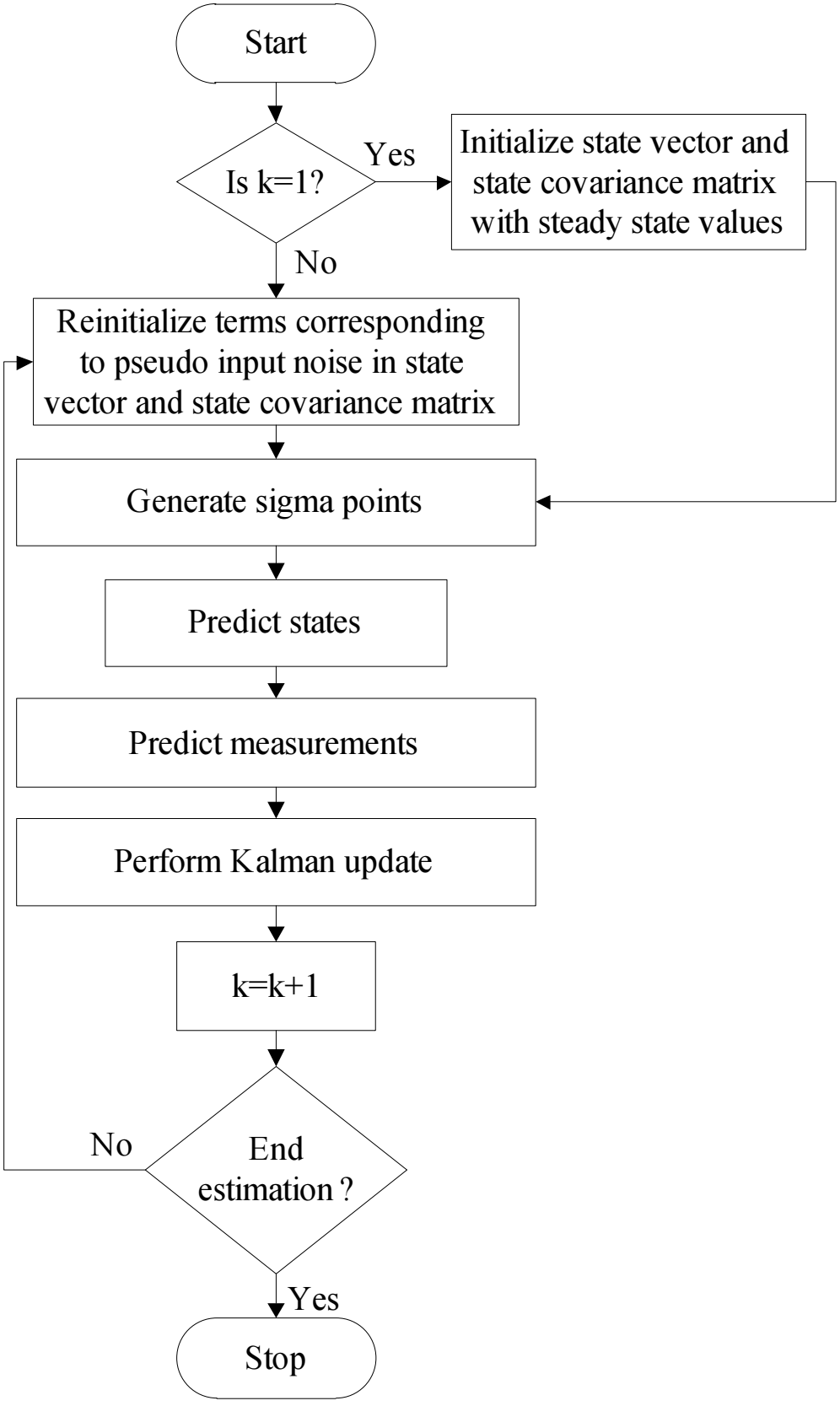

Figure 3.2: Flow chart for the steps of decentralized DSE

3.5 Case study: 68 bus test system

The 16-machine, 68-bus test system, shown in Fig. 3.3, has been used for the case study. This system is similar to the one used in last chapter, the only difference being the absence of networked control and of any FACTS device in the system.

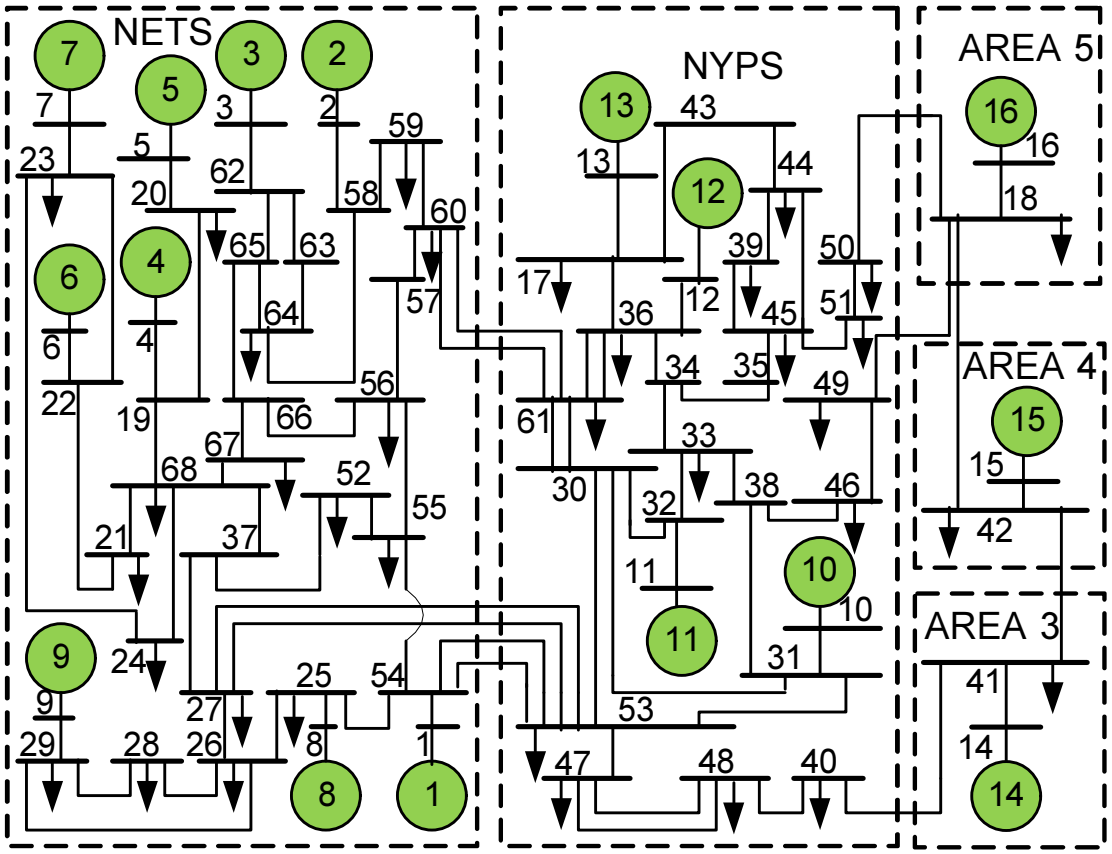

Figure 3.3: Line diagram of the 16-machine, 68-bus, power system model

A detailed system description is available in [7], which is used to simulate the system in MATLAB on a personal computer with Intel Core 2 Duo, 2.0 GHz CPU and 2 GB RAM.

There are three types of generation units in the test system. The first eight units in the system are of *type 1*: with IEEE-DC1A type of AVR, and without a PSS. The ninth unit is of *type 2*: with IEEE-ST1A type of AVR, and with a PSS installed. The rest of the units are of *type 3*: with manual excitation, and without a PSS. The state vectors for the i^{th} unit in the test system, according to these three types, are:

$$\boldsymbol{x}_i = [\delta_i, \omega_i, E'_{qi}, E'_{di}, \psi_{2qi}, \psi_{1di}, V_{ri}, V_{ai}, E_{fdi}]^T, i = 1, 2, \ldots, 8; \tag{3.56}$$

$$\boldsymbol{x}_9 = [\delta_9, \omega_9, E'_{q9}, E'_{d9}, \psi_{2q9}, \psi_{1d9}, V_{r9}, P_{s1,9}, P_{s2,9}, P_{s3,9}]^T; \tag{3.57}$$

$$\boldsymbol{x}_i = [\delta_i, \omega_i, E'_{qi}, E'_{di}, \psi_{2qi}, \psi_{1di}]^T, i = 10, 11, \ldots, 16. \tag{3.58}$$

In the time-domain simulation, the actual values of V, θ, I and ϕ were sampled at 120 Hz (T_0=8.33 ms), as system frequency is taken to be 60 Hz for the 68-bus test system and 120 Hz is the Nyquist sampling-frequency for this system frequency.

3.5.1 Noise variances

3.5.1.1 Measurement noise

All of the PMUs in the power system are time synchronized to an absolute time reference provided by GPS. IEEE standard for synchrophasor measurements for power systems specifies a basic time synchronization accuracy of ± 0.2 μs [18]. At 50 Hz, this translates to a phase-measurement accuracy of around ± 0.06 mrad. Thus, PMUs are expected to have an accuracy of around ± 0.1 mrad for phase measurements. Accuracy of PMUs in magnitude measurements is limited by accuracy of CTs and PTs (also called as instrument transformers). PMUs do not get measurements directly from field, instead they use analog values of current and voltage waveforms provided by CTs and PTs, respectively. These values are time-stamped by PMUs to an absolute reference provided by GPS in order to generate the sampled current and voltage phasors [16]. The waveforms provided by the instrument transformers have errors in both magnitude and phase, but the error in phase can be accurately compensated and calibrated out using digital signal processing (DSP) techniques [76]. The errors in magnitude of the waveforms provided by the instrument transformers are limited by accuracy class of these instruments. There are two main standards according to which instrument transformers are designed: IEC 60044 [77] and IEEE C57.13 [78]. Both of these standards specify accuracies in the range of $\pm 0.1\%$ to $\pm 0.3\%$ for the measurement of voltage and current magnitudes using modern CTs and PTs.

Thus, noises in the generated phase measurements were assumed to have standard deviation of 0.1 mrad (or 10^{-4} rad), while noises in the generated magnitude measurements were assumed to have standard deviation of 0.1% (or 10^{-3} p.u.), and hence $\sigma_{\theta_{w0}} = \sigma_{\phi_{w0}} = 10^{-4}$ rad, and $\sigma_{V_{w0}} = \sigma_{I_{w0}} = 10^{-3}$ p.u. The '0' in

$\sigma_{V_{w0}}$, $\sigma_{\theta_{w0}}$, $\sigma_{I_{w0}}$ and $\sigma_{\phi_{w0}}$ denotes that these are base-case values. The variances for the generated noises for all the units were made equal to the base-case values, and hence $\boldsymbol{P}_{zi} = \boldsymbol{P}_{z0} = \text{diag}\{10^{-6}, 10^{-8}\}$ and $\boldsymbol{P}_{wi} = \boldsymbol{P}_{w0} = \text{diag}\{10^{-6}, 10^{-8}\}$; $i = 1, 2, \ldots, 16$, from (3.42), (3.49).

White Gaussian noises with aforementioned variances were added to the sampled values of the actual signals in order to generate measurements. Fig. 3.4 shows the generated V_y and θ_y for the 13^{th} unit.

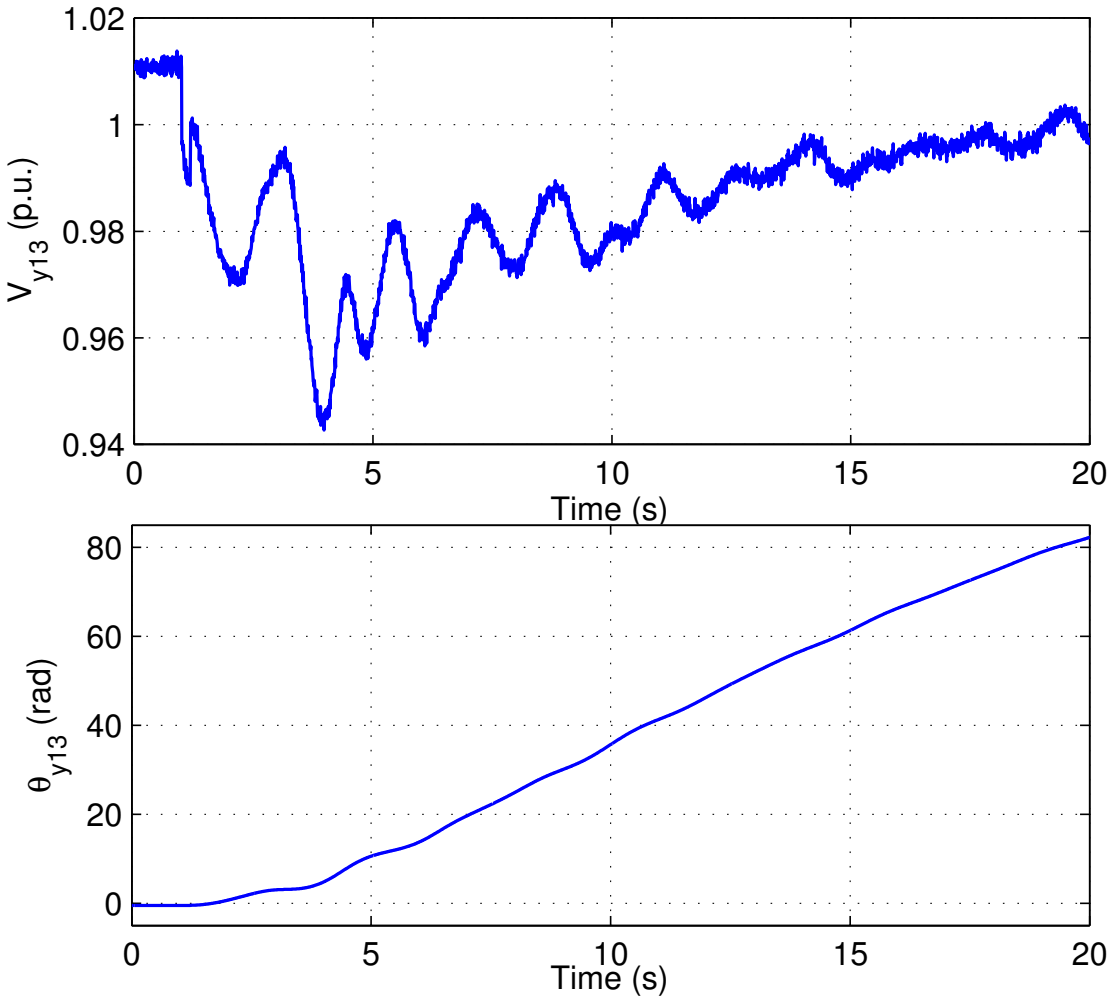

Figure 3.4: Generated measurements for V and θ for the 13^{th} generation unit

3.5.1.2 Process noise

Process noise needs to be included in a model due to modeling approximations and model integration errors. It is not as straight forward to find process noise variances as it is to find measurement noise variances. This is because it is difficult to obtain errors due to unmodeled dynamics, modeling approximations and parameter

uncertainties, and combine them with integration errors of the discrete model used by the state estimator. A practical and robust way of finding process noise variances is to estimate them using a perturbation observer [79], but this method is not required for finding process noise variances in the case study.

In the case study, as power system is simulated using known subtransient DAEs and discrete forms of the same DAEs are used by the estimator, modeling errors are absent. The only errors which are present are due to the discretization of the DAEs in the state estimator. As the DAEs are discretized according to Euler's first-order approximation, the discretization error in state x is $T_0^2\ddot{x}/2$ (also known as local truncation error of Euler's method [80]), where T_0 is the step size or sampling period of discretization. Noting that $\ddot{x} \approx \Delta(\Delta x)/T_0^2$, standard deviation (SD) of process noise in $x(k)$ is taken to be $max\{|\Delta(\Delta x(k))|\}/2$, excluding any sudden changes during faults or other such disturbances.

Here $\Delta x(k) = x(k)-x(k-1)$, $\Delta(\Delta x(k)) = \Delta x(k)-\Delta x(k-1) = x(k)-2x(k-1)+x(k-2)$, $3 \leq k \leq N$, and N is the total number of samples for which the system was simulated (for example, for a $15s$ simulation $N = (15s) \times (120Hz) = 1800$). This expression for process noise variance may be better understood with an example. Fig. 3.5 shows the state changes in δ and ω for the 13^{th} unit.

It can be observed from the figure that $max\{|\Delta(\Delta\delta_{13}(k))|\}/2$ is 6×10^{-4}, and $max\{|\Delta(\Delta\omega_{13}(k))|\}/2$ is 6×10^{-6}. Hence variances of noises in δ_{13} and ω_{13} are taken as 3.6×10^{-7} and 3.6×10^{-11}, respectively. This technique was used to find $\boldsymbol{P}_{vi}$ for all the machines. For the three different types of machines in the system $\boldsymbol{P}_{vi}$ was found to be:

$$\boldsymbol{P}_{vi} = \text{diag}\{1.6 \times 10^{-7}, 1.6 \times 10^{-11}, 4 \times 10^{-10}, 4 \times 10^{-10}, 9 \times 10^{-10}, 2.5 \times 10^{-9}, 3.6 \times 10^{-9}, 4 \times 10^{-6}, 2.5 \times 10^{-7}\},\ i = 1, 2, \ldots, 8; \quad (3.59)$$

$$\boldsymbol{P}_{v9} = \text{diag}\{1.6 \times 10^{-7}, 1.6 \times 10^{-11}, 4 \times 10^{-8}, 4 \times 10^{-10}, 9 \times 10^{-10}, 2.5 \times 10^{-9}, 3.6 \times 10^{-9}, 1 \times 10^{-12}, 2.5 \times 10^{-9}, 1.6 \times 10^{-9}\}; \quad (3.60)$$

$$\boldsymbol{P}_{vi} = \text{diag}\{3.6 \times 10^{-7}, 3.6 \times 10^{-11}, 6.4 \times 10^{-11}, 1.6 \times 10^{-9}, 2.5 \times 10^{-9}, 9 \times 10^{-10}\},\ i = 10, 11, \ldots, 16. \quad (3.61)$$

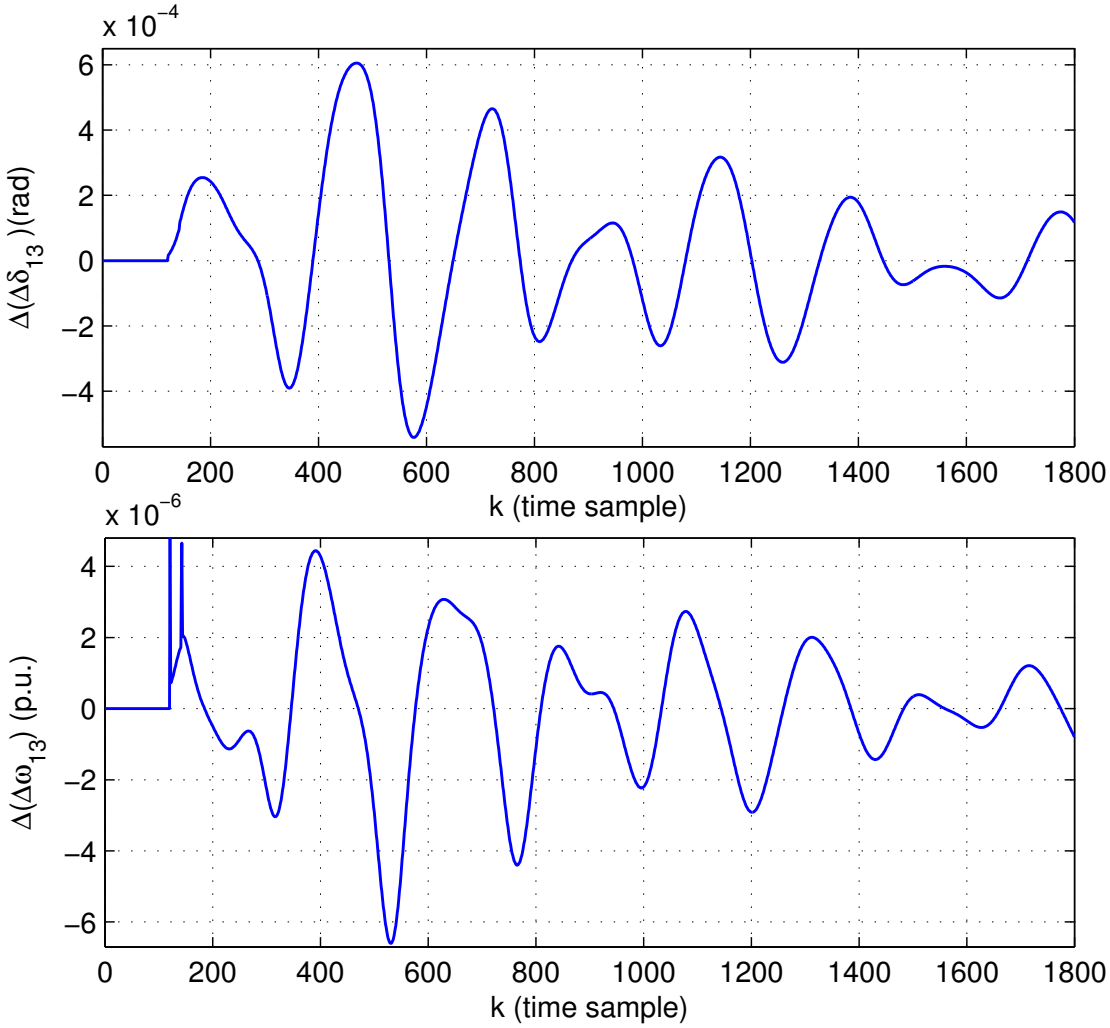

Figure 3.5: State changes in δ and ω for the 13^{th} generation unit

3.5.2 Simulation results and discussion

In the start of the simulation, the system was operating in a steady condition. Then at $t = 1s$, a disturbance was created by a three-phase fault and the fault was cleared after $0.18s$ by outage (or opening) of one of the tie-lines between buses 53-54. The i^{th} decentralized UKF algorithm, as given in Section 3.4, was running along with the simulation of the i^{th} unit. The generated measurements from each unit were given as input to the corresponding UKF. The simulated states, along with their real-time estimated values, have been plotted for each unit. Corresponding estimation errors for various states have also been plotted. Due to space-constraints, plots for only three units (of different types) have been shown: unit 3 of type 1 (Fig. 3.6, Fig. 3.8 and Fig. 3.10, and corresponding errors in Fig. 3.7, Fig. 3.9 and Fig. 3.11, respectively), unit 9 of type 2 (Fig. B.1, Fig. B.3 and Fig. B.5, and corresponding errors in Fig. B.2, Fig. B.4 and Fig. B.6, respectively), and unit

13 of type 3 (Fig. B.7 and Fig. B.9, and corresponding errors in Fig. B.8 and Fig. B.10, respectively). The plots for unit 9 and unit 13 are given in Appendix B.

3.5.2.1 Estimation accuracy

It can be seen in Fig. 3.6 - Fig. 3.11 and Fig. B.1 - Fig. B.10 that for every dynamic state, the plot of estimated values almost coincides with those of the simulated values and maximum estimation error in a state remains within 2% of maximum deviation in the state (not considering the errors during and just after a disturbance). Thus, it is evident that the decentralized UKF scheme generates accurate estimates of all the dynamic states of a generating unit. As all the generator states have been estimated with high accuracies, they can be reliably used for further control and security decisions.

3.5.2.2 Computational feasibility

The proposed algorithm was tested on two more standard IEEE test systems to assess its scalability. As the measurements are updated every 8.33 ms ($T_0 = 8.33$ ms), a single iteration of the algorithm should not require more than 8.33 ms, otherwise the algorithm would not run in real-time. The average time for one iteration has been tabulated in Table 3.1 for the three test systems. A centralized scheme for DSE (given in [30]) was also implemented on all the test systems, and the corresponding average iteration times have been tabulated in Table 3.1. It can be inferred from Table 3.1 that the computational speed of the proposed decentralized algorithm is very fast and it remains independent of size of the system, while the centralized algorithm becomes slow and infeasible for large systems (68-bus and 145-bus systems).

Table 3.1: Comparison of computational speeds

	Average computational time for one iteration (in ms)	
Test system	Decentralized algorithm	Centralized algorithm
IEEE 30-bus	0.33	1.45
IEEE 68-bus	0.33	12.4
IEEE 145-bus	0.33	139

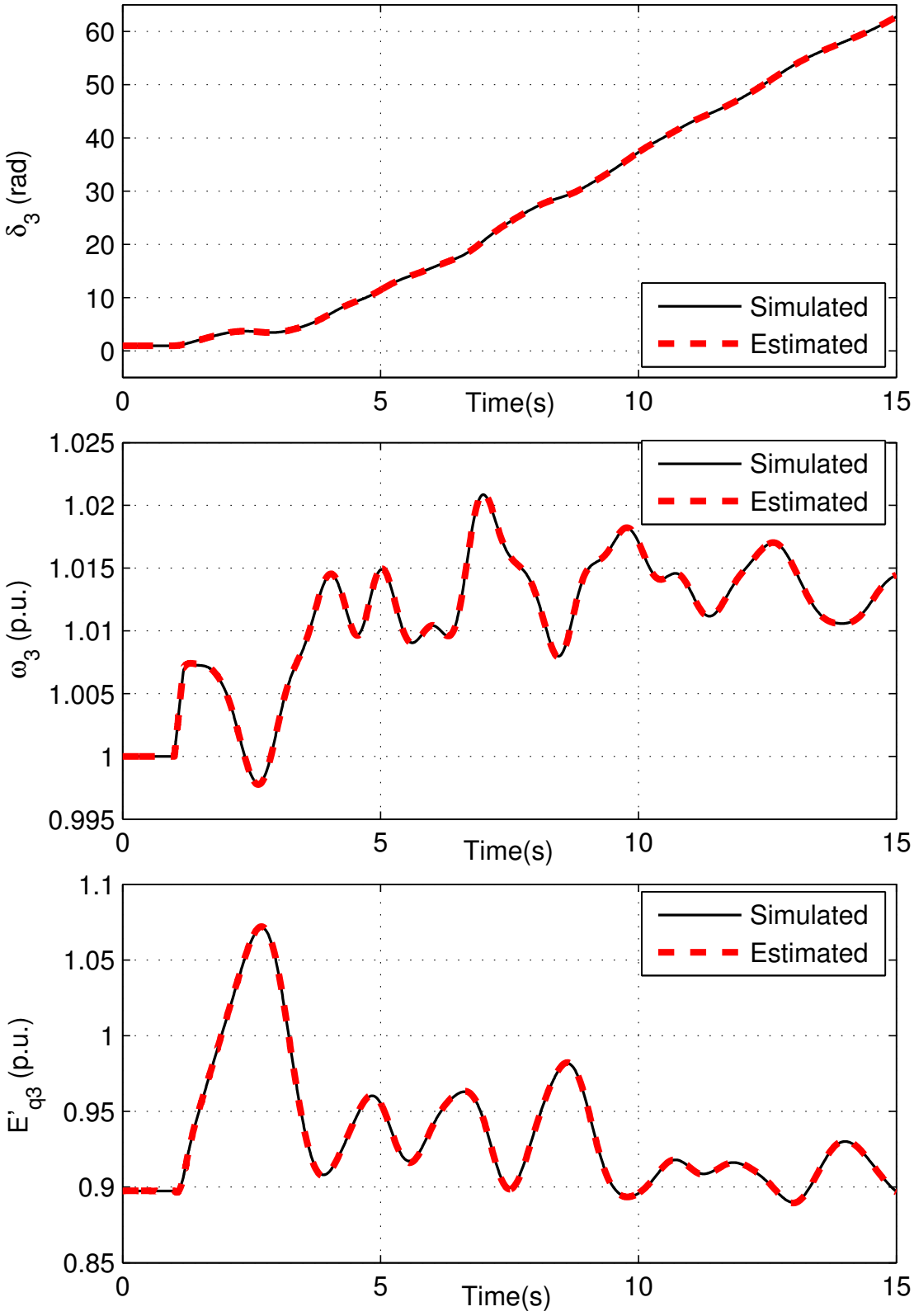

Figure 3.6: Estimated vs simulated values for δ, ω and E'_q of the 3^{rd} unit

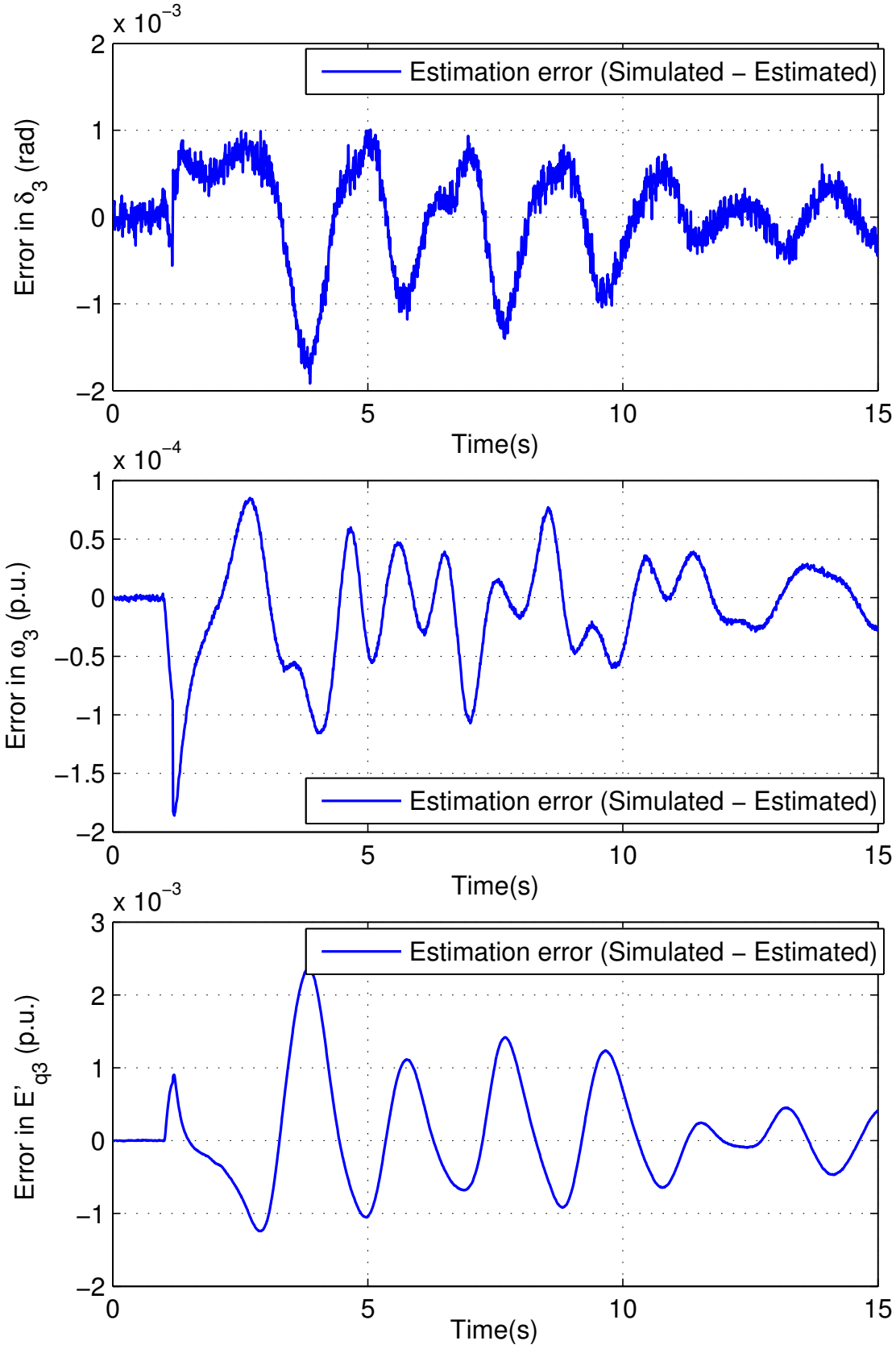

Figure 3.7: Estimation errors for δ, ω and E'_q of the 3^{rd} unit

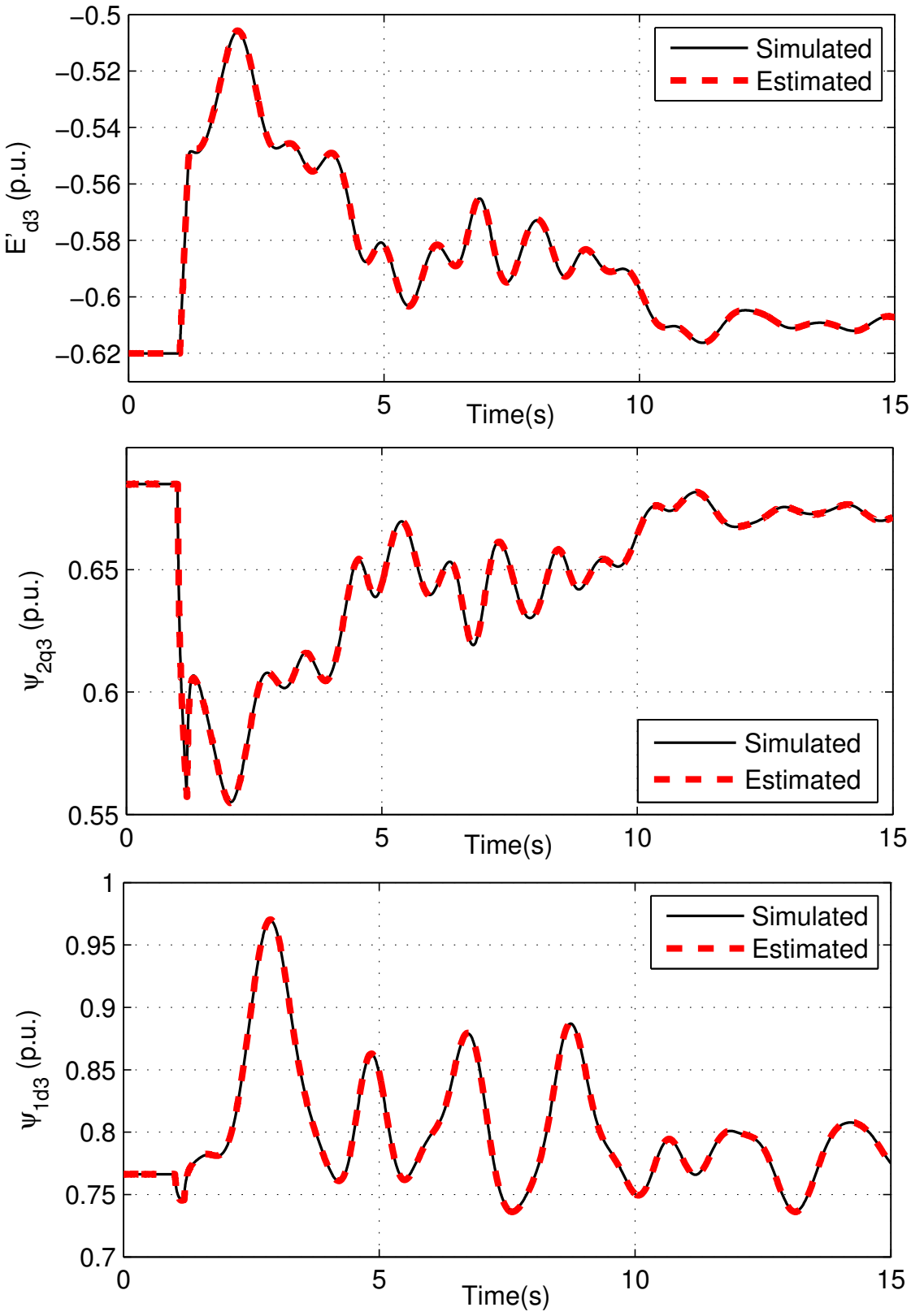

Figure 3.8: Estimated vs simulated values for E'_d, Ψ_{2q} and Ψ_{1d} of the 3^{rd} unit

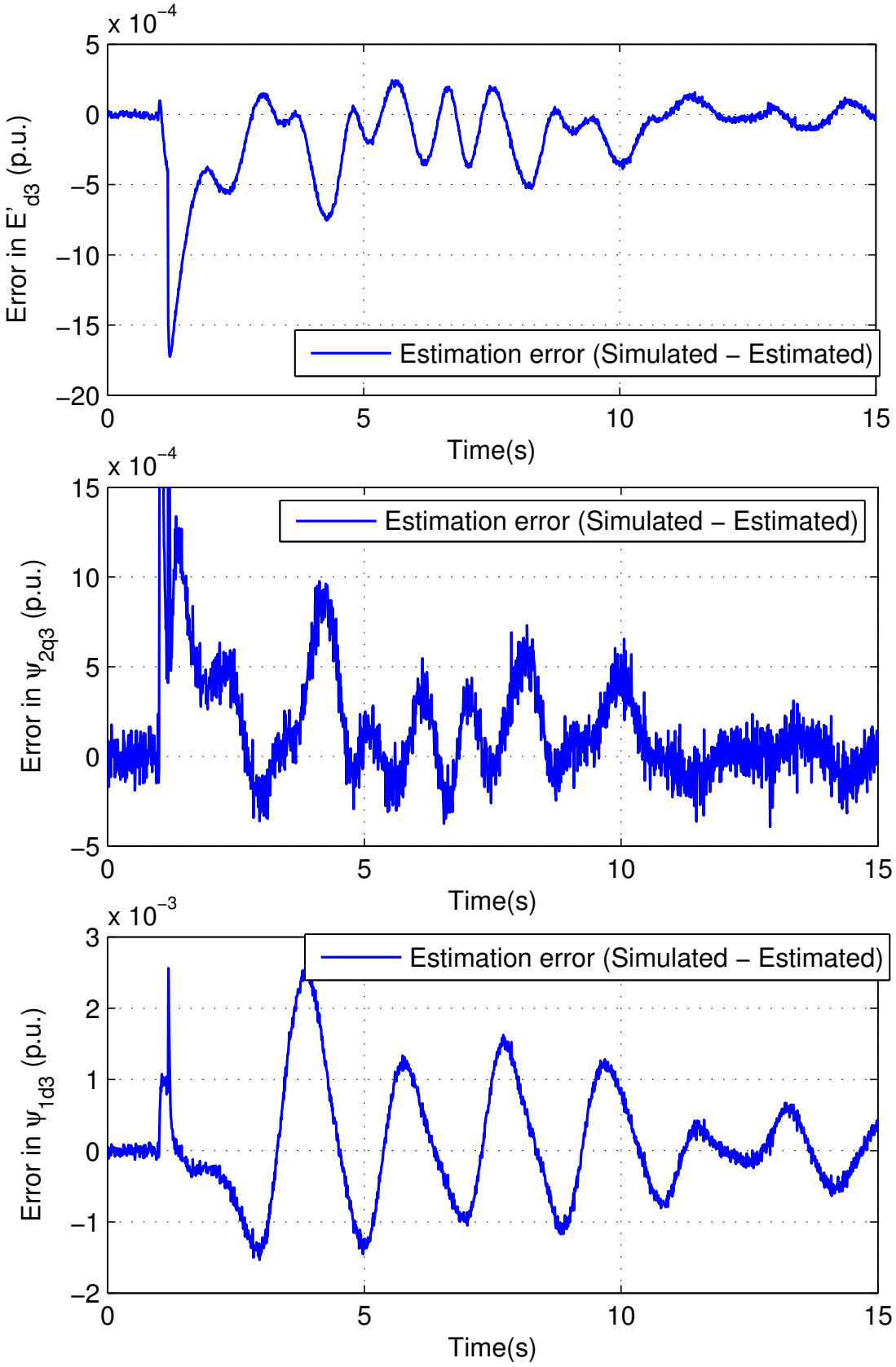

Figure 3.9: Estimation errors for E'_d, Ψ_{2q} and Ψ_{1d} of the 3^{rd} unit

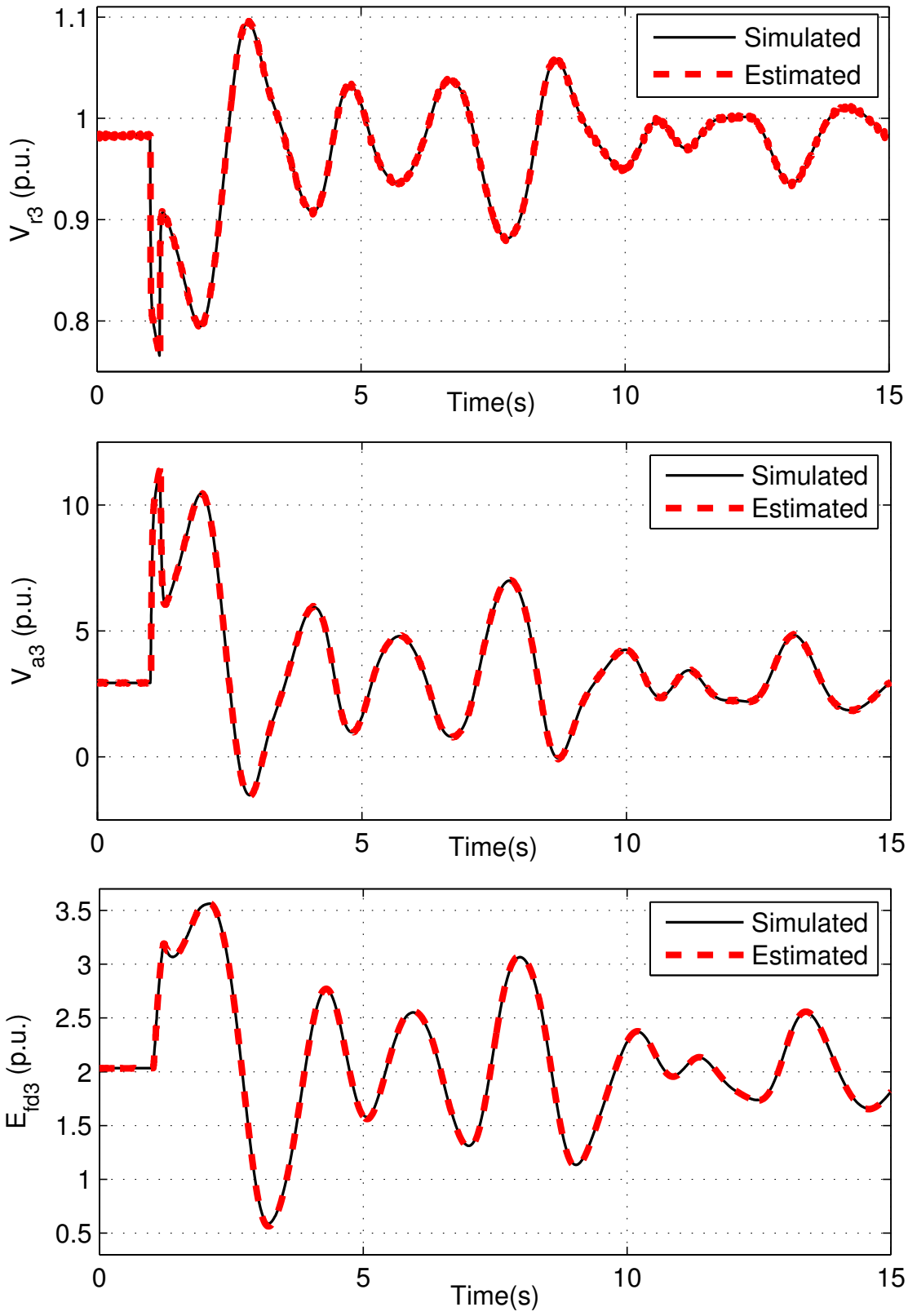

Figure 3.10: Estimated vs simulated values for V_{r3}, V_{a3} and E_{fd3} of the 3^{rd} unit

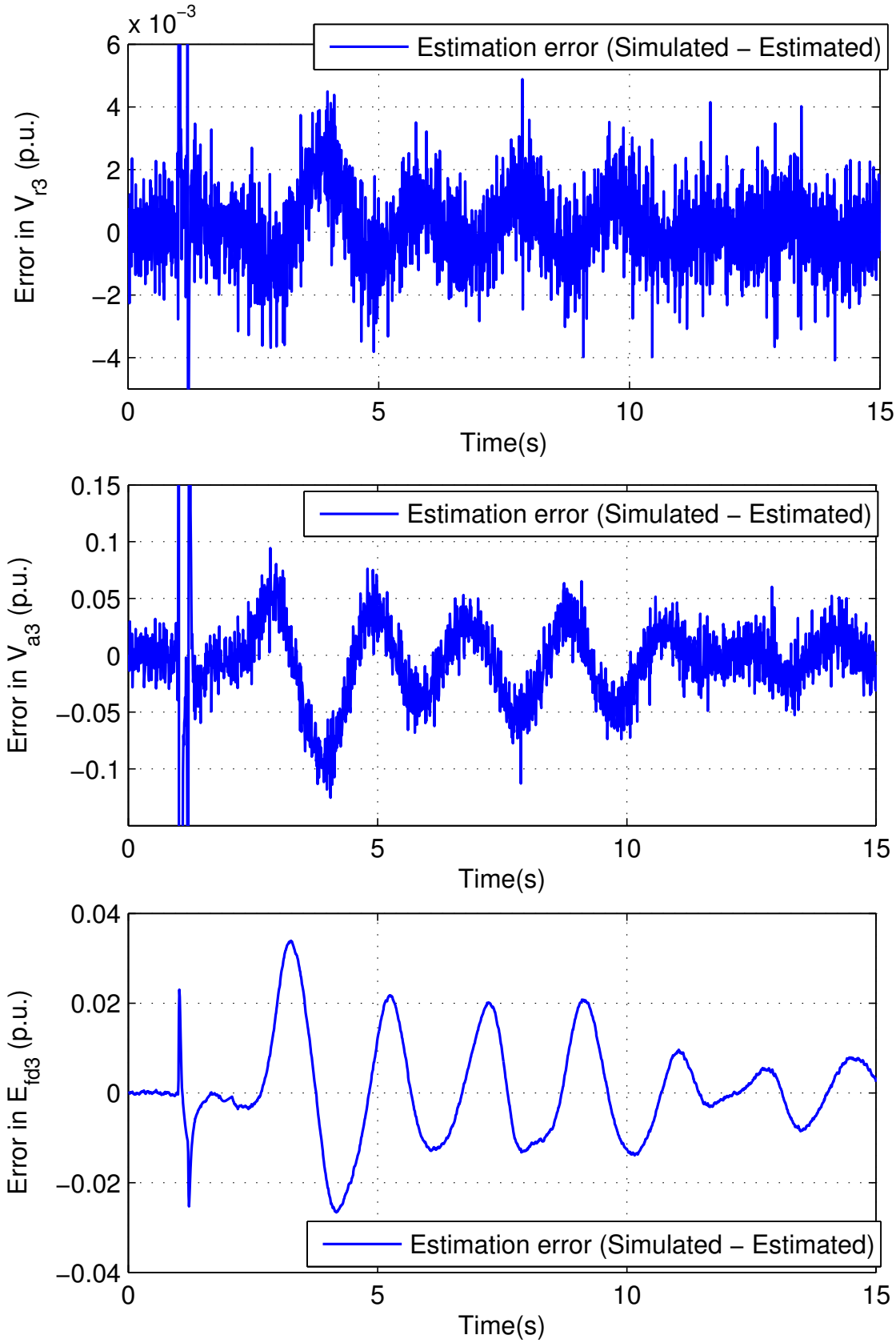

Figure 3.11: Estimation errors for V_{r3}, V_{a3} and E_{fd3} of the 3^{rd} unit

3.5.2.3 Sensitivity to noise

The robustness of the proposed algorithm to higher noise variances was also tested. For this, the variances $\boldsymbol{P}_{zi}$ and $\boldsymbol{P}_{wi}$ were varied in multiples of tens of their base-case values, $\boldsymbol{P}_{z0}$ and $\boldsymbol{P}_{w0}$, and the effect on estimation-accuracy was observed. Fig. 3.12 shows the effect of variations in noise-variances on the estimation of ω for the *type 2* of generation unit, and Fig. 3.13 shows the corresponding estimation errors. The plots have been shown for a portion of the total simulation time for clarity.

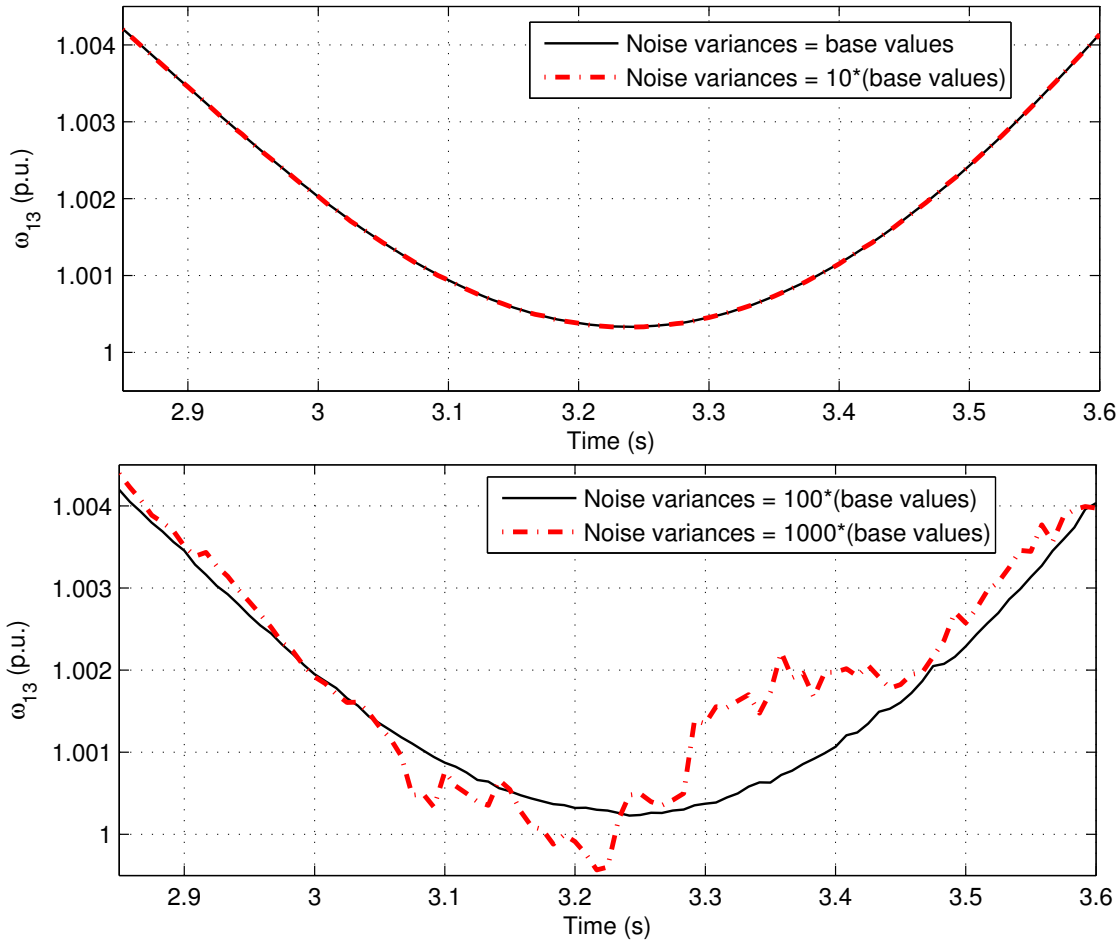

Figure 3.12: Effect of noise variances on the accuracy of estimation

It is evident from Fig. 3.12 and Fig. 3.13 that the algorithm is robust, with minor errors in estimated values, even when the noise-variances are hundred times their base-case values. When the noise-variances are thousand times the base-case variances, the estimated states have significant errors and deviations, and hence become unusable.

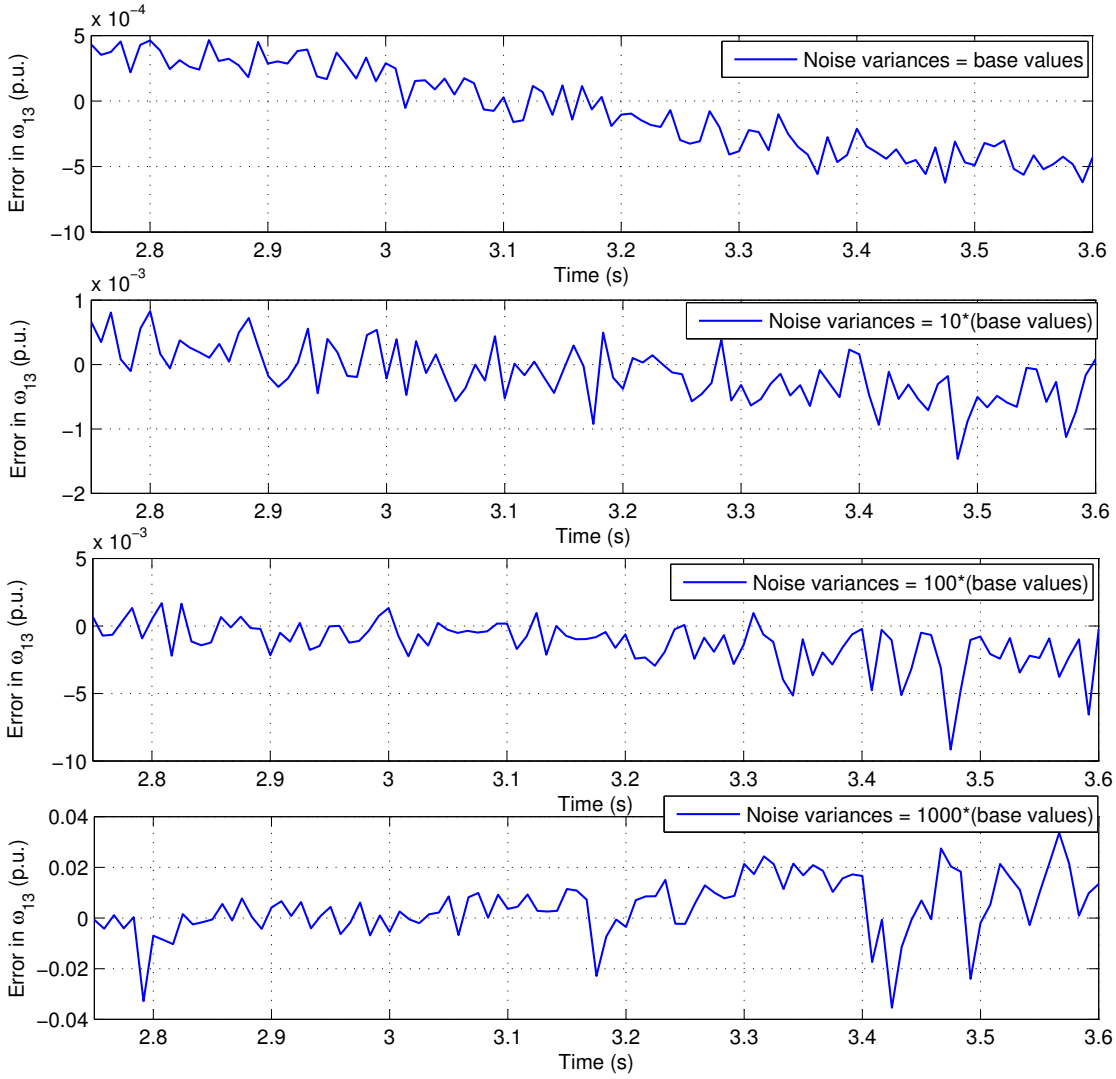

Figure 3.13: Effect of noise variances on estimation errors

3.6 Bad-data detection

PMU signals not only suffer from noise, but they are also prone to gross errors; and therefore a bad-data detection algorithm is required for the proposed decentralized estimator. Bad data detection in UKF is based on the fact that the ratio between the deviation of actual measurement from the predicted measurement and the expected standard deviation of the predicted measurement remains bounded in a narrow band in the absence of any bad data; and this ratio is called as normalized innovation ratio [30], [31]. Mathematically, this fact may be stated using (3.62) and (3.63), where $\lambda_{y_{i,1}}$ and $\lambda_{y_{i,2}}$ are the normalized innovation ratios for the two measurements $y_{i,1} = I_{yi}$ and $y_{i,2} = \phi_{yi}$, respectively (Recall that $\boldsymbol{y}_i = [I_{yi}, \phi_{yi}]^T$); $\hat{\boldsymbol{y}}_i^- = [\hat{y}_{i,1}^-, \hat{y}_{i,2}^-]^T$; $P_{yi,1}^-$ is the first diagonal element of $\boldsymbol{P}_{yi}^-$; and $P_{yi,2}^-$ is the second

diagonal element of $\boldsymbol{P}_{yi}^{-}$.

$$\lambda_{y_{i,1}} < \lambda_0; \text{ where } \lambda_{y_{i,1}} = \frac{|y_{i,1} - \hat{y}_{i,1}^{-}|}{\sqrt{P_{yi,1}^{-}}} \tag{3.62}$$

$$\lambda_{y_{i,2}} < \lambda_0; \text{ where } \lambda_{y_{i,2}} = \frac{|y_{i,2} - \hat{y}_{i,2}^{-}|}{\sqrt{P_{yi,2}^{-}}} \tag{3.63}$$

λ_0 depends on type of the system, and it may be found using off-line simulations [30], [31]. For the system in case study, λ_0 was found to be 10. Hence, a measurement is labeled as a bad measurement if its normalized innovation ratio comes out to be more than λ_0 in a given sample, and is thus discarded and the actual measurement is assumed to be same as the predicted measurement for that sample.

The above technique for bad data detection would have worked flawlessly if there wasn't any bad data present in the states or input. But since pseudo-inputs are used in the decentralized UKF algorithm, which are in reality measurements, bad-data may also be present in these pseudo-inputs. Innovation ratios are not defined for pseudo-inputs, and hence we cannot directly detect bad-data in them; but an indirect method may be used to do so. This method is based on the fact that the predicted measurements are influenced by bad-data in the pseudo-inputs but the actual measurements remain independent of these bad-data, and hence in the case of bad-data in pseudo-inputs no correlation exists between the actual measurements and the predicted measurements. In other words, if bad data is introduced in one or more pseudo-input(s) in a given sample, then both $\hat{\boldsymbol{y}}_i^{-}$ and $\boldsymbol{P}_{yi}^{-}$ would change significantly from their correct values, and this change will be completely uncorrelated with $\boldsymbol{y}_i$, even if bad data is present in $\boldsymbol{y}_i$ as well (assuming that all the bad-data are introduced randomly and independently), and thus the values of both $\lambda_{y_{i,1}}$ and $\lambda_{y_{i,2}}$ are expected to exceed λ_0 in such an event. Thus, we need to modify the technique in the previous paragraph, and discard all the pseudo-inputs if both $\lambda_{y_{i,1}}$ and $\lambda_{y_{i,2}}$ exceed λ_0 in a given sample, and use the latest uncorrupted pseudo-inputs instead. Thus, the bad-data detection for the k^{th} sample takes place according to the following algorithm.

Algorithm 2: Bad-data detection in the i^{th} generation unit

STEP 1:

Perform the first four steps of **Algorithm 1**.

STEP 2:

Find $\lambda_{y_{i,1}}$ and $\lambda_{y_{i,2}}$ according to (3.62) and (3.63), respectively.

STEP 3:

if $\lambda_{y_{i,1}} < \lambda_0$ and $\lambda_{y_{i,2}} < \lambda_0$ **then** goto **STEP 5**

else

if $\lambda_{y_{i,1}} > \lambda_0$ and $\lambda_{y_{i,2}} < \lambda_0$ **then** $y_{i,1} = \hat{y}_{i,1}^{-}$, goto **STEP 5**

else

if $\lambda_{y_{i,1}} < \lambda_0$ and $\lambda_{y_{i,2}} > \lambda_0$ **then** $y_{i,2} = \hat{y}_{i,2}^{-}$, goto **STEP 5**

else

if $\lambda_{y_{i,1}} > \lambda_0$ and $\lambda_{y_{i,2}} > \lambda_0$ **then** discard $\boldsymbol{u_i'}$ and again perform the first four steps of **Algorithm 1** using the latest uncorrupted value of $\boldsymbol{u_i'}$. Again find $\lambda_{y_{i,1}}$ and $\lambda_{y_{i,2}}$ according to (3.62) and (3.63), respectively.

STEP 4:

if $\lambda_{y_{i,1}} < \lambda_0$ and $\lambda_{y_{i,2}} < \lambda_0$ **then** goto **STEP 5**

else

if $\lambda_{y_{i,1}} > \lambda_0$ and $\lambda_{y_{i,2}} < \lambda_0$ **then** $y_{i,1} = \hat{y}_{i,1}^{-}$, goto **STEP 5**

else

if $\lambda_{y_{i,1}} < \lambda_0$ and $\lambda_{y_{i,2}} > \lambda_0$ **then** $y_{i,2} = \hat{y}_{i,2}^{-}$, goto **STEP 5**

else

if $\lambda_{y_{i,1}} > \lambda_0$ and $\lambda_{y_{i,2}} > \lambda_0$ **then** $y_{i,1} = \hat{y}_{i,1}^{-}$ and $y_{i,2} = \hat{y}_{i,2}^{-}$.

STEP 5:

Perform the last two steps of **Algorithm 1**.

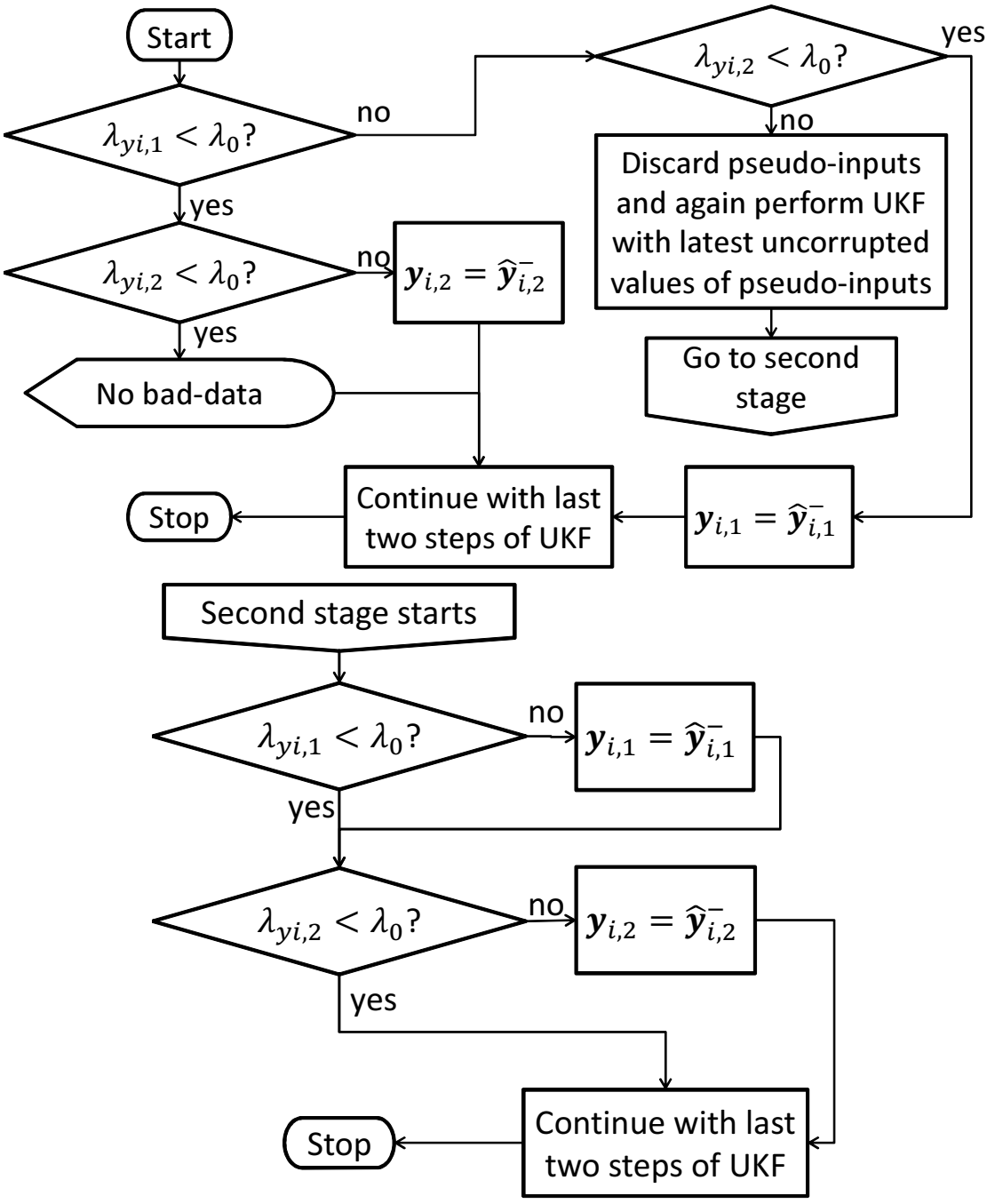

Figure 3.14: Flowchart for bad data detection

A bad-data detector based on **Algorithm 2** was implemented and integrated in the decentralized UKF algorithm. Values of $\lambda_{y_{i,1}}$ and $\lambda_{y_{i,2}}$, and estimated rotor velocity for $i = 13$, have been shown for three cases, all in Fig. 3.15:

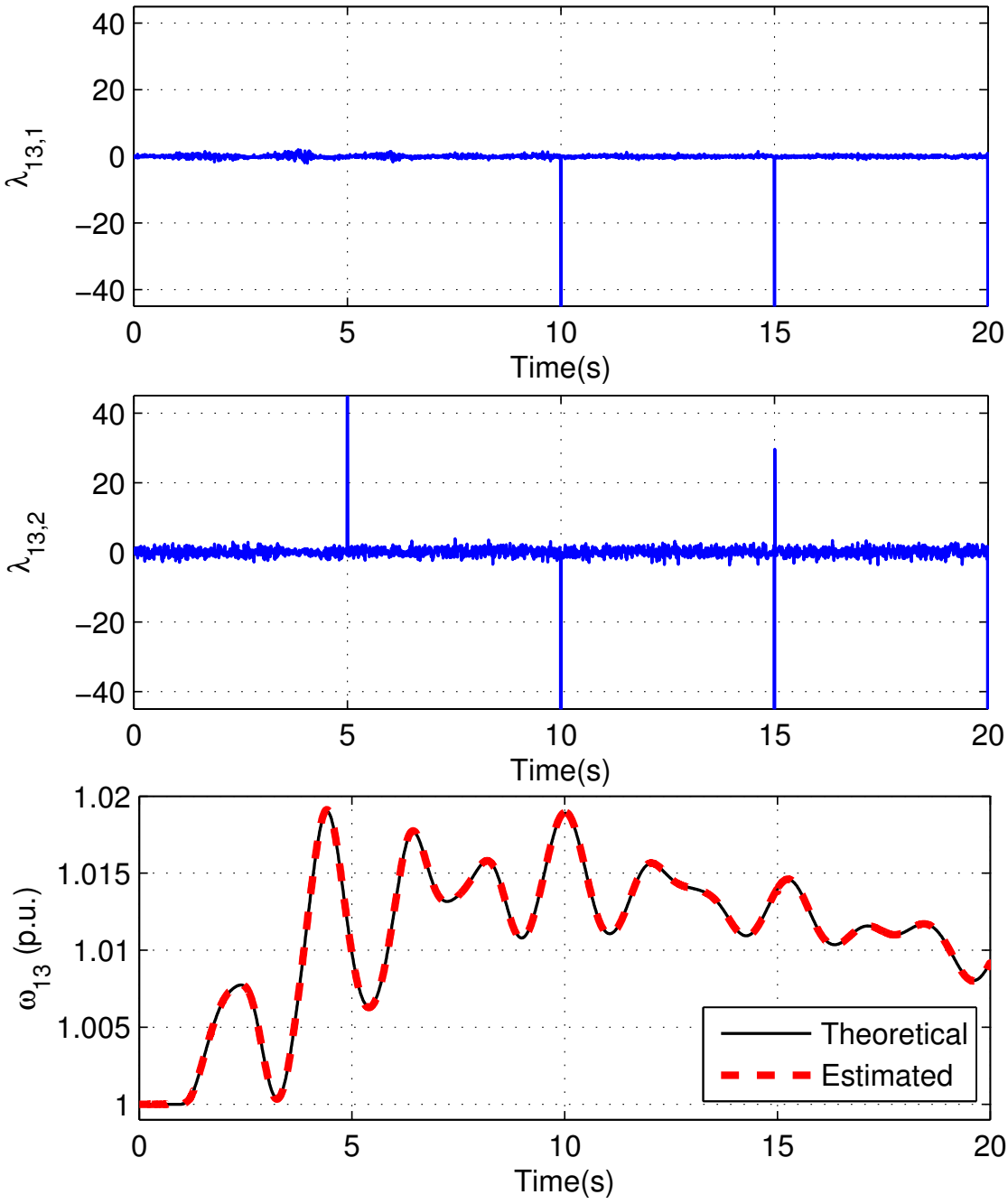

Figure 3.15: Bad-data detection

1. *Bad-data present only in one of the measurements:* In this case bad-data is introduced in the measurement ϕ_{y13} of magnitude +0.4 p.u. (i.e. the measured value of ϕ_{y13} is 0.01 p.u. above its true value), at time t = 5s. It

may be observed that the bad-data detector effectively handles this anomaly, and there is no effect on $\lambda_{y_{13,1}}$, and the estimation process remains unaffected.

2. *Bad-data present only in one of the pseudo-inputs:* In this case bad-data is introduced in the pseudo-input V_{y13} of magnitude +0.2, at time $t = 10s$. It may be observed that both $\lambda_{y_{13,1}}$ and $\lambda_{y_{13,2}}$ become unbounded, but the bad-data detector effectively handles this anomaly as well, as the estimation process remains unaffected.

3. *Bad-data present simultaneously in one of the measurements and in one of the pseudo-inputs:* In this case bad-data is introduced in the measurement ϕ_{y13} of magnitude +0.4 p.u., and another bad-data is introduced in the pseudo-input V_{y13} of magnitude +0.2 p.u., both at $t = 15s$. It may be observed that both $\lambda_{y_{13,1}}$ and $\lambda_{y_{13,2}}$ become unbounded, as in previous case, but the bad-data detector effectively handles this anomaly as well.

Thus, the proposed two-stage bad data detector successfully filters out bad-data in all the three possible cases. This bad-data detector is another important contribution of the thesis.

3.7 Summary

A scheme for decentralized estimation of the dynamic states of a power system has been proposed in this chapter. The scheme preserves non-linearity in the system and improves efficiency over other non-linear filters through unscented Kalman filtering. The basic idea of decentralization in the scheme is based on treating some of the measured signals as pseudo inputs. The advantages of the proposed scheme over the centralized schemes have been presented in terms of speed, feasibility, simplicity and high accuracy. The scheme is also robust to moderately-high noise levels and gross errors in measurement signals.

The key advantages of the proposed scheme may be summarized as follows:

1. The signals required for estimation (which are the generator voltage and current) are easy to measure using PMUs.

2. Each distributed estimator has to estimate only local states of the corresponding generation unit. Therefore the estimator is very fast and its speed

remains independent of the size of the system, unlike a centralized scheme. This is the biggest advantage over a centralized scheme as for a large power system, the number of states a central estimator has to estimate is very large, requiring huge computational capacity for real-time estimation.

3. Remote signals need not be transmitted; therefore the estimation process is not affected by network problems such as transmission delays and losses. Also, the signal sampling rates are not limited by network bandwidth.

4. State estimation for one generation unit is completely independent from estimation for other units. Thus, errors in estimation remain isolated and are easier to pin-point than in a centralized estimation scheme.

5. PMUs only need to be installed at each generation unit, and most power stations are likely to have installation of PMUs.

The proposed scheme should serve as a highly practical method of dynamic state estimation for dynamic control and dynamic security assessment in modern power systems.

Chapter 4

Extended linear quadratic regulator

This chapter aims to provide a decentralized control law using dynamic state estimates which were obtained in the last chapter. The control law should be such that it minimizes the state deviation costs and the required control effort. The theory of optimal control of dynamic systems is appropriate in this context, as it involves cost effective operation of a system by optimizing the sum of costs associated with system states and control inputs. Also, linear control is the most developed and widely adopted technology for ensuring small-signal stability in power systems (as a non-linear power system can be approximated with a linear equivalent if deviations from equilibrium point are small). Therefore, this chapter focuses on linear optimal control theory.

The particular case of optimal control in which dynamics of a system are described by linear differential equations, and cost is a quadratic function of states and control-effort, is called linear quadratic (LQ) problem [53], [81]. Solution to the LQ problem is provided by linear quadratic regulator (LQR), which is a state feedback controller [73].

The decentralized DAEs used in the last chapter involved pseudo-inputs. As pseudo-inputs are actually measurements, they can neither be disabled nor be manipulated, unlike traditional inputs given to a system. Pseudo-inputs are very similar to exogenous inputs found in control literature. Some examples of dynamic systems with exogenous inputs can be found in [82], [83] and [84]. Pseudo-inputs will be referred to as exogenous inputs in this chapter in order to develop a generalized framework for control of linear systems with such inputs.

The problem of optimal control of LTI systems with exogenous inputs has been termed as the extended linear quadratic (ELQ) problem in this chapter. It is assumed in the LQR solution that all of the inputs given to the system are normal inputs, which means that each of the input can be manipulated by the controller. The ELQ problem cannot be addressed by the LQR solution, as the exogenous inputs can neither be avoided nor be changed. So, they alter the dynamic behaviour of the system and the associated costs. A solution for the ELQ problem will need to incorporate feedback terms corresponding to the exogenous inputs. As a solution to the ELQ problem, or a related problem, is not available in the control literature, the objective of this chapter is to clearly state the ELQ problem and to provide its solution.

Rest of the chapter is organized as follows. Section 4.1 formally states the ELQ problem. Section 4.2 explains the classical LQR solution, while Section 4.3 describes the ELQ problem and its solution. This solution is demonstrated on an example LTI system in Section 4.4; and Section 4.5 concludes the chapter.

4.1 Problem statement

Some preliminary definitions:

Definition 1: A 'normal input' given to an LTI system is an input whose magnitude can be decided and changed as per any required control scheme. This is the input in the traditional sense system theory.

Definition 2: An 'exogenous input' given to an LTI system is an input which cannot be removed from the system and whose magnitude cannot be decided or changed. This input is an unavoidable quantity which cannot be used as a control input in corrective actions.

Using the above two definitions, the ELQ problem is stated as follows:

For a discrete-time open-loop LTI system in which both normal and exogenous inputs are present, find an optimal control law such that the sum of the quadratic costs associated with the system states, the exogenous inputs and the normal inputs is minimized.

Thus, the aim of the ELQ problem is to control the system via its normal inputs under the constraints of exogenous inputs.

4.2 Classical LQR control (without exogenous inputs)

A discrete-time open-loop LTI system without any exogenous input is represented by the following equation:

$$\boldsymbol{x}_{k+1} = \boldsymbol{A}\boldsymbol{x}_k + \boldsymbol{B}\boldsymbol{u}_k \tag{4.1}$$

The quadratic cost function for (4.1) for N samples is given by:

$$\boldsymbol{J} = \sum\nolimits_{k=0}^{N-1} [\boldsymbol{x}_k^T \boldsymbol{Q} \boldsymbol{x}_k + \boldsymbol{u}_k^T \boldsymbol{R} \boldsymbol{u}_k] \text{ where } \boldsymbol{Q} \geq 0,\ \boldsymbol{R} > 0 \tag{4.2}$$

Minimizing $\boldsymbol{J}$ with respect to $\boldsymbol{u}_k$ gives the following LQR solution:

$$\boldsymbol{u}_k = -\boldsymbol{F}_k \boldsymbol{x}_k, \quad k = 0, 1, \ldots, (N-1),\ \boldsymbol{u}_N = \boldsymbol{0}; \tag{4.3}$$

$$\boldsymbol{F}_{k-1} = (\boldsymbol{R} + \boldsymbol{B}^T \boldsymbol{P}_k \boldsymbol{B})^{-1} \boldsymbol{B}^T \boldsymbol{P}_k \boldsymbol{A},\ \boldsymbol{P}_N = \boldsymbol{Q}, \tag{4.4}$$

$$\text{and, } \boldsymbol{P}_{k-1} = \boldsymbol{Q} + \boldsymbol{A}^T [\boldsymbol{P}_k - \boldsymbol{P}_k \boldsymbol{B} (\boldsymbol{R} + \boldsymbol{B}^T \boldsymbol{P}_k \boldsymbol{B})^{-1} \boldsymbol{B}^T \boldsymbol{P}_k] \boldsymbol{A} \tag{4.5}$$

If N is finite then the above optimal control policy is called as finite horizon LQR; otherwise it is infinite horizon LQR. Moreover, $\boldsymbol{P}_k$ and $\boldsymbol{F}_k$ for the infinite horizon case are bounded and have a steady-state solution if and only if the pair $(\boldsymbol{A}, \boldsymbol{B})$ is stabilizable, and the steady-state solution is found by solving the following discrete-time algebraic Riccati equation (ARE):

$$\boldsymbol{P} = \boldsymbol{Q} + \boldsymbol{A}^T [\boldsymbol{P} - \boldsymbol{P}\boldsymbol{B} (\boldsymbol{R} + \boldsymbol{B}^T \boldsymbol{P}\boldsymbol{B})^{-1} \boldsymbol{B}^T \boldsymbol{P}] \boldsymbol{A}; \tag{4.6}$$

$$\boldsymbol{F} = (\boldsymbol{R} + \boldsymbol{B}^T \boldsymbol{P}\boldsymbol{B})^{-1} \boldsymbol{B}^T \boldsymbol{P}\boldsymbol{A} \tag{4.7}$$

4.3 Extended LQR (ELQR) control (with exogenous inputs)

A discrete-time open-loop LTI system with both normal and exogenous inputs is given by the following equation:

$$\boldsymbol{x}_{k+1} = \boldsymbol{A}\boldsymbol{x}_k + \boldsymbol{B}\boldsymbol{u}_k + \boldsymbol{B}'\boldsymbol{u}'_k \tag{4.8}$$

The discrete system equation in (4.8) has an extra term (corresponding to the exogenous inputs) as compared to the system given by (4.1). Thus the quadratic-cost for this system gets modified. For N samples it is given by:

$$\boldsymbol{J'} = \sum_{k=0}^{N-1} [\boldsymbol{x}_k^T \boldsymbol{Q} \boldsymbol{x}_k + \boldsymbol{u}_k^T \boldsymbol{R} \boldsymbol{u}_k + \boldsymbol{u}_k'^T \boldsymbol{R}' \boldsymbol{u}'_k], \quad \text{where, } \boldsymbol{Q} \geq 0,\ \boldsymbol{R} > 0,\ \boldsymbol{R}' \geq 0; \tag{4.9}$$

The optimal control policy for (4.8) can be found by minimizing $\boldsymbol{J'}$ in (4.9) with respect to $\boldsymbol{u}_k$, and has been rigorously derived, giving the following theorem:

Theorem 4.1. *For an LTI system with exogenous inputs or pseudo-inputs (as given by* (4.8)*), provided* $\boldsymbol{u}'_k = \boldsymbol{0}\ \forall\ k \geq N$*, the optimal control policy for* $0 \leq k < N$ *is given by* (4.10)-(4.13) *(and for* $k \geq N, \boldsymbol{u}_k = \boldsymbol{0}$*).*

$$\boldsymbol{u}_k = -(\boldsymbol{F}_k \boldsymbol{x}_k + \boldsymbol{G}_k \boldsymbol{u}'_k + \boldsymbol{G}'_k); \tag{4.10}$$

$$\boldsymbol{G}_k = \boldsymbol{F}_k (\boldsymbol{P}_k - \boldsymbol{Q})^{-1} \boldsymbol{S}_k,\ \boldsymbol{G}'_k = \boldsymbol{F}_k (\boldsymbol{P}_k - \boldsymbol{Q})^{-1} \boldsymbol{S}'_k; \tag{4.11}$$

$$\boldsymbol{S}_N = \boldsymbol{0}, \boldsymbol{S}'_N = \boldsymbol{0}, \boldsymbol{S}_k = (\boldsymbol{A} - \boldsymbol{B}\boldsymbol{F}_k)^T (\boldsymbol{P}_{k+1}\boldsymbol{B}' + \boldsymbol{S}_{k+1}), \tag{4.12}$$

$$\boldsymbol{S}'_k = (\boldsymbol{A} - \boldsymbol{B}\boldsymbol{F}_k)^T (\boldsymbol{S}_{k+1}(\boldsymbol{u}'_{k+1} - \boldsymbol{u}'_k) + \boldsymbol{S}'_{k+1}) \tag{4.13}$$

$\boldsymbol{F}_k$ *and* $\boldsymbol{P}_k$ *remain same as the LQR case (given by* (4.4)-(4.5)*).*

Proof. A preliminary modification needs to be done in the system given by (4.8) for the derivation of Theorem 4.1, by adding a constant exogenous input at the end of the column vector $\boldsymbol{u}'_k$, as:

$$\boldsymbol{x}_{k+1} = \boldsymbol{A}\boldsymbol{x}_k + \boldsymbol{B}\boldsymbol{u}_k + \boldsymbol{B}_1\boldsymbol{v}_k; \text{ where, } \boldsymbol{v}_k = \begin{bmatrix} \boldsymbol{u}'_k \\ 1 \end{bmatrix}, \ \boldsymbol{B}_1 = \begin{bmatrix} \boldsymbol{B}' & \boldsymbol{0}_{m\times 1} \end{bmatrix}; \tag{4.14}$$

Also, $\boldsymbol{v}_k = \boldsymbol{E}_k\boldsymbol{v}_{k-1}$,

$$\text{where, } \boldsymbol{E}_k = \begin{bmatrix} \boldsymbol{I}_r & \Delta\boldsymbol{u}'_k \\ \boldsymbol{0}_{1\times r} & 1 \end{bmatrix}, \text{ and, } \Delta\boldsymbol{u}'_k = \boldsymbol{u}'_k - \boldsymbol{u}'_{k-1}; \tag{4.15}$$

$$\boldsymbol{B}_1\boldsymbol{v}_k = \begin{bmatrix} \boldsymbol{B}' & \boldsymbol{0}_{m\times 1} \end{bmatrix} \begin{bmatrix} \boldsymbol{u}'_k \\ 1 \end{bmatrix} = \boldsymbol{B}'\boldsymbol{u}'_k + \boldsymbol{0}_{m\times 1} = \boldsymbol{B}'\boldsymbol{u}'_k \tag{4.16}$$

Here m is the number of elements in $\boldsymbol{x}_k$ and r is the number of elements in $\boldsymbol{u}'_k$. It should be understood that because of (4.16), the above modification has no effect on the dynamics of the original system. The modification is needed to get an iterative expression for the optimal control policy. On its own, $\boldsymbol{u}'_k$ cannot be expressed in terms of $\boldsymbol{u}'_{k-1}$. But when a new pseudo-input vector $\boldsymbol{v}_k$ is defined by appending a constant value 1 at the end of $\boldsymbol{u}'_k$, then $\boldsymbol{v}_k$ can be expressed in terms of $\boldsymbol{v}_{k-1}$ using (4.15). The quadratic-cost for the modified system (given by (4.14)) for N samples is given by:

$$\boldsymbol{J'} = \sum\nolimits_{k=0}^{N-1} [\boldsymbol{x}_k^T\boldsymbol{Q}\boldsymbol{x}_k + \boldsymbol{u}_k^T\boldsymbol{R}\boldsymbol{u}_k + \boldsymbol{v}_k^T\boldsymbol{R}_1\boldsymbol{v}_k], \tag{4.17}$$

$$\text{where, } \boldsymbol{R}_1 = \begin{bmatrix} \boldsymbol{R}' & \boldsymbol{0}_{r\times 1} \\ \boldsymbol{0}_{1\times r} & 0 \end{bmatrix}, \boldsymbol{Q} \geq 0, \boldsymbol{R} > 0, \boldsymbol{R}' \geq 0 \tag{4.18}$$

$$\boldsymbol{v}_k^T\boldsymbol{R}_1\boldsymbol{v}_k = \begin{bmatrix} \boldsymbol{u}_k'^T & 1 \end{bmatrix} \begin{bmatrix} \boldsymbol{R}' & \boldsymbol{0}_{r\times 1} \\ \boldsymbol{0}_{1\times r} & 0 \end{bmatrix} \begin{bmatrix} \boldsymbol{u}'_k \\ 1 \end{bmatrix} = \boldsymbol{u}_k'^T\boldsymbol{R}'\boldsymbol{u}'_k \tag{4.19}$$

Equation (4.19) and the definition of $\boldsymbol{R}_1$ (given by (4.18)) ensure that the constant exogenous input in $\boldsymbol{v}_k$ has zero cost, so that the quadratic-costs for the modified

system and the original system (as given by (4.17) and (4.9), respectively) are identical.

As it is given that $\boldsymbol{u}'_k = \mathbf{0}\ \forall\ k \geq N$, and the system reaches its final steady state, $\boldsymbol{x}_N$, at $k = N$, hence the optimal input required is $\boldsymbol{u}_k = \mathbf{0}\ \forall\ k \geq N$. The optimal cost for $k = N$ is therefore $\boldsymbol{J}'^{opt}_N = \boldsymbol{x}^T_N \boldsymbol{Q} \boldsymbol{x}_N = \boldsymbol{x}^T_N \boldsymbol{P}_N \boldsymbol{x}_N$. The combined quadratic cost for $k = N-1$ and $k = N$, provided that the cost for $k = N$ is optimal (which is $\boldsymbol{J}'^{opt}_N$), is given by $\boldsymbol{J}'_{N-1}$ as:

$$\boldsymbol{J}'_{N-1} = \boldsymbol{x}^T_{N-1} \boldsymbol{Q} \boldsymbol{x}_{N-1} + \boldsymbol{u}^T_{N-1} \boldsymbol{R} \boldsymbol{u}_{N-1} + \boldsymbol{v}^T_{N-1} \boldsymbol{R}_1 \boldsymbol{v}_{N-1} + \boldsymbol{J}'^{opt}_N \tag{4.20}$$

Substituting $\boldsymbol{J}'^{opt}_N = \boldsymbol{x}^T_N \boldsymbol{P}_N \boldsymbol{x}_N$ and $\boldsymbol{x}_N = \boldsymbol{A}\boldsymbol{x}_{N-1} + \boldsymbol{B}\boldsymbol{u}_{N-1} + \boldsymbol{B}_1 \boldsymbol{v}_{N-1}$ in (4.20):

$$\begin{aligned} \boldsymbol{J}'_{N-1} = {} & \boldsymbol{x}^T_{N-1} \boldsymbol{Q} \boldsymbol{x}_{N-1} + \boldsymbol{u}^T_{N-1} \boldsymbol{R} \boldsymbol{u}_{N-1} + \boldsymbol{v}^T_{N-1} \boldsymbol{R}_1 \boldsymbol{v}_{N-1} \\ & + (\boldsymbol{A}\boldsymbol{x}_{N-1} + \boldsymbol{B}\boldsymbol{u}_{N-1} + \boldsymbol{B}_1 \boldsymbol{v}_{N-1})^T \boldsymbol{P}_N (\boldsymbol{A}\boldsymbol{x}_{N-1} + \boldsymbol{B}\boldsymbol{u}_{N-1} + \boldsymbol{B}_1 \boldsymbol{v}_{N-1}) \end{aligned} \tag{4.21}$$

Finding the partial derivative of $\boldsymbol{J}'_{N-1}$ in above equation with respect to $\boldsymbol{u}_{N-1}$, $\partial \boldsymbol{J}'_{N-1} / \partial \boldsymbol{u}_{N-1}$ comes as:

$$\partial \boldsymbol{J}'_{N-1} / \partial \boldsymbol{u}_{N-1} = 2[\boldsymbol{R}\boldsymbol{u}_{N-1} + \boldsymbol{B}^T \boldsymbol{P}_N (\boldsymbol{A}\boldsymbol{x}_{N-1} + \boldsymbol{B}\boldsymbol{u}_{N-1} + \boldsymbol{B}_1 \boldsymbol{v}_{N-1})] \tag{4.22}$$

$$\because \partial \boldsymbol{J}'_{N-1} / \partial \boldsymbol{u}_{N-1} = \mathbf{0},\ \text{for}\ \boldsymbol{u}_{N-1} = \boldsymbol{u}^{opt}_{N-1}, \tag{4.23}$$

$$\therefore \boldsymbol{R}\boldsymbol{u}^{opt}_{N-1} + \boldsymbol{B}^T \boldsymbol{P}_N (\boldsymbol{A}\boldsymbol{x}_{N-1} + \boldsymbol{B}\boldsymbol{u}^{opt}_{N-1} + \boldsymbol{B}_1 \boldsymbol{v}_{N-1}) = \mathbf{0}, \tag{4.24}$$

$$\Rightarrow \boldsymbol{u}^{opt}_{N-1} = -(\boldsymbol{F}_{N-1} \boldsymbol{x}_{N-1} + \boldsymbol{H}_{N-1} \boldsymbol{v}_{N-1}), \tag{4.25}$$

$$\text{where,}\ \boldsymbol{F}_{N-1} = (\boldsymbol{R} + \boldsymbol{B}^T \boldsymbol{P}_N \boldsymbol{B})^{-1} \boldsymbol{B}^T \boldsymbol{P}_N \boldsymbol{A}, \tag{4.26}$$

$$\boldsymbol{H}_{N-1} = (\boldsymbol{R} + \boldsymbol{B}^T \boldsymbol{P}_N \boldsymbol{B})^{-1} \boldsymbol{B}^T \boldsymbol{P}_N \boldsymbol{B}_1 \tag{4.27}$$

Also, as $\partial^2 \boldsymbol{J}'_{N-1}/(\partial \boldsymbol{u}_{N-1})^2 = (\boldsymbol{R} + \boldsymbol{B}^T \boldsymbol{P}_N \boldsymbol{B}) > 0$ (as $\boldsymbol{R} > 0, \boldsymbol{P}_N \geq 0$) , and $\boldsymbol{J}'_{N-1}$ is quadratic function of $\boldsymbol{u}_{N-1}$, thus, $\boldsymbol{u}^{opt}_{N-1}$ gives global minimum for $\boldsymbol{J}'_{N-1}$. Substituting $\boldsymbol{u}^{opt}_{N-1}$ from (4.25) for $\boldsymbol{u}_{N-1}$ in (4.20):

$$\boldsymbol{J}'^{opt}_{N-1} = \boldsymbol{x}^T_{N-1} \boldsymbol{P}_{N-1} \boldsymbol{x}_{N-1} + 2\boldsymbol{x}^T_{N-1} \boldsymbol{U}_{N-1} \boldsymbol{v}_{N-1} + \boldsymbol{v}^T_{N-1} \boldsymbol{W}_{N-1} \boldsymbol{v}_{N-1}; \tag{4.28}$$

$$\text{where, } \boldsymbol{P}_{N-1} = \boldsymbol{Q} + \boldsymbol{F}^T_{N-1} \boldsymbol{R} \boldsymbol{F}_{N-1} + (\boldsymbol{A} - \boldsymbol{B}\boldsymbol{F}_{N-1})^T \boldsymbol{P}_N (\boldsymbol{A} - \boldsymbol{B}\boldsymbol{F}_{N-1}), \tag{4.29}$$

$$\boldsymbol{U}_{N-1} = \boldsymbol{F}^T_{N-1} \boldsymbol{R} \boldsymbol{H}_{N-1} + (\boldsymbol{A} - \boldsymbol{B}\boldsymbol{F}_{N-1})^T \boldsymbol{P}_N (\boldsymbol{B}_1 - \boldsymbol{B}\boldsymbol{H}_{N-1}), \tag{4.30}$$

$$\boldsymbol{W}_{N-1} = \boldsymbol{R}_1 + \boldsymbol{H}^T_{N-1} \boldsymbol{R} \boldsymbol{H}_{N-1} + (\boldsymbol{B}_1 - \boldsymbol{B}\boldsymbol{H}_{N-1})^T \boldsymbol{P}_N (\boldsymbol{B}_1 - \boldsymbol{B}\boldsymbol{H}_{N-1}) \tag{4.31}$$

Again, the combined quadratic cost for $k = (N-2)$, $(N-1)$ and N, provided that the combined cost for $k = (N-1)$ and N is optimal (which is $\boldsymbol{J}'^{opt}_{N-1}$), is given by $\boldsymbol{J}'_{N-2} = \boldsymbol{x}^T_{N-2} \boldsymbol{Q} \boldsymbol{x}_{N-2} + \boldsymbol{u}^T_{N-2} \boldsymbol{R} \boldsymbol{u}_{N-2} + \boldsymbol{v}^T_{N-2} \boldsymbol{R}_1 \boldsymbol{v}_{N-2} + \boldsymbol{J}'^{opt}_{N-1}$, and following the same aforementioned steps applied to find $\boldsymbol{J}'^{opt}_{N-1}$, the values of $\boldsymbol{u}^{opt}_{N-2}$ and $\boldsymbol{J}'^{opt}_{N-2}$ come as:

$$\boldsymbol{u}^{opt}_{N-2} = -(\boldsymbol{F}_{N-2} \boldsymbol{x}_{N-2} + \boldsymbol{H}_{N-2} \boldsymbol{v}_{N-2}), \tag{4.32}$$

$$\text{where, } \boldsymbol{F}_{N-2} = (\boldsymbol{R} + \boldsymbol{B}^T \boldsymbol{P}_{N-1} \boldsymbol{B})^{-1} \boldsymbol{B}^T \boldsymbol{P}_{N-1} \boldsymbol{A}, \tag{4.33}$$

$$\boldsymbol{H}_{N-2} = (\boldsymbol{R} + \boldsymbol{B}^T \boldsymbol{P}_{N-1} \boldsymbol{B})^{-1} \boldsymbol{B}^T (\boldsymbol{P}_{N-1} \boldsymbol{B}_1 + \boldsymbol{U}_{N-1} \boldsymbol{E}_{N-1}); \tag{4.34}$$

$$\boldsymbol{J}'^{opt}_{N-2} = \boldsymbol{x}^T_{N-2} \boldsymbol{P}_{N-2} \boldsymbol{x}_{N-2} + 2\boldsymbol{x}^T_{N-2} \boldsymbol{U}_{N-2} \boldsymbol{v}_{N-2} + \boldsymbol{v}^T_{N-2} \boldsymbol{W}_{N-2} \boldsymbol{v}_{N-2}, \tag{4.35}$$

$$\text{where, } \boldsymbol{P}_{N-2} = (\boldsymbol{A} - \boldsymbol{B}\boldsymbol{F}_{N-2})^T \boldsymbol{P}_{N-1}(\boldsymbol{A} - \boldsymbol{B}\boldsymbol{F}_{N-2}) + \boldsymbol{F}_{N-2}^T \boldsymbol{R}\boldsymbol{F}_{N-2} + \boldsymbol{Q}, \quad (4.36)$$

$$\begin{aligned}\boldsymbol{U}_{N-2} = (\boldsymbol{A} - \boldsymbol{B}\boldsymbol{F}_{N-2})^T \boldsymbol{P}_{N-1}(\boldsymbol{B}_1 - \boldsymbol{B}\boldsymbol{H}_{N-2}) \\ + (\boldsymbol{A} - \boldsymbol{B}\boldsymbol{F}_{N-2})^T \boldsymbol{U}_{N-1}\boldsymbol{E}_{N-1} + \boldsymbol{F}_{N-2}^T \boldsymbol{R}\boldsymbol{H}_{N-2}, \quad (4.37)\end{aligned}$$

$$\begin{aligned}\boldsymbol{W}_{N-2} = (\boldsymbol{B}_1 - \boldsymbol{B}\boldsymbol{H}_{N-2})^T [\boldsymbol{P}_{N-1}(\boldsymbol{B}_1 - \boldsymbol{B}\boldsymbol{H}_{N-2}) + \boldsymbol{U}_{N-1}\boldsymbol{E}_{N-1}] \\ + \boldsymbol{E}_{N-1}^T \boldsymbol{W}_{N-1}\boldsymbol{E}_{N-1} + \boldsymbol{H}_{N-2}^T \boldsymbol{R}\boldsymbol{H}_{N-2} + \boldsymbol{R}_1 \quad (4.38)\end{aligned}$$

Next, when the terms $\boldsymbol{u}_{N-3}^{opt}$ and $\boldsymbol{J}_{N-3}^{\prime opt}$ are evaluated, their expressions are similar to (4.32) and (4.35), respectively, with the only change that $N-2$ is replaced by $N-3$, and $N-1$ is replaced by $N-2$. Similar expressions come for the rest of $\boldsymbol{u}_k^{opt}$ and $\boldsymbol{J}_k^{\prime opt}$(that is for $k < N-3$). Thus, using initial conditions $\boldsymbol{U}_N = \boldsymbol{0}_{m\times(r+1)}$ and $\boldsymbol{P}_N = \boldsymbol{Q}$, and applying induction for $k < N$, the optimal cost for $\boldsymbol{J}'$ in (4.17) comes as $\boldsymbol{J}_0^{\prime opt}$ (and is found by iteratively evaluating the sequence $\boldsymbol{J}_N^{\prime opt}$, $\boldsymbol{J}_{N-1}^{\prime opt}$, $\ldots$, $\boldsymbol{J}_1^{\prime opt}$, $\boldsymbol{J}_0^{\prime opt}$) and the corresponding optimal control policy required to arrive at this optimal cost is given by:

$$\boldsymbol{u}_k^{opt} = -(\boldsymbol{F}_k \boldsymbol{x}_k + \boldsymbol{H}_k \boldsymbol{v}_k),\ 0 \le k < N; \quad (4.39)$$

$$\text{where, } \boldsymbol{F}_k = (\boldsymbol{R} + \boldsymbol{B}^T \boldsymbol{P}_{k+1}\boldsymbol{B})^{-1} \boldsymbol{B}^T \boldsymbol{P}_{k+1}\boldsymbol{A} \quad (4.40)$$

$$\boldsymbol{H}_k = (\boldsymbol{R} + \boldsymbol{B}^T \boldsymbol{P}_{k+1}\boldsymbol{B})^{-1} \boldsymbol{B}^T (\boldsymbol{P}_{k+1}\boldsymbol{B}_1 + \boldsymbol{U}_{k+1}\boldsymbol{E}_{k+1}) \quad (4.41)$$

$$\boldsymbol{P}_k = \boldsymbol{Q} + \boldsymbol{F}_k^T \boldsymbol{R}\boldsymbol{F}_k + (\boldsymbol{A} - \boldsymbol{B}\boldsymbol{F}_k)^T \boldsymbol{P}_{k+1}(\boldsymbol{A} - \boldsymbol{B}\boldsymbol{F}_k) \quad (4.42)$$

$$\boldsymbol{U}_k = \boldsymbol{F}_k^T \boldsymbol{R}\boldsymbol{H}_k + (\boldsymbol{A} - \boldsymbol{B}\boldsymbol{F}_k)^T [\boldsymbol{P}_{k+1}(\boldsymbol{B}_1 - \boldsymbol{B}\boldsymbol{H}_k) + \boldsymbol{U}_{k+1}\boldsymbol{E}_{k+1}] \quad (4.43)$$

It may be noted that $\boldsymbol{W}_k$ has no role in deciding $\boldsymbol{u}_k^{opt}$. Also, $\boldsymbol{P}_k$ (using (4.42)) can be rewritten as:

$$\boldsymbol{P}_k = \boldsymbol{Q} + \boldsymbol{F}_k^T(\boldsymbol{R} + \boldsymbol{B}^T\boldsymbol{P}_{k+1}\boldsymbol{B})\boldsymbol{F}_k - \boldsymbol{F}_k^T\boldsymbol{B}^T\boldsymbol{P}_{k+1}\boldsymbol{A} + \boldsymbol{A}^T\boldsymbol{P}_{k+1}(\boldsymbol{A} - \boldsymbol{B}\boldsymbol{F}_k) \quad (4.44)$$

$$\because \boldsymbol{F}_k^T(\boldsymbol{R} + \boldsymbol{B}^T\boldsymbol{P}_{k+1}\boldsymbol{B})\boldsymbol{F}_k = \boldsymbol{F}_k^T\boldsymbol{B}^T\boldsymbol{P}_{k+1}\boldsymbol{A} \text{ (from (4.40))} \quad (4.45)$$

$$\therefore \boldsymbol{P}_k = \boldsymbol{Q} + \boldsymbol{A}^T\boldsymbol{P}_{k+1}(\boldsymbol{A} - \boldsymbol{B}\boldsymbol{F}_k), \quad (4.46)$$

Substituting $\boldsymbol{F}_k$ from (4.40) in (4.46) gives:

$$\boldsymbol{P}_k = \boldsymbol{Q} + \boldsymbol{A}^T(\boldsymbol{P}_{k+1}\boldsymbol{B}(\boldsymbol{R} + \boldsymbol{B}^T\boldsymbol{P}_{k+1}\boldsymbol{B})^{-1}\boldsymbol{B}^T\boldsymbol{P}_{k+1})\boldsymbol{A} \quad (4.47)$$

Similarly, $\boldsymbol{U}_k$ (using (4.43)) can be rewritten as:

$$\boldsymbol{U}_k = (\boldsymbol{A} - \boldsymbol{B}\boldsymbol{F}_k)^T(\boldsymbol{P}_{k+1}\boldsymbol{B}_1 + \boldsymbol{U}_{k+1}\boldsymbol{E}_{k+1}) + \boldsymbol{F}_k^T(\boldsymbol{R} + \boldsymbol{B}^T\boldsymbol{P}_{k+1}\boldsymbol{B})\boldsymbol{H}_k - \boldsymbol{A}^T\boldsymbol{P}_{k+1}\boldsymbol{B}\boldsymbol{H}_k, \quad (4.48)$$

$$\because \boldsymbol{F}_k^T(\boldsymbol{R} + \boldsymbol{B}^T\boldsymbol{P}_{k+1}\boldsymbol{B})\boldsymbol{H}_k = \boldsymbol{A}^T\boldsymbol{P}_{k+1}\boldsymbol{B}\boldsymbol{H}_k \text{ (using (4.40))}, \quad (4.49)$$

$$\therefore \boldsymbol{U}_k = (\boldsymbol{A} - \boldsymbol{B}\boldsymbol{F}_k)^T(\boldsymbol{P}_{k+1}\boldsymbol{B}_1 + \boldsymbol{U}_{k+1}\boldsymbol{E}_{k+1}) \quad (4.50)$$

Also, from (4.46):

$$(\boldsymbol{A} - \boldsymbol{B}\boldsymbol{F}_k)^T = (\boldsymbol{P}_k - \boldsymbol{Q})\boldsymbol{A}^{-1}\boldsymbol{P}_{k+1}^{-1} \quad (4.51)$$

Substituting $(\boldsymbol{A} - \boldsymbol{B}\boldsymbol{F}_k)^T$ from (4.51) in (4.50):

$$\boldsymbol{U}_k = (\boldsymbol{P}_k - \boldsymbol{Q})\boldsymbol{A}^{-1}(\boldsymbol{B}_1 + \boldsymbol{P}_{k+1}^{-1}\boldsymbol{U}_{k+1}\boldsymbol{E}_{k+1}) \quad (4.52)$$

Using (4.40), $\boldsymbol{H}_k$ in (4.41) can be rewritten as:

$$\boldsymbol{H}_k = \boldsymbol{F}_k \boldsymbol{A}^{-1}(\boldsymbol{B}_1 + \boldsymbol{P}_{k+1}^{-1}\boldsymbol{U}_{k+1}\boldsymbol{E}_{k+1}); \tag{4.53}$$

$$\text{and using (4.52)} \Rightarrow \boldsymbol{H}_k = \boldsymbol{F}_k(\boldsymbol{P}_k - \boldsymbol{Q})^{-1}\boldsymbol{U}_k \tag{4.54}$$

Partitioning $\boldsymbol{U}_k$ in (4.50) as $\begin{bmatrix}\boldsymbol{S}_k & \boldsymbol{S}'_k\end{bmatrix}, \boldsymbol{S}_k \in \mathbb{R}^{m\times r}, \boldsymbol{S}'_k \in \mathbb{R}^{m\times 1}$:

$$\begin{bmatrix}\boldsymbol{S}_k & \boldsymbol{S}'_k\end{bmatrix} = (\boldsymbol{A} - \boldsymbol{B}\boldsymbol{F}_k)^T(\boldsymbol{P}_{k+1}\boldsymbol{B}_1 + \begin{bmatrix}\boldsymbol{S}_{k+1} & \boldsymbol{S}'_{k+1}\end{bmatrix}\boldsymbol{E}_{k+1}) \tag{4.55}$$

$$\begin{aligned}\Rightarrow \begin{bmatrix}\boldsymbol{S}_k & \boldsymbol{S}'_k\end{bmatrix} = (\boldsymbol{A} - \boldsymbol{B}\boldsymbol{F}_k)^T(\boldsymbol{P}_{k+1}&\begin{bmatrix}\boldsymbol{B}' & \boldsymbol{0}_{m\times 1}\end{bmatrix} \\ &+ \begin{bmatrix}\boldsymbol{S}_{k+1} & \boldsymbol{S}'_{k+1}\end{bmatrix}\begin{bmatrix}\boldsymbol{I}_r & \Delta\boldsymbol{u}'_{k+1} \\ \boldsymbol{0}_{1\times r} & 1\end{bmatrix})\end{aligned} \tag{4.56}$$

$$\Rightarrow \boldsymbol{S}_k = (\boldsymbol{A} - \boldsymbol{B}\boldsymbol{F}_k)^T(\boldsymbol{P}_{k+1}\boldsymbol{B}' + \boldsymbol{S}_{k+1}), \text{ and,} \tag{4.57}$$

$$\boldsymbol{S}'_k = (\boldsymbol{A} - \boldsymbol{B}\boldsymbol{F}_k)^T(\boldsymbol{S}_{k+1}(\boldsymbol{u}'_{k+1} - \boldsymbol{u}'_k) + \boldsymbol{S}'_{k+1}) \tag{4.58}$$

Partitioning $\boldsymbol{H}_k$ in (4.39) as $\begin{bmatrix}\boldsymbol{G}_k & \boldsymbol{G}'_k\end{bmatrix}, \boldsymbol{G}_k \in \mathbb{R}^{p\times r}, \boldsymbol{G}'_k \in \mathbb{R}^{p\times 1}$, where p is the number of elements in $\boldsymbol{u}_k$:

$$\boldsymbol{u}_k^{opt} = \; -\left(\boldsymbol{F}_k\boldsymbol{x}_k + \begin{bmatrix}\boldsymbol{G}_k & \boldsymbol{G}'_k\end{bmatrix}\begin{bmatrix}\boldsymbol{u}'_k \\ 1\end{bmatrix}\right), \tag{4.59}$$

$$\Rightarrow \boldsymbol{u}_k^{opt} = -(\boldsymbol{F}_k\boldsymbol{x}_k + \boldsymbol{G}_k\boldsymbol{u}'_k + \boldsymbol{G}'_k) \tag{4.60}$$

$$\text{and using (4.54)}, \begin{bmatrix}\boldsymbol{G}_k & \boldsymbol{G}'_k\end{bmatrix} = \boldsymbol{F}_k(\boldsymbol{P}_k - \boldsymbol{Q})^{-1}\begin{bmatrix}\boldsymbol{S}_k & \boldsymbol{S}'_k\end{bmatrix}$$

$$\Rightarrow \boldsymbol{G}_k = \boldsymbol{F}_k(\boldsymbol{P}_k - \boldsymbol{Q})^{-1}\boldsymbol{S}_k;\ \boldsymbol{G}'_k = \boldsymbol{F}_k(\boldsymbol{P}_k - \boldsymbol{Q})^{-1}\boldsymbol{S}'_k \tag{4.61}$$

Hence, with (4.40), (4.47), (4.57)-(4.61), Theorem 4.1 stands proved.□

□

The optimal control solution in Theorem 4.1 has been termed as the extended linear quadratic regulator (ELQR) solution and it is an original contribution of the thesis. If the pair $(\boldsymbol{A}, \boldsymbol{B})$ is stabilizable, then infinite horizon solutions for $\boldsymbol{P}_k$, $\boldsymbol{F}_k$, $\boldsymbol{G}_k$ and $\boldsymbol{S}_k$ exist, and are given by $\boldsymbol{F}$, $\boldsymbol{P}$ as in (4.6)-(4.7), and $\boldsymbol{S}$, $\boldsymbol{G}$ as in (4.64)-(4.66).

$$\boldsymbol{S} = (\boldsymbol{A} - \boldsymbol{B}\boldsymbol{F})^T(\boldsymbol{P}\boldsymbol{B}' + \boldsymbol{S}) = (\boldsymbol{P} - \boldsymbol{Q})\boldsymbol{A}^{-1}(\boldsymbol{B}' + \boldsymbol{P}^{-1}\boldsymbol{S}), \tag{4.62}$$

$$\text{(this is because } (\boldsymbol{A} - \boldsymbol{B}\boldsymbol{F})^T = (\boldsymbol{P} - \boldsymbol{Q})\boldsymbol{A}^{-1}\boldsymbol{P}^{-1} \text{ from (4.51))} \tag{4.63}$$

$$\Rightarrow \boldsymbol{S} = (\boldsymbol{A}(\boldsymbol{P} - \boldsymbol{Q})^{-1} - \boldsymbol{P}^{-1})^{-1}\boldsymbol{B}' \tag{4.64}$$

$$\boldsymbol{G} = \boldsymbol{F}(\boldsymbol{P} - \boldsymbol{Q})^{-1}\boldsymbol{S}, \text{ substituting } \boldsymbol{S} \text{ from (4.64):} \tag{4.65}$$

$$\Rightarrow \boldsymbol{G} = \boldsymbol{F}(\boldsymbol{A} - \boldsymbol{P}^{-1}(\boldsymbol{P} - \boldsymbol{Q}))^{-1}\boldsymbol{B}' \tag{4.66}$$

Although the terms $\boldsymbol{F}_k$ and $\boldsymbol{P}_k$ for the ELQR case remain same as the LQR case, this needs to be mathematically derived and hence the above derivation is important. The terms $\boldsymbol{G}_k$ and $\boldsymbol{S}_k$ are independent of the sequence of $\boldsymbol{u}'_k$, and hence they can be easily calculated if $\boldsymbol{A}$, $\boldsymbol{B}$, $\boldsymbol{B}'$, $\boldsymbol{Q}$ and $\boldsymbol{R}$ are known. On the other hand, the terms $\boldsymbol{G}'_k$ and $\boldsymbol{S}'_k$ require the knowledge of the sequence of $\boldsymbol{u}'_k$ for all the future and present samples.

4.4 Implementation example: Control of a third-order LTI system

The ELQR control can be implemented on any system whose equations can be reduced to the form given by (4.8). An illustrative examples has been presented as follows, in which a simple third-order LTI system is controlled using the ELQR methodology.

4.4.1 System description

The various state-space matrices of the test system, whose equation is given by (4.8), are as follows:

$$\boldsymbol{A} = \begin{bmatrix} 1.4 & 0.2 & -0.1 \\ -0.2 & 0.8 & -0.3 \\ 0.1 & 0.1 & 0.9 \end{bmatrix}, \boldsymbol{B} = \begin{bmatrix} 0.1 & 0.8 \\ 1.1 & 0.3 \\ 0.9 & 0.5 \end{bmatrix} \text{and } \boldsymbol{B}' = \begin{bmatrix} 1.2 \\ 0.1 \\ 0.2 \end{bmatrix} \tag{4.67}$$

Hence, the above system has three states, two normal inputs and one exogenous input. Initially, all the states and inputs are zero, that is, $\boldsymbol{x}_0 = \boldsymbol{0}_{3\times1}$, $\boldsymbol{u}_0 = \boldsymbol{0}_{2\times1}$, and $\boldsymbol{u}'_0 = 0$. For $k \geq 1$, the exogenous input is applied as follows:

$$\boldsymbol{u}'_k = (0.95)^k,\ k \geq 1 \tag{4.68}$$

As $\boldsymbol{u}'_k$ in (4.68) is an exponentially decreasing function of time-sample, and it becomes zero only when $k \to \infty$, therefore the infinite horizon case of ELQR needs to be used to optimally control this system. Using equations (4.6),(4.7),(4.64) and (4.66), and cost weighting matrices $\boldsymbol{Q}$ and $\boldsymbol{R}$ as $\boldsymbol{I}_3$ and $\boldsymbol{I}_2$, respectively, the following infinite horizon values of $\boldsymbol{P}$, $\boldsymbol{F}$, $\boldsymbol{S}$ and $\boldsymbol{G}$ are evaluated (rounded-off to two decimal places):

$$\boldsymbol{P} = \begin{bmatrix} 3.60 & 0.55 & -1.26 \\ 0.55 & 2.28 & -2.37 \\ -1.26 & -2.37 & 6.32 \end{bmatrix}, \boldsymbol{F} = \begin{bmatrix} -0.42 & 0.11 & 0.60 \\ 1.14 & 0.12 & 0.05 \end{bmatrix}, \tag{4.69}$$

$$\boldsymbol{S} = \begin{bmatrix} 6.11 \\ 5.46 \\ -11.95 \end{bmatrix}, \text{ and } \boldsymbol{G} = \begin{bmatrix} -1.48 \\ 1.62 \end{bmatrix} \tag{4.70}$$

Also, $\boldsymbol{S}'_k$ can be evaluated by substituting $\boldsymbol{P}$ and $\boldsymbol{S}$ for $\boldsymbol{P}_k$ (or $\boldsymbol{P}_{k+1}$) and $\boldsymbol{S}_k$, respectively, in (4.13), and solving for $\boldsymbol{S}'_k$ iteratively. $\boldsymbol{S}'_k$ is then substituted in (4.11) to find $\boldsymbol{G}'_k$. The final solutions for $\boldsymbol{S}'_k$ and $\boldsymbol{G}'_k$ are given as (rounded-off to two decimal places):

$$\boldsymbol{S}'_k = \begin{bmatrix} -0.67 \\ -1.11 \\ 2.46 \end{bmatrix} \times (0.95)^k = \begin{bmatrix} -0.67 \\ -1.11 \\ 2.46 \end{bmatrix} \boldsymbol{u}'_k, \text{ and, } \boldsymbol{G}'_k = \begin{bmatrix} 0.27 \\ -0.02 \end{bmatrix} \boldsymbol{u}'_k \tag{4.71}$$

4.4.2 Results and discussion

Substituting the values of $\boldsymbol{F}$, $\boldsymbol{G}$, and $\boldsymbol{G}'_k$ from (4.70) and (4.71) in (4.10), the optimal control policy for ELQR comes as:

$$\boldsymbol{u}_k = -\begin{bmatrix} -0.42 & 0.11 & 0.60 \\ 1.14 & 0.12 & 0.05 \end{bmatrix} \boldsymbol{x}_k - \begin{bmatrix} -1.48 \\ 1.62 \end{bmatrix} \boldsymbol{u}'_k - \begin{bmatrix} 0.27 \\ -0.02 \end{bmatrix} \boldsymbol{u}'_k \tag{4.72}$$

$$= -\begin{bmatrix} -0.42 & 0.11 & 0.60 \\ 1.14 & 0.12 & 0.05 \end{bmatrix} \boldsymbol{x}_k - \begin{bmatrix} -1.21 \\ 1.60 \end{bmatrix} \boldsymbol{u}'_k \tag{4.73}$$

The classical LQR control is also applied on the test system for performance comparison with ELQR control, and as only the state-feedback gain $\boldsymbol{F}$ is required for classical LQR, and it is same as the state-feedback gain for ELQR control, the classical LQR control policy comes as:

$$\boldsymbol{u}_k^{LQR} = -\begin{bmatrix} -0.42 & 0.11 & 0.60 \\ 1.14 & 0.12 & 0.05 \end{bmatrix} \boldsymbol{x}_k \tag{4.74}$$

The weighted norms of the states and the control-inputs (given by $\boldsymbol{x}_k^T \boldsymbol{Q} \boldsymbol{x}_k$ and $\boldsymbol{u}_k^T \boldsymbol{R} \boldsymbol{u}_k$, respectively) can be used as measures of control performance of a control method. These weighted norms are also the quadratic costs associated with the control method for the k^{th} sample, as can be inferred from the constituent terms of $\boldsymbol{J'}$ in (4.9). The cost associated with the exogenous inputs, given by $\boldsymbol{u}_k'^T \boldsymbol{R}' \boldsymbol{u}'_k$ remains independent of the control method. This is because $\boldsymbol{u}'_k$ is not dependent on the control method.

The test system has been simulated in MATLAB, and the weighted norms of states and control inputs have been plotted in Fig. 4.1. It should be noted that $\boldsymbol{x}_k^T \boldsymbol{Q} \boldsymbol{x}_k = \boldsymbol{x}_k^T \boldsymbol{x}_k$ and $\boldsymbol{u}_k^T \boldsymbol{R} \boldsymbol{u}_k = \boldsymbol{u}_k^T \boldsymbol{u}_k$ for the test system.

Table 4.1 presents a comparison of quadratic costs associated with the states and the control-inputs for the two methods.

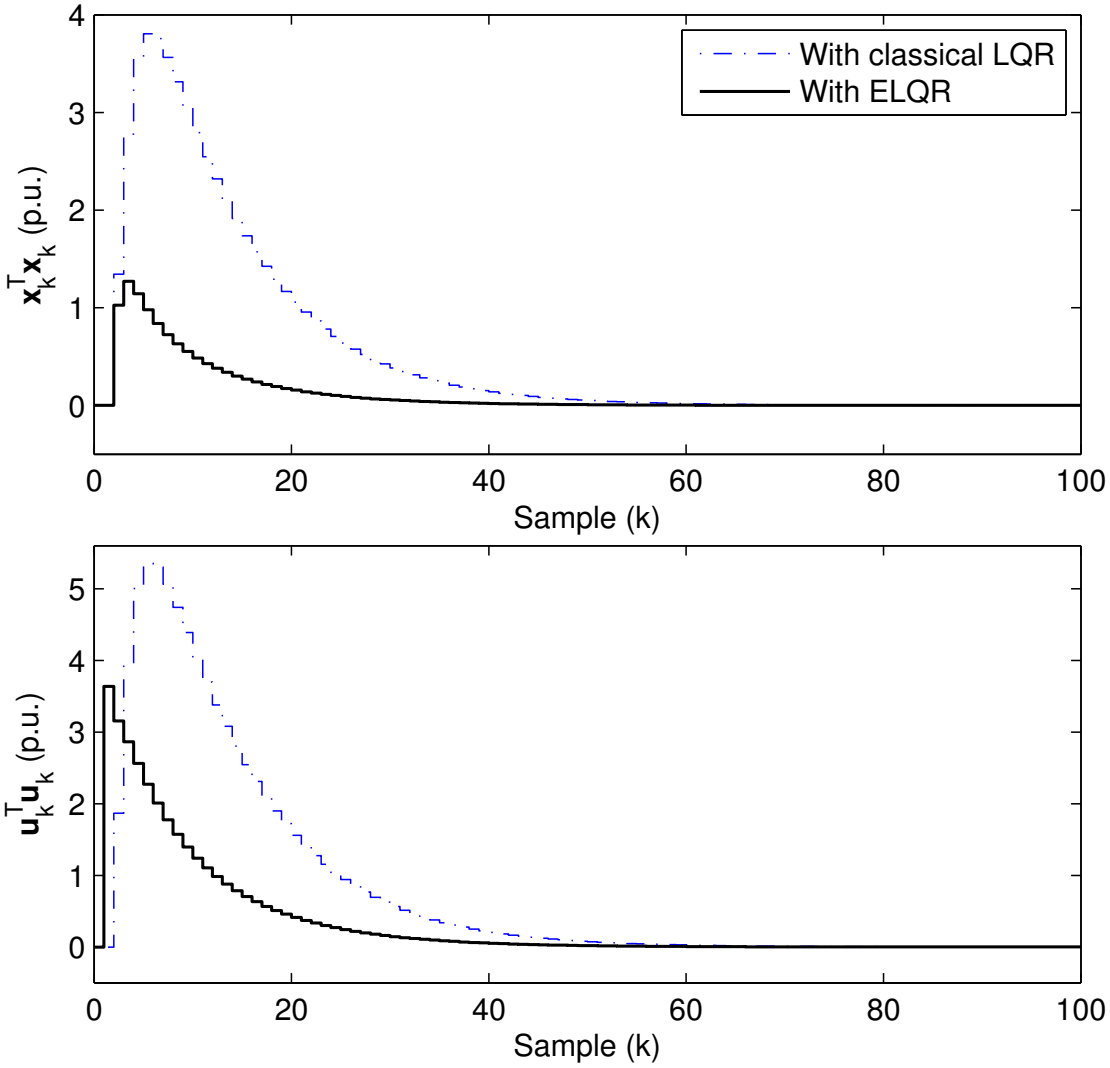

Figure 4.1: Control performance comparison of ELQR with classical LQR

Table 4.1: Comparison of quadratic costs

Quadratic costs (p.u.)	ELQR	Classical LQR
State-deviation cost ($\sum \boldsymbol{x}_k^T \boldsymbol{Q} \boldsymbol{x}_k$)	11.76	54.97
Control-effort ($\sum \boldsymbol{u}_k^T \boldsymbol{R} \boldsymbol{u}_k$)	33.28	79.37
Total cost	45.04	134.34

It may be inferred from Fig. 4.1 and Table 4.1 that ELQR is much more efficient than classical LQR in presence of exogenous inputs, and for the test system the total quadratic cost for the states and the control-inputs is reduced by 66.5% as compared to the classical LQR control.

4.5 Summary

A control scheme has been presented for the optimal control of a special case of LTI systems in which both normal and exogenous inputs are present. The scheme is termed as extended LQR, and it is shown to be significantly more cost effective than the classical LQR scheme. The applicability of the scheme has been shown on a simple model LTI system.

Chapter 5

Decentralized control of power systems using ELQR

This chapter integrates decentralized DSE and ELQR control scheme developed in the last two chapters and uses them to control and to provide adequate damping to the small signal oscillatory dynamics observed in power systems. The integrated control scheme is completely decentralized. It is a practical alternative to the centralized approach to dynamic system identification and control.

Centralized approach of control of power systems using traditional LQR control scheme has been reported by many research groups ([85], [86], [87], [88]). However this approach, just like every other centralized approach, needs strong and fast communication network to transmit information and data to control center. As power systems still lack in such a communication infrastructure (as elaborated in first two chapters), the centralized approach remains more theoretical than being practical. This chapter aims to address this limitation using the integrated decentralized control scheme.

Rest of the chapter is organized as follows. Section II describes the architecture of the problem formulation. Section III explains the concept used for decentralization, while Section IV briefly explains DSE. The control methodology is detailed in Section V; and Section VI describes the results on a power system model. Section VII concludes the chapter.

5.1 Proposed architecture of control

Electromechanical oscillations in power network are global in nature as they involve large number of generators, loads and significant part of the network. As every generator contributes to these oscillations in varying degrees, each of them can provide suitable control to dampen them out. In the proposed architecture of control, the dynamic states that are obtained for every individual generator from local PMUs measurements would be utilized to design a controller that contributes to the overall damping of the system-wide oscillations besides any local oscillation. The combined efforts of all the decentralized controllers must produce the desired response of the system at all operating conditions.

An overview of the complete system is given in Fig. 5.1. In the proposed architecture, each machine is assumed to have a PMU at its terminal that feeds voltage and current phasors to the dynamic state estimator which works on the algorithm presented in Chapter 3. The state estimates and the measurements are then sent to the local controller, which works on a modified version of the ELQR algorithm (presented in Chapter 4) to calculate an optimal control signal for the AVR, which in turn controls the excitation of the machine, thereby closing the control loop. The control gains are updated after a small interval (say after every second), so that the control law remains robust to any operating condition. Functionally even though dynamic state estimator and controller are two components, they can be implemented in the same location. The output from PSS can also be combined with the output of ELQR, but it is not required as such. It should be understood here that a PSS is not necessary when there is an ELQR in the system, and hence an ELQR can completely replace a PSS.

It may be noted here that the ELQR controller behaves like a PSS as its output signal directly controls the excitation system of the machine, but there is a fundamental difference between the two. The control-gains of the ELQR controller are updated in real-time so that the controller works for any operating point of the system, while the control-gain and phase compensator time constants for the PSS are obtained offline for a particular operating condition (or a finite set of operating conditions) using model based design and then implemented through electronic hardware and/or software.

PMUs form an essential part of the proposed schemes of estimation and control, and although their functioning has been briefly described in Chapter 3 in Sections

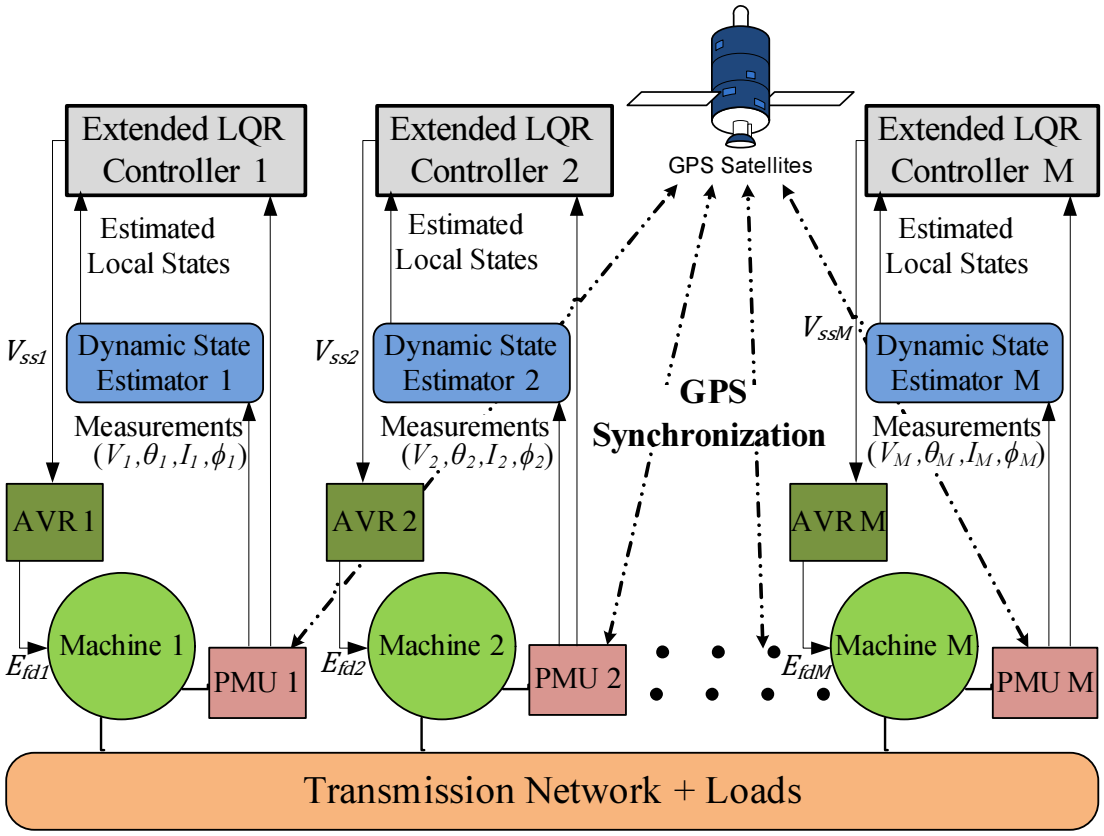

Figure 5.1: Overview of the system and the methodology

3.1.2 and 3.5.1.1, their effects on control performance still needs to be considered and have been described as follows.

Effects of PMU dynamics on controller performance: The dynamic response of a PMU depends on the combined response of its constituent components, which are the analog and digital filters and the sampler. The waveforms produced by instrument transformers are processed by the filters for surge suppression and anti-aliasing filtering in order to filter-out high frequency transients generated during faults and switching operations. There is also an issue of possible aliasing effects due to inadequate sampling rates of the sampler for higher swing frequencies in the network. This issue is rectified by using a decimation filter or a simple averaging-filter. Using these functions, PMUs measure the phasors accurately (provided the instrument transformers and GPS satellites are accurate) for both oscillatory and steady state modes of operation for all practical power systems [16]. Thus, PMU dynamics have no effect on controller performance.

Effects of PMU accuracy on controller performance: The accuracy of PMUs is dependent on the instrument transformers and GPS satellites on which

they rely for waveform acquisition and time-synchronization, respectively. The waveforms provided by the instrument transformers have errors in both magnitude and phase, but the error in phase can be accurately compensated and calibrated out using digital signal processing (DSP) techniques [76]. Hence the errors in phase are limited only by the time synchronization accuracy of GPS. The errors in magnitude of these phasors are limited by accuracy class of the instrument transformers used. These errors in phasors obtained by PMUs can be represented by noises of finite variances, and large errors are considered as bad-data. These noises and bad-data can be filtered-out from the dynamic state estimates in the state estimation stage, as shown in Chapter 3, and have negligible effect on controller performance, as also demonstrated in Section 5.4.6.

5.2 Decentralization of control

As explained in previous chapters, the dynamic behavior of a power system is modeled using a set of continuous-time non-linear differential and algebraic equations (DAEs), which may be written as:

$$\dot{\boldsymbol{x}}_c(t) = \boldsymbol{g}(\boldsymbol{x}_c(t), \boldsymbol{u}_c(t), \boldsymbol{y}_c(t)); \boldsymbol{y}_c(t) = \boldsymbol{h}(\boldsymbol{x}_c(t), \boldsymbol{u}_c(t)); \tag{5.1}$$

$$\Rightarrow \dot{\boldsymbol{x}}_c(t) = \boldsymbol{g}(\boldsymbol{x}_c(t), \boldsymbol{u}_c(t), \boldsymbol{h}(\boldsymbol{x}_c(t), \boldsymbol{u}_c(t))) \tag{5.2}$$

The subscript c in the above equation stands for continuous-time. A central control scheme which tunes itself in real-time requires complete knowledge of the differential function $\boldsymbol{g}$, the various states $\boldsymbol{x}_c$, inputs $\boldsymbol{u}_c$ and either the algebraic quantities $\boldsymbol{y}_c$ or the algebraic function $\boldsymbol{h}$. Obtaining such information centrally in real-time is very difficult. However, the local states for the generation unit can be obtained locally in real-time using decentralized dynamic state estimation. The equation for a single unit is written in a standard form as (5.3):

$$\dot{\boldsymbol{x}}_{ci}(t) = \boldsymbol{g}_i(\boldsymbol{x}_{ci}(t), \boldsymbol{u}_{ci}(t), \boldsymbol{u}'_{ci}(t)); \text{ where } \boldsymbol{u}_{ci} = V_{ssi}, \tag{5.3}$$

$$\boldsymbol{x}_{ci} = [\delta_i \ \omega_i \ E'_{di} \ E'_{qi} \ \Psi_{1di} \ \Psi_{2qi} \ E'_{dci} \ V_{ri}]^T, \boldsymbol{u}'_{ci} = [V_i \ \theta_i]^T. \tag{5.4}$$

Similar excitation systems (specifically static excitation) have been assumed for all the machines in above equations so that each machine contributes similarly in the net control effort. The subscript i in the above equation stands for the i^{th} generation unit. $\boldsymbol{u}_{ci}$, which constitutes V_{ssi}, is the control input to AVR of the i^{th} unit. $\boldsymbol{u}'_{ci}$, which constitutes V_i and θ_i (the stator voltage phasors), is the pseudo-input vector for the i^{th} unit, as explained in Chapter 3.

The multimachine dynamic model given by (5.1)-(5.3) is formulated considering reference angle for a rotational system. Thus, each δ_i and θ_i is defined with respect to a suitable reference angle, which can either be the rotor angle of a particular reference machine, or can be the center of inertia angle, δ_{COI}. This fact is illustrated in detail in [50]. But doing this would require the knowledge of rotor angle of the reference machine (or worse, the knowledge of rotor angles of all the machines, in case of δ_{COI}) at each decentralized location, and would therefore defeat the purpose of decentralization. A way of dealing with this problem is by defining a new state $\alpha_i = (\delta_i - \theta_i)$. As δ_i and θ_i have a common reference angle, it gets cancelled in the definition of α_i. The dynamic equation of α_i is given by:

$$\dot{\alpha}_i = (\dot{\delta}_i - \dot{\theta}_i) = \omega_B(\omega_i - f_i) \tag{5.5}$$

After incorporating α_i in $\boldsymbol{x}_{ci}$ in (5.3), and replacing the pseudo-input θ_i with its time derivative in p.u., f_i, (5.3) gets redefined to:

$$\dot{\boldsymbol{x}}_{ci}(t) = \boldsymbol{g}_i(\boldsymbol{x}_{ci}(t), \boldsymbol{u}_{ci}(t), \boldsymbol{u}'_{ci}(t)); \text{ where } \boldsymbol{u}_{ci} = V_{ssi}, \tag{5.6}$$

$$\boldsymbol{x}_{ci} = [\alpha_i \ \omega_i \ E'_{di} \ E'_{qi} \ \Psi_{1di} \ \Psi_{2qi} \ E'_{dci} \ V_{ri}]^T, \boldsymbol{u}'_{ci} = [V_i \ f_i]^T. \tag{5.7}$$

The non-linear equation given by (5.6) needs to be linearized before it can be used in a linear controller. Linearizing (5.6) about an operating point given by $(\boldsymbol{x}_{ci}(t_0), \boldsymbol{u}_{ci}(t_0), \boldsymbol{u}'_{ci}(t_0))$:

$$\Delta\dot{\boldsymbol{x}}_{ci}(t) = \boldsymbol{A}_{ci}\Delta\boldsymbol{x}_{ci}(t) + \boldsymbol{B}_{ci}\Delta\boldsymbol{u}_{ci}(t) + \boldsymbol{B}'_{ci}\Delta\boldsymbol{u}'_{ci}(t); \tag{5.8}$$

$$\text{where, } \boldsymbol{A}_{ci} = \frac{\partial \boldsymbol{g}_i(t_0)}{\partial \boldsymbol{x}_{ci}(t_0)}, \boldsymbol{B}_{ci} = \frac{\partial \boldsymbol{g}_i(t_0)}{\partial \boldsymbol{u}_{ci}(t_0)}, \boldsymbol{B}'_{ci} = \frac{\partial \boldsymbol{g}_i(t_0)}{\partial \boldsymbol{u}'_{ci}(t_0)}, \tag{5.9}$$

$$\Delta \boldsymbol{x}_{ci}(t) = \boldsymbol{x}_{ci}(t) - \boldsymbol{x}_{ci}(t_0),\ \Delta \boldsymbol{u}_{ci}(t) = \boldsymbol{u}_{ci}(t) - \boldsymbol{u}_{ci}(t_0), \tag{5.10}$$

$$\Delta \boldsymbol{u}'_{ci}(t) = \boldsymbol{u}'_{ci}(t) - \boldsymbol{u}'_{ci}(t_0),\ \text{and}\ t \geq t_0 \tag{5.11}$$

Appendix A gives the details of the differential and algebraic functions which constitute $\boldsymbol{g}_i$ and Appendix C gives the details of $\boldsymbol{A}_{ci}$, $\boldsymbol{B}_{ci}$ and $\boldsymbol{B}'_{ci}$.

Remark: It should be understood that (5.8) remains valid for any operating point of the system, as long as the operating point remains close to an equilibrium point. As (5.8) is used in calculating the ELQR control gains (as explained in subsequent sections), the ELQR control gains also remain valid for every operating point of the system which comes under small-signal dynamic behaviour of power systems. The only exception to this fact takes place during a contigency (such as a system fault) during which some of the system states may become transiently unbounded, and the system equations can no longer be linearized. Therefore, before linearization and update of control gains it should be checked whether every machine state is within safe operating limits and if not, control gains from the previous sample should be used.

Discretizing (5.8) at a sampling period T_0 (T_0 is the sampling period of the dynamic state estimator) gives (see [53]):

$$\boldsymbol{x}_{i(k+1)} = \boldsymbol{A}_i \boldsymbol{x}_{ik} + \boldsymbol{B}_i \boldsymbol{u}_{ik} + \boldsymbol{B}'_i \boldsymbol{u}'_{ik}; \tag{5.12}$$

$$\text{where},\ \boldsymbol{x}_{ik}{=}\Delta \boldsymbol{x}_{ci}(kT_0),\ \boldsymbol{u}_{ik}{=}\Delta \boldsymbol{u}_{ci}(kT_0),\ \boldsymbol{u}'_{ik}{=}\Delta \boldsymbol{u}'_{ci}(kT_0), \tag{5.13}$$

$$\boldsymbol{A}_i = e^{\boldsymbol{A}_{ci}T_0}, \boldsymbol{B}_i = \boldsymbol{A}_{ci}^{-1}(\boldsymbol{A}_i - \boldsymbol{I})\boldsymbol{B}_{ci}, \boldsymbol{B}'_i = \boldsymbol{A}_{ci}^{-1}(\boldsymbol{A}_i - \boldsymbol{I})\boldsymbol{B}'_{ci} \tag{5.14}$$

Writing (5.12) in simplified form by dropping suffix i:

$$\boldsymbol{x}_{k+1} = \boldsymbol{A}\boldsymbol{x}_k + \boldsymbol{B}\boldsymbol{u}_k + \boldsymbol{B}'\boldsymbol{u}'_k \tag{5.15}$$

Remark: The frequencies of the electromechanical modes of a machine lie in the range of 1.5-3.0 Hz [51]. As the ELQR controllers need to control and properly

damp these modes, the minimum required sampling frequency for the controller is 6.0 Hz according to the Nyquist-Shannon sampling theorem (i.e. a maximum allowed sampling period of 0.17 s). This upper limit is also the threshold requirement for the sampling period. The lower limit is decided by the rate at which the dynamic states are provided to the controllers, which is given by T_0. As it is desired that the controllers operate at the fastest update rate possible, T_0 is also used as the sampling period for finding the discrete model and the control laws.

Remark: It should also be noted that the PMUs are required not only for DSE, but also for the ELQR control. The ELQR requires the dynamic state estimates provided by DSE and the phasor measurements provided by the PMU for the calculation of control gains, as shown in Fig. 5.1.

5.3 Integrated ELQR control

The discrete equation in (5.15) has an extra term (corresponding to the pseudo-inputs) as compared to the general discrete-time LTI system given by (4.1). It should be understood that the extra term $\boldsymbol{u}'_k$ cannot be absorbed in $\boldsymbol{u}_k$ as $\boldsymbol{u}'_k$ is an exogenous input while $\boldsymbol{u}_k$ is a normal control input. Thus the optimal control policy for (5.15) gets modified from traditional LQR to ELQR (Theorem 4.1), as explained in the last chapter.

The terms $\boldsymbol{G}_k$ and $\boldsymbol{S}_k$ in Theorem 4.1 remain independent of the sequence of $\boldsymbol{u}'_k$, and hence they can be easily calculated if $\boldsymbol{A}$, $\boldsymbol{B}$, $\boldsymbol{B}'$, $\boldsymbol{Q}$ and $\boldsymbol{R}$ are known. On the other hand, the terms $\boldsymbol{G}'_k$ and $\boldsymbol{S}'_k$ require the knowledge of the sequence of $\boldsymbol{u}'_k$ for all the future and present samples, hence they cannot be calculated for a practical power system as only the past and present values of the sequence of $\boldsymbol{u}'_k$ are available. Moreover, using offline values of the pseudo-inputs (which are V and θ) it was found that $\boldsymbol{G}'_k$ has very small contribution in the control law given by Theorem 4.1. Thus, while implementing ELQR, $\boldsymbol{G}'_k$ is ignored and only the optimal gains $\boldsymbol{F}_k$ and $\boldsymbol{G}_k$ are calculated in real-time. Also, Theorem 4.1 requires that $\boldsymbol{u}'_k = 0 \; \forall \; k \geq N$. This condition can be taken into account if $N \to \infty$, that is, if no limit is imposed on the time within which the power system comes to a steady state. As $N \to \infty$ is the infinite horizon case, the final decentralized control policy (using Theorem 4.1), after including suffix i for the i^{th} unit (whose equation is given by (5.12)), is written as:

$$\boldsymbol{u}_{ik} = -(\boldsymbol{F}_i \boldsymbol{x}_{ik} + \boldsymbol{G}_i \boldsymbol{u}'_{ik});\ k \geq 0,\ \boldsymbol{Q}_i \geq 0,\ \boldsymbol{R}_i > 0; \tag{5.16}$$

$$\boldsymbol{F}_i = (\boldsymbol{R}_i + \boldsymbol{B}_i^T \boldsymbol{P}_i \boldsymbol{B}_i)^{-1} \boldsymbol{B}_i^T \boldsymbol{P}_i \boldsymbol{A}_i, \tag{5.17}$$

$$\boldsymbol{P}_i = \boldsymbol{Q}_i + \boldsymbol{A}_i^T [\boldsymbol{P}_i - \boldsymbol{P}_i \boldsymbol{B}_i (\boldsymbol{R}_i + \boldsymbol{B}_i^T \boldsymbol{P}_i \boldsymbol{B}_i)^{-1} \boldsymbol{B}_i^T \boldsymbol{P}_i] \boldsymbol{A}_i; \tag{5.18}$$

$$\boldsymbol{G}_i = \boldsymbol{F}_i (\boldsymbol{A}_i - \boldsymbol{P}_i^{-1} (\boldsymbol{P}_i - \boldsymbol{Q}_i))^{-1} \boldsymbol{B}'_i \tag{5.19}$$

5.3.1 Damping control

The stable response of power system requires that all the electromechanical modes in the system should have damping ratios more than a certain percentage (typically more than ten percent). This can be achieved by ensuring that each unit provides a minimum damping to the intra-plant mode it observes, and the collective damping efforts of all the units leads to damping of all the intra-area and inter-area oscillations in the system. This constraint implies that the electromechanical poles observed at a unit should lie within a conic-section in the left half of the s-plane. In z-plane, the conic-section maps to a logarithmic-spiral [89], and hence the discrete-domain poles should lie within the spiral. But confining the closed-loop poles within a logarithmic spiral is not practical; rather, a practical alternative is to substitute the spiral with a disk, and confine the closed-loop poles of the system within that disk. It is this technique that has been used in this paper for damping control.

Using Theorem 4.1 in Chapter 4 and Theorem 2 in [90] it can be shown that the decentralized control policy of ELQR for confining the closed-loop poles within a disk of radius r and center $(\beta, 0)$ remains same as in (5.16)-(5.19) except that $\boldsymbol{A}_i$, $\boldsymbol{B}_i$ and $\boldsymbol{B}'_i$ are replaced by $(\boldsymbol{A}_i - \beta \boldsymbol{I})/r$, $\boldsymbol{B}_i/r$ and $\boldsymbol{B}'_i/r$, respectively. This technique requires a circle which coincides with the logarithmic spiral at the points where the electromechanical poles should lie. As electromechanical poles have high participation from the states of δ and ω, there is only one pair of electromechanical intra-plant mode for a machine (as each machine has only one pair of δ and ω). Let the modal-frequency of this intra-plant mode be f_m and let the minimum damping ratio to which this mode needs to be damped be d_{min}. Since it is desired that

the substituting circle should exactly coincide with the logarithmic spiral at the point corresponding to (f_m, d_{min}), hence the substituting circle should intersect the spiral at this point and it should also be inside the spiral. This can only happen when the circle is tangential to the spiral at this point from within the spiral. This substitution of spiral with a circle can be better understood from Fig. 5.2.

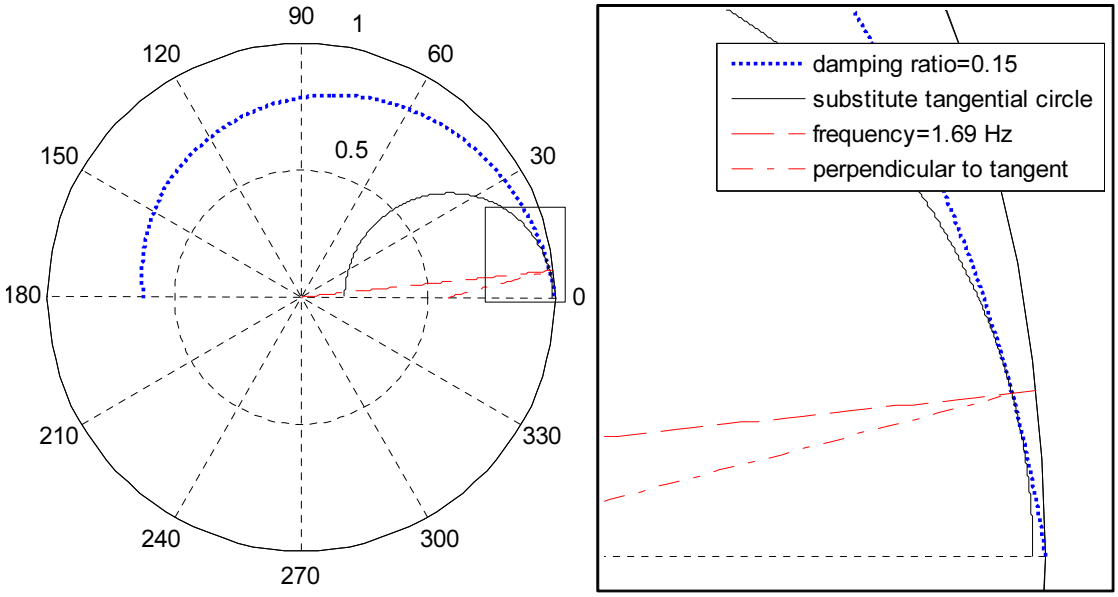

Figure 5.2: Circle substituting a logarithmic spiral

In Fig. 5.2, the blue-dotted spiral corresponds to a constant damping-ratio of $d_{min} = 0.15$ (only upper half has been shown, lower half will be its mirror-image), the red-dashed line corresponds to a constant frequency of $f_m = 1.69Hz$ (this is the modal frequency of the intra-plant mode of the 9^{th} machine; all the calculations for this machine have been shown in the case study in Section 5.4) and the black-solid curve is the substituting circle. All the curves are inside the unity circle. The substituting circle should be tangent at the point where the constant frequency line intersects the constant damping ratio spiral. The black-solid curve denotes this tangential circle. For clarity, the right sub-figure in Fig. 5.2 shows the magnified version of the region enclosed by the small rectangle in the left sub-figure. This substituting circle ensures a damping ratio of more than or equal to d_{min} for all the poles of the machine, as the circle is completely inside the spiral, and the damping ratio of d_{min} is exactly ensured for the intra-plant mode of modal frequency f_m as the circle will be tangential to the spiral at the point corresponding to (f_m, d_{min}). Thus, the parameters of this circle can be used in deriving the modified ELQR law for damping the intra-plant modes. Using coordinate geometry, the parameters r and β for the circle for given f_m and d_{min} are found as follows.

$$\beta = R(\cos\theta_m - \frac{\sin\theta_m}{M}),\ r = \sqrt{R^2 + \beta^2 - 2\beta R\cos\theta_m};$$
$$\text{where, } R = e^{-d_m\theta_m}, d_m = \cot(\cos^{-1} d_{min}), \theta_m = 2\pi f_m T_0,$$
$$\text{and } M = (\sin\theta_m + d_m\cos\theta_m)/(\cos\theta_m - d_m\sin\theta_m) \quad (5.20)$$

5.4 Case study

5.4.1 System Description

The test system remains same as the one used in Chapter 3 (Fig. 3.3). As explained in Appendix D, this system has four inter-area modes in the range 0.2-1.0 Hz, three of which are poorly damped with damping ratios less than 10%.

Each machine in the system is assumed to be equipped with excitation system controller, a PSS, a dynamic state estimator, and an ELQR controller. PSS control is used only for comparison, that is, in one case only ELQR is working and in second case only PSS is working. They are not working together in any case. The control case when only PSS is working has been termed as 'PSS control', while the case when only ELQR is working has been termed as 'ELQR control'.

The matrices $\boldsymbol{Q}$ and $\boldsymbol{R}$ are positive semi-definite and positive definite matrices, respectively, and their values depend on how costs/penalties are assigned to the deviations of the states and inputs, respectively, from their steady state values. In the case study it is desired that the sum of the squares of deviations for all the states and all the inputs for a machine is minimized for all the time samples, so that all the state and input deviations get uniform penalties in the control law. Hence the state cost for the i^{th} machine is taken as $\sum_{k=0}^{N-1}(\sum_{j=1}^{7}|x_{ijk}|^2)$ for the seven states of the i^{th} machine. Since $\sum_{j=1}^{7}|x_{ijk}|^2 = \boldsymbol{x}_{ik}^T\boldsymbol{x}_{ik} = \boldsymbol{x}_{ik}^T\boldsymbol{I}_7\boldsymbol{x}_{ik}$, hence $\boldsymbol{Q} = \boldsymbol{I}_7$ for each machine ($\boldsymbol{I}_7$ is an identity matrix of order 7). Similarly, control cost is $\sum_{k=0}^{N-1}(|u_{ik}|^2)$ (as there is only one control-input); and since $|u_{ik}|^2 = u_{ik}u_{ik} = u_{ik}.1.u_{ik}$, hence $\boldsymbol{R} = 1$.

The state estimator provides estimates every 8.33 ms, while the state matrices and the control gains of the ELQR are updated every second. As an example, the complete calculation process for finding the control gains for one of the machines

(the 9^{th} machine) at $t = 0$ has been shown as follows. The calculation process remains same for rest of the machines in the system.

The constant parameters for the 9^{th} machine, using the data for the 68-bus system from Appendix D, are:

$X_l = 0.0298$ p.u.; $R_a = 0$ p.u.; $X_d = 0.2106$ p.u.; $X'_d = 0.057$ p.u.; $X'_d = 0.045$ p.u.; $X_q = 0.205$ p.u.; $X'_q = 0.05$ p.u.; $X'_q = 0.045$ p.u.; $T'_{d0} = 4.79$ s; $T''_{d0} = 0.05$ s; $T'_{q0} = 1.96$ s; $T''_{q0} = 0.035$ s; $D = 14$ p.u.; $H = 34.5$ s; $\omega_B = 376.99$ rad/s; $K_a = 10$ p.u.; $T_r = 0.01$ s

The values of the states and algebraic variables for the 9^{th} machine at $t = 0$, found using DSE, are:

$\alpha = 0.950$ rad; $\omega = 1$ p.u.; $E'_d = -0.630$ p.u.; $E'_q = 0.978$ p.u.; $\Psi_{1d} = 0.796$ p.u.; $\Psi_{2q} = 0.713$ p.u.; $E'_{dc} = 0$ p.u.; $V_r = 1.025$ p.u.; $E_{fd} = 2.005$ p.u.; $I_d = -6.687$ p.u.; $I_q = 4.067$ p.u.; $V_d = -0.834$ p.u.; $V_q = 0.596$ p.u.; $T_e = 8$ p.u.

As $X''_d = X''_q$ for all the machines of the 68-bus system, E'_{dc} remains constant (equal to zero) and can be eliminated from the DAEs and the linearized equations in Appendix A. Thus, there are effectively seven dynamic states for each machine in the system. The following system matrices are found for the 9^{th} machine after substituting the above values of parameters and states into the expressions for $\boldsymbol{A}_c$, $\boldsymbol{B}_c$ and $\boldsymbol{B}'_c$ in Appendix A and eliminating expressions corresponding to E'_{dc}:

$$\boldsymbol{B}_c = \begin{bmatrix} 0 \\ 0 \\ 0 \\ 2.088 \\ 0 \\ 0 \\ 0 \end{bmatrix}; \boldsymbol{B}'_c = \begin{bmatrix} 0 & -376.9 \\ -0.113 & 0 \\ -1.076 & 0 \\ 0.232 & 0 \\ 7.034 & 0 \\ 10.43 & 0 \\ 100 & 0 \end{bmatrix}; \tag{5.21}$$

$$\boldsymbol{A}_c = \begin{bmatrix} 0 & 376.9 & 0 & 0 & 0 & 0 & 0 \\ -0.347 & -0.203 & -0.145 & -0.150 & -0.118 & 0.048 & 0 \\ -0.789 & 0 & -2.474 & 0 & 0 & -0.642 & 0 \\ -0.332 & 0 & 0 & -0.951 & 0.344 & 0 & -2.088 \\ -10.08 & 0 & 0 & 13.24 & -25.33 & 0 & 0 \\ 7.649 & 0 & -18.92 & 0 & 0 & -31.75 & 0 \\ 0 & 0 & 0 & 0 & 0 & 0 & -100 \end{bmatrix} \tag{5.22}$$

The discrete forms of above matrices, using (4.9) ($T_0 = 0.00833$ s), come as:

$$\boldsymbol{B} = \begin{bmatrix} 0 \\ 0 \\ 0 \\ 0.017 \\ 0.001 \\ 0 \\ 0 \end{bmatrix}; \boldsymbol{B'} = \begin{bmatrix} -0.002 & -3.137 \\ -0.001 & 0.004 \\ -0.009 & 0.010 \\ -0.004 & 0.004 \\ 0.053 & 0.123 \\ 0.077 & -0.092 \\ 0.565 & 0 \end{bmatrix}; \tag{5.23}$$

$$\boldsymbol{A} = \begin{bmatrix} 0.996 & 3.134 & -0.002 & -0.002 & -0.001 & 0.001 & 0 \\ -0.003 & 0.994 & -0.001 & -0.001 & -0.001 & 0.000 & 0 \\ -0.007 & -0.010 & 0.980 & 0 & 0 & -0.005 & 0 \\ -0.003 & -0.004 & 0 & 0.992 & 0.003 & 0 & -0.012 \\ -0.076 & -0.123 & 0 & 0.099 & 0.810 & 0 & -0.001 \\ 0.056 & 0.092 & -0.137 & 0 & 0 & 0.768 & 0 \\ 0 & 0 & 0 & 0 & 0 & 0 & 0.435 \end{bmatrix} \tag{5.24}$$

Using the above value of $\boldsymbol{A}$, the intra-plant modes are found as -0.895 ± 10.617. The modal frequency for this pair of modes is $f_m = 10.617/(2\pi) = 1.69Hz$. Finally, using equations (5.16)-(5.19) after replacing $\boldsymbol{A}$, $\boldsymbol{B}$ and $\boldsymbol{B'}$ with $(\boldsymbol{A} - \beta\boldsymbol{I})/r$, $\boldsymbol{B}/r$ and $\boldsymbol{B'}/r$, respectively (as explained in Section 5.3.1); taking $r = 0.411$, $\beta = 0.581$ (which are found using (5.20), after taking $f_m = 1.69Hz$ and $d_{min} = 0.15$) and taking $\boldsymbol{Q}$ and $\boldsymbol{R}$ as identity matrices, the gain matrices $\boldsymbol{F}$ and $\boldsymbol{G}$ for the 9^{th} machine are found to be:

$$\boldsymbol{F} = \begin{bmatrix} 2.448 & -20.524 & 2.143 & 3.378 & 0.288 & -0.110 & -0.070 \end{bmatrix}; \tag{5.25}$$

$$\boldsymbol{G} = \begin{bmatrix} 0.098 & 12.316 \end{bmatrix} \tag{5.26}$$

At each unit, a washout filter with time constant of $10s$ is also applied to the ELQR output signal. This ensures that the steady-state output of the ELQR is zero to allow operation of the system at off-nominal frequency. The output signal from the ELQR can also get unbounded transiently during contingencies; therefore its output is limited just like a PSS, with $|V_{ss}| < 0.01p.u.$. Although the parameters for the AVR, PSS and the washout filter can be tuned individually for each machine in the system, in the case study standard parameters have been

used as given in Appendix D. This is done so that the performance of the ELQR methodology is evaluated in a standard framework. The system is simulated in MATLAB Simulink. Level-2 S-functions are used for dynamic update of state matrices and control-gains.

5.4.2 Control performance

In the simulation, the system starts from steady state, and then a balanced three phase fault is applied in one of the tie-lines between buses 53-54 followed by immediate outage of this tie-line. Fig. 5.3 shows the plots of relative rotor speed between machines 13-16 and the power flow in inter-area tie-lines between buses 60-61 for two cases. In first case each machine is controlled using PSS control, while in second case each machine is controlled using ELQR control. Table 5.1 shows the modal frequencies and damping ratios for the four poorly damped inter-area modes. It can be observed that although the modal frequencies for the ELQR case decrease as compared to the case of without control, this decrease is strongly compensated by the increase in damping ratios of these modes, and all the modes are damped to damping ratios of 10% or more. Similar improvement in damping performance is not observed for the case of PSS control. Thus, Fig. 5.3 and Table 5.1 show that the control and damping performance of ELQR control is significantly better than PSS control.

Table 5.1: Modal analysis for the four inter-area modes

	Without control	PSS control	ELQR control	WADC control
Mode-1 frequency (Hz)	0.39	0.44	0.31	0.44
Mode-1 damping ratio (%)	2.1	14.8	21.9	20.6
Mode-2 frequency (Hz)	0.52	0.54	0.47	0.52
Mode-2 damping ratio (%)	2.7	7.1	10.9	17.2
Mode-3 frequency (Hz)	0.60	0.63	0.54	0.66
Mode-3 damping ratio (%)	1.9	7.0	12.1	11.4
Mode-4 frequency (Hz)	0.79	0.81	0.76	0.80
Mode-4 damping ratio (%)	4.8	7.0	10.5	12.8

5.4.3 Robustness to different operating conditions

As the state matrices and control-gains are updated every second and get adapted to the current system conditions, the control remains valid for any operating point.

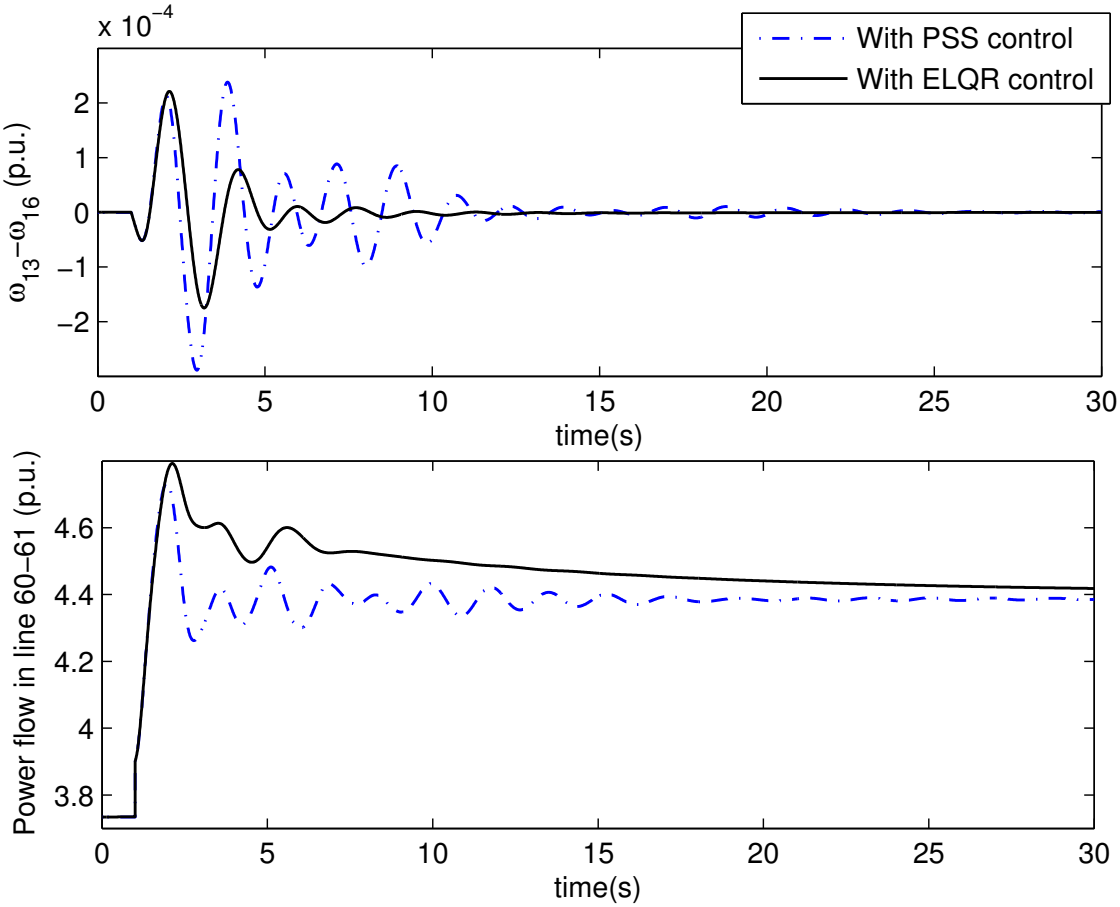

Figure 5.3: Dynamic performance of PSS control vs ELQR control

The power flow in line 60-61 has been shown for three operating cases. The total power flow from the area NETS to the area NYPS is varied in the three cases, which is 700MW for the first case (Fig. 5.3, second plot), 100MW for the second case (Fig. 5.4, first plot), and 900MW for the third case (Fig. 5.4, second plot). It can be observed that ELQR control remains robust in varying operating conditions.

5.4.4 Control efforts and state costs

Fig. 5.5 shows the 13^{th} unit's control signal (which is V_{ss13}) for PSS control and ELQR control. It can be seen that ELQR has a lower magnitude for the control signal than PSS control. But, the value of control signal for a unit (or even for all the units, if each unit is considered separately), is inconclusive. Better metrics for evaluating the quality of a control method are control efforts and state costs associated with that method. Table 5.2 presents a comparison of total cost given by $\sum_{i=1}^{m}\sum_{k=0}^{N-1}\{\boldsymbol{u}_{ik}^T\boldsymbol{u}_{ik} + \boldsymbol{x}_{ik}^T\boldsymbol{x}_{ik}\}$, which is the sum of control efforts (or the control-cost $= \sum_{i=1}^{m}\sum_{k=0}^{N-1}\{\boldsymbol{u}_{ik}^T\boldsymbol{u}_{ik}\}$) and state-costs ($= \sum_{i=1}^{m}\sum_{k=0}^{N-1}\{\boldsymbol{x}_{ik}^T\boldsymbol{x}_{ik}\}$). Three

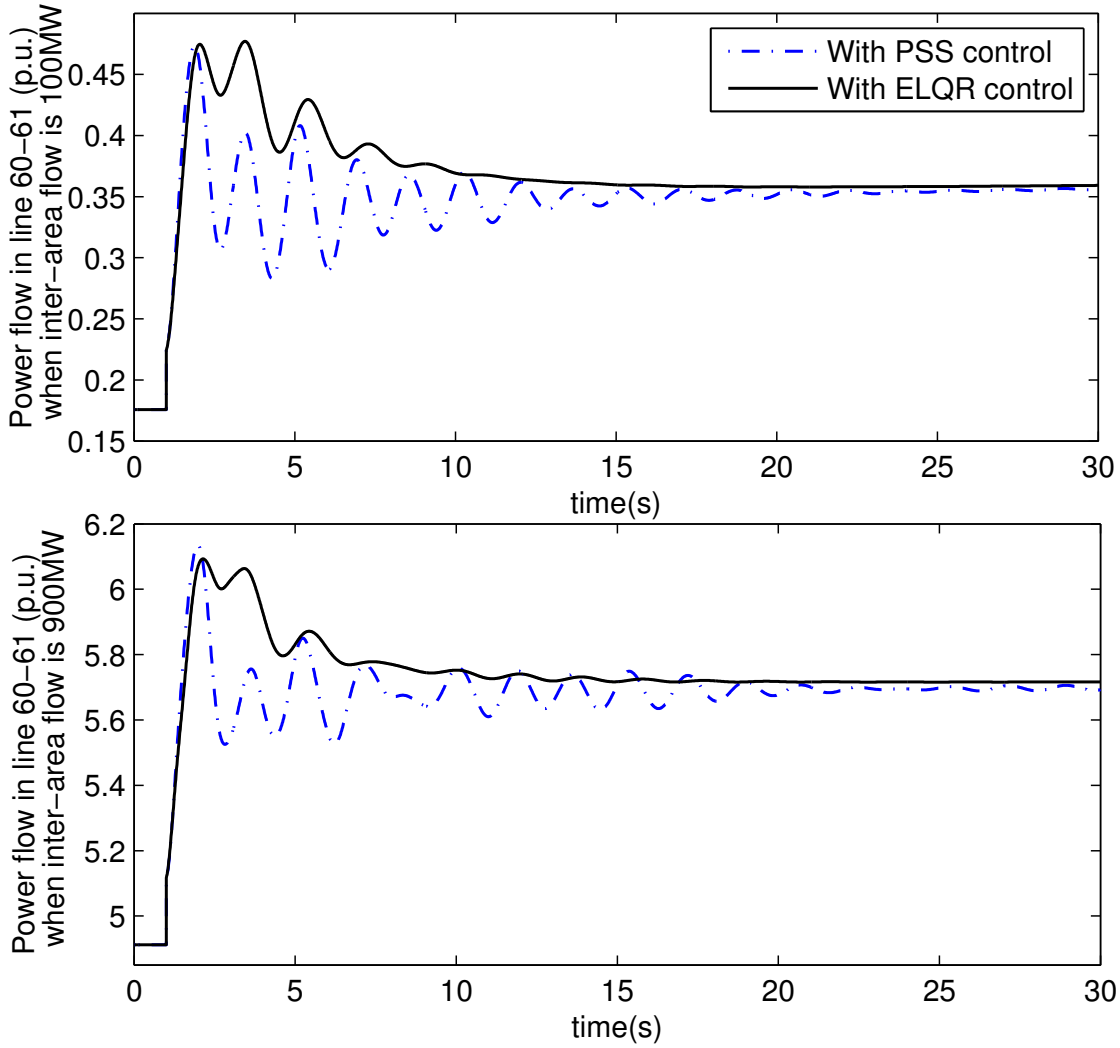

Figure 5.4: Dynamic performance for different operating conditions

more operating cases are shown in Table 5.2 in which the faulted tie-line has been changed. It can be observed that although the control-costs for PSS control and ELQR control are similar, the state-costs are reduced by an average of 28.2% and total costs are reduced by an average of 24.3% for ELQR control as compared to PSS control.

5.4.5 Comparison with centralized wide-area based control

A wide-area damping control (WADC) based control given in [20] has also been used for comparison with the proposed scheme. In this scheme, wide-area signals which have high observability of the intra-area and inter-area electromechanical modes are used to control excitation systems of several machines which have high controllability of those modes. The control signal V_{ss} is used for this purpose,

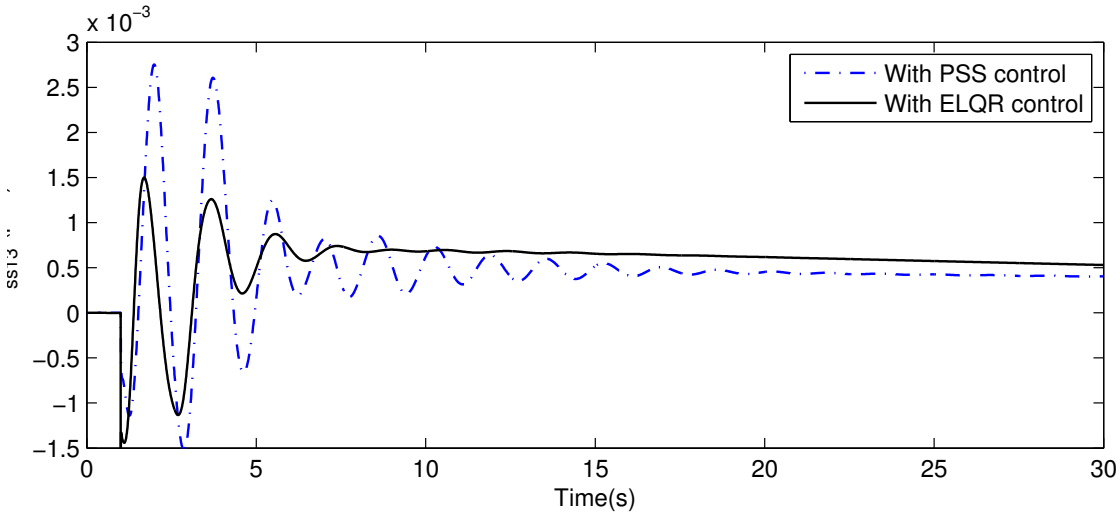

Figure 5.5: Comparison of the values of control signal for unit 13

Table 5.2: Comparison of total costs

Operating condition: interarea powerflow and faulted tie-line	Total cost (state-cost + control-cost) for PSS control (p.u.)	Total cost (state-cost + control-cost) for ELQR control (p.u.)
700 MW, 53-54	2.244 (1.908 + 0.336)	1.679 (1.391 + 0.288)
100 MW, 53-54	0.360 (0.312 + 0.048)	0.214 (0.165 + 0.049)
900 MW, 53-54	3.732 (3.228 + 0.504)	2.951 (2.491 + 0.460)
700 MW, 27-53	0.212 (0.192 + 0.020)	0.184 (0.155 + 0.029)
100 MW, 27-53	0.148 (0.132 + 0.016)	0.102 (0.084 + 0.018)
900 MW, 27-53	0.259 (0.228 + 0.031)	0.221 (0.191 + 0.030)

which is same as the control signal used by a PSS or a ELQR. The design of the centralized WADC controller is done using the linearized and reduced model of the whole system and its tuning is based on mixed H_2/H_∞ optimization with pole placement constraints as detailed in [20]. Seven power flow signals are used as output measurements and they are P_{13-17}, P_{16-18}, P_{3-62}, P_{9-29}, P_{15-42}, P_{10-31} and P_{20-19}. Each one of these signals has highest observability of one or more intra-area/inter-area modes of the system. Using these signals and the designed controller, control inputs (V_{ss}) are sent to the excitation system of each machine in the system. It is possible to select only some machines for wide-area control, but as all the machines are controlled in decentralized ELQR, in centralized WADC also all of the 16 machines have been selected for uniformity in comparison. Comparisons of time-domain simulation, modal response and control/state costs are shown in Figure 5.6, Table 5.1 and Table 5.3, respectively.

It can be observed from Figure 5.6 and Table 5.1 that the damping performance

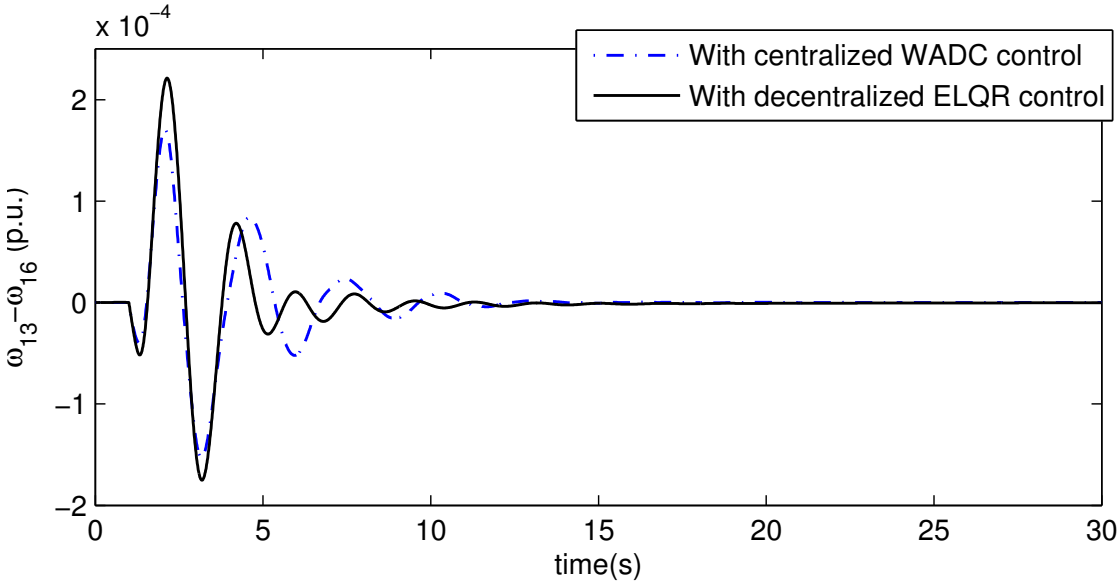

Figure 5.6: Oscillation damping comparison for WADC and ELQR

Table 5.3: Comparison of total costs for WADC vs ELQR

Operating condition: interarea powerflow and faulted tie-line	Total cost (state-cost + control-cost) for WADC control (p.u.)	Total cost (state-cost + control-cost) for ELQR control (p.u.)
700 MW, 53-54	2.580 (2.424 + 0.156)	1.679 (1.391 + 0.288)
100 MW, 53-54	0.372 (0.348 + 0.024)	0.214 (0.165 + 0.049)
900 MW, 53-54	4.440 (4.164 + 0.276)	2.951 (2.491 + 0.460)
700 MW, 27-53	0.276 (0.264 + 0.012)	0.184 (0.155 + 0.029)
100 MW, 27-53	0.184 (0.180 + 0.004)	0.102 (0.084 + 0.018)
900 MW, 27-53	0.312 (0.298 + 0.014)	0.221 (0.191 + 0.030)

of ELQR control and WADC are comparable, and WADC gives better damping ratios to the second and fourth inter-area modes, while ELQR control gives better damping to the first and third modes. The costs (as shown in Table 5.3), are not as uniformly distributed between state costs and control efforts as in the case of ELQR control, and thus the total costs are higher for WADC than ELQR control. This is expected as mixed H_2/H_∞ optimization is not as optimal as ELQR control as far as net quadratic costs are concerned. Thus, it can be concluded that the proposed scheme performs at par (or even better than) an established wide-area based centralized damping control method. Considering the facts that WADC requires information of the whole system for controller design and requires a fast and reliable communication network for transmission of measurements and control signals, decentralized ELQR is a better choice over centralized WADC.

5.4.6 Effect of noise/bad-data on control performance

ELQR control is affected by noise and bad-data in the measurements, but the effect is too small to make any impact on the control performance. All the aforementioned results of the case study have been obtained considering noise and bad-data in the measurements. For comparison, results have also been obtained without considering any noise or bad-data in the measurements, and the costs are shown in Table 5.4.

Table 5.4: Comparison of total cost with and without noise/bad-data

Condition: interarea flow, faulted tie-line	Total cost with noise (state-cost+control-cost) for ELQR control (p.u.)	Total cost without noise (state-cost+control-cost) for ELQR control (p.u.)
700 MW, 53-54	1.679 (1.391 + 0.288)	1.675 (1.390 + 0.285)
100 MW, 53-54	0.214 (0.165 + 0.049)	0.212 (0.164 + 0.048)
900 MW, 53-54	2.951 (2.491 + 0.460)	2.947 (2.490 + 0.457)
700 MW, 27-53	0.184 (0.155 + 0.029)	0.183 (0.154 + 0.029)
100 MW, 27-53	0.102 (0.084 + 0.018)	0.102 (0.084 + 0.018)
900 MW, 27-53	0.221 (0.191 + 0.030)	0.220 (0.190 + 0.030)

It can be observed from Table 5.4 that the results of case study remain almost same with and without noise in the measurements, and the state-costs differ by an average of 0.2% and control costs differ by an average of 0.5%. First reason for such a small change is that majority of the contribution in the ELQR control output comes from the seven state estimates from which noise and bad-data have been filtered out. Secondly, the level of noise in the measurements is very small: the standard deviation of the noise in magnitude measurements is 0.1% of true values and in phase measurements it is 0.1 *mrad*, for both voltage and current signals. These noise levels are as per IEC 60044/IEEE C57.13 standards for CTs and PTs and IEEE C37.118.1-2011 standard for PMUs as explained in Chapter 3. Such a small level of noise implies that the measurements deviate very little from their true values. Lastly, bad-data in the measurements is detected, removed and replaced with latest correct-data using the bad-data detection algorithm given in Chapter 3. Thus, noise and bad-data have negligible impact on the ELQR control performance.

5.4.7 Computational feasibility

The complete simulation of the power system, along with the dynamic estimators and the ELQR controllers at each of the 16 machines, runs in real-time. In the case study, a 30 s simulation takes an average running time of 5.5 s on a personal computer with Intel Core 2 Duo, 2.0 GHz CPU and 2 GB RAM. Hence the computational requirements at one machine can be easily met for both DSE and ELQR control.

5.5 Summary

A control scheme has been presented for the decentralized control of power system dynamics. The scheme utilizes dynamic state estimation using local PMU measurements and machine parameters, and employs the concept of pseudo-inputs for decentralization. It is based on an extended version of linear quadratic regulator which self-tunes in real-time to varying operating condition of the system. The scheme is also computationally feasible and easily implementable. The main advantages of this architecture are:

1. Besides being optimal, the control is completely decentralized and only local measurements and machine parameters are needed, and hence communication requirements are minimized.
2. Computational requirements are less intensive; so can be easily met by a personal computer.
3. Existing PMU in each decentralized location is adequate; no extra investment is required.
4. The control law remains valid for any operating condition, and the control gains are updated in real-time. This indirectly renders the control scheme adaptive to current operating point.
5. The scheme can be seamlessly integrated with the control devices which are already present, such as PSSs, FACTS controllers.

To summarize, research findings show that the integrated scheme which has been proposed in this thesis is very practical for reliable estimation and control of the power systems of the 21^{st} century.

Chapter 6

Conclusion and future work

The work described in this thesis is concerned with the study and development of decentralized methods for estimation and control in power systems. It has been shown that the developed methods are practical for current power systems and these methods have also been demonstrated on a benchmark power system model. The work also has a wide scope for future research and extensions. The conclusions of this thesis and recommendations for future work are presented as follows.

6.1 Thesis conclusions

The importance of robust control of power systems, so that they operate within their stability margins, is undisputed in today's age of growing power requirements and bulky power system architecture. Having elaborated on the limitation of control and monitoring tools in present power systems, reliant on EMSs and steady state analysis, this research has sought to address the constraint in dynamic estimation and control of power systems, that is, the unavailability of a fast, reliable and secure communication network. Specifically, this research has

1. studied the impact of introducing packet based communication network in the control loops of power systems on the overall system stability, and
2. proposed a decentralized algorithm for dynamic state estimation and used the estimates, thus obtained, to generate a decentralized control law. The integrated control scheme has been demonstrated to be completely decentralized, thereby providing a practical alternative for eliminating the requirement of

a fast and reliable communication network necessary for centralized control approach.

In analyzing the stability effects of introducing a packet-based communication network in the control loops of a power system, this research has developed a generalized framework to assess the effects of packet-dropout on the oscillatory stability response of a networked controlled power system (NCPS). A formal approach has also been devised to compute the lower limit on the probability of packet dropout to guarantee the specified damping and stability margins for any operating condition of a power system.

The NCPS model, however, assumes applicability only with update-rates of faster communication networks than that used in present day power-systems. Hence, the research progresses to the next logical examination of performing the dynamic estimation and control of power system in a decentralized manner, as an alternative for fast and reliable communication network. First, a scheme for decentralized estimation of the dynamic states and parameters of a power system has been proposed. The scheme rests on the new concept of treating some of the measured signals as pseudo-inputs and utilizes unscented Kalman filtering for dynamic state estimation of power systems. The feasibility, speed, simplicity and accuracy of the proposed scheme over centralized schemes has been demonstrated. A comparison of the results obtain clearly establishes the proposed method to be much advantageous for dynamic state estimation for dynamic control and dynamic security assessment in modern power systems. Next, the research proceeds to provide a decentralized control law using the dynamic states obtained. A control scheme, termed as extended linear quadratic regulator (ELQR), has been developed for the optimal control of a linear system in which both traditional inputs and pseudo-inputs are present. Demonstrating the applicability of the control scheme on a simple model LTI system, the control law has been found to significantly minimize the state deviation costs and the required control effort, over the classical LQR scheme.

The concepts of decentralized DSE and ELQR are integrated for the ultimate objective of decentralized estimation and control of a power system. The decentralized estimation and control scheme has been successfully implemented and validated on a benchmark 68-bus 16-machine system in MATLAB. The results obtained and comparisons with centralized LQR control prove that the fully decentralized integrated control scheme is not only optimal, computationally feasible and easily implementable, but also potentially dispenses with the communication

requirements of the centralized control schemes. Thus, this research proposes and successfully demonstrates a very practical and reliable estimation and control scheme for the power systems of the 21^{st} century.

6.2 Recommendations for future work

Although the results presented in the thesis have demonstrated the applicability of the decentralized estimation and control schemes for power systems, the work may be further developed in a number of ways:

6.2.1 Integration of renewable sources and HVDC

The power system model used in this thesis considers the most widely used components in current power systems, namely synchronous machines, AC transmission network (consisting of lines and transformers), FACTS devices and loads. New distributed sources of energy, such as wind and solar, and new transmission technology of high voltage direct current (HVDC) are increasingly being integrated in present power systems and are likely to form a significant part of future systems. The technique of decentralized estimation and control is very relevant to these stochastic and distributed sources of generation, and more research needs to be undertaken to extend this technique to a unified power system model in which old and new technologies of both generation and transmission are integrated together.

6.2.2 Eliminating PMUs from the decentralized DSE algorithm

The decentralized DSE algorithm presented in this thesis relies on PMU measurements for the estimation process. The reason for this is that both magnitude and phase information of voltage and current signals are required in the filtering equations. PMUs provide the phase information using GPS synchronization, and hence the presented DSE algorithm relies heavily on GPS synchronization. This is not very desirable as DSE would fail if GPS synchronization fails. A challenging and very useful extension to this method would involve finding a technique which only requires voltage and current magnitudes and other locally measurable quantities which do not require GPS synchronization.

6.2.3 Development of model-less methods

The algorithms for decentralized estimation and control require the knowledge of machine model and its parameters. If this knowledge is not accurate, or if the parameters deviate from the values which are used in these methods (due to factors such as operating temperature), then the state estimates and control law would also deviate from their desired values. A solution to this problem is constant monitoring of system parameters. Another solution is application of 'model-less' techniques, such as those given in [91], for development of decentralized estimation and control algorithms.

6.2.4 Development of non-linear decentralized control algorithms

Although the DSE algorithm which has been presented in the thesis is a non-linear estimation algorithm, the control law still requires linearization of the non-linear machine equations. This limits the applicability of the control law to small signal stability which involves small disturbances from the steady state operating point. Further research can be undertaken to develop non-linear control algorithms for decentralized and real-time control of even large disturbances occurring in power systems. This can involve application and development of traditional non-linear techniques based on energy functions and Lyapunov theory [92], [36].

Thus, a lot of scope exists for further research and development in the area of decentralized estimation and control of power systems, and the work undertaken in this thesis is a step in this direction.

Appendix A

DAEs of a generating unit

The DAEs of a generating unit in a power system (that is, the equations of a machine and its excitation system (assuming a static excitation system)) are given as follows ([50], [51]).

$$\dot{\boldsymbol{x}} = \boldsymbol{g}(\boldsymbol{x}, \boldsymbol{u}, \boldsymbol{u}') = \boldsymbol{g}, \text{ where } \boldsymbol{u} = V_{ss}, \ \boldsymbol{u}' = [V \ f]^T, \tag{A.1}$$

$$\boldsymbol{x} = [\alpha \ \omega \ E'_d \ E'_q \ \Psi_{1d} \ \Psi_{2q} \ E'_{dc} \ V_r]^T; \text{ or, } \boldsymbol{x} = [\delta \ \omega \ E'_d \ E'_q \ \Psi_{1d} \ \Psi_{2q} \ E'_{dc} \ V_r]^T \tag{A.2}$$

In the definition of state vector $\boldsymbol{x}$ (in (A.2)) either α or δ can be taken as a state. The vector $\boldsymbol{g}$ consists of eight functions corresponding to the eight states in $\boldsymbol{x}$, $\boldsymbol{g} = [g_\alpha \ g_\omega \ g_{E'_d} \ g_{E'_q} \ g_{\Psi_{1d}} \ g_{\Psi_{2q}} \ g_{E'_{dc}} \ g_{V_r}]^T$ or $\boldsymbol{g} = [g_\delta \ g_\omega \ g_{E'_d} \ g_{E'_q} \ g_{\Psi_{1d}} \ g_{\Psi_{2q}} \ g_{E'_{dc}} \ g_{V_r}]^T$. The DAEs for a generating unit are as follows:

$$\dot{\alpha} = \omega_b(\omega - f) = g_\alpha, \tag{A.3}$$

$$\dot{\delta} = \omega_b(\omega - 1) = g_\delta, \tag{A.4}$$

$$\dot{\omega} = (T_m - T_e - D(\omega - 1))/(2H) = g_\omega, \tag{A.5}$$

$$\dot{E}'_d = -(E'_d + (X_q - X'_q)\{K_{q1}I_q + K_{q2}\frac{\Psi_{2q} + E'_d}{X'_q - X_l}\})/T'_{q0} = g_{E'_d}, \tag{A.6}$$

$$\dot{E}'_q = [E_{fd} + (X_d - X'_d)\{K_{d1}I_d + K_{d2}\frac{\Psi_{1d} - E'_q}{X'_d - X_l}\} - E'_q]/T'_{d0} = g_{E'_q}, \tag{A.7}$$

$$\dot{\Psi}_{1d} = (E'_q + (X'_d - X_l)I_d - \Psi_{1d})/T''_{d0} = g_{\Psi_{1d}}, \tag{A.8}$$

$$\dot{\Psi}_{2q} = (-E'_d + (X'_q - X_l)I_q - \Psi_{2q})/T''_{q0} = g_{\Psi_{2q}}, \tag{A.9}$$

$$\dot{E}'_{dc} = ((X''_d - X''_q)I_q - E'_{dc})/T_c = g_{E'_{dc}}, \tag{A.10}$$

$$\dot{V}_r = (V - V_r)/T_r = g_{V_r}; \tag{A.11}$$

$$\text{where, } E_{fd} = K_a(V_{ref} + V_{ss} - V_r),\ E_{fdmin} \leq E_{fd} \leq E_{fdmax}, \tag{A.12}$$

$$I_d = (R_a(E'_d K_{q1} - \Psi_{2q}K_{q2} + E'_{dc} - V_d) - X''_d(E'_q K_{d1} + \Psi_{1d}K_{d2} - V_q))/Z_a^2, \tag{A.13}$$

$$I_q = (R_a(E'_q K_{d1} + \Psi_{1d}K_{d2} - V_q) + X''_d(E'_d K_{q1} - \Psi_{2q}K_{q2} + E'_{dc} - V_d))/Z_a^2, \tag{A.14}$$

$$V_d = -V\sin\alpha = -V\sin(\delta - \theta), \tag{A.15}$$

$$V_q = V\cos\alpha = V\cos(\delta - \theta), \tag{A.16}$$

$$T_e = E'_d I_d K_{q1} + E'_q I_q K_{d1} + \Psi_{1d} I_q K_{d2} - \Psi_{2q} I_d K_{q2} + I_d I_q (X''_d - X''_q). \tag{A.17}$$

If a DC1A type of excitation is used, then the eqautions change as follows:

$$\dot{V}_r = (V - V_r)/T_r, \tag{A.18}$$

$$\dot{V}_a = [K_a(V_{ref} + V_{ss} - V_r) - V_a]/T_a; \tag{A.19}$$

$$\dot{E}_{fd} = -[E_{fd}(K_x + A_x e^{B_x E_{fd}}) - V_a]/T_x; \text{ where } E_{fdmin} \leq E_{fd} \leq E_{fdmax}. \tag{A.20}$$

Appendix B

Dynamic state estimation plots for unit 9 and unit 13

The dynamic state estmation plots for the 9^{th} and the 13^{th} generating units are as follows.

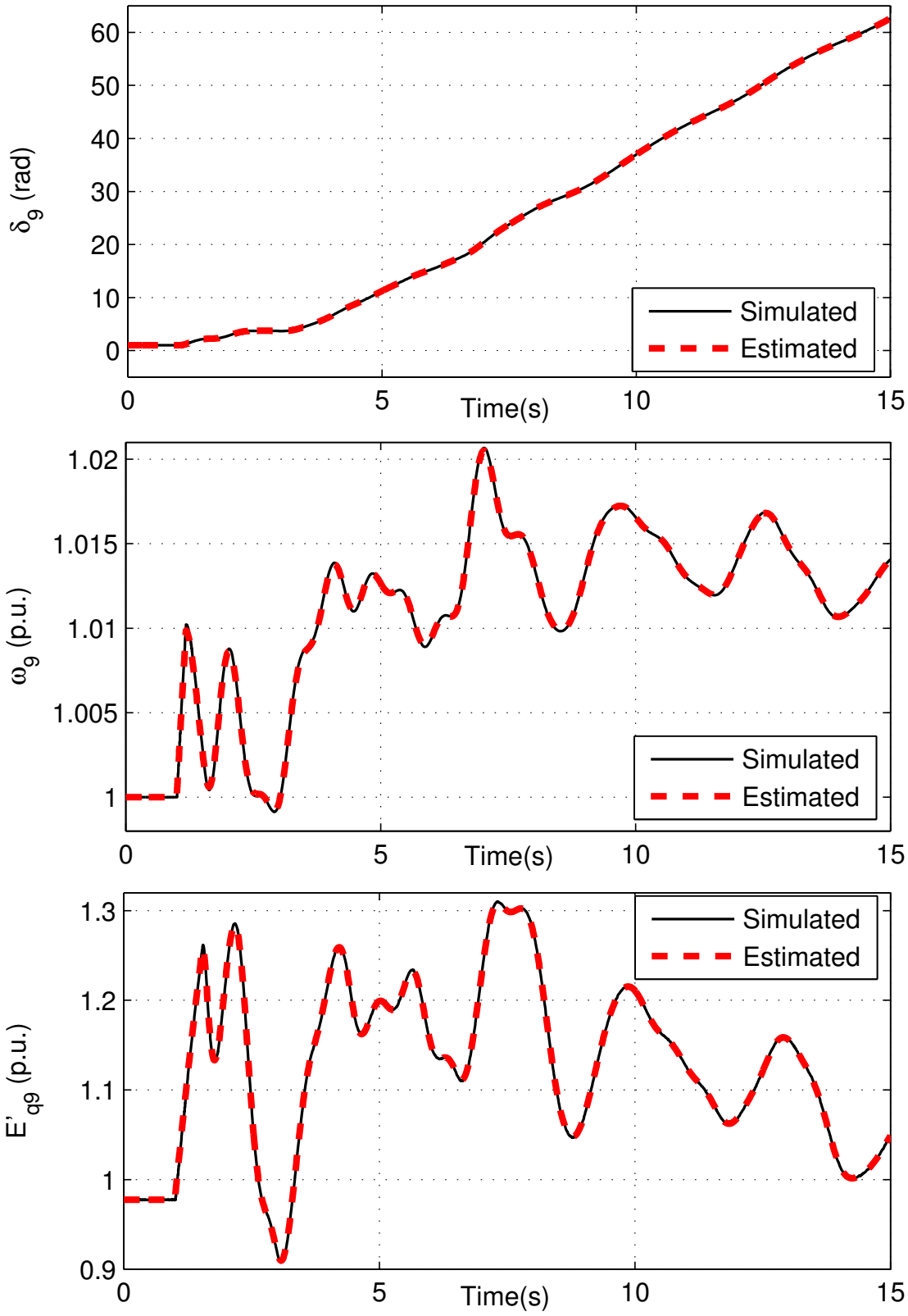

Figure B.1: Estimated vs simulated values for δ, ω and E'_q of the 9^{th} unit

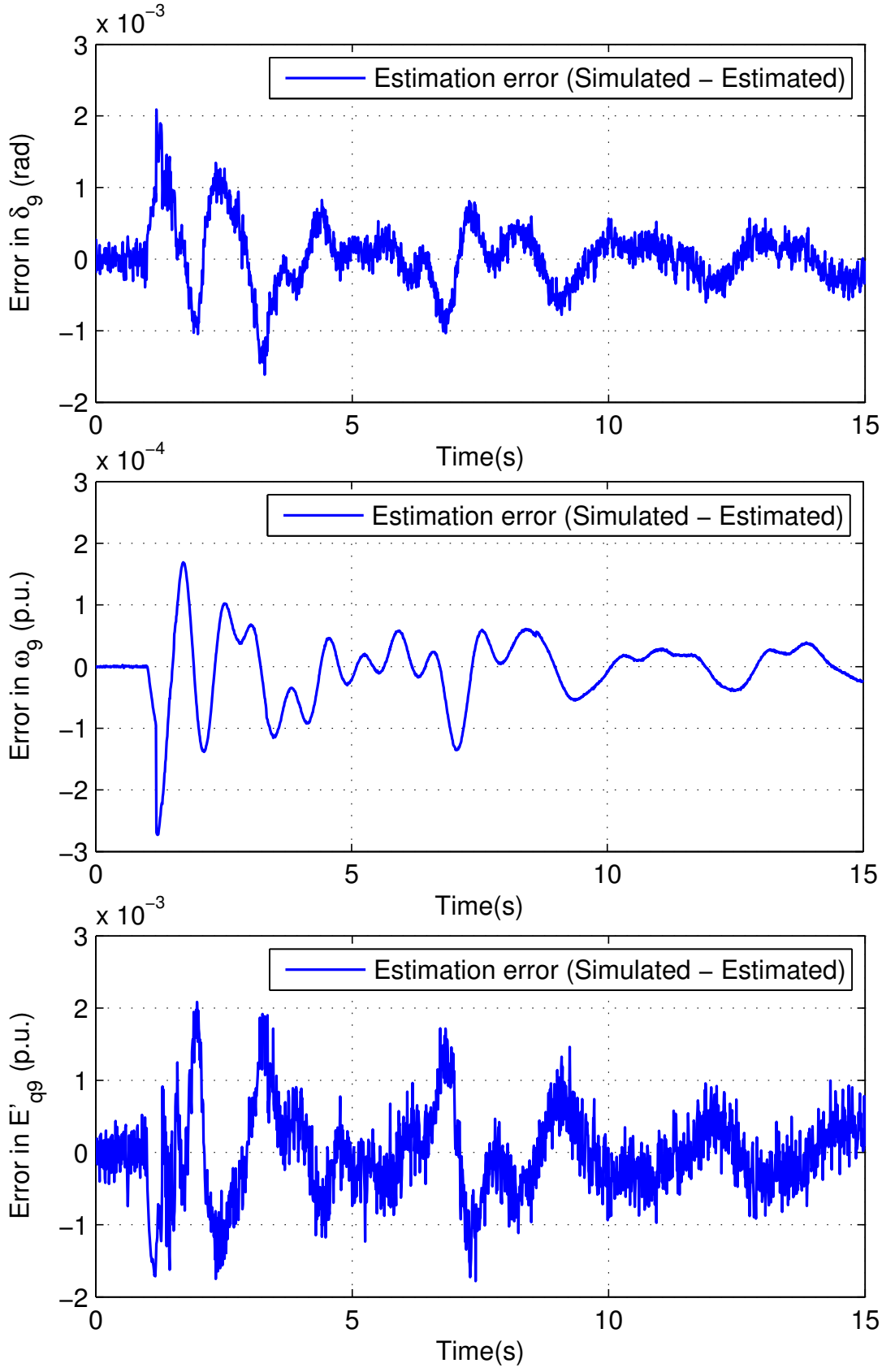

Figure B.2: Estimation errors for δ, ω and E'_q of the 9^{th} unit

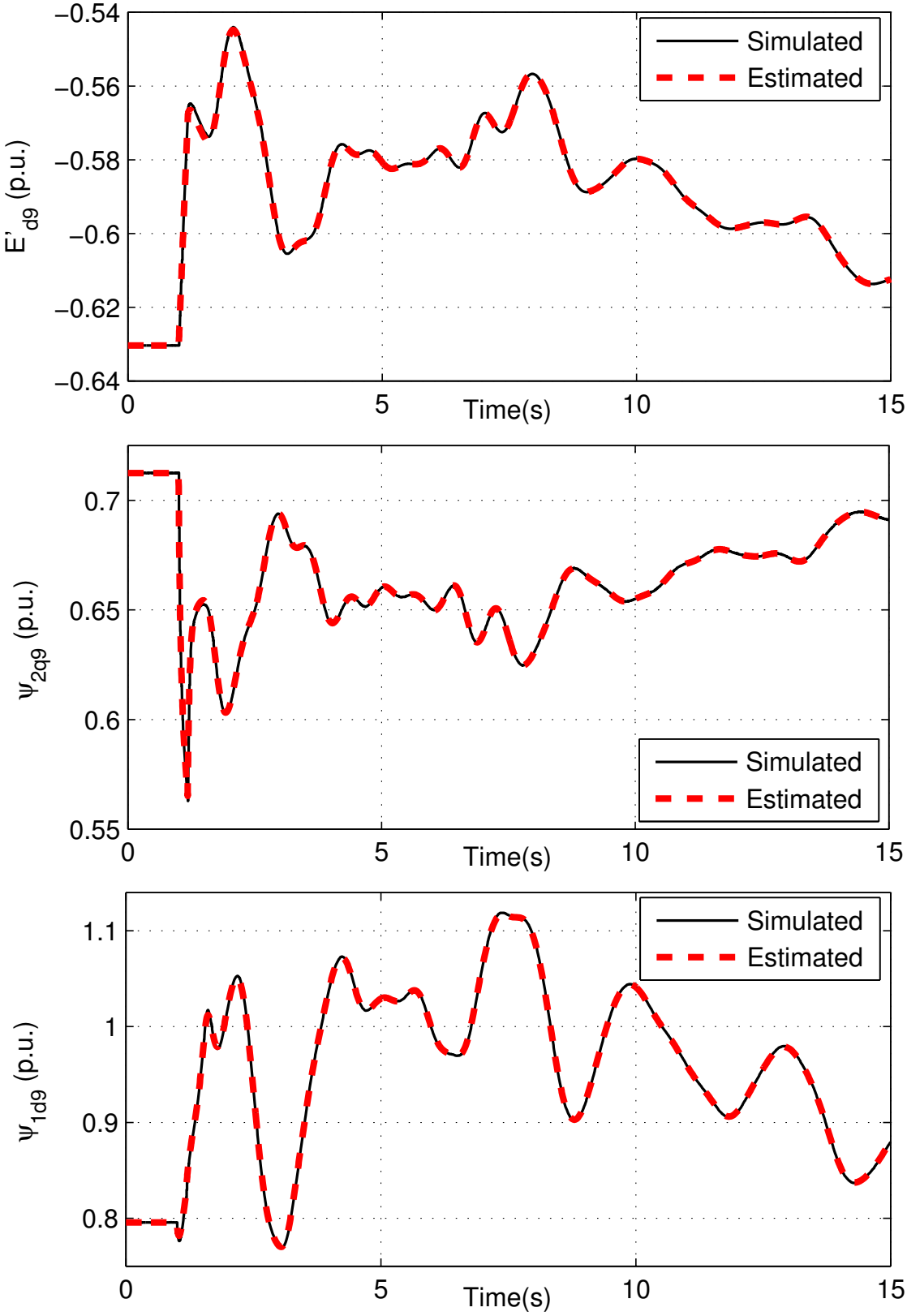

Figure B.3: Estimated vs simulated values for E'_d, Ψ_{2q} and Ψ_{1d} of the 9^{th} unit

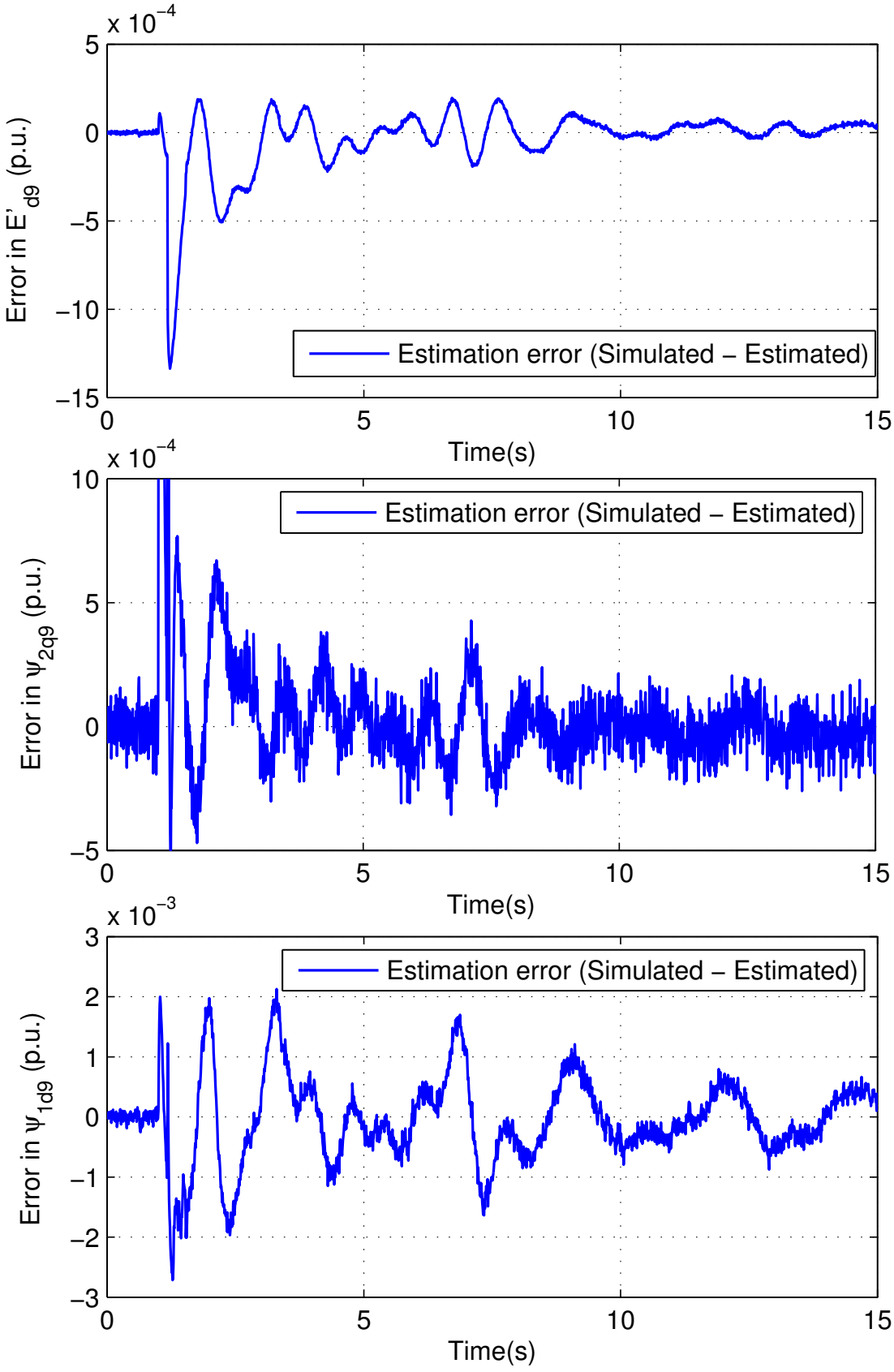

Figure B.4: Estimation errors for E'_d, Ψ_{2q} and Ψ_{1d} of the 9^{th} unit

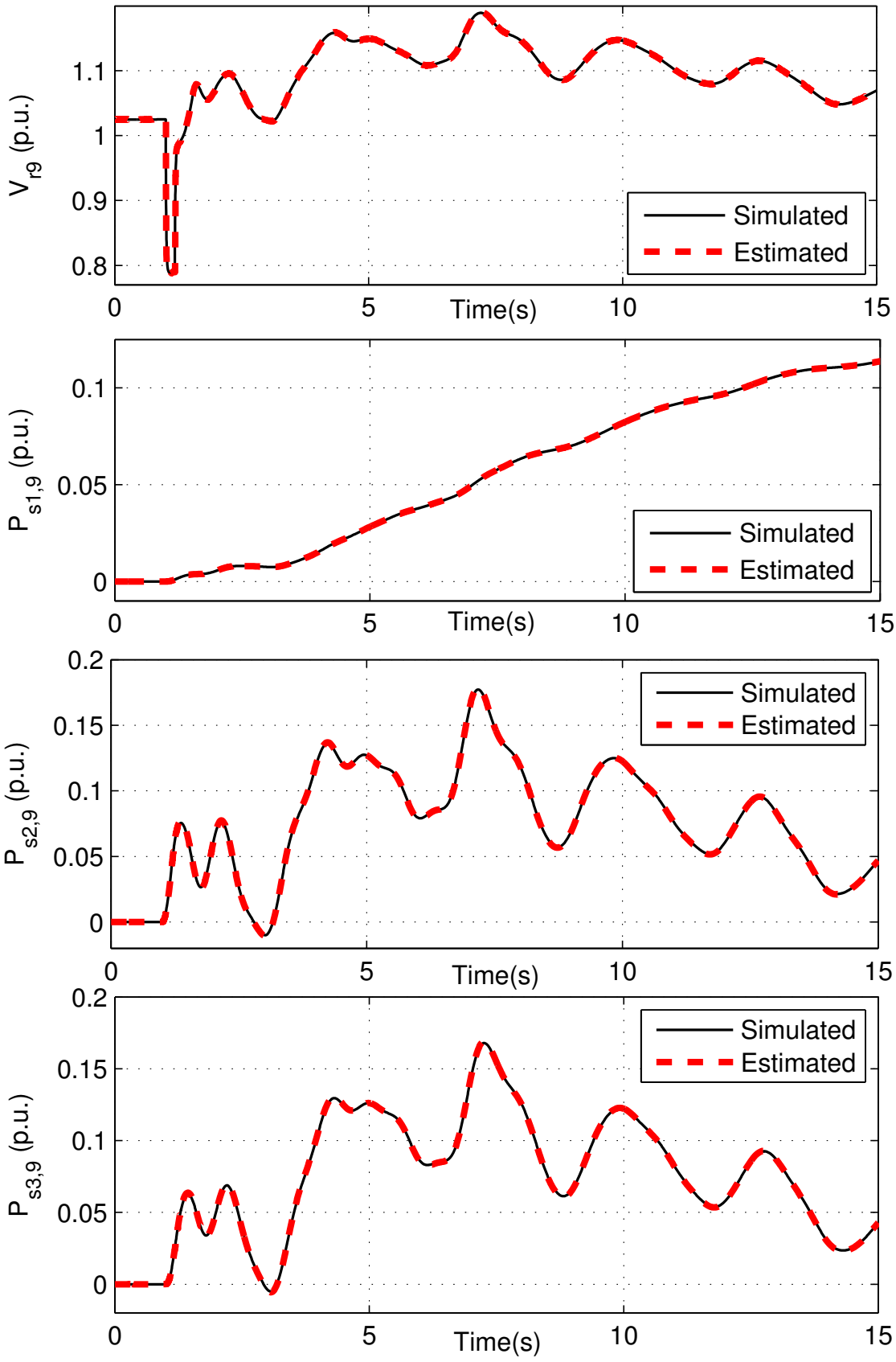

Figure B.5: Estimated vs simulated values for V_{r9} & PSS states of the 9^{th} unit

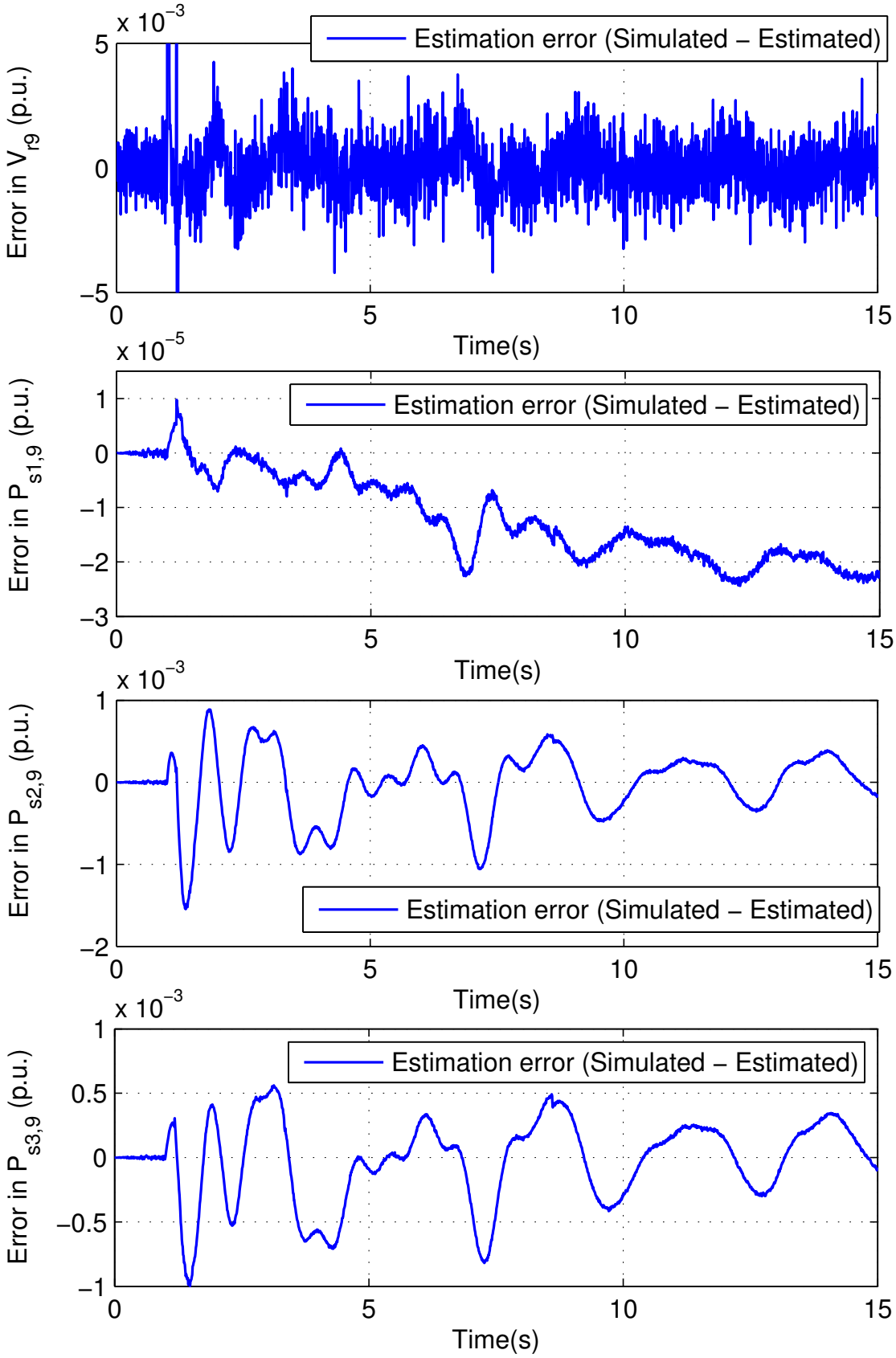

Figure B.6: Estimation errors for V_{r9} & PSS states of the 9^{th} unit

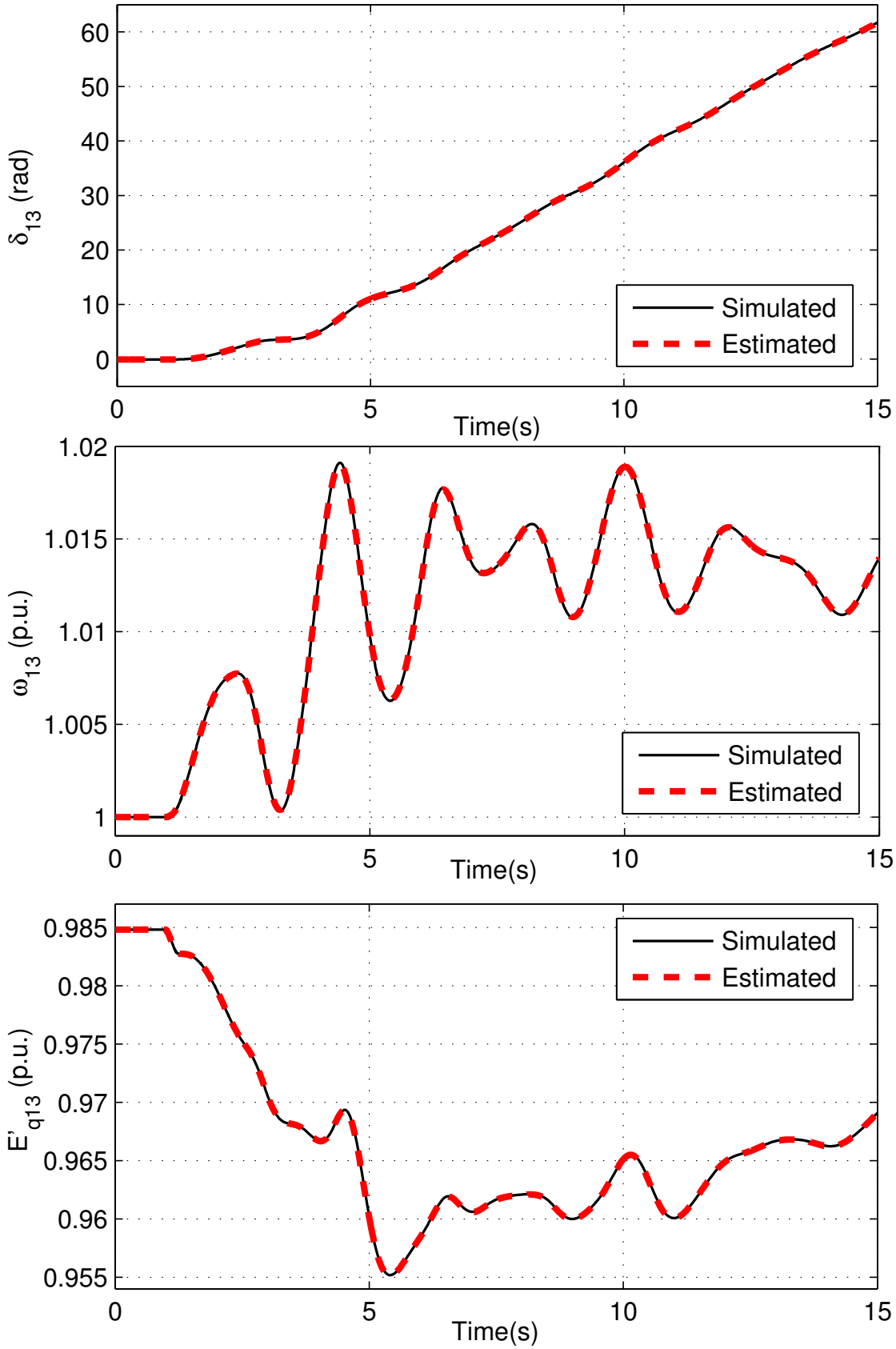

Figure B.7: Estimated vs simulated values for δ, ω and E'_q of the 13^{th} unit

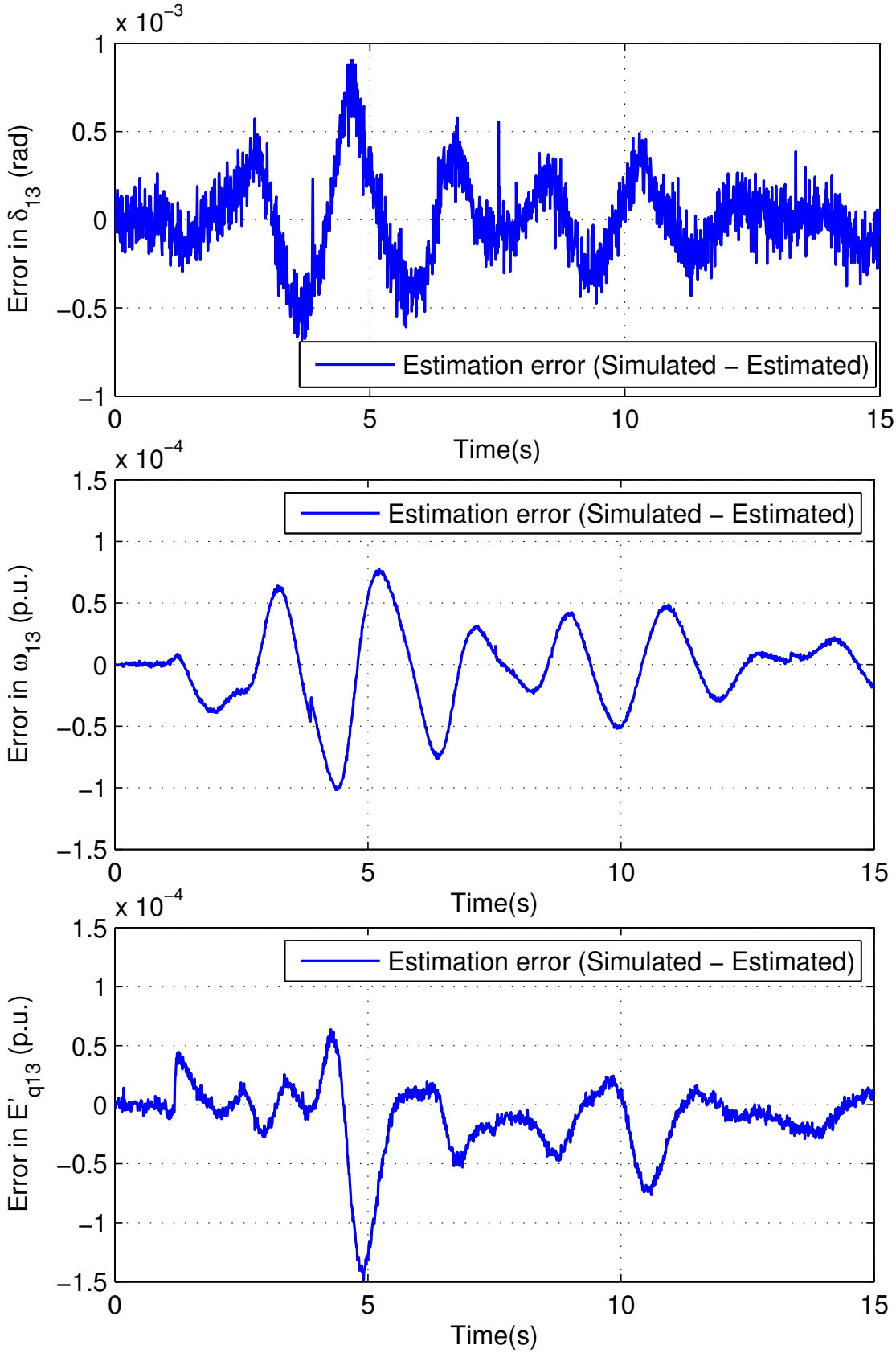

Figure B.8: Estimation errors for δ, ω and E'_q of the 13^{th} unit

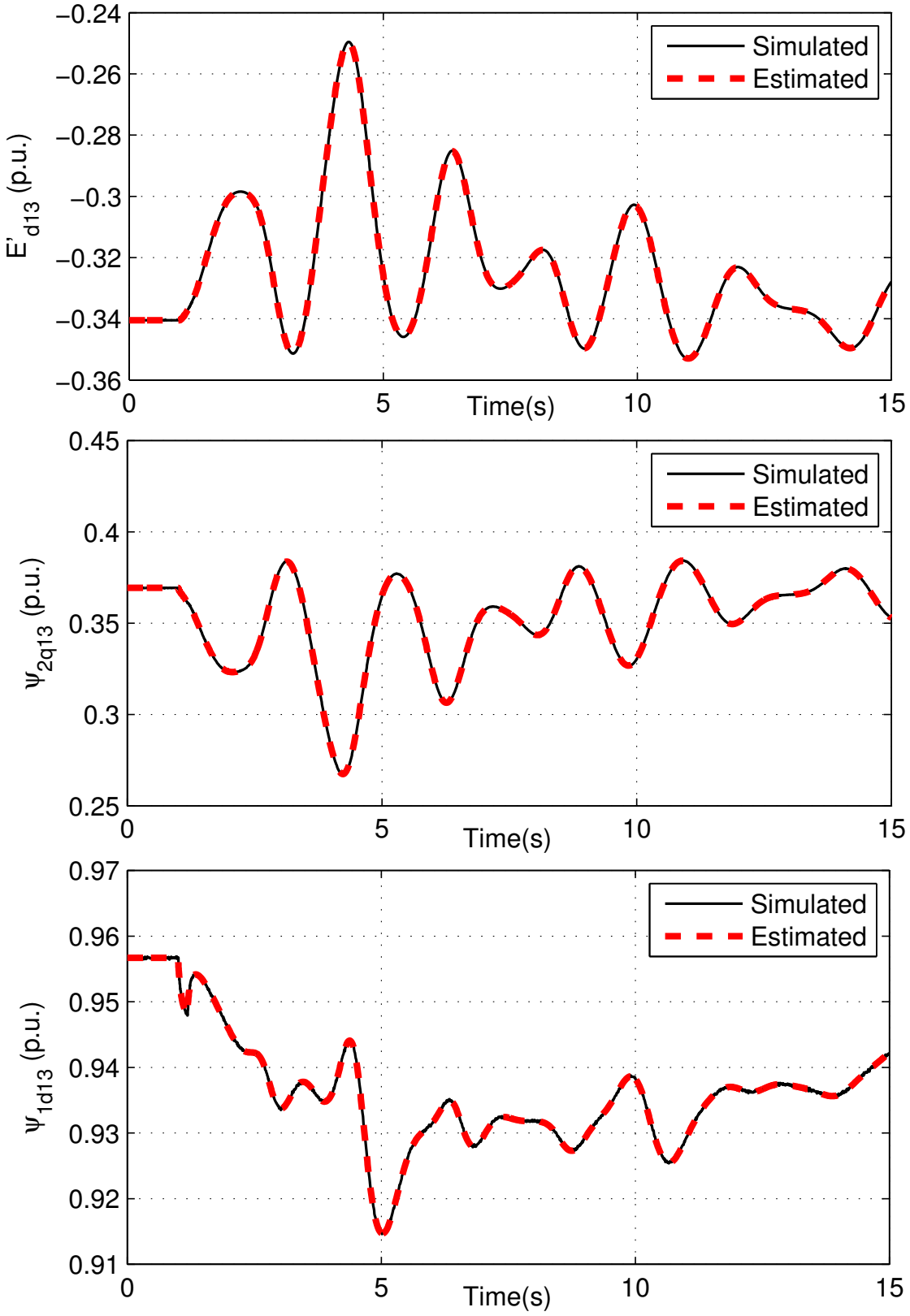

Figure B.9: Estimated vs simulated values for E'_d, Ψ_{2q} and Ψ_{1d} of the 13^{th} unit

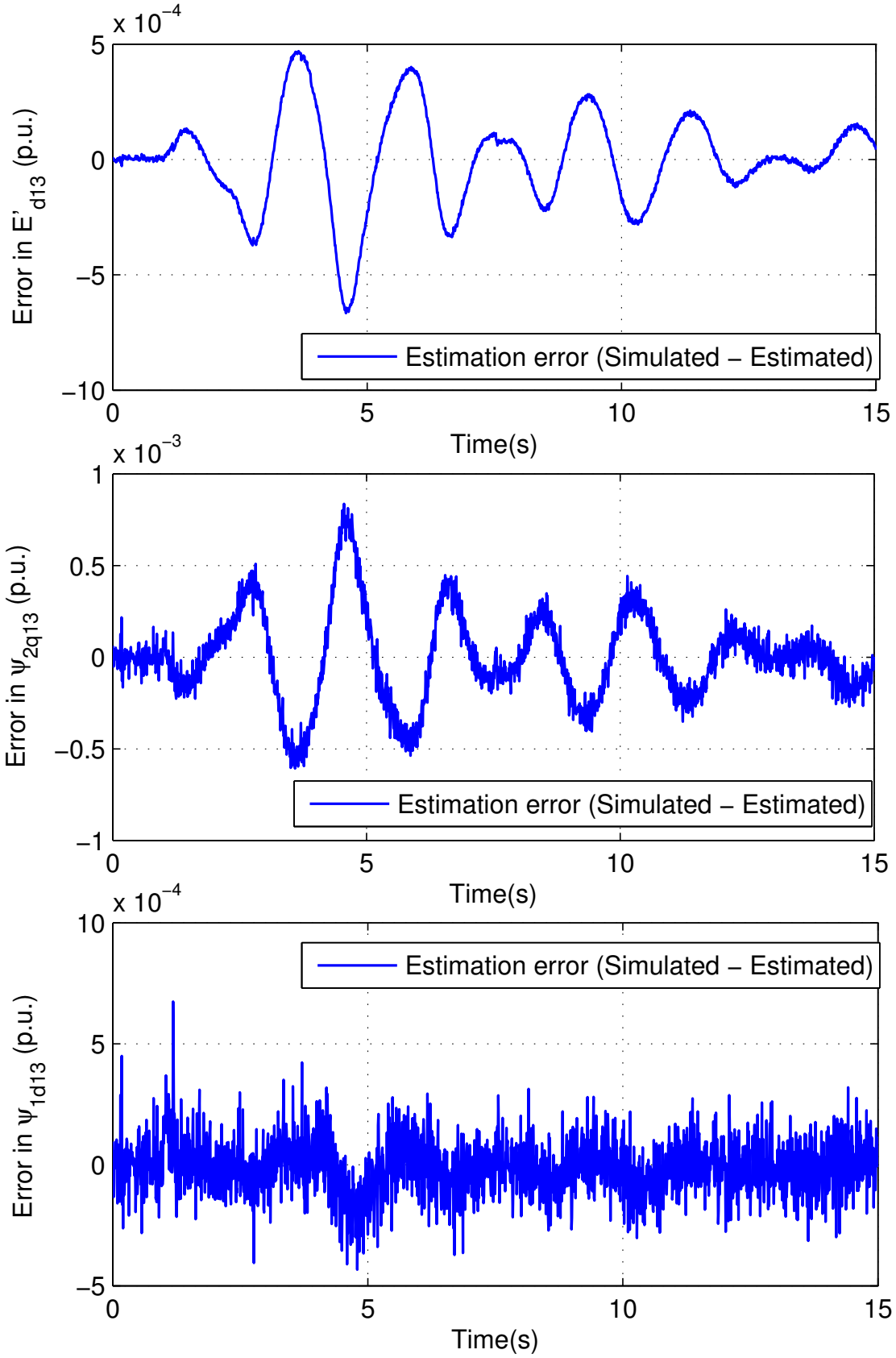

Figure B.10: Estimation errors for E'_d, Ψ_{2q} and Ψ_{1d} of the 13^{th} unit

Appendix C

Details of state matrices used in integrated ELQR

Linearizing (A.1) in Appendix A gives:

$$\Delta\dot{\boldsymbol{x}} = \boldsymbol{A}\Delta\boldsymbol{x} + \boldsymbol{B}\Delta\boldsymbol{u} + \boldsymbol{B}'\Delta\boldsymbol{u}', \tag{C.1}$$

$$\text{where, } \boldsymbol{A} = \frac{\partial \boldsymbol{g}}{\partial \boldsymbol{x}}, \boldsymbol{B} = \frac{\partial \boldsymbol{g}}{\partial \boldsymbol{u}}, \boldsymbol{B}' = \frac{\partial \boldsymbol{g}}{\partial \boldsymbol{u}'} \tag{C.2}$$

Next, some intermediate partial derivatives are calculated using the DAEs in Appendix A:

$$\frac{\partial I_d}{\partial \alpha} = \frac{V(R_a \cos\alpha - X''_d \sin\alpha)}{Z_a^2}, \tag{C.3}$$

$$\frac{\partial I_q}{\partial \alpha} = \frac{V(R_a \sin\alpha + X''_d \cos\alpha)}{Z_a^2}, \tag{C.4}$$

$$\frac{\partial I_d}{\partial E'_d} = \frac{R_a K_{q1}}{Z_a^2}, \tag{C.5}$$

$$\frac{\partial I_q}{\partial E'_d} = \frac{X''_d K_{q1}}{Z_a^2}, \tag{C.6}$$

$$\frac{\partial I_d}{\partial E'_q} = \frac{-X''_d K_{d1}}{Z_a^2}, \tag{C.7}$$

$$\frac{\partial I_q}{\partial E'_q} = \frac{R_a K_{d1}}{Z_a^2}, \tag{C.8}$$

$$\frac{\partial I_d}{\partial \Psi_{1d}} = \frac{-X''_d K_{d2}}{Z_a^2}, \tag{C.9}$$

$$\frac{\partial I_q}{\partial \Psi_{1d}} = \frac{R_a K_{d2}}{Z_a^2}, \tag{C.10}$$

$$\frac{\partial I_d}{\partial \Psi_{2q}} = \frac{-R_a K_{q2}}{Z_a^2}, \tag{C.11}$$

$$\frac{\partial I_q}{\partial \Psi_{2q}} = \frac{-X''_d K_{q2}}{Z_a^2}, \tag{C.12}$$

$$\frac{\partial I_d}{\partial E'_{dc}} = \frac{R_a}{Z_a^2}, \tag{C.13}$$

$$\frac{\partial I_q}{\partial E'_{dc}} = \frac{X''_d}{Z_a^2}, \tag{C.14}$$

$$\frac{\partial T_e}{\partial I_d} = E'_d K_{q1} - \Psi_{2q} K_{q2} - I_q (X''_d - X''_q), \tag{C.15}$$

$$\frac{\partial T_e}{\partial I_q} = E'_q K_{d1} - \Psi_{1d} K_{d2} - I_d (X''_d - X''_q), \tag{C.16}$$

$$\frac{\partial I_d}{\partial V} = \frac{R_a \sin\alpha + X''_d \cos\alpha}{Z_a^2}, \tag{C.17}$$

$$\frac{\partial I_q}{\partial V} = \frac{-R_a \cos\alpha + X''_d \sin\alpha}{Z_a^2} \tag{C.18}$$

Using (C.1), the DAEs in Appendix A and the above intermediate derivatives, the various non-zero terms of $\boldsymbol{A}$, $\boldsymbol{B}$ and $\boldsymbol{B'}$ are given as:

$$\boldsymbol{A}_{1,2} = \frac{\partial g_\alpha}{\partial \omega} = \omega_B \tag{C.19}$$

$$\boldsymbol{A}_{2,1} = \frac{\partial g_\omega}{\partial \alpha} = \frac{-1}{2H}\left(\frac{\partial T_e}{\partial I_d}\frac{\partial I_d}{\partial \alpha} + \frac{\partial T_e}{\partial I_q}\frac{\partial I_q}{\partial \alpha}\right) \tag{C.20}$$

$$\boldsymbol{A}_{2,2} = \frac{\partial g_\omega}{\partial \omega} = \frac{-D}{2H} \tag{C.21}$$

$$\boldsymbol{A}_{2,3} = \frac{\partial g_\omega}{\partial E'_d} = \frac{-1}{2H}\left(I_d K_{q1} + \frac{\partial T_e}{\partial I_d}\frac{\partial I_d}{\partial E'_d} + \frac{\partial T_e}{\partial I_q}\frac{\partial I_q}{\partial E'_d}\right) \tag{C.22}$$

$$\boldsymbol{A}_{2,4} = \frac{\partial g_\omega}{\partial E'_q} = \frac{-1}{2H}\left(I_q K_{d1} + \frac{\partial T_e}{\partial I_d}\frac{\partial I_d}{\partial E'_q} + \frac{\partial T_e}{\partial I_q}\frac{\partial I_q}{\partial E'_q}\right) \tag{C.23}$$

$$\boldsymbol{A}_{2,5} = \frac{\partial g_\omega}{\partial \Psi_{1d}} = \frac{-1}{2H}\left(I_q K_{d2} + \frac{\partial T_e}{\partial I_d}\frac{\partial I_d}{\partial \Psi_{1d}} + \frac{\partial T_e}{\partial I_q}\frac{\partial I_q}{\partial \Psi_{1d}}\right) \tag{C.24}$$

$$\boldsymbol{A}_{2,6} = \frac{\partial g_\omega}{\partial \Psi_{2q}} = \frac{-1}{2H}\left(-I_d K_{q2} + \frac{\partial T_e}{\partial I_d}\frac{\partial I_d}{\partial \Psi_{2q}} + \frac{\partial T_e}{\partial I_q}\frac{\partial I_q}{\partial \Psi_{2q}}\right) \tag{C.25}$$

$$\boldsymbol{A}_{2,7} = \frac{\partial g_\omega}{\partial E'_{dc}} = \frac{-1}{2H}\left(\frac{\partial T_e}{\partial I_d}\frac{\partial I_d}{\partial E'_{dc}} + \frac{\partial T_e}{\partial I_q}\frac{\partial I_q}{\partial E'_{dc}}\right) \tag{C.26}$$

$$\boldsymbol{A}_{3,1} = \frac{\partial g_{E'_d}}{\partial \alpha} = \frac{-1}{T'_{q0}}\left((X_q - X'_q)K_{q1}\frac{\partial I_q}{\partial \alpha}\right) \tag{C.27}$$

$$\boldsymbol{A}_{3,3} = \frac{\partial g_{E'_d}}{\partial E'_d} = \frac{-1}{T'_{q0}}\left(1 + (X_q - X'_q)\left(K_{q1}\frac{\partial I_q}{\partial E'_d} + \frac{K_{q2}}{X'_q - X_l}\right)\right) \tag{C.28}$$

$$\boldsymbol{A}_{3,4} = \frac{\partial g_{E'_d}}{\partial E'_q} = \frac{-1}{T'_{q0}}\left((X_q - X'_q)K_{q1}\frac{\partial I_q}{\partial E'_q}\right) \tag{C.29}$$

$$\boldsymbol{A}_{3,5} = \frac{\partial g_{E'_d}}{\partial \Psi_{1d}} = \frac{-1}{T'_{q0}}\left((X_q - X'_q)K_{q1}\frac{\partial I_q}{\partial \Psi_{1d}}\right) \tag{C.30}$$

$$\boldsymbol{A}_{3,6} = \frac{\partial g_{E'_d}}{\partial \Psi_{2q}} = \frac{-1}{T'_{q0}}(X_q - X'_q)\left(K_{q1}\frac{\partial I_q}{\partial \Psi_{2q}} + \frac{K_{q2}}{X'_q - X_l}\right) \tag{C.31}$$

$$\boldsymbol{A}_{3,7} = \frac{\partial g_{E'_d}}{\partial E'_{dc}} = \frac{-1}{T'_{q0}} \left((X_q - X'_q) K_{q1} \frac{\partial I_q}{\partial E'_{dc}} \right) \tag{C.32}$$

$$\boldsymbol{A}_{4,1} = \frac{\partial g_{E'_q}}{\partial \alpha} = \frac{1}{T'_{d0}} \left((X_d - X'_d) K_{d1} \frac{\partial I_d}{\partial \alpha} \right) \tag{C.33}$$

$$\boldsymbol{A}_{4,3} = \frac{\partial g_{E'_q}}{\partial E'_d} = \frac{1}{T'_{d0}} \left((X_d - X'_d) K_{d1} \frac{\partial I_d}{\partial E'_d} \right) \tag{C.34}$$

$$\boldsymbol{A}_{4,4} = \frac{\partial g_{E'_q}}{\partial E'_q} = \frac{-1}{T'_{d0}} \left(1 + (X_d - X'_d) \left(-K_{d1} \frac{\partial I_d}{\partial E'_q} + \frac{K_{d2}}{X'_d - X_l} \right) \right) \tag{C.35}$$

$$\boldsymbol{A}_{4,5} = \frac{\partial g_{E'_q}}{\partial \Psi_{1d}} = \frac{1}{T'_{d0}} \left((X_d - X'_d) \left(K_{d1} \frac{\partial I_d}{\partial \Psi_{1d}} + \frac{K_{d2}}{X'_d - X_l} \right) \right) \tag{C.36}$$

$$\boldsymbol{A}_{4,6} = \frac{\partial g_{E'_q}}{\partial \Psi_{2q}} = \frac{1}{T'_{d0}} \left((X_d - X'_d) K_{d1} \frac{\partial I_d}{\partial \Psi_{2q}} \right) \tag{C.37}$$

$$\boldsymbol{A}_{4,7} = \frac{\partial g_{E'_q}}{\partial E'_{dc}} = \frac{1}{T'_{d0}} \left((X_d - X'_d) K_{d1} \frac{\partial I_d}{\partial E'_{dc}} \right) \tag{C.38}$$

$$\boldsymbol{A}_{4,8} = \frac{\partial g_{E'_q}}{\partial V_r} = \frac{-K_a}{T'_{d0}} \tag{C.39}$$

$$\boldsymbol{A}_{5,1} = \frac{\partial g_{\Psi_{1d}}}{\partial \alpha} = \frac{X'_d - X_l}{T''_{d0}} \frac{\partial I_d}{\partial \alpha} \tag{C.40}$$

$$\boldsymbol{A}_{5,3} = \frac{\partial g_{\Psi_{1d}}}{\partial E'_d} = \frac{1}{T''_{d0}} \left((X'_d - X_l) \frac{\partial I_d}{\partial E'_d} \right) \tag{C.41}$$

$$\boldsymbol{A}_{5,4} = \frac{\partial g_{\Psi_{1d}}}{\partial E'_q} = \frac{1}{T''_{d0}} \left(1 + (X'_d - X_l) \frac{\partial I_d}{\partial E'_q} \right) \tag{C.42}$$

$$\boldsymbol{A}_{5,5} = \frac{\partial g_{\Psi_{1d}}}{\partial \Psi_{1d}} = \frac{1}{T''_{d0}} \left((X'_d - X_l) \frac{\partial I_d}{\partial \Psi_{1d}} - 1 \right) \tag{C.43}$$

$$\boldsymbol{A}_{5,6} = \frac{\partial g_{\Psi_{1d}}}{\partial \Psi_{2q}} = \frac{1}{T''_{d0}} \left((X'_d - X_l) \frac{\partial I_d}{\partial \Psi_{2q}} \right) \tag{C.44}$$

$$\boldsymbol{A}_{5,7} = \frac{\partial g_{\Psi_{1d}}}{\partial E'_{dc}} = \frac{1}{T''_{d0}} \left((X'_d - X_l) \frac{\partial I_d}{\partial E'_{dc}} \right) \tag{C.45}$$

$$\boldsymbol{A}_{6,1} = \frac{\partial g_{\Psi_{2q}}}{\partial \alpha} = \frac{X'_q - X_l}{T''_{q0}} \frac{\partial I_q}{\partial \alpha} \tag{C.46}$$

$$\boldsymbol{A}_{6,3} = \frac{\partial g_{\Psi_{2q}}}{\partial E'_d} = \frac{1}{T''_{q0}} \left((X'_q - X_l) \frac{\partial I_q}{\partial E'_d} - 1 \right) \tag{C.47}$$

$$\boldsymbol{A}_{6,4} = \frac{\partial g_{\Psi_{2q}}}{\partial E'_q} = \frac{X'_q - X_l}{T''_{q0}} \frac{\partial I_q}{\partial E'_q} \tag{C.48}$$

$$\boldsymbol{A}_{6,5} = \frac{\partial g_{\Psi_{2q}}}{\partial \Psi_{1d}} = \frac{X'_q - X_l}{T''_{q0}} \frac{\partial I_q}{\partial \Psi_{1d}} \tag{C.49}$$

$$\boldsymbol{A}_{6,6} = \frac{\partial g_{\Psi_{2q}}}{\partial \Psi_{2q}} = \frac{1}{T''_{q0}} \left((X'_q - X_l) \frac{\partial I_q}{\partial \Psi_{2q}} - 1 \right) \tag{C.50}$$

$$\boldsymbol{A}_{6,7} = \frac{\partial g_{\Psi_{2q}}}{\partial E'_{dc}} = \frac{X'_q - X_l}{T''_{q0}} \frac{\partial I_q}{\partial E'_{dc}} \tag{C.51}$$

$$\boldsymbol{A}_{7,1} = \frac{\partial g_{E'_{dc}}}{\partial \alpha} = \frac{X''_d - X''_q}{T_c} \frac{\partial I_q}{\partial \alpha} \tag{C.52}$$

$$\boldsymbol{A}_{7,3} = \frac{\partial g_{E'_{dc}}}{\partial E'_d} = \frac{X''_d - X''_q}{T_c} \frac{\partial I_q}{\partial E'_d} \tag{C.53}$$

$$\boldsymbol{A}_{7,4} = \frac{\partial g_{E'_{dc}}}{\partial E'_q} = \frac{X''_d - X''_q}{T_c} \frac{\partial I_q}{\partial E'_q} \tag{C.54}$$

$$\boldsymbol{A}_{7,5} = \frac{\partial g_{E'_{dc}}}{\partial \Psi_{1d}} = \frac{X''_d - X''_q}{T_c} \frac{\partial I_q}{\partial \Psi_{1d}} \tag{C.55}$$

$$\boldsymbol{A}_{7,6} = \frac{\partial g_{E'_{dc}}}{\partial \Psi_{2q}} = \frac{X''_d - X''_q}{T_c} \frac{\partial I_q}{\partial \Psi_{2q}} \tag{C.56}$$

$$\boldsymbol{A}_{7,7} = \frac{\partial g_{E'_{dc}}}{\partial E'_{dc}} = \frac{1}{T_c}\left(\frac{\partial I_q}{\partial E'_{dc}}(X''_d - X''_q) - 1\right) \tag{C.57}$$

$$\boldsymbol{A}_{8,8} = \frac{\partial g_{V_r}}{\partial V_r} = \frac{-1}{T_r} \tag{C.58}$$

$$\boldsymbol{B}_{4,1} = \frac{\partial g_{E'_q}}{\partial V_{ss}} = \frac{K_a}{T'_{d0}} \tag{C.59}$$

$$\boldsymbol{B}'_{1,2} = \frac{\partial g_{\alpha}}{\partial f} = -\omega_B \tag{C.60}$$

$$\boldsymbol{B}'_{2,1} = \frac{\partial g_{\omega}}{\partial V} = \frac{-1}{2H}\left(\frac{\partial T_e}{\partial I_d}\frac{\partial I_d}{\partial V} + \frac{\partial T_e}{\partial I_q}\frac{\partial I_q}{\partial V}\right) \tag{C.61}$$

$$\boldsymbol{B}'_{3,1} = \frac{\partial g_{E'_d}}{\partial V} = \frac{-(X_q - X'_q)K_{q1}}{T'_{q0}}\frac{\partial I_q}{\partial V} \tag{C.62}$$

$$\boldsymbol{B}'_{4,1} = \frac{\partial g_{E'_q}}{\partial V} = \frac{(X_d - X'_d)K_{d1}}{T'_{d0}}\frac{\partial I_d}{\partial V} \tag{C.63}$$

$$\boldsymbol{B}'_{5,1} = \frac{\partial g_{\Psi_{1d}}}{\partial V} = \frac{X'_d - X_l}{T''_{d0}}\frac{\partial I_d}{\partial V} \tag{C.64}$$

$$\boldsymbol{B}'_{6,1} = \frac{\partial g_{\Psi_{2q}}}{\partial V} = \frac{X'_q - X_l}{T''_{q0}}\frac{\partial I_q}{\partial V} \tag{C.65}$$

$$\boldsymbol{B}'_{7,1} = \frac{\partial g_{E'_{dc}}}{\partial V} = \frac{X''_d - X''_q}{T_c}\frac{\partial I_q}{\partial V} \tag{C.66}$$

$$\boldsymbol{B}'_{8,1} = \frac{\partial g_{V_r}}{\partial V} = \frac{1}{T_r} \tag{C.67}$$

Appendix D

Description of the 16-machine, 68-bus, 5-area test system

The 68-bus system (whose line diagram has been shown in Fig. 3.3) is a reduced order equivalent of the interconnected New England test system (NETS) (containing G1 to G9) and New York power system (NYPS) (containing G10 to G13), with five geographical regions out of which NETS and NYPS are represented by a group of generators whereas, the power import from each of the three other neighboring areas are approximated by equivalent generator models (G14 to G16).

There are three major tie-lines between NETS and NYPS (connecting buses 60-61, 53-54 and 27-53). All the three are double-circuit tie-lines. Generators G1 to G8 have DC excitation systems of type IEEE-DC1A; G9 has fast static excitation of type IEEE-ST1A, while the rest of the generators have manual excitation. G9 is also equipped with a PSS in order to damp a local mode. Data for the system has been extracted from [63], and is given as follows.

D.1 System data

D.1.1 Bus data

Base MVA for the system is taken as 100 MVA. Table D.1 presents bus data for the system. Bus type in last column has been denoted as 1 for swing bus, 2 for generator bus (PV bus) and 3 for load bus (PQ bus).

Table D.1: Bus data for the 68-bus system

Bus no.	V (p.u.)	P_G (p.u.)	Q_G (p.u.)	P_L (p.u.)	Q_L (p.u.)	Bus type
1	1.045	2.5	0	0	0	2
2	0.98	5.45	0	0	0	2
3	0.983	6.5	0	0	0	2
4	0.997	6.32	0	0	0	2
5	1.011	5.05	0	0	0	2
6	1.05	7	0	0	0	2
7	1.063	5.6	0	0	0	2
8	1.03	5.4	0	0	0	2
9	1.025	8	0	0	0	2
10	1.01	5	0	0	0	2
11	1	10	0	0	0	2
12	1.0156	13.5	0	0	0	2
13	1.011	35.91	0	0	0	2
14	1	17.85	0	0	0	2
15	1	10	0	0	0	2
16	1	40	0	0	0	1
17	1	0	0	60	3	3
18	1	0	0	24.7	1.23	3
19	1	0	0	0	0	3
20	1	0	0	6.8	1.03	3
21	1	0	0	2.74	1.15	3
22	1	0	0	0	0	3
23	1	0	0	2.48	0.85	3
24	1	0	0	3.09	-0.92	3
25	1	0	0	2.24	0.47	3
26	1	0	0	1.39	0.17	3
27	1	0	0	2.81	0.76	3
28	1	0	0	2.06	0.28	3
29	1	0	0	2.84	0.27	3
30	1	0	0	0	0	3
31	1	0	0	0	0	3
32	1	0	0	0	0	3
33	1	0	0	1.12	0	3
34	1	0	0	0	0	3

Continued on next page

Table D.1 – continued from previous page

Bus no.	V (p.u.)	P_G (p.u.)	Q_G (p.u.)	P_L (p.u.)	Q_L (p.u.)	Bus type
35	1	0	0	0	0	3
36	1	0	0	1.02	-0.1946	3
37	1	0	0	0	0	3
38	1	0	0	0	0	3
39	1	0	0	2.67	0.126	3
40	1	0	0	0.6563	0.2353	3
41	1	0	0	10	2.5	3
42	1	0	0	11.5	2.5	3
43	1	0	0	0	0	3
44	1	0	0	2.6755	0.0484	3
45	1	0	0	2.08	0.21	3
46	1	0	0	1.507	0.285	3
47	1	0	0	2.0312	0.3259	3
48	1	0	0	2.412	0.022	3
49	1	0	0	1.64	0.29	3
50	1	0	0	1	-1.47	3
51	1	0	0	3.37	-1.22	3
52	1	0	0	1.58	0.3	3
53	1	0	0	2.527	1.1856	3
54	1	0	0	0	0	3
55	1	0	0	3.22	0.02	3
56	1	0	0	2	0.736	3
57	1	0	0	0	0	3
58	1	0	0	0	0	3
59	1	0	0	2.34	0.84	3
60	1	0	0	2.088	0.708	3
61	1	0	0	1.04	1.25	3
62	1	0	0	0	0	3
63	1	0	0	0	0	3
64	1	0	0	0.09	0.88	3
65	1	0	0	0	0	3
66	1	0	0	0	0	3
67	1	0	0	3.2	1.53	3
68	1	0	0	3.29	0.32	3

D.1.2 Line data

Table D.2 presents line data for the system.

Table D.2: Line data for the 68-bus system

From bus	To bus	R_L (p.u.)	X_L (p.u.)	Line charging (p.u.)	Tap ratio
1	54	0	0.0181	0	1.025
2	58	0	0.025	0	1.07
3	62	0	0.02	0	1.07
4	19	0.0007	0.0142	0	1.07
5	20	0.0009	0.018	0	1.009
6	22	0	0.0143	0	1.025
7	23	0.0005	0.0272	0	1
8	25	0.0006	0.0232	0	1.025
9	29	0.0008	0.0156	0	1.025
10	31	0	0.026	0	1.04
11	32	0	0.013	0	1.04
12	36	0	0.0075	0	1.04
13	17	0	0.0033	0	1.04
14	41	0	0.0015	0	1
15	42	0	0.0015	0	1
16	18	0	0.003	0	1
17	36	0.0005	0.0045	0.32	1
18	49	0.0076	0.1141	1.16	1
18	50	0.0012	0.0288	2.06	1
19	68	0.0016	0.0195	0.304	1
20	19	0.0007	0.0138	0	1.06
21	68	0.0008	0.0135	0.2548	1
22	21	0.0008	0.014	0.2565	1
23	22	0.0006	0.0096	0.1846	1
24	23	0.0022	0.035	0.361	1
24	68	0.0003	0.0059	0.068	1
25	54	0.007	0.0086	0.146	1
26	25	0.0032	0.0323	0.531	1

Continued on next page

Table D.2 – continued from previous page

From bus	To bus	R_L (p.u.)	X_L (p.u.)	Line charging (p.u.)	Tap ratio
27	37	0.0013	0.0173	0.3216	1
27	26	0.0014	0.0147	0.2396	1
28	26	0.0043	0.0474	0.7802	1
29	26	0.0057	0.0625	1.029	1
29	28	0.0014	0.0151	0.249	1
30	53	0.0008	0.0074	0.48	1
30	61	0.00095	0.00915	0.58	1
31	30	0.0013	0.0187	0.333	1
31	53	0.0016	0.0163	0.25	1
32	30	0.0024	0.0288	0.488	1
33	32	0.0008	0.0099	0.168	1
34	33	0.0011	0.0157	0.202	1
34	35	0.0001	0.0074	0	0.946
36	34	0.0033	0.0111	1.45	1
36	61	0.0011	0.0098	0.68	1
37	68	0.0007	0.0089	0.1342	1
38	31	0.0011	0.0147	0.247	1
38	33	0.0036	0.0444	0.693	1
40	41	0.006	0.084	3.15	1
40	48	0.002	0.022	1.28	1
41	42	0.004	0.06	2.25	1
42	18	0.004	0.06	2.25	1
43	17	0.0005	0.0276	0	1
44	39	0	0.0411	0	1
44	43	0.0001	0.0011	0	1
45	35	0.0007	0.0175	1.39	1
45	39	0	0.0839	0	1
45	44	0.0025	0.073	0	1
46	38	0.0022	0.0284	0.43	1
47	53	0.0013	0.0188	1.31	1
48	47	0.00125	0.0134	0.8	1
49	46	0.0018	0.0274	0.27	1
51	45	0.0004	0.0105	0.72	1
51	50	0.0009	0.0221	1.62	1
52	37	0.0007	0.0082	0.1319	1

Continued on next page

Table D.2 – continued from previous page

From bus	To bus	R_L (p.u.)	X_L (p.u.)	Line charging (p.u.)	Tap ratio
52	55	0.0011	0.0133	0.2138	1
54	53	0.0035	0.0411	0.6987	1
55	54	0.0013	0.0151	0.2572	1
56	55	0.0013	0.0213	0.2214	1
57	56	0.0008	0.0128	0.1342	1
58	57	0.0002	0.0026	0.0434	1
59	58	0.0006	0.0092	0.113	1
60	57	0.0008	0.0112	0.1476	1
60	59	0.0004	0.0046	0.078	1
61	60	0.0023	0.0363	0.3804	1
63	58	0.0007	0.0082	0.1389	1
63	62	0.0004	0.0043	0.0729	1
63	64	0.0016	0.0435	0	1.06
65	62	0.0004	0.0043	0.0729	1
65	64	0.0016	0.0435	0	1.06
66	56	0.0008	0.0129	0.1382	1
66	65	0.0009	0.0101	0.1723	1
67	66	0.0018	0.0217	0.366	1
68	67	0.0009	0.0094	0.171	1
27	53	0.032	0.32	0.41	1

D.1.3 Machine parameters

Tables D.3, D.4 and D.5 present parameters of the 16 machines in the system.

Table D.3: Machine data for the 68-bus system (A)

Machine no.	Bus	Base MVA	X_l (p.u.)	R_a (p.u.)	H (s)	D (p.u.)
1	1	100	0.0125	0	42	4
2	2	100	0.035	0	30.2	9.75
3	3	100	0.0304	0	35.8	10
4	4	100	0.0295	0	28.6	10

Continued on next page

Table D.3 – continued from previous page

Machine no.	Bus	Base MVA	X_l (p.u.)	R_a (p.u.)	H (s)	D (p.u.)
5	5	100	0.027	0	26	3
6	6	100	0.0224	0	34.8	10
7	7	100	0.0322	0	26.4	8
8	8	100	0.028	0	24.3	9
9	9	100	0.0298	0	34.5	14
10	10	100	0.0199	0	31	5.56
11	11	100	0.0103	0	28.2	13.6
12	12	100	0.022	0	92.3	13.5
13	13	200	0.003	0	248	33
14	14	100	0.0017	0	300	100
15	15	100	0.0017	0	300	100
16	16	200	0.0041	0	225	50

Table D.4: Machine data for the 68-bus system (B)

Machine no.	X_d (p.u.)	X'_d (p.u.)	X''_d (p.u.)	T'_{d0} (s)	T''_{d0} (s)
1	0.1	0.031	0.025	10.2	0.05
2	0.295	0.0697	0.05	6.56	0.05
3	0.2495	0.0531	0.045	5.7	0.05
4	0.262	0.0436	0.035	5.69	0.05
5	0.33	0.066	0.05	5.4	0.05
6	0.254	0.05	0.04	7.3	0.05
7	0.295	0.049	0.04	5.66	0.05
8	0.29	0.057	0.045	6.7	0.05
9	0.2106	0.057	0.045	4.79	0.05
10	0.169	0.0457	0.04	9.37	0.05
11	0.128	0.018	0.012	4.1	0.05
12	0.101	0.031	0.025	7.4	0.05
13	0.0296	0.0055	0.004	5.9	0.05
14	0.018	0.00285	0.0023	4.1	0.05
15	0.018	0.00285	0.0023	4.1	0.05
16	0.0356	0.0071	0.0055	7.8	0.05

Table D.5: Machine data for the 68-bus system (C)

Machine no.	X_q (p.u.)	X'_q (p.u.)	X''_q (p.u.)	T'_{q0} (s)	T''_{q0} (s)
1	0.069	0.028	0.025	1.5	0.035
2	0.282	0.06	0.05	1.5	0.035
3	0.237	0.05	0.045	1.5	0.035
4	0.258	0.04	0.035	1.5	0.035
5	0.31	0.06	0.05	0.44	0.035
6	0.241	0.045	0.04	0.4	0.035
7	0.292	0.045	0.04	1.5	0.035
8	0.28	0.05	0.045	0.41	0.035
9	0.205	0.05	0.045	1.96	0.035
10	0.115	0.045	0.04	1.5	0.035
11	0.123	0.015	0.012	1.5	0.035
12	0.095	0.028	0.025	1.5	0.035
13	0.0286	0.005	0.004	1.5	0.035
14	0.0173	0.0025	0.0023	1.5	0.035
15	0.0173	0.0025	0.0023	1.5	0.035
16	0.0334	0.006	0.0055	1.5	0.035

D.1.4 Excitation system parameters

IEEE-DC1A type of excitation system has following parameters:

$$T_r = 0.01\ s, K_a = 40.0\ p.u., T_a = 0.02\ s, K_x = 1.0\ p.u., T_x = 0.785\ p.u.,$$
$$A_x = 0.07\ p.u., B_x = 0.91\ p.u., E_{fdmin} = -10\ p.u., E_{fdmax} = 10\ p.u.$$

IEEE-ST1A type of excitation system has following parameters:

$$T_r = 0.01\ s, K_a = 200.0\ p.u., E_{fdmin} = -5\ p.u., E_{fdmax} = 5\ p.u.$$

D.1.5 PSS parameters

PSS has following parameters:

$$K_{pss} = 12\ (p.u.), T_w = 10\ p.u., T_{11} = 0.1\ s, T_{12} = 0.2\ s, T_{21} = 0.1\ s,$$
$$T_{22} = 0.2\ s, V_{ssmin} = -0.05\ p.u., V_{ssmax} = 0.2\ p.u.$$

D.1.6 TCSC parameters

TCSC (if present on a line) has following parameters:

$$K_c = 0.5\ p.u., K_{cmin} = 0.1\ p.u., K_{cmax} = 0.8\ p.u., T_{tcsc} = 0.02\ s.$$

D.2 System analysis

D.2.1 Load flow

Initial condition of the system is found by first finding the initial bus voltage magnitudes and phases using load flow calculation, and then using these values to find the steady state values of the system states using the DAEs given in Appendix A. Table D.6 presents the results of load flow for the system.

Table D.6: Load flow for the 68-bus system

Bus no.	V (p.u.)	θ (degree)	P_G (p.u.)	Q_G (p.u.)	Bus type
1	1.045	-8.9563	2.5	1.96	2
2	0.98	-0.9835	5.45	0.7001	2
3	0.983	1.6129	6.5	0.8078	2
4	0.997	1.6683	6.32	0.0027	2
5	1.011	-0.6276	5.05	1.1657	2
6	1.05	3.8425	7	2.5449	2
7	1.063	6.0307	5.6	2.9083	2
8	1.03	-2.841	5.4	0.4907	2

Continued on next page

Table D.6 – continued from previous page

Bus no.	V (p.u.)	θ (degree)	P_G (p.u.)	Q_G (p.u.)	Bus type
9	1.025	2.6524	8	0.5981	2
10	1.01	-9.6439	5	-0.131	2
11	1	-7.2245	10	0.0832	2
12	1.0156	-22.6313	13.5	2.8006	2
13	1.011	-28.6539	35.91	8.8504	2
14	1	10.962	17.85	0.4748	2
15	1	0.0168	10	0.7673	2
16	1	0	33.7953	0.9364	1
17	0.9499	-36.0269	0	0	3
18	1.0023	-5.8054	0	0	3
19	0.932	-4.2634	0	0	3
20	0.9806	-5.8744	0	0	3
21	0.9602	-7.0539	0	0	3
22	0.9937	-1.801	0	0	3
23	0.9961	-2.1606	0	0	3
24	0.9587	-9.8767	0	0	3
25	0.9981	-9.9995	0	0	3
26	0.9869	-11.0194	0	0	3
27	0.9679	-12.8571	0	0	3
28	0.9897	-7.4968	0	0	3
29	0.9921	-4.5464	0	0	3
30	0.9762	-19.71	0	0	3
31	0.9838	-17.464	0	0	3
32	0.9699	-15.2375	0	0	3
33	0.9738	-19.758	0	0	3
34	0.98	-26.1159	0	0	3
35	1.043	-27.0886	0	0	3
36	0.9606	-28.8273	0	0	3
37	0.9555	-11.788	0	0	3
38	0.989	-18.7593	0	0	3
39	0.9915	-39.2902	0	0	3
40	1.0442	-13.64	0	0	3
41	0.9996	9.4272	0	0	3
42	0.999	-0.8435	0	0	3
43	0.9765	-37.9088	0	0	3

Continued on next page

Table D.6 – continued from previous page

Bus no.	V (p.u.)	θ (degree)	P_G (p.u.)	Q_G (p.u.)	Bus type
44	0.9775	-37.9863	0	0	3
45	1.0471	-29.3626	0	0	3
46	0.9903	-20.5314	0	0	3
47	1.0184	-19.4976	0	0	3
48	1.0337	-18.3761	0	0	3
49	0.9936	-19.8196	0	0	3
50	1.0602	-19.0521	0	0	3
51	1.0634	-27.2882	0	0	3
52	0.9545	-12.8334	0	0	3
53	0.9863	-18.9373	0	0	3
54	0.9857	-11.537	0	0	3
55	0.9571	-13.2179	0	0	3
56	0.9208	-11.9593	0	0	3
57	0.9102	-11.2129	0	0	3
58	0.909	-10.4023	0	0	3
59	0.9037	-13.311	0	0	3
60	0.9062	-14.0368	0	0	3
61	0.9556	-23.2222	0	0	3
62	0.9121	-7.3117	0	0	3
63	0.9096	-8.37	0	0	3
64	0.8367	-8.377	0	0	3
65	0.9128	-8.1847	0	0	3
66	0.9194	-10.1909	0	0	3
67	0.928	-11.4299	0	0	3
68	0.9483	-10.0712	0	0	3

D.2.2 Small signal analysis

For small signal analysis, the system is first linearized at $t = 0$ using the calculated steady state values, and then state space matrices and eigenvalues for the linearized system are found.

D.2.2.1 Eigenvalues

Fig. D.1 shows the plot of the eigenvalues of the test system. The system is small signal stable as all the eigenvalues have negative real parts, but with so many eigenvalues outside the 10% damping line, the system is poorly damped.

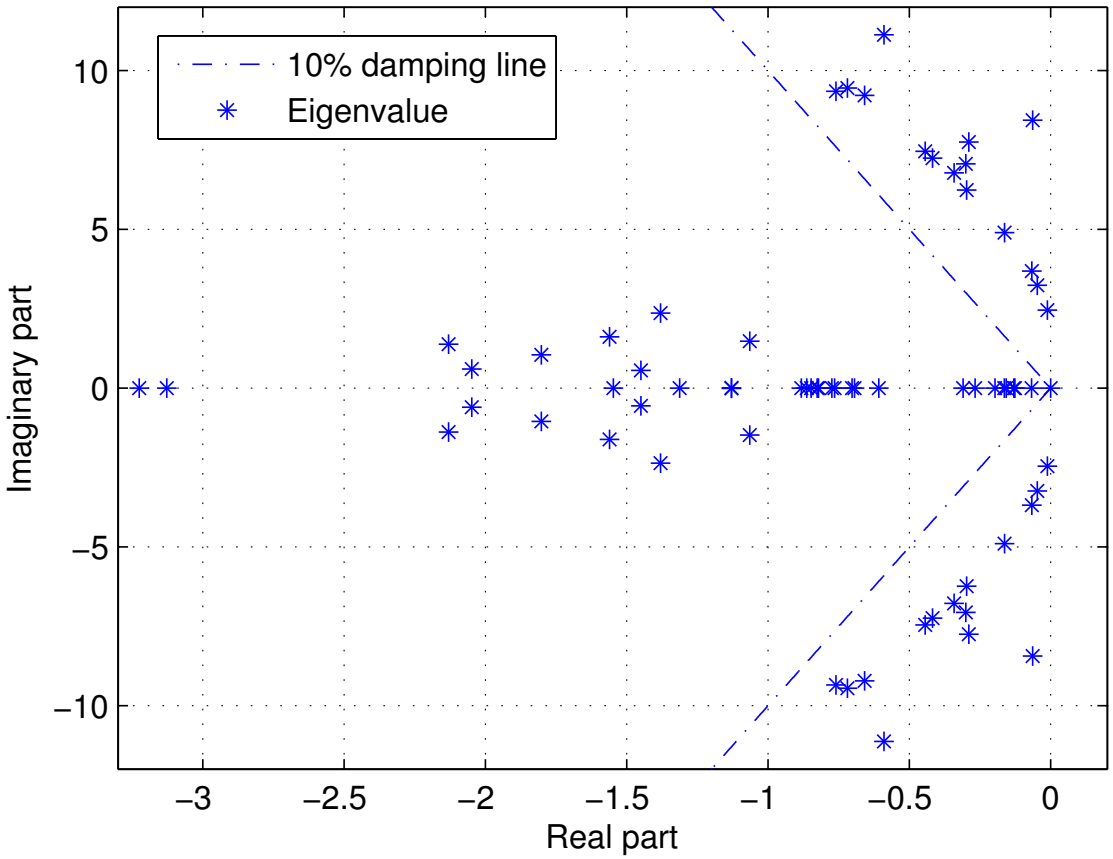

Figure D.1: Plot of the eigenvalues of the 68-bus system

D.2.2.2 Electromechanical modes

A detailed modal analysis of the modes (mode is another name for eigenvalue) of the test system is required to find which machines have high participations in them. It was found that all the poorly damped (damping ratio less than 10%) modes of the test system have high participation from rotor angles and rotor speeds of various machines. Such modes are called as electromechanical modes. The electromechanical modes with frequencies in the range 0.1 to 1 Hz are the interarea modes, while the rest of them are local machine modes. Table D.7 shows the electromechanical modes for the test system. The top four modes in the table are inter-area modes while the rest are local modes. For each mode the highest

participating states are also tabulated in Table D.7 and arranged in increasing order of normalized participation factors.

Table D.7: Electromechanical modes with normalized participation factors

No.	Damping Ratio (%)	Frequency (Hz)	State	PF	State	PF
1	0.486	0.391	δ_{13}	1	ω_{15}	0.93
2	1.476	0.516	δ_{14}	1	ω_{16}	0.63
3	1.827	0.587	δ_{13}	1	ω_{13}	0.738
4	3.343	0.779	δ_{15}	1	ω_{15}	0.755
5	4.772	0.993	δ_{2}	1	ω_{2}	0.992
6	5.036	1.079	δ_{12}	1	ω_{12}	0.984
7	4.245	1.124	δ_{1}	1	ω_{1}	0.992
8	5.766	1.153	δ_{6}	1	ω_{6}	0.998
9	5.952	1.187	δ_{2}	1	ω_{2}	1
10	3.732	1.234	δ_{10}	1	ω_{10}	0.992
11	0.759	1.343	δ_{9}	1	ω_{9}	0.803
12	7.122	1.468	δ_{8}	1	ω_{8}	1
13	8.097	1.488	δ_{4}	1	ω_{4}	1
14	7.582	1.505	δ_{7}	1	ω_{7}	1
15	5.299	1.771	δ_{11}	1	ω_{11}	0.993

D.2.2.3 Inter-area modes and mode shapes

The inter-area modes are named so because in these modes the participating machines divide into two groups, and the two groups oscillate against each other. If the inter-area modes are poorly damped, or unstable, then the two groups may lose synchronism completely and this leads to system breakdown. Also, as the inter-area modes have low frequencies as compared to other modes, for a given damping ratio they take much more time to die down than the other modes. A 10% or more damping ratio for all the inter-area modes gives an acceptable system performance, and hence control methods are designed to give at least 10% damping ratio to all the inter-area modes.

The phenomenon of all the machines dividing into two groups may be better understood by the help of mode shapes. Mode shapes are the polar plots of the

eigenvectors of a mode corresponding to the desired states. In Matlab, 'feather' or 'compass' functions may be used for plotting the mode shapes. Fig. D.2 shows the mode shapes of the inter-area modes, in which the eigenvectors (corresponding to each machine's rotor speed) of all the inter-area modes are plotted. The division of machines into two opposing groups is evident in all the inter-area modes.

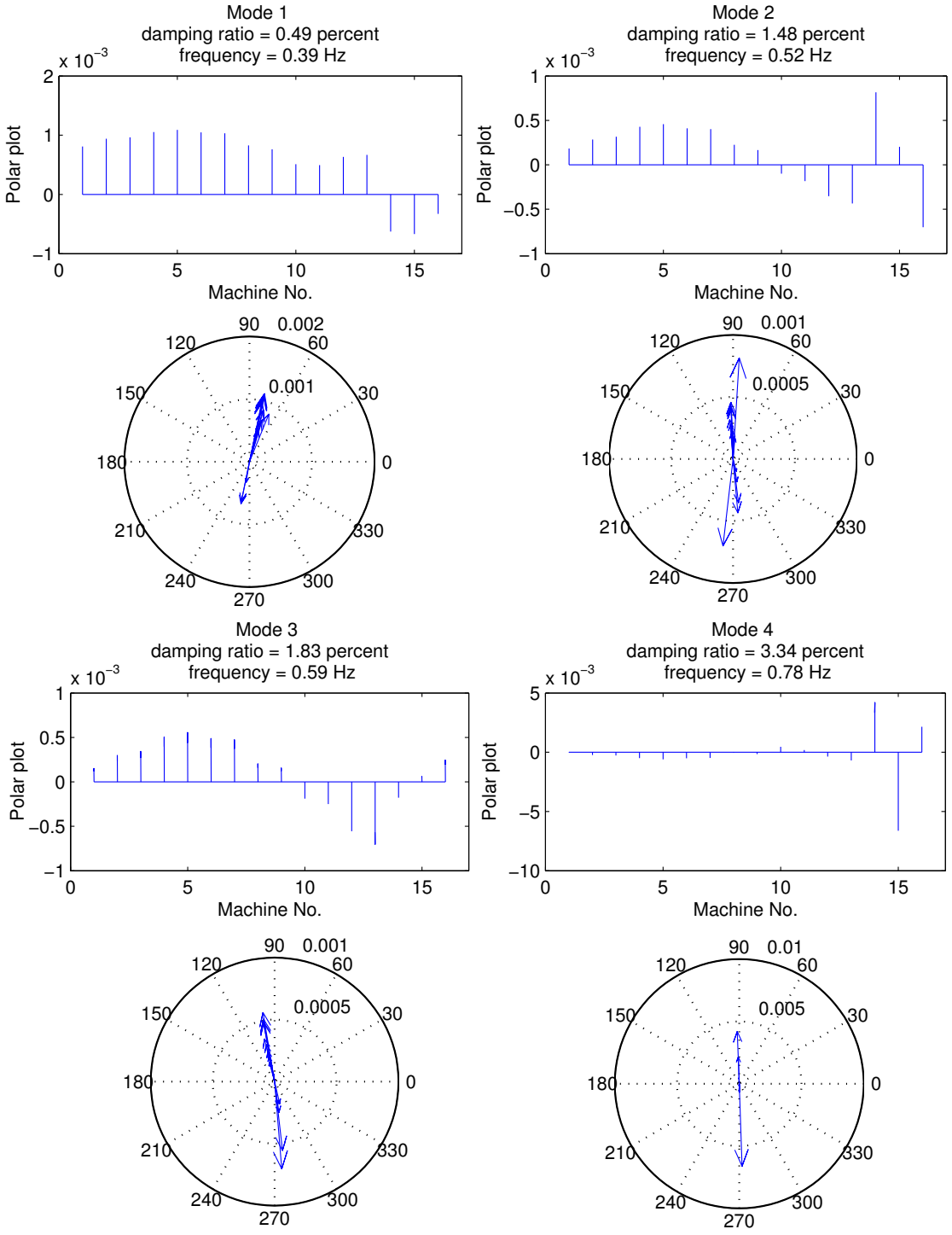

Figure D.2: Mode shapes for inter-area modes

Appendix E

Level-2 S-function used in integrated ELQR

Code for Level-2 S-function used for dynamic update of system matrices and control law for the integrated ELQR block is as follows:

```
function LQR_Integrated(block)
%Level-2 MATLAB file S-Function for damped  ELQR function.
setup(block);
%endfunction

function setup(block)

%% Register number of input and output ports
block.NumInputPorts  = 4;%1st input=states, 2nd ...
    input=pseudo-inputs, 3rd input=machine parameters, 4th ...
    input=sampling period
block.NumOutputPorts = 2;%1st output= state gains, 2nd ...
    output=pseudo-input gains
%% Setup functional port properties to dynamically inherited.
block.SetPreCompInpPortInfoToDynamic;
block.SetPreCompOutPortInfoToDynamic;

block.RegBlockMethod('SetInputPortDimensions', @SetInpPortDims);

block.RegBlockMethod('SetInputPortSamplingMode', ...
    @SetInpPortFrameData);

%% Set block sample time to inherited
block.SampleTimes = [-1 0];
```

```
21
22 %% Set the block simStateCompliance to default (i.e., same as ...
       a built-in block)
23 block.SimStateCompliance = 'DefaultSimState';
24
25 %% Run accelerator on TLC
26 block.SetAccelRunOnTLC(true);
27
28 %% Register methods
29 block.RegBlockMethod('Outputs',@Output);
30 %endfunction
31
32 function Output(block)
33
34 Prm=block.InputPort(3).Data;%machine parameters
35 T=block.InputPort(4).Data;%the sampling period
36
37 xls=   Prm(:,1);
38 % Ra=    Prm(:,2); %not needed as Ra=0;
39 xd=    Prm(:,3);
40 xdd=   Prm(:,4);
41 xddd=  Prm(:,5);
42 xq=    Prm(:,6);
43 xqd=   Prm(:,7);
44 xqdd=  Prm(:,8);
45 Td0d=  Prm(:,9);
46 Td0dd= Prm(:,10);
47 Tq0d=  Prm(:,11);
48 Tq0dd= Prm(:,12);
49 D=     Prm(:,13);
50 M=     Prm(:,14);
51 wB=    Prm(:,15);
52 Ka=    Prm(:,16);
53 Tr=    Prm(:,17);
54 kd1=(xddd-xls)./(xdd-xls);
55 kd2=(xdd-xddd)./(xdd-xls);
56 kq1=(xqdd-xls)./(xqd-xls);
57 kq2=(xqd-xqdd)./(xqd-xls);
58 N_Machine=size(Prm,1);%total no. of machines
59
60 x0=block.InputPort(1).Data;%states
61 alpha0=   x0(:,1);
62 Ed_dash0= x0(:,3);
63 Eq_dash0= x0(:,4);
64 Psi1d0=   x0(:,5);
65 Psi2q0=   x0(:,6);
```

```
%State Edcd is identically zero as xddd=xqdd

u0=block.InputPort(2).Data;%pseudo inputs
Vg=  u0(:,1);
iq0= (Ed_dash0.*kq1-Psi2q0.*kq2+Vg.*sin(alpha0))./xddd;
id0= -(Eq_dash0.*kd1+Psi1d0.*kd2-Vg.*cos(alpha0))./xddd;

%%%%%%%%%%%%%partial derivatives%%%%%%%%%%%%%%%%%%%
dIq_by_dEdd       =kq1./xddd;
dIq_by_dEqd       =0;
dIq_by_dPsi1d     =0;
dIq_by_dPsi2q     =-kq2./xddd;
dIq_by_dalpha     =Vg.*cos(alpha0)./xddd;
dIq_by_dV         =sin(alpha0)./xddd;

dId_by_dEdd       =0;
dId_by_dEqd       =-kd1./xddd;
dId_by_dPsi1d     =-kd2./xddd;
dId_by_dPsi2q     =0;
dId_by_dalpha     =-Vg.*sin(alpha0)./xddd;
dId_by_dV         =cos(alpha0)./xddd;

dTe_by_dId        =kq1.*Ed_dash0-iq0.*(xddd-xqdd)-Psi2q0.*kq2;
dTe_by_dIq        =kd1.*Eq_dash0-id0.*(xddd-xqdd)+Psi1d0.*kd2;

dTe_by_dEdd       ...
   =id0.*kq1+dTe_by_dId.*dId_by_dEdd+dTe_by_dIq.*dIq_by_dEdd;
dTe_by_dEqd       ...
   =iq0.*kd1+dTe_by_dId.*dId_by_dEqd+dTe_by_dIq.*dIq_by_dEqd;
dTe_by_dPsi1d     ...
   =iq0.*kd2+dTe_by_dId.*dId_by_dPsi1d+dTe_by_dIq.*dIq_by_dPsi1d;
dTe_by_dPsi2q     ...
   =-id0.*kq2+dTe_by_dId.*dId_by_dPsi2q+dTe_by_dIq.*dIq_by_dPsi2q;
dTe_by_dalpha     ...
   =dTe_by_dId.*dId_by_dalpha+dTe_by_dIq.*dIq_by_dalpha;
dTe_by_dV         =dTe_by_dId.*dId_by_dV+dTe_by_dIq.*dIq_by_dV;

dfSm_by_dEdd      =-dTe_by_dEdd./M;
dfSm_by_dEqd      =-dTe_by_dEqd./M;
dfSm_by_dPsi1d    =-dTe_by_dPsi1d./M;
dfSm_by_dPsi2q    =-dTe_by_dPsi2q./M;
dfSm_by_dSm       =-D./M;
dfSm_by_dalpha    =-dTe_by_dalpha./M;
dfSm_by_dV        =-dTe_by_dV./M;

```

```
106 dfEdd_by_dEdd      ...
       =-(1./Tq0d).*(1+(xq-xqd).*(kq1.*dIq_by_dEdd+kq2./(xqd-xls)));
107 dfEdd_by_dPsi2q    ...
       =-(1./Tq0d).*(xq-xqd).*(kq1.*dIq_by_dPsi2q+kq2./(xqd-xls));
108 dfEdd_by_dalpha    =-(1./Tq0d).*(xq-xqd).*kq1.*dIq_by_dalpha;
109 dfEdd_by_dV        =-(1./Tq0d).*(xq-xqd).*kq1.*dIq_by_dV;
110
111 dfEqd_by_dEqd      ...
       =-(1./Td0d).*(1+(xd-xdd).*(-kd1.*dId_by_dEqd+kd2./(xdd-xls)));
112 dfEqd_by_dPsi1d    ...
       =(1./Td0d).*(xd-xdd).*(kd1.*dId_by_dPsi1d+kd2./(xdd-xls));
113 dfEqd_by_dalpha    =(1./Td0d).*(xd-xdd).*kd1.*dId_by_dalpha;
114 dfEqd_by_dV        =(1./Td0d).*(xd-xdd).*kd1.*dId_by_dV;
115 dfEqd_by_dVr       =-Ka./Td0d;
116
117 dfPsi1d_by_dEqd    =(1./Td0dd).*(1+(xdd-xls).*dId_by_dEqd);
118 dfPsi1d_by_dPsi1d  =(1./Td0dd).*(-1+(xdd-xls).*dId_by_dPsi1d);
119 dfPsi1d_by_dalpha  =(1./Td0dd).*(xdd-xls).*dId_by_dalpha;
120 dfPsi1d_by_dV      =(1./Td0dd).*(xdd-xls).*dId_by_dV;
121
122 dfPsi2q_by_dEdd    =(1./Tq0dd).*(-1+(xqd-xls).*dIq_by_dEdd);
123 dfPsi2q_by_dPsi2q  =(1./Tq0dd).*(-1+(xqd-xls).*dIq_by_dPsi2q);
124 dfPsi2q_by_dalpha  =(1./Tq0dd).*(xqd-xls).*dIq_by_dalpha;
125 dfPsi2q_by_dV      =(1./Tq0dd).*(xqd-xls).*dIq_by_dV;
126
127 dfalpha_by_dSm     =wB;
128
129 dfVr_by_dVr        =-(1./Tr);
130 dfVr_by_dV         =(1./Tr);
131
132 dEqd_by_dVs        =Ka./Td0d;
133 %%%%%%%%%%%%%partial derivatives end%%%%%%%%%%%%%%%%
134
135 %%%%%%%%%%State matrices' formation using partial ...
       derivatives%%%%%%%%%%%%
136 Kx=zeros(size(x0));
137 Ku=zeros(size(u0));
138 N_State=size(x0,2);
139 Afull =zeros(N_State);
140 Bfull =zeros(N_State,1);
141 B1full=zeros(N_State,2);
142 for i=1:1:N_Machine
143     if Ka(i)==0
144         continue;
145     end
146
```

```
147     Afull(3,3)=dfEdd_by_dEdd(i);
148     Afull(3,6)=dfEdd_by_dPsi2q(i);
149     Afull(3,1)=dfEdd_by_dalpha(i);
150
151     Afull(4,4)=dfEqd_by_dEqd(i);
152     Afull(4,5)=dfEqd_by_dPsi1d(i);
153     Afull(4,1)=dfEqd_by_dalpha(i);
154
155     Afull(5,4)=dfPsi1d_by_dEqd(i);
156     Afull(5,5)=dfPsi1d_by_dPsi1d(i);
157     Afull(5,1)=dfPsi1d_by_dalpha(i);
158
159     Afull(6,3)=dfPsi2q_by_dEdd(i);
160     Afull(6,6)=dfPsi2q_by_dPsi2q(i);
161     Afull(6,1)=dfPsi2q_by_dalpha(i);
162
163     Afull(2,3)=dfSm_by_dEdd(i);
164     Afull(2,4)=dfSm_by_dEqd(i);
165     Afull(2,5)=dfSm_by_dPsi1d(i);
166     Afull(2,6)=dfSm_by_dPsi2q(i);
167     Afull(2,2)=dfSm_by_dSm(i);
168     Afull(2,1)=dfSm_by_dalpha(i);
169
170     Afull(1,2)=dfalpha_by_dSm(i);
171
172     Bfull(4,1)=dEqd_by_dVs(i);
173
174     B1full(1,2)=-dfalpha_by_dSm(i);
175     B1full(3,1)=dfEdd_by_dV(i);
176     B1full(4,1)=dfEqd_by_dV(i);
177     B1full(5,1)=dfPsi1d_by_dV(i);
178     B1full(6,1)=dfPsi2q_by_dV(i);
179     B1full(2,1)=dfSm_by_dV(i);
180
181     if N_State==7
182         Afull(4,7)=dfEqd_by_dVr(i);
183         Afull(7,7)=dfVr_by_dVr(i);
184         B1full(7,1)=dfVr_by_dV(i);
185     end
186     %%%%%%%%%%State matrices' formation using partial ...
      derivatives ends%%%
187
188     %%%%%%%%%%Eigenvalues%%%%%%%%%%%%%%%%%%%%%%%%%%%%%%%%%%%%
189     [¬,lambdar]=eig(Afull,'nobalance');
190     lambdar=diag(lambdar);
191     omegar=abs(imag(lambdar));
```

```
    %%%%%%%%%%Eigenvalues ...
    end%%%%%%%%%%%%%%%%%%%%%%%%%%%%%%%%%%%%%%%%%%%

    %%%%%%%%%%%%%%%%%%%%%%%Calculation of r and ...
    beta%%%%%%%%%%%%%%%%%%%%%
    w_max=max(omegar);
    min_damping_ratio=0.15;
    min_damping=cot(acos(min_damping_ratio));
    theta_spiral=w_max*T;%angle of spiral at w
    radius_spiral=exp(-min_damping*theta_spiral);%radius of ...
    spiral at w
    spiral_vector=radius_spiral*exp(1i*theta_spiral);

    slope=(sin(theta_spiral)+min_damping*cos(theta_spiral))/...
        (cos(theta_spiral)-min_damping*sin(theta_spiral));
    %slope of perpendicular to tangent of spiral at (R, tht)

    ...
    beta=radius_spiral*(cos(theta_spiral)-sin(theta_spiral)/slope);
    %intercept of the line from (R,tht) on x axis
    r=abs(spiral_vector-beta);
    %%%%%%%%%%%%%%%%%%%%%%%Calculation of r and beta ...
    ends%%%%%%%%%%%%%%%%%%

    %%%%%%%%%%Decentralized LQR%%%%%%%%%%%%%%%%%%%%%%%%%%%%%
    N_State=size(Afull,1);
    csys=ss(Afull,eye(N_State),zeros(1,N_State),0);
    dsys=c2d(csys,T);
    AD=(dsys.a-beta*eye(N_State))/r;
    BD=dsys.b*Bfull/r;
    B1D=dsys.b*B1full/r;
    Q=eye(N_State);
    [PD,¬,KD] = dare(AD,BD,Q,1);
    KVD=KD/(AD-PD\(PD-eye(N_State)))*B1D;
    Kx(i,:)=KD;
    Ku(i,:)=KVD;
end

block.OutputPort(1).Data=Kx;
block.OutputPort(2).Data=Ku;
%endfunction

function SetInpPortDims(block, idx, di)

block.InputPort(idx).Dimensions = di;
if idx==1
```

```
233     block.OutputPort(1).Dimensions  = di;
234 end
235 if idx==2
236     block.OutputPort(2).Dimensions  = di;
237 end
238 %endfunction
239
240 function SetInpPortFrameData(block, idx, fd)
241
242 block.InputPort(idx).SamplingMode = fd;
243 if idx==1
244     block.OutputPort(1).SamplingMode  = fd;
245     block.OutputPort(2).SamplingMode  = fd;
246 end
247 %endfunction
```

Bibliography

[1] P. Kundur, J. Paserba, V. Ajjarapu, G. Andersson, A. Bose, C. Canizares, N. Hatziargyriou, D. Hill, A. Stankovic, C. Taylor, T. Van Cutsem, V. Vittal, "Definition and classification of power system stability: IEEE/CIGRE joint task force on stability terms and definitions," *IEEE Trans. Power Syst.*, vol. 19, no. 3, pp. 1387–1401, Aug. 2004.

[2] P. Kundur, *Power System Stability And Control*. India: McGraw-Hill Pvt. Limited, 1994.

[3] U. Häger, C. Rehtanz, N. Voropai, *Monitoring, Control and Protection of Interconnected Power Systems*. Germany: Springer, 2014.

[4] P. Kundur, C. W. Taylor, "Blackout Experiences and Lessons, Best Practices for System Dynamic Performance, and the Role of New Technologies," *IEEE Task Force Report*, 2007.

[5] G. Andersson, P. Donalek, R. Farmer, N. Hatziargyriou, I. Kamwa, P. Kundur, N. Martins, J. Paserba, P. Pourbeik, J. Sanchez-Gasca, R. Schulz, A. Stankovic, C. Taylor, and V. Vittal, "Causes of the 2003 major grid blackouts in North America and Europe, and recommended means to improve system dynamic performance," *IEEE Trans. Power Syst.*, vol. 20, no.4, pp. 1922–1928, Nov. 2005.

[6] D. N. Kosterev, C. W. Taylor, W. A. Mittelstadt, "Model validation for the August 10, 1996 WSCC system outage," *IEEE Trans. Power Syst.*, vol. 14, no. 3, pp. 967– 979, Aug. 1999.

[7] B. Pal and B. Chaudhuri, *Robust Control in Power Systems*. New York, U.S.A.: Springer, 2005.

[8] M. Klein, G.J. Rogers, P. Kundur, "A fundamental study of inter-area oscillations in power systems" *IEEE Trans. Power Syst.*, vol. 6, no. 3, pp. 914–921, Aug. 1991.

[9] J. Paserba, "Analysis and control of power system oscillations," *CIGRE special publication 38.01.07, Technical Brochure no. 111*, 1996.

[10] E. Vaahedi, *Practical Power System Operation, Ch. 10: Energy Management Systems*. U.S.A.: Wiley IEEE Press, 2014.

[11] D. Bailey and E. Wright *Practical SCADA for Industry*. U.K.: Newnes, 2003.

[12] K. Barnes, B. Johnson, R. Nickelson, "Review of Supervisory Control and Data Acquisition (SCADA) Systems," *Idaho National Engineering and Environmental Laboratory, report Prepared for the U.S. Department of Energy*, Jan. 2004.

[13] D. T. Askounis, E. Kalfaoglou, "The Greek EMS-SCADA: from the contractor to the user," *IEEE Trans. Power Syst.*, vol. 15, no. 4, pp. 1423–1427, Nov. 2000.

[14] C. L. Su, C. N. Lu, M. C. Lin, "Wide area network performance study of a distribution management system," *International Journal of Electrical Power & Energy Systems* vol. 22, no. 1, pp. 9–14 vol.1, Jan. 2000.

[15] F. Maghsoodlou, R. Masiello, T. Ray, "Energy management systems," *IEEE Power and Energy Magazine*, vol. 2, no. 5, pp. 49–57, Sept.-Oct. 2004.

[16] A. G. Phadke and J. S. Thorp, *Synchronized Phasor Measurements and Their Applications*. U.S.A.: Springer, 2008.

[17] A. G. Phadke, "Synchronized phasor measurements in power systems," *IEEE Computer Applications in Power*, vol.6, no.2, pp.10–15, Apr. 1993.

[18] *IEEE Standard for Synchrophasor Measurements for Power Systems*, IEEE Std C37.118.1-2011, Dec. 2011.

[19] X. P. Zhang, C. Rehtanz and B. Pal, *Flexible AC Transmission Systems: Modeling and Control*, Berlin, Germany: Springer, 2006.

[20] Y. Zhang; A. Bose, "Design of Wide-Area Damping Controllers for Interarea Oscillations," *IEEE Trans. Power Syst.*, vol. 23, no. 3, pp. 1136–1143, Aug. 2008.

[21] C. W. Taylor, D. C. Erickson, K. E. Martin, R. E. Wilson, V. Venkatasubramanian, "WACS-Wide-Area Stability and Voltage Control System: R&D and Online Demonstration," *Proc. of the IEEE*, vol. 93, no. 5, pp. 892–906, May 2005.

[22] C. Hauser, D. Bakken, and A. Bose, "A failure to communicate: next generation communication requirements, technologies, and architecture for the electric power grid," *IEEE Power and Energy Magazine*, vol. 3, pp. 47– 55, Mar.-Apr. 2005.

[23] K. Tomsovic, D. Bakken, V. Venkatasubramanian, and A. Bose, "Designing the next generation of real-time control, communication, and computations for large power systems," *Proc. of the IEEE*, vol. 93, pp. 965–979, May 2005.

[24] Z. Xie, G. Manimaran, V. Vittal, A. Phadke, and V. Centeno, "An information architecture for future power systems and its reliability analysis," *IEEE Trans. Power Syst.*, vol. 17, pp. 857–863, Aug. 2002.

[25] E. Ghahremani, I. Kamwa, "Dynamic State Estimation in Power System by Applying the Extended Kalman Filter With Unknown Inputs to Phasor Measurements," *IEEE Trans. Power Syst.*, vol. 26, no. 4, pp.2556–2566, 2011.

[26] G. K. Gharban, B. J. Cory, "Non-linear dynamic power system state estimation," *IEEE Trans. Power Syst.*, vol. 1, no. 3, pp. 276–283, 1986.

[27] W. Miller, J. Lewis, "Dynamic state estimation in power systems," *IEEE Trans. Autom. Control*, vol. 16, no. 6, pp. 841–846, Dec. 1971.

[28] E. Ghahremani, I. Kamwa, "Online State Estimation of a Synchronous Generator Using Unscented Kalman Filter From Phasor Measurements Units," *IEEE Trans. Energy Conv.*, vol. 26, no. 4, pp.1099–1108, 2011.

[29] N. Zhou, D. Meng, S. Lu, "Estimation of the Dynamic States of Synchronous Machines Using an Extended Particle Filter," *IEEE Trans. Power Syst.*, vol. 28, no. 4, pp. 4152–4161, Nov. 2013.

[30] S. Wang, W. Gao, A.P.S. Meliopoulos, "An Alternative Method for Power System Dynamic State Estimation Based on Unscented Transform," *IEEE Trans. Power Syst.*, vol. 27, no. 2, pp. 942–950, May 2012.

[31] G. Valverde, V. Terzija, "Unscented Kalman filter for power system dynamic state estimation," *IET Gener., Transm. and Dist.* vol. 5, no. 1, pp.29–37, Jan. 2011.

[32] C. Liu, K. Sun, Z. H. Rather, Z. Chen, C. L. Bak, P. Thogersen, P. Lund, "A Systematic Approach for Dynamic Security Assessment and the Corresponding Preventive Control Scheme Based on Decision Trees," *IEEE Trans. Power Syst.*, vol. 29, no. 2, pp. 717–730, Mar. 2014.

[33] Y. Xu, Z. Y. Dong, J. H. Zhao, P. Zhang, K. P. Wong, "A Reliable Intelligent System for Real-Time Dynamic Security Assessment of Power Systems," *IEEE Trans. Power Syst.*, vol. 27, no. 3, pp. 1253–1263, Aug. 2012.

[34] A. Fuchs, M. Imhof, T. Demiray, M. Morari, "Stabilization of Large Power Systems Using VSC-HVDC and Model Predictive Control," *IEEE Trans. Power Delivery*, vol. 29, no. 1, pp. 480–488, Feb. 2014.

[35] J. Licheng, R. Kumar, N. Elia, "Model Predictive Control-Based Real-Time Power System Protection Schemes," *IEEE Trans. Power Syst.*, vol. 25, no. 2, pp. 988–998, May 2010.

[36] H. Liu, Z. Hu, Y. Song, "Lyapunov-Based Decentralized Excitation Control for Global Asymptotic Stability and Voltage Regulation of Multi-Machine Power Systems," *IEEE Trans. Power Syst.*, vol. 27, no. 4, pp.2262–2270, Nov. 2012.

[37] A. E. Leon, J. M. Mauricio, J. A. Solsona, "Multi-machine power system stability improvement using an observer-based nonlinear controller" *Electric Power Syst. Research*, vol. 89, pp. 204–214, Aug. 2012.

[38] R. Yan, Z. Y. Dong, T. K. Saha, R. Majumder, "A power system nonlinear adaptive decentralized controller design," *Automatica*, vol. 46, no. 2, pp. 330–336, Feb. 2010.

[39] M.A.M Ariff, *Adaptive Protection and Control for Wide-Area Blackout Prevention*, Ph.D. Thesis: Imperial College London, U.K., Jun. 2014.

[40] F. Y. Wang, D. Liu, *Networked Control Systems: Theory and Applications*, London, U.K.: Springer, 2008.

[41] J. E. Flood, *Telecommunication Networks*, 2nd ed., IET 1997.

[42] L. Zhang, H. Gao, O. Kaynak, "Network-Induced Constraints in Networked Control Systems - A Survey," *IEEE Trans. Industrial Informatics*, vol. 9, no. 1, pp. 403–416, Feb. 2013.

[43] M. C. F. Donkers, W. P. M. H. Heemels, N. van de Wouw, L. Hetel, "Stability Analysis of Networked Control Systems Using a Switched Linear Systems Approach," *IEEE Trans. Autom. Control*, vol. 56, no. 9, pp. 2101–2115, Sep. 2011.

[44] W. P. M. H. Heemels, A. R. Teel, N. van de Wouw, D. Nesic, "Networked Control Systems With Communication Constraints: Trade offs Between Transmission Intervals, Delays and Performance," *IEEE Trans. Autom. Control*, vol. 55, no. 8, pp. 1781–1796, Aug. 2010.

[45] W. Zhang, M. Branicky, and S. Phillips, "Stability of networked control systems," *IEEE Control Syst.*, vol. 21, pp. 84–99, Feb. 2001.

[46] S. Wang, X. Meng, and T. Chen, "Wide-area control of power systems through delayed network communication," *IEEE Trans. Control Syst. Tech.*, vol. 20, pp. 495–503, Mar. 2012.

[47] H. Li, M. Y. Chow, and Z. Sun, "Eda-based speed control of a networked dc motor system with time delays and packet losses," *IEEE Trans. Industrial Electronics*, vol. 56, pp. 1727–1735, May 2009.

[48] N. R. Chaudhuri, D. Chakraborty, and B. Chaudhuri, "An architecture for FACTS controllers to deal with bandwidth-constrained communication," *IEEE Trans. Power Del.*, vol. 1, pp. 188–196, Mar. 2011.

[49] S. H. Horowitz and A. G. Phadke, *Power System Relaying*, 3rd ed. West Sussex, U.K.: John Wiley & Sons Ltd,, 2008.

[50] M. A. Pai and P. W. Sauer, *Power System Dynamics and Stability*. New Jersey, U.S.A.: Prentice Hall, 1998.

[51] K. R. Padiyar, *Power System Dynamics: Stability and Control*. Tunbridge Wells, U.K.: Anshan Limited, 2004.

[52] M. G. Chiang and R. Y. Safonov, "A Schur method for balanced model reduction," *IEEE Trans. Autom. Control*, vol. AC-34, pp. 729–733, 1989.

[53] K. Ogata, *Modern Control Engineering*, 4th ed. Upper Saddle River, NJ, USA: Prentice Hall PTR, 2001.

[54] D. P. Bertsekas, *Dynamic Programming and Optimal Control*, 1st ed. Belmont, MA, USA: Athena Scientific, 1995.

[55] B. Sinopoli, L. Schenato, M. Franceschetti, K. Poolla, and S. Sastry, "Optimal linear LQG control over lossy networks without packet acknowledgment," *Asian Journal of Control*, vol. 10, pp. 3–13, Jan. 2008.

[56] X. Yu, J. W. Modestino, X. Tian, "The Accuracy of Markov Chain Models in Predicting Packet-Loss Statistics for a Single Multiplexer," *IEEE Trans. Information Theory*, vol. 54, no. 1, pp. 489–501, Jan. 2008.

[57] W. D. Koning, "Infinite horizon optimal control of linear discrete time systems with stochastic parameters," *Automatica*, vol. 18, pp. 443–453, Apr. 1982.

[58] B. Sinopoli, L. Schenato, M. Franceschetti, K. Poolla, M. Jordan, and S. Sastry, "Kalman filtering with intermittent observations," *IEEE Trans. Autom. Control*, vol. 49, pp. 1453–1464, Sep. 2004.

[59] L. E. Ghaoui and M. A. Rami, "Robust state-feedback stabilization of jump linear systems via LMIs," *Int. J. of Robust & Nonlinear Control*, vol. 6, pp. 1015–1022, Nov. 1996.

[60] Y. Loparo and K. A. Fang, "Stochastic stability of jump linear systems," *IEEE Trans. Autom. Control*, vol. 47, pp. 1204–1208, Jul. 2002.

[61] M. Chilali and P. Gahinet, "H_∞ design with pole placement constraints: an LMI approach," *IEEE Trans. Autom. Control*, vol. 41, pp. 358–367, Mar. 1996.

[62] D. Arzelier, J. Bernussou, and G. Garcia, "Pole assignment of linear uncertain systems in a sector via a Lyapunov-type approach," *IEEE Trans. Autom. Control*, vol. 38, pp. 1128–1132, Jul. 1993.

[63] G. Rogers, *Power System Oscillations*. U.S.A.: Springer, 2000.

[64] N. Martins, L.T.G. Lima, "Determination of suitable locations for power system stabilizers and static VAR compensators for damping electromechanical oscillations in large scale power systems," *IEEE Trans. Power Syst.*, vol. 5, pp. 1455–1469, Nov. 1990.

[65] L.P. Kunjumuhammed, R. Singh, and B.C. Pal, "Robust signal selection for damping of inter-area oscillations," *Gener., Transm., Dis., IET*, vol.6, no.5, pp.404–416, May 2012.

[66] A. Heniche, and I. Kamwa, "Control loops selection to damp inter-area oscillations of electrical networks," *IEEE Trans. Power Syst.*, vol. 17, no. 2, pp. 378–384, May 2002.

[67] H. Wang, "Selection of robust installing locations and feedback signals of FACTS-based stabilizers in multi-machine power systems," *IEEE Trans. Power Syst.*, vol. 14, no. 2, pp. 569–574, May 1999.

[68] M.E. Aboul-Ela, "Damping controller design for power system oscillations using global signals," *IEEE Trans. Power Syst.*, vol.11, no.2, pp. 767–773, May 1996.

[69] L. Fan, Y. Wehbe, "Extended Kalman filtering based real-time dynamic state and parameter estimation using PMU data," *Electric Power Systems Research*, vol. 103, pp. 168–177, Oct. 2013.

[70] J. K. Uhlmann, "Algorithms for multiple target tracking," *American Scientist*, vol. 80, no. 2, pp. 128–141, 1992.

[71] J. K. Uhlmann, "Simultaneous map building and localization for real-time applications," Transfer thesis. University of Oxford, 1994.

[72] S. J. Julier, J. K. Uhlmann, "A new extension of the Kalman filter to nonlinear systems," *The Proceedings of AeroSense: The 11th International Symposium on Aerospace/Defense Sensing, Simulation and Controls, Orlando, Florida, SPIE,* 1997.

[73] R. E. Kalman, "A New Approach to Linear Filtering and Prediction Problems," *Journal of Basic Engineering*, vol. 82 D, pp. 35–45, 1960.

[74] S. Julier, J. Uhlmann, H. F. Durrant-Whyte, "A new method for the nonlinear transformation of means and covariances in filters and estimators," *IEEE Trans. Autom. Control*, vol. 45, no. 3, pp. 477–482, Mar. 2000.

[75] I. Markovsky and B. D. Moor, "Linear dynamic filtering with noisy input and output," *Automatica*, vol. 41, pp. 167–171, 2005.

[76] K. Tam, "Current-Transformer Phase-Shift Compensation and Calibration," *Application Report, Texas Instruments*, Literature Number SLAA122 pp. 1–6, Feb. 2001.

[77] *IEC Standard for Instrument Transformers*, IEC Std 60044 ed. 1.2, 2003.

[78] *IEEE Standard Requirements for Instrument Transformers*, IEEE Std C57.13-2008 (Revision of IEEE Std C57.13-1993), pp. c1-82, Jul. 28, 2008.

[79] S. Kwon, W. Chung, "Combined synthesis of state estimator and perturbation observer," *ASME Journal of Dynamic Syst., Meas., and Control*, vol. 125, no. 1, pp. 19–26 Mar. 2003.

[80] A. Iserles, *A First Course in the Numerical Analysis of Differential Equations*. U.K.: Cambridge University Press, 2008.

[81] H. Kwakernaak; R. Sivan, *Linear optimal control systems*. vol. 1. New York: Wiley-Interscience, 1972.

[82] E. Menguy; J. L. Boimond; L. Hardouin; J. L. Ferrier, "Just-in-time control of timed event graphs: update of reference input, presence of uncontrollable input," *IEEE Trans. Autom. Control*, vol. 45, no. 11, pp. 2155–2159, Nov. 2000.

[83] J. M. Yang; S. W. Kwak, "Model Matching for Asynchronous Sequential Machines with Uncontrollable Inputs," *IEEE Trans. Autom. Control*, vol. 56, no. 9, pp. 2140–2145, Sep. 2011.

[84] J. M. Yang; S. W. Kwak, "Corrective control of asynchronous machines with uncontrollable inputs: application to single-event-upset error counters," *IET Control Theory & Applications*, vol. 4, no. 11, pp. 2454–2462, Nov. 2010

[85] A. C. Zolotas, B. Chaudhuri, I. M. Jaimoukha, P. Korba, "A Study on LQG/LTR Control for Damping Inter-Area Oscillations in Power Systems," *IEEE Trans. Control Syst. Tech.*, vol. 15, no. 1, pp. 151–160, Jan. 2007.

[86] H. S. Ko, J. Jatskevich, "Power Quality Control of Wind-Hybrid Power Generation System Using Fuzzy-LQR Controller," *IEEE Trans. Energy Conv.*, vol. 22, no. 2, pp. 516–527, Jun. 2007.

[87] K. M. Son, J. K. Park, "On the robust LQG control of TCSC for damping power system oscillations," *IEEE Trans. Power Syst.*, vol. 15, no. 4, pp. 1306–1312, Nov. 2000.

[88] J. C. Seo, T. H. Kim, J. K. Park, S. I. Moon, "An LQG based PSS design for controlling the SSR in power systems with series-compensated lines," *IEEE Trans. Energy Conv.*, vol. 11, no. 2, pp. 423–428, Jun. 1996.

[89] Charles L. Philips and H. Troy Nagel, *Digital Control System Analysis and Design*. 3rd ed. U.S.A.: Prentice Hall, 1994.

[90] K. Furuta, S. Kim, "Pole assignment in a specified disk," *IEEE Trans. Autom. Control*, vol. 32, no. 5, pp. 423–427, May 1987.

[91] Y. Susuki, I. Mezic, "Nonlinear Koopman Modes and Power System Stability Assessment Without Models," *IEEE Trans. Power Syst.*, vol. 29, no. 2, pp. 899–907, Mar. 2014.

[92] K. R. Padiyar, *Structure Preserving Energy Functions in Power Systems: Theory and Applications*. Florida, U.S.A.: CRC Press, 2013.